Aus dem
Comprehensive Pneumology Center Munich des
Helmholtz Zentrum München
Direktor: Prof. Dr. med. Oliver Eickelberg

und dem
Institut für experimentelle Pneumologie des
Klinikum der Universität München
Direktor: Prof. Dr. med. Oliver Eickelberg

Defining Molecular Signatures of Fibroblast Phenotypes in Pulmonary Fibrosis

Dissertation

zum Erwerb des Doktorgrades der Naturwissenschaften

an der Medizinischen Fakultät der Ludwig-Maximilians-Universität München

vorgelegt von

Bettina Madeleine Oehrle

aus Spaichingen

2015

Gedruckt mit Genehmigung der Medizinischen Fakultät der Ludwig-Maximilians-Universität München

Betreuerin: PD. Dr. rer. nat. Silke Meiners
Zweitgutachter: Prof. Dr. rer. nat. Alexander Dietrich
Dekan: Prof. Dr. med. Dr.h.c. Maximilian Reiser, FACR, FRCR
Tag der mündlichen Prüfung: 12.05.2015

EIDESSTATTLICHE VERSICHERUNG

Ich, Bettina Madeleine Oehrle, erkläre hiermit an Eides statt, dass ich die vorliegende Dissertation mit dem Thema

Defining Molecular Signatures of Fibroblast Phenotypes in Pulmonary Fibrosis

selbständig verfasst, mich außer der angegebenen keiner weiteren Hilfsmittel bedient und alle Erkenntnisse, die aus dem Schrifttum ganz oder annähernd übernommen sind, als solche kenntlich gemacht und nach ihrer Herkunft unter Bezeichnung der Fundstelle einzeln nachgewiesen habe. Ich erkläre des Weiteren, dass die hier vorgelegte Dissertation nicht in gleicher oder in ähnlicher Form bei einer anderen Stelle zur Erlangung eines akademischen Grades eingereicht wurde.

Ort, Datum

Unterschrift

EIDESSTATTLICHE VERSICHERUNG ..... **i**
LIST OF ABBREVIATIONS ..... **ii**
ZUSAMMENFASSUNG ..... **vii**
SUMMARY ..... **viii**
1. INTRODUCTION **1**
1.1 Interstitial lung disease (ILD) 1
1.2 Idiopathic pulmonary fibrosis (IPF) 1
1.2.1 Diagnosis and treatment strategies of IPF 2
1.2.2 Pathologic features of IPF 4
1.2.3 IPF pathogenesis 5
1.2.4 Molecular mechanisms of IPF 6
1.3 Lung fibroblast biology 8
1.3.1 Activated fibroblasts in IPF 8
1.3.2 Interstitial cell migration 10
1.4 Extracellular matrix (ECM) 12
1.4.1 ECM remodeling processes in IPF 13
1.4.2 ECM model systems 15
1.5 Objectives 16
2. MATERIALS AND METHODS **17**
2.1 Materials 17
2.1.1 Antibodies 17
2.1.2 Buffers and solutions 18
2.1.3 Cell lines and primary cells 20
2.1.1 Laboratory equipment and software 22
2.1.2 Chemicals and Consumables 24
2.1.3 Enzymes 25
2.1.4 Oligonucleotides 26
2.1.4.1 Quantitative RT-PCR 26
2.1.5 Standards and kits 27
2.2 Methods 27
2.2.1 Cell biological methods 27
2.2.1.1 Isolation of primary human fibroblast 27
2.2.1.2 Cryopreservation of mammalian cells 28
2.2.1.3 Culturing and sub-culturing of mammalian cells 28
2.2.1.4 Liposome-based cell transfection 29

2.2.1.5 Growth factor treatment of cells 29
2.2.1.6 Live cell imaging in 3D 30
2.2.1.7 Live cell imaging in 2D 30
2.2.2 3D cell culture models 31
2.2.2.1 Preparation of collagen G matrices 31
2.2.2.2 3D collagen-based invasion assay 31
2.2.2.3 3D collagen-based separation assay 32
2.3 Molecular biological methods 33
2.3.1 RNA analysis 33
2.3.1.1 mRNA isolation from 3D cell culture 33
2.3.1.2 mRNA isolation from 2D cell culture 33
2.3.1.3 cDNA-synthesis 33
2.3.1.4 Quantitative real-time Polymerase Chain reaction (qRT-PCR) 34
2.3.1.5 Verification of amplicons by agarose gel electrophoresis 35
2.3.1.6 Microarray 35
2.3.2 Proteinbiochemistry 35
2.3.2.1 Protein isolation from 3D cell culture 35
2.3.2.2 Protein isolation from 2D cell culture 36
2.3.2.2.1 Protein isolation from cell lysates 36
2.3.2.2.2 Protein isolation from cell supernatants 36
2.3.2.3 Determination of protein concentration by bicinchoninic acid assay (BCA) ... 36
2.3.2.4 Sodium dodecyl sulphate polyacrylamide gel electrophoresis (SDS-PAGE) and Western blotting 37
2.3.2.5 Enzyme-linked Immunosorbent Assay (ELISA) 37
2.3.2.6 Luciferase reporter assay 37
2.3.2.7 Immunocytochemistry and immunofluorescence microscopy 37
2.4 In silico analysis 38
2.4.1 Quantification of cell morphology 38
2.4.2 Quantification of invasion capacity 39
2.4.3 Bioinformatical analysis 39
2.4.4 Statistical analysis 39
3. RESULTS 41
3.1 Establishment of novel 3D collagen-based invasion assays 41
3.1.1 Invasion assay 41
3.1.2 Characterization of the invasive fibroblast phenotype 45

3.1.3 Separation assay 49
3.2 Growth factor induced fibroblast invasion 50
3.3 Molecular characterization of the invading fibroblast phenotype 52
3.3.1 Gene profile of the invasive fibroblast phenotype 52
3.3.2 Identification of TGFβ1-mediated transcriptomic invasion signature 59
3.3.3 Gene array verification 66
3.4 Secreted frizzled-related protein 1 (Sfrp1) 68
3.4.1 Sfrp1 within the molecular signature of invading fibroblasts 68
3.4.2 Growth factor induced regulation of Sfrp1 70
3.4.3 Sfrp1 expression in interstitial lung disease (ILD) 72
3.4.4 Functional characterization of Sfrp1 in invading fibroblasts 77
4. DISCUSSION 81
4.1 3D ECM model systems for extensive profiling of invasive cell types 81
4.2 Growth factor mediated fibroblast invasion 83
4.3 Phenotypic characterization of fibroblasts cultured in 3D 84
4.4 Analysis of the gene profile of fibroblast invasion 85
4.5 TGFβ1-induced invasion gene profile and strategy for target selection 88
4.6 Sfrp1 as functional target for fibroblast invasion 89
4.7 Regulation of Sfrp1 in interstitial lung disease (ILD)-related environments 92
4.8 Conclusion and future directions 94
5. REFERENCES 96
List of Tables 113
List of Figures 114
6. APPENDIX 116
6.1 Scheme for cell morphology quantification 116
6.2 Gene expression lists 117
ACKNOWLEDGEMENTS 144

LIST OF ABBREVIATIONS

A

αSMA	Alpha smooth muscle actin
Adamts	A Metallopeptidase with Thrombospondin Type 1 Motif
Adam	A Disintegrin and Metalloproteinase domain-containing protein
ANOVA	Analysis of variance
APS	Ammonium peroxodisulfate
ATI	Alveolar type I
ATII	Alveolar type II

B

BAL	Bronchoalveolar lavage
BH	Benjamini-Hochberg
BMP4	Bone morphogenic protein 4
BSA	Bovine serum albumin

C

C1qtnf3	C1q and tumor necrosis factor related protein 3
Cav1	Caveolin 1
CAF	Cancer associated fibroblasts
CCL	Chemokine (CC-motif) ligand
CCN	Cyr61 CTGF NOV
cDNA	Complementary DNA
CD29	Cluster of differentiation 29
Cdc42	Cell division cycle 42 protein
Col1a1	Collagen type 1 a 1
CTGF	Connective tissue growth factor
Cyr61	Cysteine-rich angiogenic protein 61
°C	Degrees Celsius

D

D	Day(s)
Da	Dalton
DAPI	4',6-diamidino-2-phenylindole
DKK	Dickkopf protein family
DMEM	Dulbecco's Modified Eagle's Medium
DMSO	Dimethyl sulfoxide
DNA	Deoxyribonucleic acid
dNTP	Desoxy-nucleotide-tri-phosphate
DPLD	Diffuse parenchymal lung disease
DTT	Dithiothreitol

E

ECM	Extracellular matrix
EDTA	Ethylenediaminetetraacetic acid
EGF	Epidermal growth factor
ELISA	Enzyme-linked immunosorbent assay
EMT	Epithelial mesenchymal transition
EndoMT	Endothelial mesenchymal transition
Enpp2	Ectonucleotide Pyrophosphatase/Phosphodiesterase 2
ER	Endoplasmatic reticulum

F

FBS	Fetal bovine serum
FD	Fold difference
FDR	False discovery rate
FGF	Fibroblast growth factors
FW	Forward
FZD	Frizzled

G

G	Gram
GAPDH	Glyceraldehyde 3-phosphate dehydrogenase
Grem2	Gremlin-2
Gly	Glycin

H

H	Hour(s)
HAS	Hyaluronan synthase
hCLUST	Hierachical clustering
HEPES	N-2-hydroxyethylpiperazine-N-2-ethane sulfonic acid
HGF	Hepatocyte growth factor
HRCT	High resolution computer tomography
HRP	Horseradish peroxidase

I

IGF	Insulin-like growth factor
IgG	Immunoglobulin protein G
IL	Interleukin
ILD	Interstitial lung disease
INF	Interferone
IPA	Ingenuity® Pathway Analysis
IPF	Idiopathic pulmonary fibrosis

K

K	Kilo

L

L	Liter
LEF	Lymphocyte enhancer factor
LOXL	Lysyl oxidase-like
LPA	Lysophosphatidic acid

M

M	Milli
M	Molar
mA	Milli Ampere
Min	Minutes
MMP	Matrix Metallo-proteinase
mRNA	Messenger RNA
MUC5B	Mucin 5B
µ	Micro

N

N	Nano
NLK	Nemo-like kinase
NOV	Nephroblastoma overexpressed

O

Ogn	Osteoglycin
ON	Over night

P

P	Pico
PAGE	Polyacrylamide gel electrophoresis
PBS	Phosphatate buffered saline
PCR	Polymerase chain reaction
PDGFR	Platelet-derived growth factor receptor
pEGFP-N2	Enhanced green fluorescent protein N2 vector
PET	Polyethylenterephthalat
PFA	Paraformaldehyde
PGE2	Prostaglandin E2
PMC	Pleural mesothelial cells
PI3K/Akt	Phosphatidylinositol-3-kinase/Ak strain transforming
Pten	Phosphatase and tensin homologue deleted on chromosome 10

Q

qRT-PCR	Quantitative real-time Polymerase chain reaction

R

Rac1	Ras-related C3 botulinum toxin substrate 1
RFU	Relative fluorescence units
RhoA	Ras homologous A
RIN	RNA integrity number
RIPA	Radio-immunoprecipitation assay
RMA	Robust multi-array average
RNA	Ribonucleic acid
ROC	Receiver operating characteristic curve

S

S	Seconds
SDS	Sodium dodecyl sulphate
Serpina3n	Serine (or cysteine) peptidase inhibitor, clade A, member 3N
SFTPA2	Surfactant protein A2
SFTPC	Surfactant protein C
Sfrp1	Secreted frizzled-related protein 1
Sike1	Suppressor of IKBKE 1
SNP	Single nucleotide polymorphism
SOX9	SRY (sex determining region Y)-box 9

T

TAE	Tris-acetate-EDTA
TBS	Tris-buffered saline
TBS-T	Tris-buffered saline with TWEEN®20
TCF	T cell factor
TEMED	N,N,N',N'-Tetramethylendiamin
TERC	Telomerase RNA component
TERT	Telomerase reverse transcriptase
TGF	Transforming growth factor
TIMP	Tissue inhibitor of metalloproteinase
TNF	Tumor necrosis factor
TRIS	Tris(hydroxymethyl)-aminomethane

U

U	Unit
UIP	Usual interstitial pneumonia

V

V	Volt
V	Volume
VEGFR	Vascular endothelial growth factor receptor

W

W	Weight
WIF-1	Wnt inhibitory factor-1
WISP	WNT1 inducible signaling pathway protein
Wnt	Wingless/integrase-1

ZUSAMMENFASSUNG

Die idiopatische pulmonale Fibrose (IPF) ist eine schwerwiegende, chronische interstitielle Lungenerkrankung (ILD). IPF ist gekennzeichnet durch eine progressive Äthiopathologie, einer Beeinträchtigung und Hyperplasie des Epithels sowie, einer extensiven Anlagerung von extrazellulärer Matrix (ECM) im Lungeninterstitium. Diese pathologischen Prozesse, die primär von einem anomalen Umbau des Gewebes gesteuert werden, resultieren in einem beeinträchtigten Gasaustausch, der zum Tod führt. Der dynamische Prozess des Gewebeumbaus ist auf einen aktiven und wandlungsfähigen Fibroblastenphänotyp angewiesen. Dieser Fibroblastenphänotyp besitzt eine besonders ausgeprägte Fähigkeit, in stromales Gewebe einzuwandern. Die Zielsetzung der vorliegenden Studie umfasste die umfangreiche Charakterisierung dieses aktivierten, invasiven Fibroblastenphänotyps und die Identifizierung zugrundeliegender potenzieller Regulatoren. Hierfür wurden zunächst kollagenbasierte, phänotypische Assays der dreidimensionalen (3D) Fibroblasteninvasion entwickelt *(Burgstaller, Oehrle et al., 2013)*. Unter Verwendung dieser neuartigen Assays wurde der invasive Fibroblastenphänotyp auf morphologischer und molekularer Ebene charakterisiert. Für mesenchymale Zellen, die physiologisch in der 3D Struktur der Lunge angesiedelt sind, sind adaptive und reziproke Interaktionen zwischen Zellen und der sie umgebenden ECM weithin anerkannt und spiegeln sich in der Zellmorphologie wider. Demgemäß wurde ein signifikanter Unterschied der zellulären Morphologie zwischen Fibroblasten, die in 2D und 3D Zellkultursystemen kultiviert wurden, identifiziert. Um den invasiven Fibroblastenphänotyp auf molekularer Ebene zu charakterisieren, wurden transkriptom-weite Signaturen der Fibroblasteninvasion generiert (microarrays) unter der Verwendung einer murinen Fibroblastenzelllinie (MLg) *(Oehrle, Burgstaller et al. 2015 – in press)*. Die resultierenden Genexpressionsprofile der invasiven und nicht-invasiven Fibroblasten setzen sich deutlich voneinander ab: 1049 Gene waren unterschiedlich reguliert (>1,5-fach). Eine *in silico* Analyse der Transkriptomsignatur der Invasion deckte eine Anreicherung der funktionalen Cluster „invasion of cells“, „IPF“ und „metastasis“ auf. Anschließend wurden die Invasionsassays mit dem profibrotischen Zytokin transforming growth factor (TGF) β1 implementiert, was das Invasionsvermögen der MLg Zellen erhöhte. Daraufhin, wurde eine Transkriptionsanalyse der TGFβ1-induzierten Fibroblasteninvasion durchgeführt. In der sich überschneidenden Signatur der nicht induzierten und TGFβ1-induzierten Invasion wurde der Inhibitor der Wingless/Integrase-1 (Wnt) Signalwege, secreted frizzled-related protein (Sfrp) 1, als negativer Regulator für Fibroblasteninvasion identifiziert. Stimulierung mit TGFβ1 erniedrigte signifikant die Expression von Sfrp1 und die spezifische Inhibierung von Sfrp1 durch ein Diarylsulfon-Sulfonamid Derivat erhöhte die 3D Invasion ohne die 2D Motilität zu beeinflussen. Primäre humane Fibroblasten (phF) von ILD Patienten exprimierten geringe Sfrp1 Spiegel, was invers mit deren Invasionskapazität korrelierte.

SUMMARY

Idiopathic pulmonary fibrosis (IPF) is a severe, chronic interstitial lung disease (ILD). IPF is characterized by a progressive ethiopathology, damage and hyperplasia of the epithelium as well as extensive deposition of extracellular matrix (ECM) within the lung interstitium. These pathological processes, which are primarily driven by aberrant tissue remodeling, ultimately result in impaired gas exchange and death by asphyxiation. The dynamic process of tissue remodeling depends on an activated, versatile fibroblast phenotype. This fibroblast phenotype exhibits an exceptional and distinct capacity to invade stromal tissue.

The objective of the current study was to comprehensively characterize this activated, invasive fibroblast phenotype and to identify potential underlying regulators. For this purpose, three dimensional (3D) collagen-based phenotypic assays of fibroblast invasion were established *(published in Burgstaller, Oehrle et al., 2013)*. Using these novel assays, the invading fibroblast phenotype was characterized on morphological and molecular levels. For mesenchymal cells, physiologically residing in the 3D structure of the lung interstitium, adaptive and reciprocal interactions between cells and surrounding ECM are well recognized and are reflected in the cell morphology. Accordingly, significant differences of cellular morphology between fibroblasts cultured in 2D and 3D cell culture systems were identified. To characterize the invading fibroblast phenotype on molecular level, transcriptome-wide signatures of fibroblast invasion were generated (microarrays) using a murine lung fibroblast cell line (MLg) *(Oehrle, Burgstaller et al. 2015 – in press)*. The resulting gene expression profiles of invading and non-invading fibroblasts were highly distinct: 1049 genes were differentially regulated (>1.5-fold). *In silico* analysis of this invasion transcriptome signature revealed a significant enrichment for the functional clusters “invasion of cells”, “IPF”, and “metastasis”. Subsequently, the invasion assays were implemented with the profibrotic cytokine, transforming growth factor (TGF) β1, which increased the invasion capacity of MLg cells. Transcriptome analysis of the TGFβ1-induced fibroblast invasion was then performed. Within overlapping signatures of baseline and TGFβ1-induced invasion, the Wingless/Integrase-1 (Wnt) signaling pathway inhibitor, secreted frizzled-related protein (Sfrp) 1, was identified as a negative regulator of fibroblast invasion. Sfrp1 expression was significantly lowered upon TGFβ1 stimulation and specific chemical inhibition of Sfrp1 by a diarylsulfone sulfonamide derivate increased 3D invasion, without affecting 2D motility. Furthermore, primary human lung fibroblasts derived from ILD patients expressed low Sfrp1 levels, which inversely correlated with the invasion capacity.

1. INTRODUCTION

1.1 Interstitial lung disease (ILD)

Interstitial lung disease (ILD) or diffuse parenchymal lung disease (DPLD) designates a group of lung pathologies that affects the epithelium, endothelium, the basal membrane as well as the perivascular and perilymphatic tissues of the lung. ILD is associated with high morbidity and mortality rates (Antoniou, Margaritopoulos et al. 2014). The term ILD comprises more than 150 different subgroups of the same clinical, pathological, physiological, and radiological manifestations but varying underlying etiologies and molecular pathophysiologies (Eickelberg and Selman 2010). ILDs can be subclassified according to their causes, which include inhaled substances (inorganic or organic), drug induced, radiation exposure, connective tissue diseases, infections, or idiopathic.

1.2 Idiopathic pulmonary fibrosis (IPF)

Idiopathic pulmonary fibrosis (IPF) shows, with a median survival of three years, the highest mortality among the ILDs (Antoniou, Margaritopoulos et al. 2014). The prevalence of IPF is estimated to be 14 - 63 cases per 100,000 in the United States and 1.25 - 23.4 cases per 100,000 in Europe, depending on the case definition used (Nalysnyk, Cid-Ruzafa et al. 2012). The prevalence rises dramatically with age, as evidenced in the United States, where 0.2% of the population older than 75 years is already affected (Wolters, Collard et al. 2014). Men are more frequently affected than women and a correlation with patients' smoking history has been reported. IPF is characterized by a progressive ethiopathology, damage, and hyperplasia of the alveolar epithelium, extensive deposition of extracellular matrix (ECM), especially collagens, within the lung interstitium, and enhanced fibroblast proliferation and activation, which causes the formation of fibroblastic foci (Selman, King et al. 2001). These processes lead to disruption of the lung architecture, impairment of gas exchange and ultimately death by asphyxiation. IPF clinically presents with dry cough, unexplained chronic exertional dyspnea, bibasilar inspiratory crackles, and finger clubbing (Raghu, Collard et al. 2011). The clinical course is often influenced by the occurrence of acute episodes of respiratory worsening. These acute exacerbations may be initiated by viral infection (Wootton, Kim et al. 2011), air pollution (Johannson, Vittinghoff et al. 2014), or microaspiration (Lee, Song et al. 2012) and are associated with a high mortality risk.

1.2.1 Diagnosis and treatment strategies of IPF

Referring to the official revised diagnosis guideline of the American Thoracic Society, European Respiratory Society, Japanese Respiratory Society and Latin American Thoracic Association, diagnosis of IPF without surgical biopsy is accomplished following the major and minor diagnosis criteria listed in Table 1.1. Importantly, IPF can only be diagnosed by excluding other causes of ILD.

Table 1.1: Diagnosis of IPF in absence of surgical lung biopsy (2000). (Wells 2013) – *modified.*

Major diagnosis criteria
- Exclusion of known causes of ILD (environmental exposure, connective tissue diseases and drug toxicities)
- Evidence of restriction and impaired gas exchange by pulmonary function studies
- HRCT scans show bibasilar reticular abnormalities with minimal ground glass opacities
- BAL and transbronchial lung biopsy do not support alternative diagnosis

Minor diagnosis criteria
- Age > 50 years
- Insidious onset of otherwise unexplained dyspnea on exertion
- Duration of illness > 3 months

Abbreviations: High-resolution computer tomography (HRCT), Bronchoalveolar lavage (BAL)

Despite intense research efforts over the past decades no effective pharmaceutical therapy has been discovered to date. Solely Pirfenidone has been approved for the treatment of IPF in Japan in 2008 and in Europe in 2011 although phase III clinical trials are still ongoing (Potts and Yogaratnam 2013). Most recently, efficacy in a phase III clinical trial has been reported for the multiple tyrosine kinase inhibitor Nintedanib (formerly known as BIBF 1120) (Richeldi, du Bois et al. 2014).

Ineffective treatment strategies to date are anti-inflammatory immunomodulators (Corticosteroid monotherapy, Cyclophosphamide, Azathioprine, Everolimus), anticoagulants (Warfarin, Heparin), endothelin receptor antagonists and vasodilators (Bosentan, Ambisentan, Macicentan, Sildenafil), and antifibrotics and cytokine/kinase-inhibitors (INFγ1b, Eternacept, Imatinib, CC-930). Further treatment strategies currently in phase III clinical trials are summarized in Table 1.2.

Nevertheless, to date, the only intervention for IPF that improves survival is lung transplantation (Rafii, Juarez et al. 2013).

Table 1.2: Selected ongoing clinical trials for IPF (Rafii, Juarez et al. 2013) – *modified.*

Agent/treatment	Potential mechanism	Clinical trial
Pirfenidone	Inhibitor of TGFβ, anti-inflammatory, antioxidant	ASCEND (Intermune), USA
Nintedanib	Multiple tyrosine kinase inhibitor	INPULSIS 1-2 (Boehringer Ingelheim Pharmaceuticals), UK
GC1008	Anti-TGFβ1-3 antibody	Genzyme and Cambridge Antibody Technology, UK
STX-100	Anti-αvβ6 integrin	Stromedix, USA
FG-3019	CTGF inhibitor	Fibrogen, USA
Octreotide	Somatostatin analogue	Institut National de la Santé Et de la Recherche Médicale, France
CNTO 888	Anti CCL2 antibody	Centocor, USA
QAX576, Tralokinumab	Anti-IL-13 antibody	Novartis, Switzerland, MedImmune LLC
SAR156597	Bispecific Anti-IL-13 and IL-4 antibody	Sanofi-Aventis
Thalidomide	Inhibitor of TGFβ1 signaling and VEGF expression	John Hopkins University, USA
GS-6624	Anti-LOXL2 antibody	Gilead Sciences
BIBF1120	Angiokinase inhibitor targeting FGFR, PDGFR, VEGFR	TOMORROW (Boehringer Ingelheim Pharmaceuticals), UK
Minocycline	Tetracycline with anti-inflammatory and anti-angiogenic properties	University of California, USA
Tetrathiomolybdate	Antiangiogenic	University of Michigan, USA
Doxycycline	MMP inhibitor	Indian Institute of Chemical Biology, India
Losartan	Angiotensin II inhibitor	National Cancer Institute, USA
Carbon Monoxide	Anti-proliferative diatomic gas, inhibitor of fibroblast ECM deposition	Brigham and Women's hospital, USA
Mesenchymal stem cells	Potential alveolar re-epithelialization	The Prince Charles Hospital, Australia

Abbreviations: Transforming growth factor (TGF), Connective tissue growth factor (CTGF), Chemokine (CC-motif) ligand (CCL), Interleukin (IL), Vascular endothelial growth factor (VEGF), Lysyl oxidase-like (LOXL), Fibroblast growth factor receptor (FGFR), Platelet-derived growth factor receptor (PDGFR), Matrix Metallo-proteinase (MMP).

1.2.2 Pathologic features of IPF

According to the guidelines, described in Table 1.1, HRCT is an essential tool for the diagnosis of IPF. By means of HRCT scans the histopathological feature of IPF can be identified, which is termed usual interstitial pneumonia (UIP). UIP is characterized by a spatial and temporal heterogeneity where the lung injury pattern in the periphery is highly different from that of the center of the pulmonary lobule. The subpleural/paraseptal regions are affected by scarring and microscopic honeycombing and intersect abruptly with normal lung tissue. Honeycombs are large airspaces lined by bronchiolar epithelium and filled with mucous and inflammatory cells, such as neutrophils and macrophages (Cavazza, Rossi et al. 2010). Other characteristic HRCT features of UIP are ground glass and reticular opacity.

Hallmarks of UIP are so called fibroblastic foci which are small interstitial associations of myofibroblasts, covered by hyperplastic alveolar epithelial cells or bronchiolar cells. Histopathologically, these fibrotic lesions are primarily detected by their expression of alpha smooth muscle actin (αSMA) (Figure 1.1). Fibroblastic foci mainly occur at the interface of fibrotic and less affected regions. These sites represent manifestations of proliferating spindle-shaped fibroblasts that frequently arrange parallel to the alveolar surface. Numbers of fibrotic lesions predict disease progression, as more fibroblastic foci are found in lungs of patients with a rapidly progressive form of IPF (King, Schwarz et al. 2001).

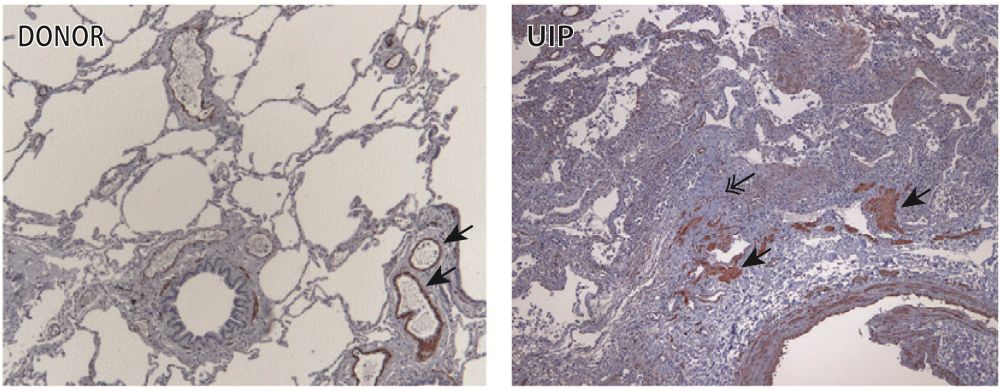

Figure 1.1: Histopathological appearance of UIP.
Immunohistochemical staining for alpha smooth muscle actin (αSMA) of tissue sections from a normal donor lung (left panel) and a lung with usual interstitial pneumonia (UIP) pattern (right panel). αSMA-staining (brown) is indicated with black solid arrows. While in donor specimens exclusively smooth muscle cells are stained, in UIP fibroblast foci show and intense signal for αSMA (solid arrow). Extensive interstitial collagen deposition in UIP is indicated with a (double-line headed arrow). (Eickelberg and Laurent 2010) – *modified*. (Reprinted with permission of the American Thoracic Society. Copyright © 2014 American Thoracic Society).

1.2.3 IPF pathogenesis

Initially, IPF was considered a disease that resulted from excessive chronic inflammation that induces lung injury and thus fibrosis. However, failure of anti-inflammatory therapeutic approaches (compare section 1.2) led to a paradigm shift to consider IPF more and more as a disease driven by excessive wound healing processes (Gross and Hunninghake 2001). Currently, epithelial cells as well as the mesenchyme are considered key components in IPF.

The pathobiology of IPF can be divided into *predisposition*, *initiation* and *progression* stages (Wolters, Collard et al. 2014).

The *predisposition* stage is mainly manifested by epithelial cell dysfunction. Familial clustering of pulmonary fibrosis suggests the existence of a genetic predisposition. Consequently, several mutations have been identified in patients suffering from pulmonary fibrosis. The major alteration identified in 2011 in a large genome-wide associated study is the SNP rs35705950, which is located 3 kb upstream of the mucin 5B (MUC5B) gene on chromosome 11. This SNP occurred in 34% of patients with IPF and induced 37.4 times higher MUC5B expression in IPF compared to healthy lungs. However, the molecular consequences of increased MUC5B expression remain to be discovered. The second most frequent genetic mutation affects the age-related genes, telomerase reverse transcriptase (TERT) and telomerase RNA component (TERC). TERT and TERC mutations are associated with shortened telomere lengths; a phenomenon that has been reported in IPF (Liu, Ullenbruch et al. 2013). The third most prominent group of mutations affects the surfactant protein family. A heterozygous mutation ($SPC^{\Delta exon4}$) in surfactant protein C encoding gene (SFTPC) was identified (Nogee, Dunbar et al. 2001). Other mutations in SFTPC affect the BRICHOS domain, which is involved in post-translational processing and has a chaperone-like function (Thomas, Lane et al. 2002), (Knight, Presto et al. 2013). In addition, mutations in surfactant protein A2 encoding gene (SFTPA2) were detected (Wang, Kuan et al. 2009). Both mutations induce endoplasmatic reticulum (ER) stress in the lung epithelium. Another aspect for the *predispositional* stage of IPF arose from the fact that the genetic mutations described did not directly induce fibrosis in animal models (Lawson, Cheng et al. 2011). (Lee, Reddy et al. 2009), (Rudolph, Chang et al. 1999). One explanation for this may be the requirement for an additional stressor. Besides aging, environmental exposures to dust, pollution and smoke may particularly act on a genetically predisposed epithelium (Sueblinvong, Neujahr et al. 2012).

The prevailing theory of fibrogenesis in IPF suggests that recurring, non-resolving microinjury of the alveolar epithelium is the main *initiation* factor. Epithelial cell dysfunction, caused by ER stress that activates the unfolded protein response (Lawson, Cheng et al. 2011), disruption of basement membrane, excessive activation of signaling pathways and release of fibrogenic mediators induce fibrocyte recruitment (Andersson-Sjoland, de Alba et al. 2008) and plasticity of

numerous other cell types. Ultimately, activated fibroblasts infiltrate the lung interstitium to form fibroblastic foci and excessively secret ECM components. Together with an aberrant re-epithelialization, these tissue remodeling processes accumulate in the distorted lung architecture and impaired lung function (du Bois 2010), (King, Pardo et al. 2011), observed in IPF.

Once initiated, IPF progresses unrelentingly. Although the detailed mechanism behind the *progressive* character of the disease is not yet uncovered, it is speculated that the pathologically remodeled ECM (Booth, Hadley et al. 2012) and excessive fibroblast proliferation (Nho, Hergert et al. 2011) significantly contribute to the disease progression. Furthermore, epigenetic changes such as the DNA methylation pattern (Rabinovich, Kapetanaki et al. 2012), (Sanders, Ambalavanan et al. 2012) and micro RNA expression changes (Pandit, Milosevic et al. 2011) are hypothesized to contribute to IPF progression (Wolters, Collard et al. 2014).

1.2.4 Molecular mechanisms of IPF

To date, numerous profibrotic mediators have been identified that contribute to fibrogenic changes by promoting fibroblast activation, invasion, differentiation and collagen production (Laurent, McAnulty et al. 2008). Among the manifold sources for the cytokines that have been reported, the epithelium presents one essential secretor for paracrine factors, acting on the mesenchyme. In the lung, epithelial and mesenchymal cells reside in close spatial proximity. Moreover in terms of IPF, fibroblastic foci are covered by hyperplastic alveolar epithelial cells (compare section 1.2.3). Given that fibrotic processes within the lung are believed to be initiated at the epithelium but ultimately result in extensive mesenchymal malfunction, it appears likely that there occurs signal transduction between both compartments. In addition to epithelial cells, macrophages, lymphocytes, smooth muscle cells and endothelial cells have been reported among others as potential sources of cytokines in IPF (Laurent, McAnulty et al. 2008).

Considering the enormous number of cell types postulated to be involved in IPF pathogenesis, unsurprisingly the network of the suggested underlying molecular mechanism is very complex. In order to identify the most interesting profibrotic mediators, Coker and Laurent proposed a list of criteria according to which profibrotic mediators must be present in the diseased lung, show profibrotic potential *in vitro*, and their inhibition should ameliorate fibrosis in animal models (Laurent, McAnulty et al. 2008). Mediators that fulfill these criteria comprise the proinflammatory cytokines TNFα, interleukin (IL)-1β and -13 (IL-13), the vasoconstrictors endothelin 1 (ET-1), and angiotensin II, platelet-derived growth factor (PDGF), insulin-like growth factor (IGF)-1 and TGFβ (Laurent, McAnulty et al. 2008). Inhibitors thereof have been tested or currently entered clinical trials (compare Table 1.2).

One pleiotropic fibrogenic cytokine, widely accepted as the key regulator of fibrosis, is TGFβ1 (Fernandez and Eickelberg 2012a). Besides its role in fibrogenesis, TGFβ signaling involvement has been revealed in embryogenesis (Wu and Hill 2009), tissue homeostasis (Massague 2012), immunity (Li, Wan et al. 2006), and cancerogenesis (Massague 2008). In humans, the TGFβ-superfamily comprises over 30 members that all signal through receptor serine/threonine kinases, including three TGFβ isoforms: TGFβ1, 2 and 3 (Massague 2012), (Fernandez and Eickelberg 2012a). Among these isoforms, TGFβ1 is most highly associated with IPF pathogenesis (Xaubet, Marin-Arguedas et al. 2003). A latent form of TGFβ is secreted and subsequently stored in the ECM. Activation is accomplished proteolytically by Matrix Metallo-proteinase (MMP) 2 and 9, by thrombospondin-1, reactive oxygen species (ROS), or under acidic conditions. Interestingly, tissue stiffness was reported as potential TGFβ1 activator in myofibroblasts via integrin-mediated contraction (Wipff, Rifkin et al. 2007, Hinz 2009). During canonical TGFβ1 signal transduction (Smad dependent), active TGFβ1 binds to a heterotetrameric receptor complex consisting of one TGFβ receptor (TGFβR) I and TGFβRII homodimer, respectively. Formation of this active complex results in phosphorylation of TGFβRI and TGFβRII which in turn induces phosphorylation of the effector proteins Smad2 and 3. Both Smads subsequently bind to the coregulator Smad 4 and translocate to the nucleus where they induce target gene expression. Activity of the receptor regulated Smads (R-Smad) 2 and 3, is controlled by inhibitory Smads (I-Smad) e.g. Smad7 (Zi, Chapnick et al. 2012).

Expression of TGFβ ligand or receptors is highly induced in fibrotic tissue of both, experimental fibrosis models (Cabrera, Selman et al. 2013) as well as pulmonary fibrosis patients (Coker, Laurent et al. 2001). Importantly, blocking TGFβ1 signaling (Bonniaud, Margetts et al. 2005) and epithelium-specific deletion of TGFβRII (Li, Krishnaveni et al. 2011) protect against pulmonary fibrosis in rodent models. On the other hand, overexpression of TGFβ1 causes persistent fibrosis (Sime, Xing et al. 1997). TGFβ acts on the epithelium as well as mesenchyme. Specifically, TGFβ1 induces apoptosis (Siegel and Massague 2003) and EMT (Willis and Borok 2007), (Willis, Liebler et al. 2005), (Kim, Kugler et al. 2006) in the epithelium. In fibroblasts, TGFβ1 induces activation, invasion, proliferation (Clark, McCoy et al. 1997), (Leask and Abraham 2004), and ECM production (Cutroneo, White et al. 2007). TGFβ1 is further integrated in interconnected networks with different signaling pathways. For instance, TGFβ1 induces expression and secretion of proinflammatory (TNFα, IL-1β, IL-13) and profibrotic cytokines (PDGF) which further intensifies fibrotic changes in the lung. Further significant insights into potential IPF causing signaling networks emerged from a system biology approach on IPF lung samples. This study revealed the reactivation of developmental signaling pathways within the

diseased lung, including in addition to TGFβ1, Sonic Hedgehog, Notch and Wingless/integrase-1 (Wnt) (Studer and Kaminski 2007), (Selman, Pardo et al. 2008).

Besides profibrotic mediators, protective factors have been identified, with prostaglandin E2 (PGE2) being the most eminent one. PGE2 was shown to inhibit fibroblast proliferation and ECM synthesis. Stimulation of fibroblasts derived from lung fibrosis patients with profibrotic mediators resulted in a reduced expression of PGE2 and attributed to a defect in cyclooxygenase (COX) mediated arachidonic acid metabolism (Wilborn, Crofford et al. 1995).

1.3 Lung fibroblast biology

Fibroblasts represent a group of ubiquitous mesenchymal cells that reside in the stroma of numerous tissues. Regarding the adult lung, they are present in the adventitia of vascular structures and airways. Fibroblasts are the main ECM-producing cells, fulfilling the function of maintaining structural tissue integrity (Hinz, Phan et al. 2012). Thus, they are key players in wound healing processes (Pechkovsky, Hackett et al. 2010). Unlike other cell types in the lung, no specific marker for fibroblasts has been identified thus far. Therefore, fibroblasts are mainly identified by means of their characteristic spindle-shaped morphology. The absence of a pertinent fibroblast marker may indicate that fibroblasts are not a distinct homogenous cell population but rather a heterogeneous conglomerate of diverse subpopulations (Phan 2008). Identification of phenotypic and functional features of these fibroblast subpopulations is currently central in fibroblast research.

1.3.1 Activated fibroblasts in IPF

The major characteristics of IPF pathology are an aberrant *accumulation of fibroblasts*, the *formation of fibroblastic foci* in the lung interstitium, and an *extensive deposition of ECM*. Therefore, although alveolar epithelial damage is recognized as the pivotal initiative factor of IPF, the majority of pathological changes are ascribed to activated fibroblasts.

The extensive *accumulation of fibroblasts* results primarily from increased fibroblast proliferation and an acquired resistance to apoptosis. Experimentally, fibroblasts derived from IPF lungs show a higher proliferative capacity when cultured on polymerized collagen (Nho, Hergert et al. 2011) and resistance to apoptosis when exposed to FAS ligand (Maher, Evans et al. 2010). Furthermore, numerous studies provide evidence that activated fibroblasts, or myofibroblasts, emerge from different cell types via cellular transition. Hence, various pathological changes, including profibrotic cytokines, in particular TGFβ1, may initiate the differentiation of resident fibroblasts into activated fibroblasts. Thus, resident fibroblasts represent one major source for

activated fibroblasts in IPF (Zhang, Rekhter et al. 1994), (Hung, Linn et al. 2013). Furthermore, through the processes of epithelial-mesenchymal transition (EMT) and endothelial-mesenchymal transition (EndoMT), type I and type II alveolar epithelial cells (AT I and ATII) and endothelial cells loose cell-cell contacts and cell polarity while increasingly expressing mesenchymal markers such as fibronectin, αSMA and vimentin (Kalluri and Neilson 2003), (Montorfano, Becerra et al. 2014). Although extensively studied, doubts about the contribution of EMT to IPF pathology recently emerged in the scientific society (reviewed in (Kage and Borok 2012)). While Marmai and colleagues provided evidence for *in vivo* EMT processes in IPF (Marmai, Sutherland et al. 2011), current lineage tracing studies disputed this observation (Rock, Barkauskas et al. 2011). Besides resident fibroblasts, epithelial and endothelial cells, several further cell types were reported as potential sources for activated fibroblasts or myofibroblasts in IPF. Thus, infiltrating fibrocytes in the fibrotic lung were speculated as one origin for activated fibroblasts (Andersson-Sjoland, de Alba et al. 2008). In addition, recent studies added pericytes (Patel, West-Mays et al. 2010), and pleural mesothelial cells (PMC) as pivotal progenitors of activated fibroblasts (Mubarak, Montes-Worboys et al. 2012). Accordingly, Hung *et al.* could show that pericytes, which are cells of mesenchymal origin that adhere to blood vessels, feature as precursor of activated fibroblast in pulmonary fibrosis (Hung, Linn et al. 2013). PMCs are a dynamic cell type that covers the lung as monolayer structure in close proximity to the lung parenchyma (Nasreen, Mohammed et al. 2009). Recently, Zolak *et al.* could proof *in vivo* a TGFβ1-induced transition of PMCs to activated fibroblasts while trafficking into the lung interstitium (Zolak, Jagirdar et al. 2013).

The different lung cell types that potentially contribute to the pool of activated fibroblasts in the fibrotic lung are summarized in Figure 1.2.

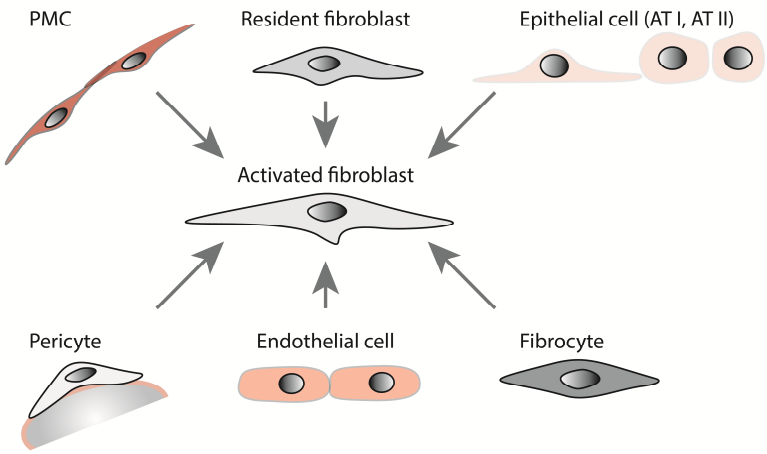

Figure 1.2: Cellular transition.

Lung cell types that contribute to the pool of activated fibroblasts in the fibrotic lung. Alveolar type I (AT I) and alveolar type II (AT II) epithelial cells, pleural mesothelial cell (PMC). Figure template from (Fernandez and Eickelberg 2012b).

While *fibroblastic foci* were long thought of as discrete entities, current studies suggest the existence of an interconnected fibroblastic reticular structure, termed the fibroblast reticulum (Cool, Groshong et al. 2006). Based on the finding of this structure, a new hypothesis for the origin and dissemination of the disease was generated. By means of computer-based 3D reconstructions of serial sections from surgical lung biopsy specimens of patients diagnosed with UIP, Cool and colleagues identified the subpleural region of the lung as the point of origin of the disease. This suggests that the pathological process is initiated at the lung periphery and progresses into the lung interstitium to build up the fibrotic reticulum. The ability of fibroblastic cells to invade interstitial lung tissue features prominently in this pathological process.

Aberrant activation and accumulation of fibroblasts in the diseased lung interstitium significantly contribute to the *extensive deposition of ECM* in IPF. This process is described in section 1.4.1 in detail.

1.3.2 Interstitial cell migration

Interstitial migration is one crucial cellular property that contributes to embryonic morphogenesis, disease stages such as cancer, atherosclerosis, arthritis, or mental retardation as well as tissue repair and remodeling. In essence, interstitial cell migration can be subclassified into two modes: amoeboid and mesenchymal (Ridley, Schwartz et al. 2003). While leukocytes mainly exhibit amoeboid mode of migration, most cancer cells and fibroblasts follow the mesenchymal mode. The amoeboid mode functions in a protease-independent fashion (“path-finding”), whereas the

mesenchymal mode depends on protease activity ("path-generating"). The multistep process of mesenchymal migration is highly complex and synchronized. Initially, cells polarize and protrusions are formed on the leading edge which forces the cell into an elongated shape. Subsequently, transmembrane adhesion receptors of the integrin family mediate adhesion of the protrusions to surrounding ECM fibers. For instance, for fibroblast adhesion to collagen fibers, integrin α2β1 fulfills this function (Cukierman, Pankov et al. 2002). These points of adhesion between protrusions and ECM provide traction for the cell, crucial for the ensuing transfer of mechanical forces. Crosslinking of α-actinin and myosin and its coupling to focal contacts by zyxin and talin results in alignment and bundling of actin filaments (Ridley, Schwartz et al. 2003). Increasing strengthening of cell contractility and proteolytic degradation of ECM initiates retraction of the trailing edge of the cell and thus forward translocation (Figure 1.3).

As outlined in section 1.3.1, invasion of pericytes and activated fibroblasts into the lung interstitium is one crucial cellular function in IPF pathogenesis. Accordingly, Li and colleagues showed *ex vivo* an increased invasive capacity of fibroblasts derived from IPF lungs compared to control fibroblasts (Li, Jiang et al. 2011). Mechanistically, the authors identified a connection between increased hyaluronan synthase (HAS) expression and the reported augmented fibroblast invasiveness in IPF. Furthermore, α5β1 integrin was found to induce an invasive phenotype in lung fibroblasts. This effect could be inhibited by α4β1 integrin through increasing activity of phosphatase and tensin homologue deleted on chromosome 10 (Pten) (White, Thannickal et al. 2003).

In disease, interstitial cell invasion can further be driven by growth factor signaling. For example, epidermal growth factor (EGF) represents one potent inducer of cellular invasion as shown for cancer cells (Lu, Jiang et al. 2001) and human dermal fibroblasts (Gobin and West 2003).

Together, these findings indicate a pivotal role of interstitial cell migration in fibrogenesis.

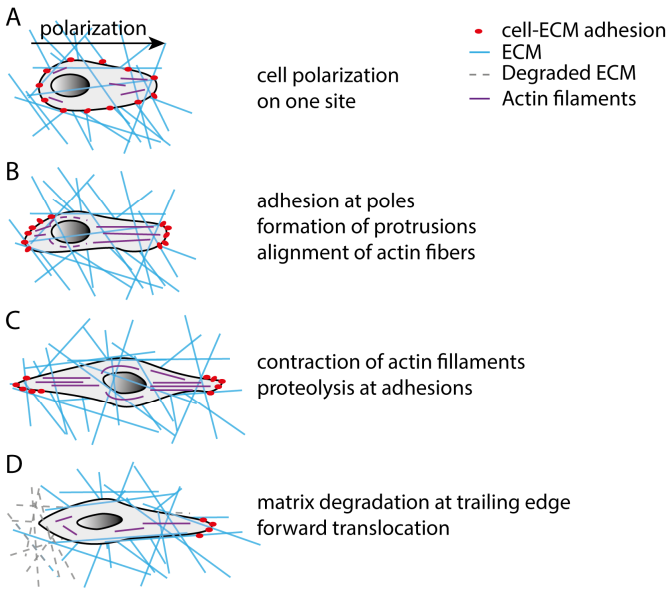

Figure 1.3: Mode of mesenchymal migration.
The cell starts to polarize in one direction as the cell interacts with surrounding extracellular matrix (ECM) **(A)**. Protrusions are shaped in direction of the polarization, cell-ECM adhesions are formed at the leading edge and actin-filaments align **(B)**. While adhesion intensifies at the leading edge, contractility of actin increases and proteolysis takes place at the trailing edge **(C)**. Forward translocation is accomplished by retraction of the trailing edge **(D)**. Figure template from (Pathak and Kumar 2011).

1.4 Extracellular matrix (ECM)

Within the extremely organized structure of the lung, functional arrangement of the cells is not only dependent on cell-cell contacts but also highly influenced by the ubiquitous extracellular matrix. Thus far, the mammalian matrisome, which comprises all proteins that contribute to matrices, includes ~300 proteins and thus makes up 1 - 1.5% of the whole proteome. The matrisome is composed of 43 collagen subunits, ~200 glycoproteins, and ~40 proteoglycans (Hynes and Naba 2012). These components are arranged to an interlocking meshwork structure. Within this structure, collagens fill a role as shaping element (Fan, Creemers et al. 2014). The major collagens are the interstitial types I and III (Clarke, Carruthers et al. 2013). Both types are characterized by their fibrillar texture and assemble from collagen subunits as homotrimers. Decisive for the fibrillar arrangement of these homotrimers is the repeat of the sequence Gly-X-Y, with X being frequently proline and Y 4-hydroxyproline (Ricard-Blum 2011). This repeat encodes the assembly of collagen subunits to rodlike trimers, which subsequently organize into oligomers and fibrils. Transglutaminase cross-linking and disulfide bonds between collagens via lysyl oxidases (LOX) and hydroxylases result in the fibrillous mesh-like structures of collagen-based ECM.

The ECM constitutes a pleiotropic bioactive environment for mesenchymal cells (Frantz, Stewart et al. 2010). Cell matrix interactions play a decisive role in guiding cellular functions such as migration, shape (Hakkinen, Harunaga et al. 2011), differentiation (Liu, Mih et al. 2010), and survival (Nho, Hergert et al. 2011). The bi-directional signal transduction between ECM and embedded cells is mainly accomplished by integrins, a large family of cell surface-adhesion receptors that assembles in heterodimers at the cell membrane (Arnaout, Mahalingam et al. 2005). Besides their function in cell-matrix adhesion, integrins enable the cell to mechanosense the surrounding environment. Thus, integrins conduct mechanotransduction to intracellular chemical signals ("outside-in signaling"). Activation of integrins can further be transmitted by growth factor or G-protein-coupled receptor signaling. These inputs can initiate a conformational change of the extracellular domain of the integrins, thereby regulating their affinity for extracellular ligands ("inside-out signaling") (reviewed in (Harburger and Calderwood 2009)). Besides its biomechanical function, the ECM serves as reservoir for diverse cytokines and growth factors (Frantz, Stewart et al. 2010). Therefore, it may contribute to both, outside-in and inside-out signaling of integrins.

As the ECM represents a highly dynamic compartment, its integrity is maintained by constant remodeling processes. Likewise ECM deposition, matrix degradation is mainly accomplished by fibroblasts as these cells not only secrete ECM molecules but also ECM degrading enzymes in a spatially and temporally controlled manner. In regards to ECM degradation, the zinc-dependent endopeptidases Matrix Metallo-proteinases (MMPs) play a decisive role. The family of MMPs, which comprises 25 enzymes, achieves cleavage of all ECM components (Overall 2002) and basement membranes (Sand, Larsen et al. 2013). Secretion of MMPs by fibroblasts represents a highly concerted process, which is counterbalanced by tissue inhibitors of metalloproteinases (TIMPs) (Willenbrock, Crabbe et al. 1993).

1.4.1 ECM remodeling processes in IPF

Balancing the dynamic processes of ECM deposition, remodeling, and resorption is highly complex. Precise control mechanisms assure the ECM homeostasis during morphogenesis and tissue repair. Disruption of the ECM homeostasis is one hallmark event of non-neoplastic and fibroproliferative diseases, such as IPF, systemic sclerosis, myelofibrosis, hepatic cirrhosis or hypertrophic scars and keloids (Huang and Ogawa 2012). Nowadays, aberrant ECM secretion and composition is seen not only as *phenotypic response* but also as *active contributor* of fibroblast activation in fibrogenesis:

As outlined in section 1.3.1, extensive secretion of ECM is one major *phenotypic response* of activated fibroblasts in IPF. One single fibroblast, activated by growth factors or mechanical stimuli, may produce up to 5,000 molecules of procollagen per minute (Lindahl, Chambers et al. 2002), (McAnulty, Campa et al. 1991). Besides collagen, fibrotic ECM is enriched with glycoproteins, such as extra domain containing fibronectin, periostin, fibulin, fibrillin, vitronectin or versican (Booth, Hadley et al. 2012). Furthermore, increased levels of proteoglycans, such as hyaluronan were found in broncheoalveolar fluid of IPF patients (Bjermer, Lundgren et al. 1989).

Extensive ECM deposition in IPF lungs might be consequence of not only increased secretion but also defective degradation by activated fibroblasts. Accordingly, current studies indicate malfunction of the ECM degrading machinery in IPF, most prominently MMPs (Pardo, Selman et al. 2008).

One further aspect of fibrotic ECM is its significantly altered structure and biomechanical properties. According to atomic force microscopy studies, experimental fibrosis significantly increases stiffness of lung parenchymal tissue (Liu, Mih et al. 2010). Consistent with that, elevated levels of LOXL2, one enzyme responsible for covalent collagen cross-linking, were found in serum of IPF patients (Chien, Richards et al. 2014).

Importantly, with doxycycline one MMP inhibitor and GS-6624 one LOXL2 antibody are currently being investigated in clinical trials as treatment options for IPF (compare Table 1.2).
As bioactive compartment, the ECM can act as *active contributor* in fibroblast activation and thus fibrogenesis. Therefore, ECM and fibroblast reciprocally influence each other's functions and extensively modified remodeling processes may result in a feed-forward loop of matrix deposition (Booth, Hadley et al. 2012), (Parker, Rossi et al. 2014). As outlined in section 1.4 the ECM serves both, biomechanical and biochemical roles. Accordingly, variations in the composition and physical properties, such as rigidity, of the ECM were found to influence cell proliferation, viability, spreading, differentiation, and migration (Naba, Clauser et al. 2012). Furthermore, signal transduction of TGFβ, Fibroblast growth factors (FGF), prostaglandine E (PGE), integrins as well as of mechanosensitive pathways such as Wingless/Integrase-1 (Wnt) β-catenin signaling are affected by the diseased ECM (Frantz, Stewart et al. 2010), (Hynes and Naba 2012).

Taking the interdependence of ECM and mesenchymal cells into consideration, it seems natural that studies on fibroblast behavior, undertaken in three-dimensional matrices, elicit more physiologically relevant results than in the absence of ECM components (Green and Yamada 2007).

1.4.2 ECM model systems

Accumulating evidence that the ECM pivotally influences behavior of cells that physiologically reside in a three dimensional (3D) environment have led to the conclusion that mesenchymal cells should be studied in an environment that closely mimics structure and dimensionality of ECM (Cukierman, Pankov et al. 2002), (Abbott 2003), (Baker and Chen 2012). Therefore, to date, a variety of 3D cell culture systems have been established and validated. ECM-coated tissue culture plastic is one simplified model that is widely used. This model is applicable for studies on signaling pathways related to ECM adhesion. However, the planar surface does not allow comprehensive conclusions regarding the 3D behavior of cells (Thannickal, Henke et al. 2014). Models using synthetic acrylamide-, or polyethylene glycol-based matrices exhibit the same dimensional limitation, yet due to the potentiality of gradient formation they are the model of choice to study matrices of varying stiffness (Saums, Wang et al. 2014).

In addition to acrylamide and hydrogels, native and engineered biopolymers represent prevailing *in vitro* ECM model systems. In contrast to artificially synthesized macromolecular structures, biopolymers more closely resemble the physiological ECM architecture (Raeber, Lutolf et al. 2005). Common protein components of these biopolymers are collagens (Silver and Pins 1992), laminin (Rodin, Antonsson et al. 2014), fibrin (Hayen, Goebeler et al. 1999), elastin (Hafemann, Ensslen et al. 1999) as well as hybrid protein based matrices, such as Matrigel (Hall and Brooks 2014). Regarding the omnipresence of collagens in the lung interstitium, type I collagen gels harbor a high biomimetic potential for the three-dimensional texture of the pulmonary ECM. Type I collagen gels can be used to study cell contractility, migration and proteolysis in 3D. Furthermore, these gels provide multiple imaging modalities allowing studies on 3D behavior of living cells. However, unlike acrylamide and hydrogels, the stiffness of type I collagen gels is not extensively adjustable (Thannickal, Henke et al. 2014).

Two additional models that mainly benefit from their physiological composition are basement membrane extract gels and fibroblast-derived matrices (Goetz, Minguet et al. 2011). Although these models most closely mimic physiological ECM, the diversity in the composition can also be disadvantageous as it negatively affects robustness and reproducibility.

Taken together, as all currently used 3D *in vitro* cell culture models exhibit advantages and disadvantages, the right choice of model system highly depends on the research question. Prospectively, acellular *ex vivo* matrices present alternative 3D model systems that circumvent biomimetic limitations (Booth, Hadley et al. 2012).

1.5 Objectives

Fibroblast activation and invasion through stromal tissue represents one dominant pathomechanism in non-neoplastic fibrotic diseases such as IPF. Aberrantly activated fibroblasts in the disease have frequently been reported to exhibit a strong invasive capacity (Li, Jiang et al. 2011), (White, Atrasz et al. 2006), which enables them to infiltrate the lung interstitium. To date, studies investigating the invasion capacity of fibroblasts have mainly focused on individual factors and have not implemented a systemic approach. The aim of this current study was to comprehensively characterize this invading fibroblast phenotype *in vitro* and to identify novel functional targets for fibroblast invasion by in-depth analysis of the invasion induced transcriptome signature.

The first aim of this study was to establish and validate two collagen-based phenotypic assays of 3D fibroblast invasion that enable the quantification of the cellular invasion capacity *(invasion assay)* and the effective separation of invading from non-invading fibroblasts *(separation assay)*. As IPF represents a disease highly driven by growth factors, further objectives comprised investigations on the impact of the two pro-invasive and pro-fibrotic cytokines, EGF and TGFβ1, on fibroblast invasion, using the novel invasion models.

The second main objective focused on unraveling the transcriptome-wide signature of fibroblast invasion, using the newly established *separation assay*. This was achieved in collaboration with Dr. Martin Irmler (Institute of Experimental Genetics, Helmholtz-Zentrum München). Subsequently, to gain insight into growth factor induced cell invasion, this signature was extended to TGFβ1-mediated fibroblast invasion.

The final goals were to evaluate both transcriptomic invasion signatures, using detailed bioinformatical analysis, and to validate single identified molecules for their role in fibroblast invasion by in-depth analysis.

2. MATERIALS AND METHODS

2.1 Materials

2.1.1 Antibodies

Table 2.1: Primary antibodies for Western blot

Antigen name	Host/Clonality	Dilution	Manufacturer
Anti-αSMA (clone 1A4)	Mouse/mc	1:1,000	Sigma; St. Louis, USA
Anti-Cav1 (D46G3) XP	Rabbit/mc	1:1,000	Cell Signaling; Danvers, USA
Anti-Col 1 (600-401-103-0.1)	Rabbit/pc	1:1,000	Rockland, Gilbertsville, USA
Anti-MMP13 (ab75606)	Rabbit/pc	1:333	Abcam; Cambridge, UK
Anti-Sfrp1 (ab126613)	Rabbit/mc	1:1,000	Abcam; Cambridge, UK
Anti-β-actin peroxidase (clone AC-15)	Mouse/mc	1:20,000	Cell Signaling; Danvers, USA

Table 2.2: Secondary antibodies for Western blot

Antigen name	Host	Dilution	Manufacturer
Goat anti-mouse	Goat	1:10,000	Cell Signaling; Danvers, USA
Goat anti-rabbit	Goat	1:10,000	Cell Signaling; Danvers, USA

Table 2.3: Primary antibodies for immunofluorescence stainings

Antigen name	Host/Clonality	Dilution	Manufacturer
Anti-αSMA (clone 1A4)	Mouse/mc	1:5,000	Sigma; St. Louis, USA
Anti-CD29 (9EG7)	Rat/mc	1:100	BD; Franklin Lakes USA
Anti-Col 1 (600-401-103-0.1)	Rabbit/pc	1:1,000	Rockland, Gilbertsville, USA
Anti-Ki67 (M7249)	Rat/mc	1:100	Dako; Hamburg, Germany
Anti-Sfrp1 (ab126613)	Rabbit/mc	1:200	Abcam; Cambridge, UK
Anti-Vimentin (C20)	Goat/pc	1:100	Santa Cruz; Dallas, USA

Table 2.4: Secondary antibodies for immunofluorescence stainings

Antigen name	Host/Clonality	Dilution	Manufacturer
Goat anti-mouse IgG DyLight™ 649 AffinityPure	Goat	1:500	Jackson ImmunoResearch Laboratories Inc./Dianova; Suffolk, UK
Goat anti-rabbit IgG Alexa Fluor 488	Goat	1:500	Invitrogen; Carlsbad, USA

Goat anti-mouse IgG Alexa Fluor 568	Goat	1:500	Invitrogen; Carlsbad, USA
Donkey anti-goat IgG Alexa Fluor 488	Donkey	1:500	Invitrogen; Carlsbad, USA
Goat anti-rat IgG Alexa Fluor 488	Goat	1:500	Invitrogen; Carlsbad, USA

2.1.2 Buffers and solutions

DNA loading buffer (6x) (Fermentas, Thermo Fisher Scientific):

Substance	Concentration
Tris/HCl, pH 7.6	10 mM
Bromophenol blue	0.03% (w/v)
Xylene cyanol FF	0.03% (v/v)
Glycerol	60% (v/v)
EDTA	60 mM

HEPES (N-2-hydroxyethylpiperazine-N-2-ethane sulfonic acid) (Sigma-Aldrich):

Substance	Concentration
HEPES	1 M

Lämli loading buffer (6x):

Substance	Concentration
SDS	12% (w/v)
Glycerol (87%)	60% (v/v)
Bromophenol blue	0.06% (w/v)
Tris/HCl, pH 6.8	375 mM
DTT	600 mM

PBS (Phosphatate buffered saline) pH 7.4 (10x):

Substance	Concentration
NaCl	1.37 M
KCl	27 mM
Na_2HPO_4	100 mM
KH_2PO_4	20 mM
NaCl	1.37 M

RIPA (radio-immunoprecipitation assay) buffer:

Substance	Concentration
Tris-Cl pH 7.4	50 mM
NaCl	150 mM
NP40	1% (v/v)
Na-deoxycholate	0.25% (v/v)

SDS (sodium dodecyl sulphate) solution (20%) (w/v):

Substance	Volume/Weight
SDS	200 g
Millipore-H_2O	1 L

SDS-PAGE (sodium dodecyl sulfate polyacrylamide gel electrophoresis) Running Buffer:

Substance	Concentration
Tris/HCl, pH 7.4	250 mM
Glycine	1.92 M
SDS	1% (w/v)

SDS-PAGE Separation Gels:

Substance	Concentration/Volume		
	7%	**10%**	**12%**
Millipore-H_2O	4.6 ml	3.7 ml	3.1 ml
1.5 M Tris/HCl pH 8.8	2.25 ml	2.25 ml	2.25 ml
SDS 20%	45 µl	45 µl	45 µl
Acrylamide	2.1 ml	3 ml	3.6 ml
APS 10%	30 µl	30 µl	30 µl
TEMED	6 µl	6 µl	6 µl

SDS-PAGE Stacking Gel (4%):

Substance	Volume
Millipore-H2O	1.8 ml
0.5 M Tris/HCl pH 6.8	750 µl
SDS 20%	15 µl
Acrylamide	400 µl
APS 10%	15 µl
TEMED	3 µl

TAE (Tris-acetate-EDTA) buffer (50x):

Substance	Concentration/amount
Tris/HCl	2 M
Glacial acetic acid	5.71% (v/v)
EDTA, pH 8	50 mM

TBS (Tris-buffered saline) (10x):

Substance	Concentration
Tris/HCl pH 7.4	10 mM
NaCl	150 mM

TBS-T (TBS with TWEEN®20) (1x):

Substance	Concentration
TBS (10x)	10% (v/v)
Tween®20	0.1% (v/v)
Millipore-H_2O	89.99% (v/v)

Transfer buffer (10x):

Substance	Concentration
Tris/HCl	250 mM
Glycine	1.92 M

Transfer buffer (1x):

Substance	Concentration
Transfer Buffer (10x)	10% (v/v)
Methanol	10% (v/v)
Millipore-H_2O	80% (v/v)

2.1.3 Cell lines and primary cells

Table 2.5: Murine cell line

Cell line name	Description	Supplier
MLg	Murine newborn lung fibroblasts	ATCC (CCL-206), LGC Standards; Wesel Germany

Table 2.6: Human cell line

Cell line name	Description	Supplier
A549	Human alveolar basal epithelial cells, lung carcinoma	Leibniz-Institute DSMZ-German Collection of Microorganisms and Cell Cultures; Braunschweig Germany

Table 2.7: Primary human fibroblast lines

Identification	Tissue information	Supplier
ASK013	Non-carcinogenic lung tissue resection from patient with lung metastasis of leiomyosarcoma of the uterus	Asklepios Klinik; Munich, Germany
ASK016	Non-carcinogenic lung tissue resection from patient with lung metastasis	Asklepios Klinik; Munich, Germany
A003	Non-carcinogenic lung tissue resection from patient with lung metastasis and COPD	Asklepios Klinik; Munich, Germany
G20Tn	Healthy lung tissue from patient after lung transplantation	Asklepios Klinik; Munich, Germany
ASK006	Non-carcinogenic lung tissue resection from patient with adenocarcinoma and COPD	Asklepios Klinik; Munich, Germany
MLT003	Lung explant/donor lung	Klinikum Großhadern; Munich, Germany
MLT013.01	Lung explant/donor lung	Klinikum Großhadern; Munich, Germany
L0023	Fibrotic origin	University of Michigan; USA (laboratory of Eric White)
L0026	Fibrotic origin	University of Michigan; USA (laboratory of Eric White)
L0028	Fibrotic origin	University of Michigan; USA (laboratory of Eric White)
L0032	Fibrotic origin	University of Michigan; USA (laboratory of Eric White)
S86A	Fibrotic origin	University of Michigan; USA (laboratory of Eric White)
S099B	Fibrotic origin	University of Michigan; USA (laboratory of Eric White)
S101BA	Fibrotic origin	University of Michigan; USA (laboratory of Eric White)
S121B	Non-fibrotic origin	University of Michigan; USA (laboratory of Eric White)

L0029	Non-fibrotic origin	University of Michigan; USA (laboratory of Eric White)
L0031	Non-fibrotic origin	University of Michigan; USA (laboratory of Eric White)
L0024	Non-fibrotic origin	University of Michigan; USA (laboratory of Eric White)
L0025	Non-fibrotic origin	University of Michigan; USA (laboratory of Eric White)
L0029	Non-fibrotic origin	University of Michigan; USA (laboratory of Eric White)
S126N	Non-fibrotic origin	University of Michigan; USA (laboratory of Eric White)

2.1.1 Laboratory equipment and software

Table 2.8: Laboratory equipment

Product	Manufacturer
-20°C freezer MediLine LGex 410	Liebherr; Biberach, Germany
Agarose gel running chamber	Biorad; Hercules, USA
Analytical scale XS20S Dual Range	Mettler Toledo; Gießen, Germany
Autoclave DX-45	Systec; Wettenberg, Germany
Autoclave VX-120	Systec; Wettenberg, Germany
Bacterial shaker Innova 42	New Brunswick; Hamburg, Germany
Cell counter Casy Modell TT	Roche Diagnostics; Mannheim, Germany
Cell culture work bench Herasafe KS180	Thermo Fisher Scientific; Darmstadt, Germany
Centrifuge MiniSpin plus	Eppendorf; Hamburg, Germany
Centrifuge Rotina 420R	Hettich; Tuttlingen, Germany
Centrifuge with cooling, Micro200R	Hettich; Tuttlingen, Germany
CO_2 cell Incubator BBD6620	Thermo Fisher Scientific; Darmstadt, Germany
Demineralized water	Thermo Fisher Scientific; Darmstadt, Germany
Dispenser, Ceramus 2-10 ml	Hirschmann Laborgeräte; Eberstadt, Germany
Dry ice container Forma 8600 Series, 8701	Thermo Fisher Scientific; Darmstadt, Germany
Electronic pipet filler	Eppendorf; Hamburg, Germany
Electrophoretic Transfer Cell, Mini Protean Tetra Cell	Biorad; Hercules, USA
Film developer Curix 60	AGFA; Morsel, Belgium
Fluorescence Mikroscope AxioImager M2	Zeiss; Jena, Germany
Fridge MediLine LKv 3912	Liebherr; Biberach, Germany
Gel electrophoresis chamber MINIeasy	Carl Roth; Karlsruhe, Germany
Gel imaging system ChemiDoc XRS+	Biorad; Hercules, USA
Ice machine ZBE 110-35	Ziegra; Hannover, Germany
Intelli-Mixer RM-2	Schubert & Weiss Omnilab; Munich, Germany
Light Cycler LC480II	Roche Diagnostics; Mannheim, Germany

Liquid nitrogen cell tank BioSafe 420SC	Cryotherm; Kirchen/Sieg, Germany
Liquid nitrogen tank Apollo 200	Cryotherm; Kirchen/Sieg, Germany
Magnetic stirrer KMO 2 basic	IKA; Staufen, Germany
Mastercycler gradient	Eppendorf; Hamburg, Germany
Mastercycler Nexus	Eppendorf; Hamburg, Germany
Microbiological Incubator HERATherm IGS60	Thermo Fisher Scientific; Darmstadt, Germany
Sartorius Micro-Dismembrator S	Thermo Fisher Scientific; Darmstadt, Germany
Microscope Axio Imager M2 (flourescence)	Zeiss; Jena, Germany
Microscope Axiovert 40	Zeiss; Jena, Germany
Microscope LSM 710 (confocal)	Zeiss; Jena, Germany
Multipette stream	Eppendorf; Hamburg, Germany
Nalgene® Freezing Container (Mr. Frosty)	Omnilab; Munich, Germany
NanoDrop 1000	PeqLab; Erlangen, Germany
pH meter InoLab pH 720	WTW; Weilheim, Germany
Pipettes Research Plus	Eppendorf; Hamburg, Germany
Plate centrifuge 5430	Eppendorf; Hamburg, Germany
Plate reader TriStar LB941	Berthold Technologies; Bad Wildbach, Germany
Plate reader Sunrise	Tecan; Crailsheim, Germany
Roll mixer	VWR International; Darmstadt, Germany
Power Supply Power Pac HC Power Supply	Biorad; Hercules, USA
Scale XS400 2S	Mettler Toledo; Gießen, Germany
Shaker Duomax 1030	Heidolph; Schwabach, Germany
Thermomixer compact	Eppendorf; Hamburg, Germany
Ultra pure water supply MilliQ Advantage A10	Merck Millipore; Darmstadt, Germany
LSM Top table centrifuge MCF-2360	Schubert & Weiss Omnilab; Munich, Germany
Vortex Mixer	IKA; Staufen, Germany
Vacuum pump NO22AN.18 with switch 2410	KNF; Freiburg, Germany
Water bath Aqua Line AL 12	Lauda; Lauda-Königshofen, Germany

Table 2.9: Software

Product	**Manufacturer**
GraphPad Prism 5	GraphPad Software; La Jolla, USA
Imaris Software, Version	Bitplane; Zurich, Switzerland
Image Lab Version	Biorad; Hercules, USA
Ingenuity® Pathway Analysis (IPA) platform	Ingenuity,Systems; Redwood City, USA
LightCycler® 480 SW 1.5	Roche Diagnostics; Mannheim, Germany
Vector NTI Advanced 9	Invitrogen, Life Technologies; Carlsbad, USA
Magelan Software	Tecan; Crailsheim, Germany
Tristar MicroWin 2000	Berthold Technologies; Bad Wildbach, Germany
Axio Imager Software	Zeiss; Jena, Germany

2.1.2 Chemicals and Consumables

Table 2.10: Chemicals

Product	Manufacturer
0.2% Trypsin - EDTA solution	Sigma-Aldrich; Taufkirchen, Germany
87% Glycerin	AppliChem; Darmstadt, Germany
Ammonium peroxodisulfate (APS)	AppliChem Darmstadt, Germany
Bovine serum albumin (BSA)	Sigma-Aldrich; Taufkirchen, Germany
Casyton	Roche Diagnostics; Mannheim, Germany
Chloroform	AppliChem; Darmstadt, Germany
Complete® Mini without EDTA (Protease-inhibitor)	Roche Diagnostics; Mannheim, Germany
Coomassie Brilliant Blue R-250 staining solution	BioRad; Hercules, USA
DAPI (4',6-diamidino-2-phenylindole)	Sigma-Aldrich; Taufkirchen, Germany
DMEM/HAM's F12	PAA, GE Healthcare; Cölbe, Germany
DMEM (high glucose; 4.5g/l)	PAA, GE Healthcare; Cölbe, Germany
Desoxyribonucleotides mix (dNTPs)	Fermentas, Thermo Fisher Scientific;
Dimethyl sulfoxide (DMSO)	Carl Roth; Karlsruhe, Germany
Dithiothreitol (DTT)	AppliChem; Darmstadt, Germany
ECL Plus Western Blotting Substrate	Pierce, Thermo Fisher Scientific; Schwerte, Germany
Ethanol (p.a.)	AppliChem; Darmstadt, Germany
Fetal bovine serum (FBS) "GOLD", heat inactivated	PAA, GE Healthcare
Fluorescence mounting medium	Dako; Hamburg, Deutschland
Gentamicin	Invitrogen, Life Technologies; Carlsbad, USA
HOECHST 33342	Pierce, Thermo Fisher Scientific; Schwerte, Germany
Isopropanol, (p.a.)	AppliChem; Darmstadt, Germany
Light Cycler 480 SybrGreen l Master Mix	Roche Diagnostics; Mannheim, Germany
Lipofectamine2000	Invitrogen, Life Technologies; Carlsbad, USA
Lipofectamine LTX with PLUS reagent	Invitrogen, Life Technologies; Carlsbad, USA
Methanol, (p.a.)	AppliChem; Darmstadt, Germany
Non-fat dried milk powder	AppliChem; Darmstadt, Germany
Nonidet P-40	AppliChem; Darmstadt, Germany
Penicillin-Streptomycin (10,000 U/ml)	Gibco, Life Technologies; Carlsbad, USA
Peptone from Casein	AppliChem; Darmstadt, Germany
Phalloidin	Invitrogen, Life Technologies; Carlsbad, USA
Ponceau S solution	Sigma-Aldrich; Taufkirchen, Germany
Poly-L-Lysine (0.01% solution)	Sigma-Aldrich; Taufkirchen Germany
Random hexamers	Applied Biosystems, Life Technologies; Carlsbad, USA
Recombinant human EGF protein	R&D Systems; Minneapolis, USA
Recombinant human TGFβ1 protein	R&D Systems; Minneapolis, USA
Recombinant human Sfrp1 protein	R&D Systems; Minneapolis, USA
Restore Plus Western Blot Stripping Buffer	Pierce, Thermo Fisher Scientific; Schwerte, Germany
Sfrp1-inhibitor sc-222310 (CHEMBL473916)	Santa Cruz; Biotechnology; Dallas, USA
SuperSignal West Dura Chemiluminescent Substrate	Pierce, Thermo Fisher Scientific; Schwerte, Germany
SuperSignal West Femto Chemiluminescent Substrate	Pierce, Thermo Fisher Scientific; Schwerte, Germany

SuperSignal West Pico Chemiluminescent Substrate	Pierce, Thermo Fisher Scientific; Schwerte, Germany

Table 2.11: Consumables

Product	Manufacturer
96 well MaxiSorp ELISA plate	Nunc; Wiesbaden, Germany
96 well plates, white, for luciferase assay	Berthold Technologies; Bad Wildbad, Germany
Amicon Ultra 3K-0.5 mL centrifugal filters	Merck Millipore; Darmstadt, Germany
Cell culture dishes	Corning, Thermo Fisher Scientific; Schwerte
Cell culture flasks	Nunc; Wiesbaden, Germany
Cell culture multi well plates	TPP Techno Plastic Products, Switzerland
Cell scraper/lifter	Corning, Thermo Fisher Scientific; Schwerte
Cryovials 1.5ml	Greiner Bio- One; Frickenhausen, Germany
Falcon tubes (5ml, 50ml)	BD Bioscience, Heidelberg, Germany
Filter tips	Biozym Scientific, Hessisch Oldendorf Germany
Glas Pasteur pipettes	VWR International, Darmstadt Germany
Hyperfilm® ECL™ Film	Amersham, GE Healthcare; Freiburg, Germany
Measuring pipettes sterile, single use (2ml, 5ml, 10ml, 25ml, 50ml)	VWR International, Darmstadt Germany
Nylon filters, pore size 70µm	BD Bioscience, Heidelberg, Germany
PCR plates, 96-well, white	Biozym Scientific, Hessisch Oldendorf Germany
PVDF membrane (0.2 or 0.45µm)	Merck Millipore; Darmstadt, Germany
Reaction tubes (0.5ml, 1.5ml)	Eppendorf; Hamburg Germany
Sealing foil for PCR plates	Kisker Biotech, Steinfurt Germany
Thincert™ 6-well cell culture inserts (pore Ø 8µm)	Greiner Bio- One; Frickenhausen, Germany
Tips	Eppendorf; Hamburg, Germany
Whatman blotting paper 3mm	GE Healthcare; Freiburg, Germany

2.1.3 Enzymes

Table 2.12: Enzymes

Product	Manufacturer
Collagenase I	Biochrom; Berlin, Germany
DNase I	AppliChem; Darmstadt, Germany
RNase inhibitor 20U/µl	Invitrogen, Life Technologies; Carlsbad, USA

2.1.4 Oligonucleotides

Table 2.13: Oligonucleotides

Product	Manufacturer
pEGFP-N2 vector	Clonetech Laboratories Inc.; Mountain View, USA
TOPFLASH pTA-Luc vector	Addgene; Cambridge, USA
FOPFLASH pGL3 vector	Addgene; Cambridge, USA

2.1.4.1 Quantitative RT-PCR

Primers for quantitative PCR (qPCR), were purchased from Eurofins MWG Operon; Ebersberg, Germany as desalted oligonucleotide lyophilisates and dissolved in DNase/RNAse - free water to a concentration of 100 µM, prior use.

Table 2.14: quantitative human qPCR primer.

Gene		Sequence 5' – 3'
GAPDH	fw	TGTGTCCGTCGTGGATCTGA
	rev	CCTGCTTCACCACCTTCTTGA
Sfrp1	fw	GGACCGGCCCATCTACCCGT
	rev	ACACCGTTGTGCCTTGGGGC
Cav1	fw	GGACATCTCTACACCGTTCCC
	rev	CTTGACCACGTCATCGTTGAG
MMP13	fw	AGGCTCCGAGAAATGCAGTC
	rev	ATCAGGAACCCCGCATCTTG
Pten	fw	TGGCGGAACTTGCAATCCTCAGT
	rev	TCCCGTCGTGTGGGTCCTGA
TGFβ1	fw	TTCGCCTTAGCGCCCACTGC
	rev	GGCCGGTAGTGAACCCGTTG

Table 2.15: quantitative mouse qPCR primer.

Gene		Sequence 5' – 3'
GAPDH	fw	TGACCTCAACTACATGGTTTACATG
	rev	TTGATTTTGGAGGGATCTCG
Sfrp1	fw	GTGCGAGCCGGTCATGCAGT
	rev	CACACGGTTGTACCTTGGGGC
Cav1	fw	CGACGACGTGGTCAAGATTGACTTT
	rev	TGCACGGTACAACCGCCCAG
MMP13	fw	ATCCCTTGATGCCATTACCA

	rev	AAGAGCTCAGCCTCAACCTG
Pten	fw	TCAGTGGCGGAACTTGCAATCCT
	rev	CGCCGCGTGGGTCCTGAAT
TGFβ1	fw	GTGGACCGCAACAACGCC
	rev	TGGGGGTCAGCAGCCGGT

2.1.5 Standards and kits

Table 2.16: Standards

Product	Manufacturer
1 kb DNA ladder	Peqlab; Erlangen, Germany
100 bp DNA ladder	Peqlab; Erlangen, Germany
Ultra low range DNA ladder I	Peqlab; Erlangen, Germany
Protein marker V	Peqlab; Erlangen, Germany

Table 2.17: Kits

Product	Manufacturer
BCA Protein Assay kit	Biochrom; Berlin, Germany
Dual luciferase reporter system	Promega; Mannheim, Germany
PeqGold RNA kit	Peqlab; Erlangen, Germany
Murine Sfrp1 ELISA kit	Uscn Life Science; Hubei, China
RNase-Free DNase set	Qiagen; Hilden, Germany
RNeasy Mini kit	Qiagen; Hilden, Germany

2.2 Methods

2.2.1 Cell biological methods

2.2.1.1 Isolation of primary human fibroblast

Primary human lung fibroblasts (phF) were isolated and cultured according to the two following protocols. At the University of Michigan, lungs were received through Gift of Life donations ("normal") or explanted during transplantation (UIP or IPF). Sample tissue was taken as close to parenchyma as possible, avoiding major airways. Fibroblast isolations were performed in the laboratory of Prof. Dr. Eric White. For this, tissue pieces were placed in 150 mm tissue culture

dishes with DMEM media pre-warmed to 37°C. Tissue was minced with a sterile scalpel blade until the remaining pieces did not exceed a size of 2 mm in diameter and incubated at 37°C with 5% CO_2. The cell culture medium was changed every 2 - 3 days. When outgrowing fibroblasts reached approximately 50 - 60% confluence (1 - 2 weeks), remaining tissue pieces were removed. Prior shipping, cells were harvested and re-suspended (at $1x10^6$ cells/ml) in freeze media and frozen in liquid nitrogen.

Specimens from lung lobes or segmental lung resections, received from the Asklepios Klinik or Klinikum Großhadern in Munich, were dissected into pieces of 1 - 2 mm^2 in size and digested by 5 mg of Collagenase I (Biochrom) at 37°C for 2 hours. Subsequently, samples were filtered through nylon filters with a pore size of 70 µm (BD Falcon). Filtrates, containing the cells, were centrifuged at 400 g, 4°C for 5 minutes. Pellets were resuspended in DMEM/F-12 medium supplemented with 20% fetal bovine serum, plated on 10 cm cell-culture dishes and cultured as described below (2.2.1.3). Fibroblast isolations were performed by Dr. Katharina Heinzelmann, Katharina Lippl, and Daniela Dietel.

2.2.1.2 Cryopreservation of mammalian cells

Cell preservation was achieved by freezing cells in liquid nitrogen in freezing medium (90% FBS supplemented with 10% DMSO). First, cells were washed with PBS (1x), detached with pre-warmed trypsin/EDTA solution at 37°C for 5 min and resuspended in complete medium. Subsequently, cells were centrifuged (400 rpm for 5 min) and resuspended in freezing medium in an approximate concentration of 1 - $2x10^6$ cells/ml. Cell suspensions were transferred to cryovials and frozen in a Mister Frosty (Omnilab) (-80°C, overnight) and kept for long-term storage in liquid nitrogen.

2.2.1.3 Culturing and sub-culturing of mammalian cells

Mouse lung fibroblasts MLg (Mlg 2908) were purchased from ATCC (CCL-206) and cultivated in DMEM/HAM's F12 (PAA) medium containing 10% FBS (PAA). PhF were isolated from lung specimens, as described above (2.2.1.1) and subsequently cultured in DMEM/HAM's F12 medium containing 20% FBS. A549 cells were cultured in DMEM (high glucose) (PAA) medium containing 10% FBS. All cells were cultivated and passaged under standard conditions (5% CO_2 and 37°C) to a maximal confluence of 80 - 90%. For sub-culturing, cells were washed with pre-warmed PBS and detached with trypsin/EDTA solution (37°C, 5 min). Cells were then resuspended and divided in the respective medium and ratio (Table 1.1). MLg fibroblasts were not

used at passage numbers higher than 15, phF were not used at passage numbers higher than 13 and A549 higher than 25.

Table 2.18: Cell type specific culturing conditions

Cell type	Culture medium	Split ratio
A549	DMEM (high glucose) (10% FBS)	1:2 – 1:10
phF	DMEM/F-12/HAM's (20% FBS) + gentamicin (15 µg/ml), penicillin/streptomycin (1%)	1:2 – 1:10
MLg	DMEM/F-12/HAM's (20% FBS)	1:3 – 1:20

2.2.1.4 Liposome-based cell transfection

For transient cell transfection, $2.5x10^5$ MLg cells were plated per well of a 6-well plate. Liposome-based transfection was performed 24 hours after seeding the cells. Solution A and B were prepared as outlined in Table 2.19. Both solutions were first incubated separately at room temperature for 5 minutes, mixed, and incubated for final formation of the liposomes at room temperature for another 20 minutes. Subsequently, 1 ml complete medium and 500 µl transfection mix were added onto the cells and incubated overnight. Re-seeding of the cells was accomplished 24 hours after transfection.

Table 2.19: Transfection protocol for one well of a 6-well plate

Solution	Reagent	Volume [µl]
A	Optimem	246
	DNA [1µg/µl]	4
B	Optimem	244
	Lipofectamin 2000	6

2.2.1.5 Growth factor treatment of cells

Fibroblasts, cultured in a 2D cell culture system, were serum starved in DMEM/HAM's F12 medium containing 1% FBS, 24 hours prior cell treatment. Treatment of cells with TGFβ1was accomplished by culturing cells in DMEM/HAM's F12 medium containing 1 % FBS for the 2D cell culture system and 1 - 5 % for the 3D cell culture assays, supplemented with 1 or 5 ng/ml

TGβ1. For treatment with epidermal growth factor (EGF), medium was supplemented with 10 or 50 ng/ml EGF.

2.2.1.6 Live cell imaging in 3D

For live cell imaging in 3D, collagen matrices were prepared according to the protocol below (2.2.2.1), supplemented with TGFβ1 (5 ng/ml) and cast in 3.5 cm cell culture dishes. Prior seeding on top of the matrices, MLg fibroblasts were stained with the cell-tracker dye CMTPX (5 mM), (Molecular Probes), according to the manufacturer's protocol. During the period of observation the cells were cultured in DMEM/HAM's F12 medium, containing 10% FBS and 15 mM HEPES. Live cell imaging was performed using a PM S1 incubator chamber (Carl Zeiss) at 37°C. Upon seeding the cells, recordings were started within one hour, and z-stacks were acquired with an EC Plan-Neofluar DICI 10x/0.3 NA objective lens (Carl Zeiss) in 30 minutes intervals, operated by ZEN2009 software (Carl Zeiss). The settings for the LSM were as follows: zoom = 0.6, pixel dwell time = 3.15 ms, average =1, master gain = 899, digital gain = 1.00, digital offset = 0.00, pinhole = 90 mm, filters = 410–556, laser line 561 nm = 2%. The confocal 4D data sets were imported into Imaris 7.4.0 software (Bitplane) and processed by applying a maximum intensity projection volume rendering algorithm.

2.2.1.7 Live cell imaging in 2D

Time-lapse microscopy was implemented on an AxioObserver (Carl Zeiss) equipped with an incubator XL S1 and an AxioCam (Carl Zeiss). Nuclear staining of cells was accomplished by incubating the cells with HOECHST for 30 minutes. 9000 cells were seeded in each well of a tissue culture treated 96-well microplate with a flat bottom. Cells were kept in DMEM/HAM's F12 medium containing 10% FBS and 15 mM HEPES during the whole period of observation. Recordings started 24 hours after seeding the cells. Images were acquired with an EC Plan-Neofluar DICI 10x/0.3 NA objective lens (Carl Zeiss) in 20 minutes intervals for 24 hours. The imaging system was operated by AxioVision 4.0 software (Carl Zeiss). The acquired time-lapse data sets were analyzed with the Imaris 7.4.0 software. Automatic tracking of the stained cell nuclei was accomplished with Imaris' spot detection algorithm. Per condition 200-500 cells were analyzed.

2.2.2 3D cell culture models

2.2.2.1 Preparation of collagen G matrices

Collagen G matrices (Biochrom AG), produced from calf skin, were prepared according to the manufacturer's protocol. In short, solution A was prepared by mixing 0.7M NaOH with 1M HEPES buffer (Sigma) in a 1:1 ratio. Subsequently, solution A was combined with 10x PBS, supplemented with 20% FCS, in a 1:1 ratio resulting in solution B (pH = 7.90 - 8.05). Solution B was mixed with collagen G in a 1:4 ratio for the final gelation step (Table 2.20). During the procedure, all reactions were kept on ice. Polymerization of the final collagen G solution was accomplished by incubation at 37°C for 2 hours. Visual quality control of the 3D collagen matrices was performed with an Axiovert 40C microscope (Zeiss). For the invasion assay, a volume of 40 µl collagen G solution was poured in each cavity of a 96-well plate and for the separation assay, 400 µl were used per membrane insert.

Table 2.20: Preparation of collagen G matrices

Solution	Composition	Ratio
A	0.7M NaOH + 1M HEPES	1:1
B	A + 10x PBS (20% FCS)	1:1
C	B + collagen G	1:4

2.2.2.2 3D collagen-based invasion assay

After gelation of the 3D collagen gel, as described in 2.2.2.1, $2x10^4$ cells per well of a 96 well-plate were seeded on top of the matrix and left for invasion under standard conditions (37°C, 5% CO_2) in DMEM/HAM's F12 medium containing 1 - 10% FBS for up to 96 hours, depending on the experiment (Table 2.21). The collagen gels containing the cells were washed once in PBS, fixed in 4% paraformaldehyde (PFA) in PBS at 37°C for 1 hour. Subsequently cells were stained with DAPI (1:2,000) and phalloidin (1:300) in PBS at room temperature for 1 hour. Staining with phalloidin was carried out in order to visually assess integrity of single cells and the cell layer, as well as to estimate cell confluence. Each well containing the in 3D collagen matrix embedded cells was imaged with a LSM710, using an EC Plan-Neofluar DICI 10x/0.3 NA objective lens (Carl Zeiss). The stage was automated to acquire a 5x5 tile z-stack at each well starting from its very center. The z-stack was set to begin 100 mm above and to end 500 mm below the surface of the 3D collagen gel. The settings for the LSM were as follows: zoom = 0.7, pixel dwell time = 1.58 ms, average = 1, master gain = 564, digital gain = 1.24, digital offset = 250.00, pinhole = 265 mm,

filters = 410–585, laser line 405 nm = 4%. Quantification of invasion capacity was accomplished according to 2.4.2.

For assessment of the cellular morphology, MLg fibroblasts were transfected with a pEGFP-N2 (Clontech) vector as described in 2.2.1.4. Subsequently, $2x10^4$ cells were seeded on top of a 3D collagen matrix, prepared as described in section 2.2.2.1. For the 2D control, $2.5\text{-}5.0x10^3$ cells were plated in each cavity of a 96-well plate with a flat bottom. Cells were then incubated for 72 hours, washed with PBS and fixed in 4% paraformaldehyde (PFA) in PBS at 37°C for 1 hour. After fixation nuclei were stained with DAPI (1:2,000) in PBS and confocal z-stacks were acquired with a LSM 710 using an LD Plan-Apochromat 256/0.8 NA objective lens (Carl Zeiss) with the following settings: zoom = 1.0, pixel dwell time = 1.58 ms, average = 2, master gain = 479, digital gain = 1.00, digital offset = 0.00, pinhole = 90 mm, filters = 410– 495, laser line 405 nm = 4% and laser line 488 nm = 4%.

Table 2.21: Culturing conditions for invasion assay

Experiment	Culture medium	Culturing period
Characterization of invading fibroblasts	1% FCS	72-96 hours
Assessment of cellular morphology	10% FCS	72 hours
Assessment of invasion capacity	5% FCS	72 hours

2.2.2.3 3D collagen-based separation assay

The separation assay is a modified setup of the invasion assay. Gelation of the 3D collagen gel was performed as described above (2.2.2.1). The 3D collagen matrix was directly put on the bottom side of tissue culture inserts for 6-well plates (ThinCertsTM, 8 mm pore size, Greiner Bio-One). After gelation of the 3D collagen gel, $2.5 - 5x10^5$ cells per well were seeded on top of the insert membrane and left for invasion under standard conditions (37°C, 5% CO_2) in DMEM/HAM's F12 medium containing 1 - 5% FBS for 72 - 96 hours. The tissue culture insert, containing membrane and 3D collagen gel, was washed twice with ice-cold PBS. Subsequently, the gel was separated from the membrane with a pair of tweezers and mRNA and protein were isolated from the two fractions as described in section 2.3.1.1 and section 2.3.2.1, respectively.

2.3 Molecular biological methods

2.3.1 RNA analysis

2.3.1.1 mRNA isolation from 3D cell culture

For RNA isolation gel and membrane were separated as mentioned in section 2.2.2.3. Three gels were directly pooled in 1 ml of QIAzol Lysis Reagent (Qiagen), incubated at room temperature for 10 minutes and mixed until the complete disintegration. For membrane samples, a minimum of three membranes was pooled in one well of a 6-well plate and incubated in 1 ml of QIAzol Lysis Reagent for 10 minutes. Subsequently, samples were transferred to 1.5 ml Eppendorf tubes and 200 µl chloroform added. After vortexing, samples were centrifuged at 12000 g at 4°C for 15 minutes for phase separation. The upper aqueous phase was transferred into a fresh tube and RNA was further purified with RNeasy Mini Kit (Qiagen) according to the manufacturer's instructions. The concentration of the isolated RNA was assessed spectrophotometrically at a wavelength of 260 nm (NanoDrop 1000).

2.3.1.2 mRNA isolation from 2D cell culture

From conventional 2D cell culture, RNA isolation was accomplished using the PeqGold RNA kit (Peqlab) according to the manufacturer's instruction. The concentration of the isolated RNA was assessed spectrophotometrically at a wavelength of 260 nm (NanoDrop 1000).

2.3.1.3 cDNA-synthesis

cDNA was synthesized with the GeneAMP PCR kit (Applied Biosystems) utilizing random hexamers. For each reaction 1 µg isolated RNA diluted in 18 µl water was used and complemented with the required reagents according to Table 2.22. Denaturation and reverse transcription were performed in an Eppendorf Mastercycler with the following settings: Denaturation: lid = 45°C, 70°C for 10 minutes and 4°C for 5 minutes. Reverse transcription: lid = 105°C, 20°C for 10 minutes, 42°C for 60 minutes and 99°C for 5 minutes. Subsequently, cDNA was diluted to a concentration of 8.33 ng/µl and stored at -20°C.

Table 2.22: Pipet scheme for reverse transcription

Reagent	Stock concentration	Volume [µl]	Final concentration
$MgCl_2$	25 mM	8	5 mM
10x Buffer	10x	4	1x
dNTPs	10 mM	4	1 mM
Random Hexamers	50 µM	2	2.5 µM
RNase Inibitor	20 u/µl	2	1 u/µl
Reverse Transcriptase	50 u/µl	2	2.5 u/µl
Denat. RNA	-	18	-
Total		**40**	

2.3.1.4 Quantitative real-time Polymerase Chain reaction (qRT-PCR)

All primers for quantitative PCR were designed with NCBI's PrimerBLAST (http://www.ncbi.nlm.nih.gov/tools/primer-blast/), according to the following criteria: amplicon size ≤ 500 bp, T_M (primer) ≈ 60°C and $|T_M(fw-primer) - T_M(rev-primer)| \leq 5K$, size of primer 18 – 24 bp, GC content ≈ 50%.

To avoid primer hybridization, T_M and ΔG for primer-dimer and hairpin formation were tested for all designed primerpairs using the oligoanalyzer tool from Integrated DNA Technologies (http://eu.idtdna.com/analyzer/applications/oligoanalyzer/#Structure%201). qRT-PCR reactions were performed in triplicates with SYBR Green I Master in a LightCycler® 480II (Roche) with standard conditions: 95°C for 5 min followed by 45 cycles of 95°C for 5 s (denaturation), 59°C for 5 s (annealing), 72°C for 20 s (elongation), 60 – 95°C for 1 min with continuous acquisition (melting curve). Prior pipetting reactions according to Table 2.23, forward and reverse primers were diluted to a concentration of 2.5 µM in DNase/RNAse - free water. Target gene expression was normalized to GAPDH expression.

Table 2.23: Reaction scheme qRT-PCR

Reagent	Stock concentration	Volume [µl]	Final concentration
SybrGreen I Master Mix	2x	5	1x
Primer Mix	10 µM each	2	0.5 µM
cDNA	8.33 ng/µl	3	25 ng/µl
Total		10	

2.3.1.5 Verification of amplicons by agarose gel electrophoresis

Size determination and review of amplicon specificity for PCR amplified DNA fragments were accomplished by electrophoretic separation on 1% agarose gels. Agarose was dissolved in 1x TAE buffer boiled in a microwave, supplemented with SybrSafe (1x final concentration) and poured into a gel electrophoresis chamber. DNA samples were mixed with 6x loading dye (1x final concentration), loaded into the pockets and electrophoretic separated in 1% TAE buffer by applying 50 V/gel. For size assessment, appropriate molecular weight markers were loaded on the outer lanes. DNA bands were visualized using the XcitaBlue™ Conversion Screen from ChemiDoc at 470 nm.

2.3.1.6 Microarray

For the microarrays, total RNA was isolated with the miRNeasy mini kit® according to the manufacturer's protocol (Qiagen). RNA quality was accessed by the Agilent 2100 Bioanalyzer and only high quality RNA (RIN > 8) was used for microarray analysis. Total RNA (150 ng) was amplified using the Ambion WT Expression Kit and the WT Terminal Labeling Kit (Affymetrix). Amplified cDNA (2.75 µg) was hybridized on Affymetrix Mouse Gene 1.0 ST arrays, containing about 28,000 probe sets. Staining (Fluidics script FS450_0007) and scanning was done according to the Affymetrix expression protocol.

2.3.2 Proteinbiochemistry

2.3.2.1 Protein isolation from 3D cell culture

For protein isolation, gel and membrane were separated as mentioned in section 2.2.2.3. A minimum of three gels was pooled in one 2 ml Eppendorf tube and the remaining PBS was aspirated. 80 µl (2120 U) of collagenase type1 (Biochrom) was added to each tube and incubated while shaking at 37°C for 30 – 60 minutes until the complete disintegration of the collagen gel. Centrifugation for 2 minutes at 500 g at 4°C resulted in a cell pellet that was washed twice with ice-cold PBS. Finally, the cell pellet was lysed in 30 – 50 µl ice-cold RIPA buffer, containing 1x Roche complete mini protease inhibitor cocktail. For protein isolation from non-invading cells, the membranes were cut out with a sharp scalpel. Next, the cells were scraped off the membrane directly into 200 µl ice-cold RIPA buffer containing 1x Roche complete mini protease inhibitor cocktail. Cells of a minimum of three membranes were pooled in one 2 ml Eppendorf tube. After incubating the samples on ice for 30 minutes, insoluble material was removed by centrifugation at

14,000 g at 4°C for 15 minutes and the supernatant was further processed as described in section 2.3.2.3 - 2.3.2.4. Protein concentrations were determined using the BCA assay described in 2.3.2.3.

2.3.2.2 Protein isolation from 2D cell culture

2.3.2.2.1 Protein isolation from cell lysates

$2.5x10^5$ MLg fibroblasts were plated per well of a 6-well plate and cells treated according to section 2.2.1.5. Prior protein isolation, cell culture medium from the adherent cells was aspirated and cells were washed with ice-cold PBS. Cell samples, fresh or frozen (-80°C), were scratched on ice in 70 – 100 µl RIPA lysis buffer (complemented with 1x Roche complete mini protease inhibitor cocktail) per well of a 6-well plate, with a cell lifter. Cell lysates were transferred to microcentrifuge tubes and incubated on ice for 30 minutes. Soluble protein fractions were purified by centrifugation at 14,000 g at 4°C for 15 minutes. Protein concentrations were determined using the BCA assay described in 2.3.2.3.

2.3.2.2.2 Protein isolation from cell supernatants

For analyzing secreted Sfrp1 protein concentrations of cell culture supernatants, $2.5x10^5$ MLg fibroblasts were plated in one well of a 6-well plate. Cells were treated as described under 2.2.1.5. For ELISAs, samples were taken 24 hours after treatment and concentrated by reducing the volume to one forth with Amicon® Ultra centrifugal filter units (Millipore). Briefly, 500 µl culture supernatant was transferred into one 3K Amicon Ultra centrifugal filter unit and subsequently centrifuged at 14,000 g at 4°C for 30 minutes. Subsequently, the centrifugal filter units were inverted and concentrated samples were recovered from the centrifugal filter units by centrifugation at 1,000 g at 4°C for 2 minutes.

2.3.2.3 Determination of protein concentration by bicinchoninic acid assay (BCA)

Protein samples were diluted 1:10 in water and protein concentration determined with the biuret reaction based BCA using the Pierce® BCA protein assay kit (Biochrom) according to the manufacturer's instruction. Absorbance was measured at 562 nm with the Sunrise multiplate reader. All BCA reactions were performed in duplicates.

2.3.2.4 Sodium dodecyl sulphate polyacrylamide gel electrophoresis (SDS-PAGE) and Western blotting

Protein samples were mixed with 6x lämli loading buffer (final concentration 1x) and proteins were separated using standard SDS (7-12%) PAGE (20 - 30 mA per gel). For immunoblotting, proteins were transferred to methanol activated PVDF (Millipore, 0.45 µm or 0.2 µm) membranes (350 mA for 60 minutes). Subsequently, membranes were blocked with 5% milk in 1xTBST (0.1% Tween®20/TBS) and incubated with primary, followed by HRP-conjugated secondary antibodies at 4°C over night and at room temperature for 1 hour, respectively. Upon antibody incubation, membranes were washed intensively. Chemiluminescence was generated by incubating the membranes with SuperSignal West Chemiluminescent Substrate (ECL). Finally, signals were documented on x-ray films.

2.3.2.5 Enzyme-linked Immunosorbent Assay (ELISA)

Sandwich enzyme immunoassay for Sfrp1 was performed using the murine Sfrp1 ELISA kit (E95880Mu) from Uscn Life Science, according to the manufacturer's protocol. Cell supernatants were concentrated (25x) using the Amicon Ultra centrifugal as described in 2.3.2.2.2. ELISAs were performed by Elisabeth Hennen. Data analysis was performed using non-linear interpolation on standards with GraphPad Prism4 (GraphPad Software).

2.3.2.6 Luciferase reporter assay

$3x10^4$ MLg cells were plated in each cavity of a 48-well plate in DMEM/Ham's F12 (10% FBS). Cells were transfected with 500 ng of TOPFLASH or FOPFLASH reporter plasmid in DMEM/Ham's F12 (1% FBS), respectively (Lipofectamine® 2000, Invitrogen). Five hours after transfection, fibroblasts were treated with Wnt3a (R&D) (100 ng/ml), Sfrp1 inhibitor CHEMBL473916 (sc-222310, Santa Cruz) (10 µM, 30 µM) and rh-Sfrp1 (R&D) (1 µg/ml) over night. Cells were lysed and luciferase activity measured with BrightGlo reagent (Promega) (TriStar LB 941, Berthold Technologies).

2.3.2.7 Immunocytochemistry and immunofluorescence microscopy

phF were seeded on borosilicate glass coverslips (25 mm diameter, VWR international) in a density of $3x10^5$ per well of a 12-well dish. Cells were cultured in DMEM/HAM'S F12 (20% FCS) at 37°C with 5% $CO_2$for 24 hours, prior starvation in DMEM/HAM'S F12 (1% FCS) for 16

hours. Subsequently, fibroblasts were treated with TGFβ1 (5 ng/ml) or EGF (50 ng/ml) in starvation medium and incubated for 24 hours. Cells were fixed in 4% PFA in PBS at 37°C for 30 minutes and permeabilized with 0.5% Triton-X in 4% PFA for 5 minutes. Primary antibodies were diluted to the appropriate concentrations in 1% bovine serum albumin (BSA, Sigma) in PBS, added to the samples and incubated at 4°C for 16 hours. Afterwards, samples were washed three times with PBS for 10 minutes each. Incubation steps for the secondary antibody were performed equally. Coverslips were mounted on microscope slides (Thermo Scientific) in Fluorescent mounting medium (DAKO). Images were acquired with a LSM 710 as z-stacks and a LD C-Apochromat 406/1.1 NA water objective lens (Carl Zeiss).

For the characterization of fibroblasts in 3D, MLg fibroblasts were seeded on top of the 3D collagen matrix, cultured as described in section 2.2.2.2, fixed in 4% paraformaldehyde (PFA) in PBS at 37°C for 1 hour and permeabilized in 4% PFA/0.5% Triton X-100 in PBS for 10 minutes. Primary and secondary antibodies were diluted in 1% BSA in PBS, incubated at 4°C for 16 hours and subsequently washed off by rinsing the cells three times with PBS for 20 minutes each, respectively. Cells were imaged in PBS with a LSM 710 as z-stacks and with an LD C-Apochromat 406/1.1 NA water objective lens (Carl Zeiss) with the following settings: zoom = 1.7, pixel dwell time = 2.55 ms, average = 4, master gain = 593, digital gain = 1.00, digital offset = 0.00, pinhole= 90 mm, filters = 410–495, laser line 488 nm = 10%, laser line 405 nm = 4% and laser line 561 nm = 2%.

2.4 In silico analysis

2.4.1 Quantification of cell morphology

For assessment of cell morphology, MLg fibroblasts were transfected with an empty pEGFP-N2 vector as described in section 2.2.1.4, cultured and imaged according to section 2.3.2.7. Confocal fluorescent z-stacks were volume rendered with Imaris 7.4.0 software (Bitplane) and its statistical analysis tool. For the numerical output of the cell shape, cell surface area ($A = 4\pi r^2$), cell volume ($V = \frac{4}{3}\pi r^3$), and sphericity ($\Psi = \frac{\pi^{\frac{1}{3}}(6V_p)^{\frac{2}{3}}}{A_p}$) were determined according to Imaris V6.0 Reference Manual (Bitplane 2007) (www.bitplane.com/download/manuals/ReferenceManual5_7_0.pdf). For length/width ratios two equations were utilized: $e_{prolate} = \frac{2a^2}{a^2+b^2} * \left(1 - \frac{a^2+b^2}{2c^2}\right)$, $e_{oblate} = \frac{2b^2}{b^2+c^2} * \left(1 - \frac{2a^2}{b^2+c^2}\right)$, where a, b and c are the lengths of semi-axes of an ellipsoid. Classification in oblate and prolate cell shape is depicted in section 6.1.

2.4.2 Quantification of invasion capacity

Acquired data sets, as described in section 2.2.2.2, were imported into Imaris 7.4.0 software (Bitplane) and cropped in 3D. Then the spot detection algorithm of the Imaris 7.4.0 software was applied to assign a spot for each fluorescent intensity of a single nucleus. The settings for the spot detection algorithm were as follows: [Algorithm] enable region of interest = false; enable region growing = false; enable tracking = false. [Source channel] source channel index = 1; estimated diameter = 15; background subtraction = true. [Classify spots] ‘‘quality’’ above 3.089. Thus, by using Imaris’ statistical analysis tool, the total number of spot objects was retrieved. Subsequently, the spot objects were filtered by their z-position (‘‘position z’’ below a threshold in mm), whereby the threshold was set at the lowest point of the collagen surface. Thus, all spot objects assigned to invading cells in the 3D collagen matrix were selected. This selection was duplicated to a new ‘‘spots object’’ and the number of invading spots by using Imaris’ statistical analysis tool was determined. Finally, by correlating the number of spots representing the invading cells to the total number of spots, the percentage of invading cells in the 3D collagen matrix was defined. Invasion depth was ascertained by using Imaris’ statistical analysis tool. Thereby, the maximal invasion depth was defined as the distance between the lowest non-invading cell (on top of the matrix) and the deepest invading cell (within the matrix).

2.4.3 Bioinformatical analysis

For the statistical transcriptome analysis, expression console (Affymetrix) was used for quality control and to obtain annotated normalized robust multiarray average approach (RMA) gene-level data (standard settings including sketch-quantile normalisation). Heatmaps were generated with CARMAweb (Rainer, Sanchez-Cabo et al. 2006) and cluster dendrograms with the R script hclust. Molecular network analysis was conducted with the web-based software application Ingenuity® Pathway Analysis (IPA) by creating a custom pathway, based on the Ingenuity Knowledge Base.

2.4.4 Statistical analysis

Statistical analysis was performed using GraphPad Prism4 (GraphPad Software). Data are presented as mean ± standard deviation (SD). Statistical analysis was performed using unpaired and paired t-tests (two-tailed) or One way ANOVA with Dunnett’s multiple comparison test. For microarray experiments statistical analyses were performed by utilizing the statistical programming environment R (R Development Core Team Ref1), implemented in CARMAweb. Genewise testing for differential expression was done employing limma t-test and Benjamini-

Hochberg (BH) multiple testing correction (FDR < 10%). Right-tailed Fisher Exact Test was utilized for statistical analysis on the IPA platform (Ingenuity Systems).

3. RESULTS

3.1 Establishment of novel 3D collagen-based invasion assays

Aberrant invasion through interstitial and stromal tissue is one dominant pathomechanism of activated fibroblasts in non-neoplastic fibrotic diseases (Li, Jiang et al. 2011) and cancer (Kalluri and Zeisberg 2006). The aim of this study was to extensively profile the invading fibroblast phenotype and to systematically investigate the molecular signatures of fibroblast invasion in order to identify potential regulators thereof. In a first step, a 3D collagen-based invasion assay was established and deployed for effective quantification of the invasive capacity of fibroblasts *(invasion assay)*. Then, a modified version of the *invasion assay* allowed the separation of invading from non-invading fibroblasts *(separation assay)* and their subsequent molecular analysis and generation of transcriptome signatures of invasion.

3.1.1 Invasion assay

To assess cellular invasion in a high-content and high-throughput setting, a 96-well microplate collagen-based 3D cell culture model was established and validated. To establish this, fibroblasts of the murine lung fibroblast line MLg 2908 were utilized.

Collagen type I was selected as ECM model system, since *in vivo* it represents the predominant structural component of the ECM of connective tissue (Vasaturo, Caserta et al. 2012), (Wolf, Alexander et al. 2009). In a first step, quality and thickness of the collagen microstructure was surveyed with a laser scanning microscope, operating in reflection mode. The polymerized collagen type I arranged in 200 - 300 µm thick matrices with a homogeneous microfibrillar structure (Figure 3.1). In the invasion model, fibroblasts were plated on top of collagen type I matrices and cultured under standard conditions.

After an invasion time of 72 to 96 hours, fibroblasts were fixed and stained with phalloidin and DAPI. Invading fibroblasts were found to exhibit a spindle-shaped morphology, characteristic for fibroblasts *in vivo* (Kalluri and Zeisberg 2006) (Figure 3.1). Morphological changes during the process of invasion were analyzed in detail with a slightly different experimental set-up as described in section 3.1.2.

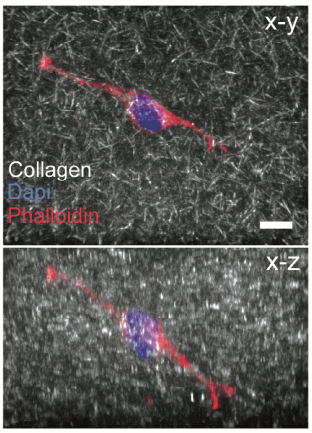

Figure 3.1: Confocal image of an invading MLg fibroblast, embedded in collagen matrix.
Microfibrillar structures are visualized using a confocal laser scanning microscope operating in reflection mode. Maximum intensity projections (x-y) **(upper panel)** and (x-z) **(lower panel)** from a generated z-stack are shown. Collagen matrix (reflection mode) is displayed in grey. Nuclei and F-actin of fibroblasts were fluorescently stained with DAPI (blue) and phalloidin (red), respectively. Scale bar, 10 µm. (Published in (Burgstaller, Oehrle et al. 2013)).

Visualizing the nuclei allowed subsequent assessment of the cell numbers and thus quantification of the invading cell fraction. With a laser scanning microscope (LSM 710) z-stacks were acquired from each well, thereby only scanning the DAPI channel. The scanning process was automated for the 96-well plate using Zen2009 (Zeiss) software and the scanning area maximized by generating a 5x5 tile image/well. Subsequently, the collective image files of the 96 well plate were split, resulting in one individual file for each well. The exported imaging data were analyzed with Imaris software (Bitplane). To avoid false-positive counts of invading cells, caused by the meniscus of the matrix, the area for analysis was minimized to the planar part in the center of each well, using the 3D-crop function. For quantification, each fluorescence signal was marked with a spot by applying the built-in spot detection algorithm. Thus, each spot represented one nucleus, equivalent to one single cell. With the built-in spot detection algorithm, the exact spatial information (x,y,z) for each cell can be determined. Accordingly, with the statistical analysis function for spot-objects, a threshold was set (red line) and invading (yellow) fibroblasts were thus distinguished from non-invading ones (white) (Figure 3.2).

To proof that the invasion assay enabled the assessment of an active cell invasion process rather than capturing matrix artifacts, the invasive fibroblast cell line MLg was compared to the non-invasive epithelial cell line, A549, in regards to invasion distance. The maximal invasion depth was defined as distance between the lowest non-invading cell (on top of the matrix) and the deepest invading cell (within the matrix). Upon invasion, MLg fibroblasts were traced at an

invasion depth of up to 136.9 ± 33.04 µm whereas A549 cells reached a maximal invasion depth of 12.72 ± 6.35 µm (Figure 3.3).

These data verified that MLg cells, found in deeper regions of the matrix, underwent active invasion.

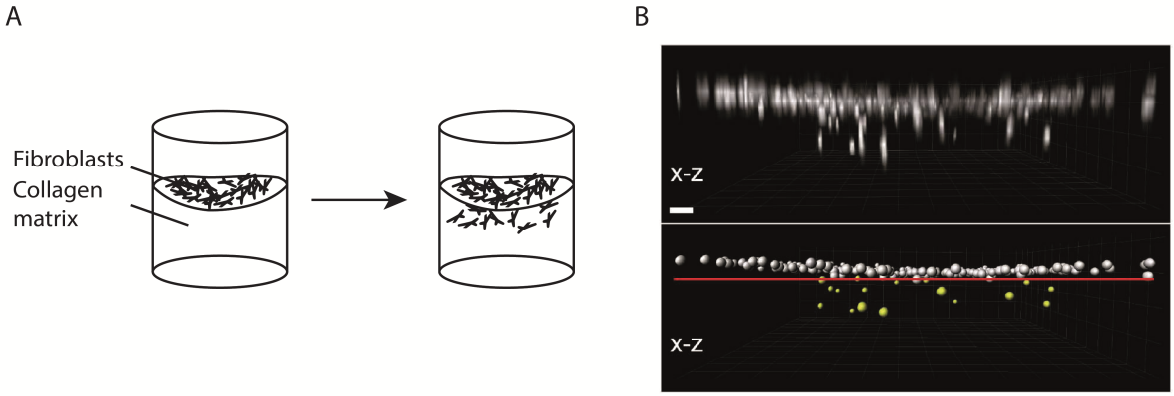

Figure 3.2: Experimental set-up and analysis of 3D collagen-based invasion assay.
Schematic representation of the experimental set-up of the established invasion assay **(A)**. MLg fibroblasts were cultured in the invasion assay for 72 hours. Maximum intensity projection (x-z) of nuclei stained with DAPI (white) **(upper panel)** and corresponding spot analysis acquired with the Imaris built-in spot algorithm **(lower panel)**. Invading cells are highlighted in yellow, non-invading in white. The threshold for z-position filtering is depicted in red **(B)**. (Published in (Burgstaller, Oehrle et al. 2013)).

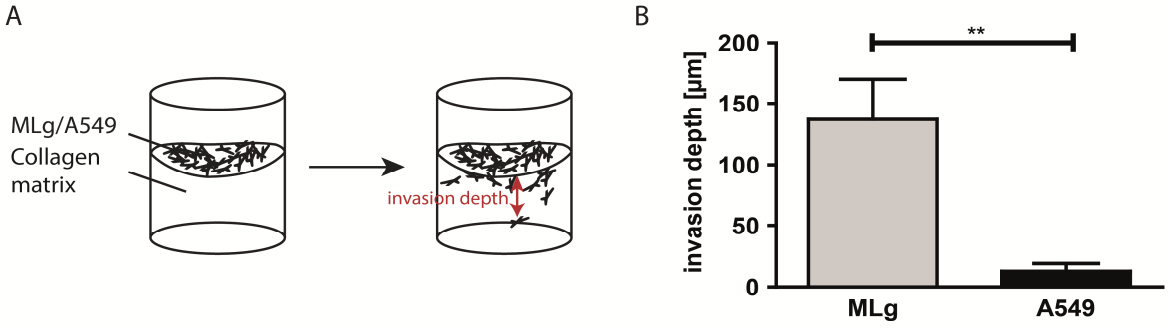

Figure 3.3: Quantification of the maximal invasion distance of MLg and A549 cells.
Schematic representation of the experimental set-up and assessment of the maximal invasion depth. The maximal invasion depth was defined as the distance between the lowest non-invading and deepest invading cell (A). Quantification of the invasion depth of MLg and A549 cells (B). Data are shown as mean invasion depth (±SD) of 3 independent experiments (n = 3). Statistical analysis: unpaired t-test. **p<0.01. (Published in (Burgstaller, Oehrle et al. 2013)– *modified*).

The dynamic process of fibroblast invasion was further analyzed by confocal 4D (z-stack over time) time-lapse microscopy. MLg fibroblasts were stained with a cell tracker dye (CMTPX), seeded on top of collagen matrices, containing 5 ng/ml TGFβ1, and live cell imaging was performed over a period of two days.

Using this method as a proof of principle, fibroblasts were traced at an invasion depth of 50 µm (1 day 7 hours), 74 µm (1 day 22 hours) and 98 µm (2 days 14 hours) and thus observed to actively invade the collagen I (Figure 3.4).

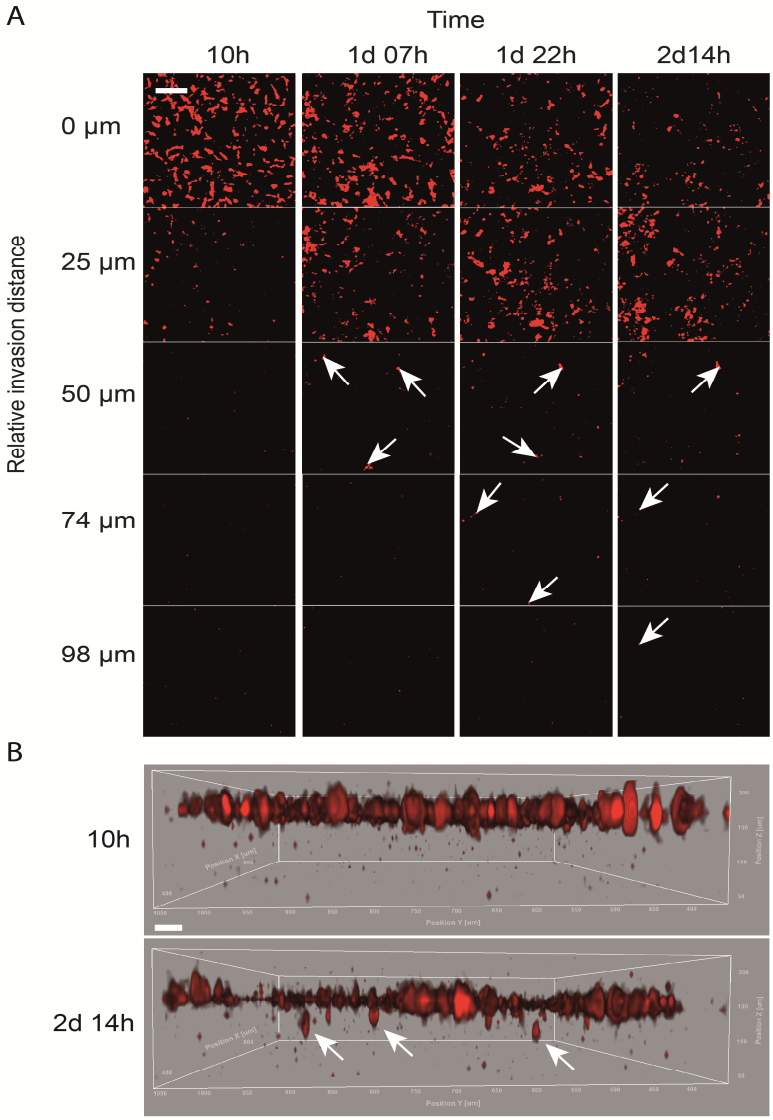

Figure 3.4: Live cell imaging showing fibroblast invasion over time.

Confocal 4D time-lapse movie of MLg fibroblasts stained with the cell tracker CMTPX dye during the process of collagen invasion in the presence of TGFβ1 (5 ng/ml). Over the time, fibroblasts appeared in deeper regions of the matrix as shown in single frames at different time points (10 hours, 1 day 7 hours, 1 day 22 hours, 2 days 14 hours). Scale bar, 80 µm **(A)**. Orthoview of maximum intensity projections at 10 hours and 2 days 14 hours **(B).** Scale bar, 50 µm. White arrows indicate invading fibroblasts found in deeper regions of the matrix. (Published in (Burgstaller, Oehrle et al. 2013)– *modified*).

3.1.2 Characterization of the invasive fibroblast phenotype

In vivo, fibroblasts reside in the 3D environment of ECM and are described as spindle-shaped elongated cells (Kalluri and Zeisberg 2006).

To further validate the established collagen-based invasion model, morphological plasticity of fibroblasts in different culturing systems as well as during the process of invasion was assessed. For this, MLg fibroblasts were transiently transfected with a pEGFP-N2 (enhanced green fluorescent protein) vector, which effected a strong fluorescent labelling of the cells' cytoplasm. Subsequently, the cells were cultured either in a conventional 2D plastic-based cell culture system or plated on top of a collagen matrix (3.2 mg/ml). In both conditions, cells were cultured for 72 hours. As fibroblasts undergo spontaneous invasion, two subpopulations formed in the 3D collagen-based experimental set-up. Cell shape, cell surface area, cell volume and cell sphericity were assessed. The morphology of the different fibroblast subtypes was quantified by means of surface rendering of acquired confocal fluorescent z-stacks.

For simplified mathematical modeling of the cell shape, cells were regarded as spheroids. Commonly, spheroids can be classified in prolate (elongated) or oblate (disk-shaped). Thereby, for prolate spheroids the polar radius is greater than the equatorial radius ($prolate: a = b < c$) while for oblate spheroids the polar radius is shorter than the equatorial radius ($oblate: a < b = c$) with a,b,c being the lengths of the semi-axes of an ellipsoid.

Hence, for the numerical output of the cell shape, the prolate ($e_{prolate}$) and oblate (e_{oblate}) factor of a representative number of cells was estimated and a morphological shift from predominantly disk-shaped spheroids ($e_{prolate} = 0.36$, $e_{oblate} = 0.37$) of conventional 2D cultured fibroblasts (Figure 3.5 right panel) to elongated cigar-shaped spheroids ($e_{prolate} = 0.67$, $e_{oblate} = 0.15$) of in 3D collagen cultured fibroblasts was quantified (Figure 3.5 left panel). Non-invading fibroblasts, which remained on the surface of the collagen matrices during culturing time, had an intermediate ellipsoid-like shape ($e_{prolate} = 0.51$, $e_{oblate} = 0.36$) (Figure 3.5 middle panel).

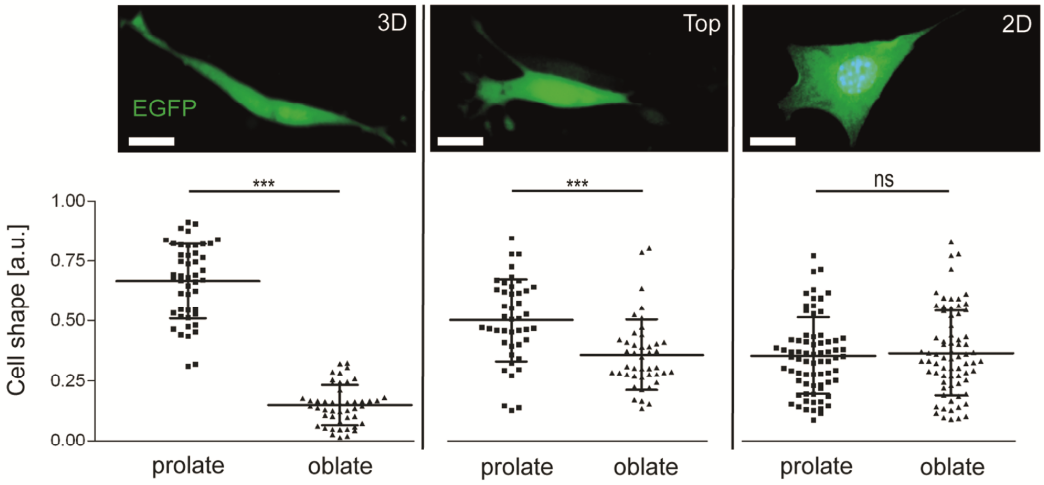

Figure 3.5: Assessment of the morphological plasticity of MLg fibroblasts.
Representative confocal images of MLg fibroblasts embedded in collagen matrix **(left)**, on top of collagen matrix **(middle)**, or cultured in 2D **(right)** **(upper panel)**. Morphological evaluation of the represented fibroblast subpopulations (prolate and oblate factor) **(lower panel)**. Data shown represent mean values (±SD) of randomly selected fibroblasts (n = 47 - 73). Statistical analysis: unpaired t-test. ***p<0.001 and ns = not significant. Scale bar, 20 µm, a.u. = arbitrary units. (Published in (Burgstaller, Oehrle et al. 2013)).

Morphological plasticity of fibroblasts is furthermore reflected in the cell surface area (A), volume (V), and sphericity (Ψ). Significant changes in all three geometric parameters between fibroblasts cultured in 2D plastic dishes (A = 2956 µm^2, V = 9601 µm^3, Ψ = 0.73), invaded the 3D collagen I matrix (A = 2254 µm^2, V = 5291 µm^3, Ψ = 0.66), or remained on top of the collagen I matrix were observed (A = 1511 µm^2, V = 4241 µm^3, Ψ = 0.83). Fibroblasts, cultured in the 2D system, exhibited increased volume and surface area when compared to cells cultured on top or within the 3D collagen I matrix. Importantly, fibroblasts embedded in the 3D collagen matrix showed lowest sphericity, indicating a more elongated phenotype than 2D cultured and non-invading fibroblasts (Figure 3.6).

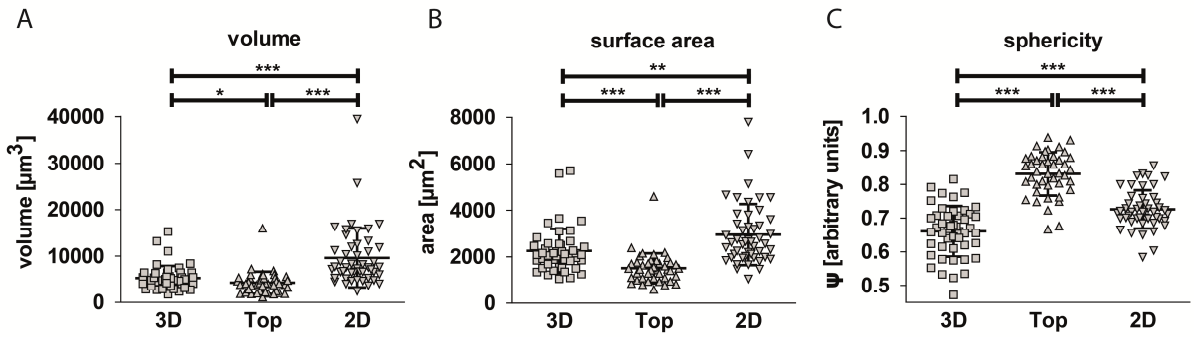

Figure 3.6: Assessment of the geometry of MLg fibroblasts in different microenvironments.
Geometric parameters (volume, surface area, and sphericity) were assessed from surface rendering of acquired confocal fluorescent z-stacks. Fibroblasts, cultured in 2D, showed highest cell volume compared to fibroblasts on top and embedded in collagen matrix. The cell volume significantly differed between culturing conditions **(A)**. Accordingly, surface area was found highest in the 2D set-up and displayed significant differences between the three groups **(B)**. Fibroblasts, remaining on top of the collagen matrix, exhibited significantly higher sphericity values compared to fibroblasts embedded in the matrix or cultured in 2D **(C)**. Data shown represent mean values (±SD) of randomly selected fibroblasts (n = 47 - 73). Statistical analysis: unpaired t-test. *p<0.05, **p<0.01,***p<0.001. (Published in (Burgstaller, Oehrle et al. 2013)).

To further characterize fibroblasts that invaded the collagen matrix, immunofluorescence stainings were performed. Adhesion of cells to the surrounding ECM via integrins is fundamental for the mesenchymal mode of migration (Cukierman, Pankov et al. 2002), (Rhee 2009). Therefore, an antibody against integrin β1 (CD29) was used to detect cell-ECM adhesions of invaded MLg fibroblasts within the 3D collagen I matrix. Thereby, fibrillar adhesion-like structures were visualized along F-actin fibres (Figure 3.7).

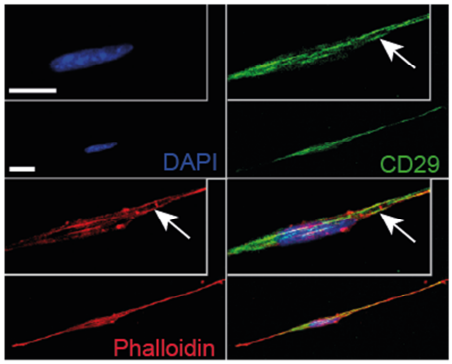

Figure 3.7: Immunofluorescence staining for integrin β1 (CD29) in invading MLg fibroblasts.
Representative image of invading MLg fibroblasts (invasion depth ≈ 100 - 200 µm) stained for integrin β1 (CD29), phalloidin, and DAPI. White boxes highlight magnification of the central part of the cells. White arrows indicate co-localization of CD29 with F-actin (phalloidin) at elongated fibrillar adhesion-like structures. Scale bars, 20 µm. (Published in (Burgstaller, Oehrle et al. 2013)).

Further cellular functional activities such as cell cycle status, ECM production and cell polarity were analyzed in the invading fibroblast fraction by immunofluorescence staining.

First, to review cellular growth of fibroblasts, embedded in the collagen matrix (invasion depth of 100 – 200µm), dividing cells were identified by the nuclear proliferation marker Ki67 (Figure 3.9, upper panel).

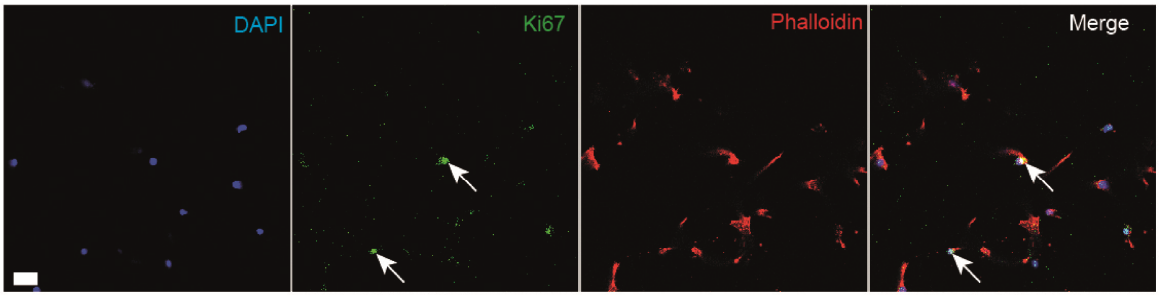

Figure 3.8: Immunofluorescence staining for Ki67.
Maximum intensity projection of confocal immunofluorescence microscopy images of MLg fibroblasts stained with Ki67-ab, residing the collagen matrix at an invasion depth of 100 - 200 µm. F-actin was stained in red (phalloidin) and nuclei in blue (DAPI). Scale bar, 20 µm. (Published in (Burgstaller, Oehrle et al. 2013) - *modified*).

As *in vivo* fibroblasts function as main ECM-producing cell type (Kendall and Feghali-Bostwick 2014) fibroblasts, residing the collagen matrix, were stained for fibronectin. These fibroblasts were found to contribute, with the production of fibronectin, to the construction of a more complex ECM structure (Figure 3.9, upper panel).

Additionally invading fibroblasts were found to be highly positive for vimentin, a major cytoskeletal component of motile mesenchymal cells (Shabbir, Cleland et al. 2014) (Figure 3.9, lower panel).

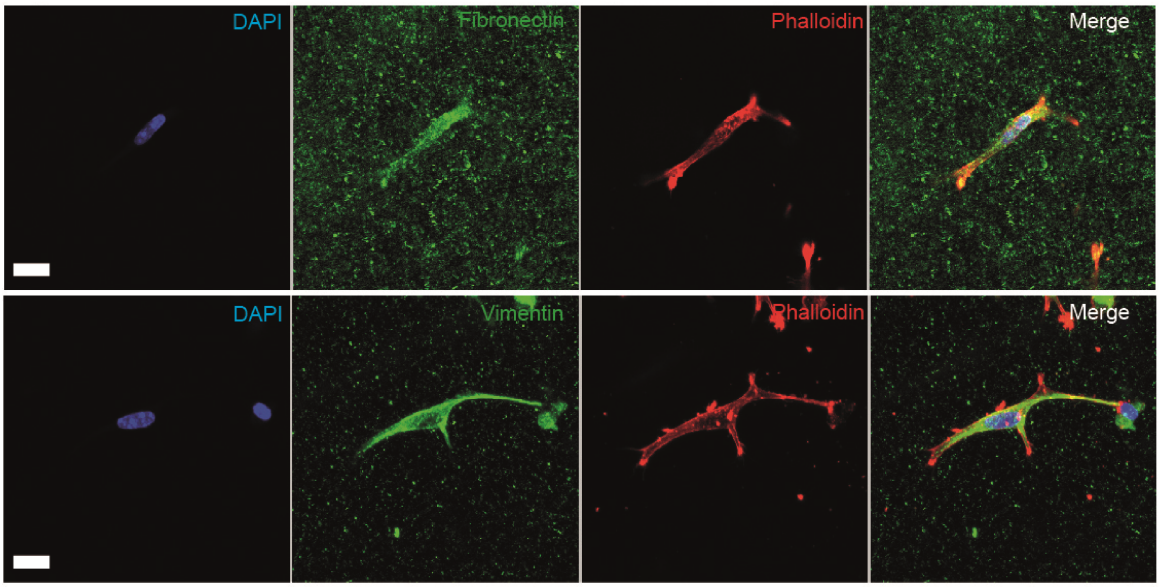

Figure 3.9: Immunofluorescence staining fibronectin and vimentin in invading MLg fibroblasts.
Maximum intensity projection of confocal immunofluorescence microscopy images of MLg fibroblasts, residing the collagen matrix at an invasion depth of 100 – 200 µm. Fibronectin **(middle panel)** and vimentin **(lower panel)** were stained in green. F-actin (phalloidin) was stained in red and DAPI in blue. Scale bar 10 µm. (Published in (Burgstaller, Oehrle et al. 2013) - *modified*).

3.1.3 Separation assay

To analyze the molecular properties of the invading fibroblast phenotype, a 3D collagen-based separation assay was established. Porous Polyethylenterephthalat (PET) membrane inserts (Ø of pore = 8 µm) were coated with collagen matrix on the underside. Fibroblasts were plated onto the membrane, opposite to the collagen matrix plug and cultured for 72 hours and 96 hours. Invading fibroblasts migrated through the pores of the membrane into the collagen matrix.

To physically split the two fractions, the membranes, which were colonized with the non-invading cells, were detached from the collagen matrices, which contained the invading cells. Subsequently, RNA and protein were extracted from the fractions and subjected to detailed molecular analysis (Figure 3.10).

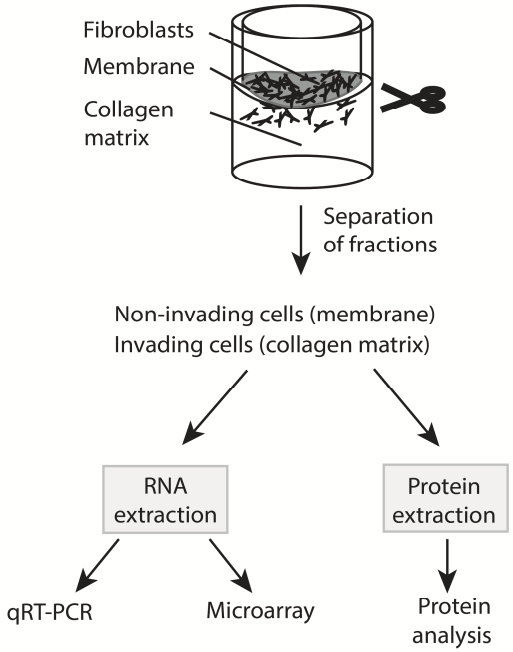

Figure 3.10: Experimental set-up of 3D collagen-based separation assay.
Schematic representation of the experimental set-up of the separation assay, indicating the application range of the assay. Fibroblasts are initially plated on top of the membrane inserts and invade over a period of 72 to 96 hours through the pores of the membrane into the collagen matrix. Subsequently, invading fibroblasts (collagen matrix fraction) are separated from non-invading fibroblasts (membrane fraction). Either RNA or protein is extracted from both fractions and finally used for various molecular and biochemical analysis.

3.2 Growth factor induced fibroblast invasion

Growth factor signaling, eminently TGFβ1 (Santibanez, Quintanilla et al. 2011) and EGF (Baughman, Lower et al. 1999), are profoundly altered in fibrotic lung diseases. Hence, the impact of TGFβ1 and EGF on fibroblast invasion was evaluated with the 3D collagen invasion assay.

MLg fibroblasts were cultured on top of collagen matrices for 24 hours and subsequently stimulated with TGFβ1 (1 and 5 ng/ml) or EGF (10 and 50 ng/ml). 48 hours after stimulation with the growth factors, the invasion capacity was assessed. Figure 3.11 A and B represent 3D reconstructions of the acquired z-stacks with a spot analysis and z-position dependent color coding (A-B). TGFβ1 significantly induced invasion into the 3D collagen matrices from 11.52 ± 4.56% to 16.26 ± 7.00% (1 ng/ml) and 15.63 ± 5.93% (5 ng/ml) (Figure 3.11 C). Treatment with EGF resulted in 19.15 ± 4.71 (10 ng/ml) and 21.36 ± 5.62% (50 ng/ml) (Figure 3.11 D).

Of note, for further experiments TGFβ1 and EGF were used in a concentration of 5 ng/ml and 50 ng/ml, respectively.

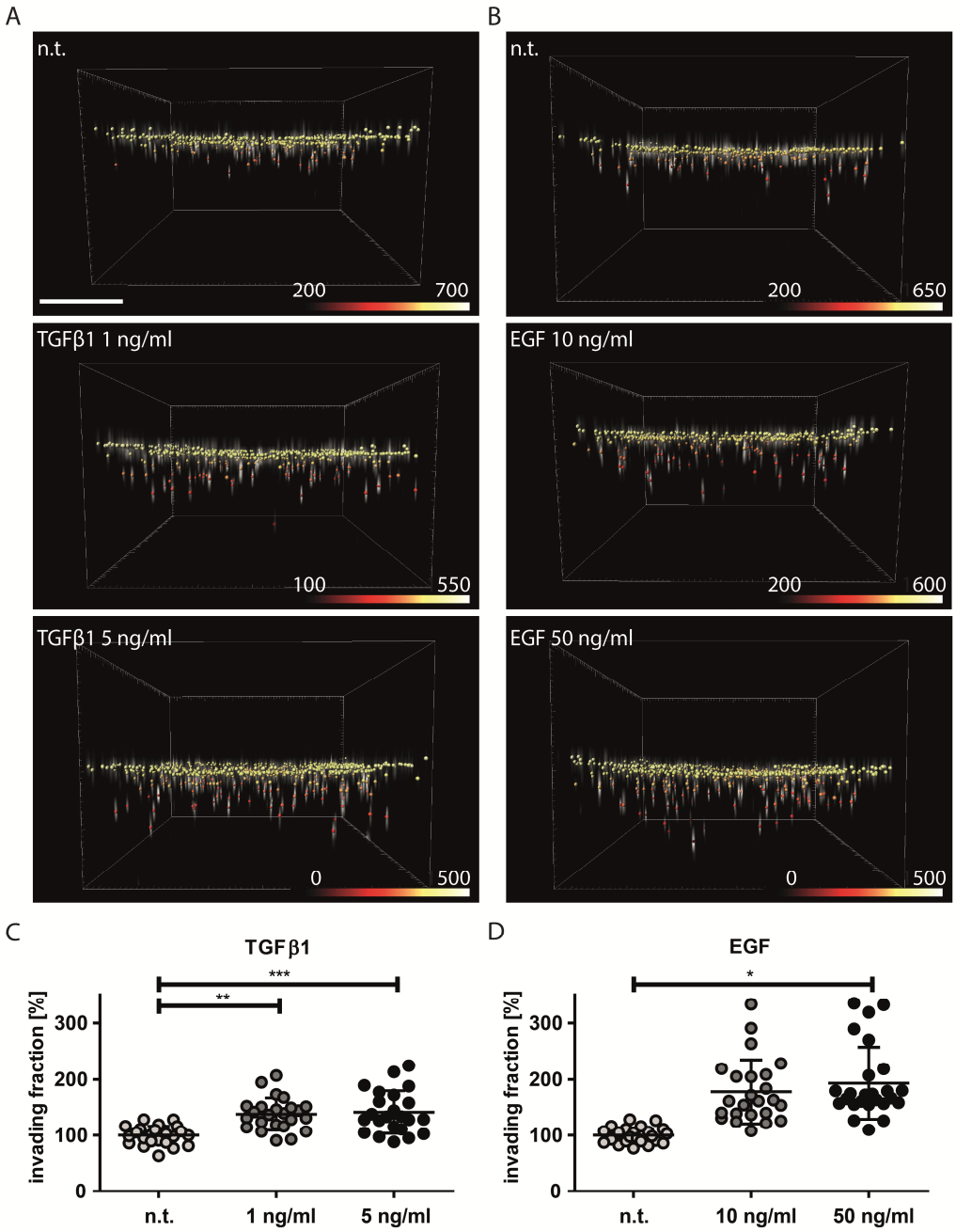

Figure 3.11: TGFβ1 and EGF induce MLg fibroblast invasion.
Software-based quantification of fibroblast nuclei (stained with DAPI) within and on top of collagen matrices by means of 3D reconstructed confocal z-stacks allowed the assessment of the invasion capacity of MLg fibroblasts. TGFβ1 (1 ng/ml and 5 ng/ml) significantly induced fibroblast invasion as assessed 48 hours after treatment **(A)**. By applying the same conditions, treatment of the cells with EGF resulted in a strong pro-invasive effect (10 ng/ml and 50 ng/ml) **(B)**. Data are shown in five technical replicates per each of the five independent experiments (n = 5) (±SD). Statistical analysis: One way ANOVA with Dunnett's multiple comparison test. (n.t. = non-treated). *p<0.05, **p<0.01, ***p<0.001. Scale bar, 300 µm. (Published in (Oehrle, Burgstaller et al. 2015) *(in press) - modified*).

3.3 Molecular characterization of the invading fibroblast phenotype

3.3.1 Gene profile of the invasive fibroblast phenotype

To comprehensively characterize the invading fibroblast phenotype, not only by morphology but also on molecular levels, invading and non-invading MLg fibroblasts were separated by utilizing the established 3D collagen-based separation system described in section 3.1.2. Subsequently, differences in the gene profile were uncovered applying whole transcriptome analysis (Affymetrix Mouse Gene 1.0 ST arrays). Microarrays, gene clustering and initial data processing, and statistical analyses were performed by Dr. Martin Irmler (Institute of Experimental Genetics, Helmholtz-Zentrum München). Initially, microarrays were conducted after 72 and 96 hours of invasion. For quality control of the microarray performance, the ratio of the area under the curve (AUC) for a receiver operating characteristic curve (ROC) of detection of positive versus negative controls was determined. AUC ratios of all samples ranged between 0.91 and 0.95 and thus meet the required standard criteria. Data were normalized with RMA in standard settings including sketch quantile normalization. Genewise testing for differential expression was done employing the (limma) t-test and Benjamini-Hochberg multiple testing correction. Transcripts with a false discovery rate (FDR) lower than 10% were considered as statistically significant and thus used for analysis. The comparison of invading to non-invading fibroblast fractions, after 72 hours of invasion, revealed a signature of 1086 targets with expression ratios > 1.5-fold and 163 targets with differential expression ratios > 2-fold. After 96 hours of invasion, 1049 probes with a differential regulation of > 1.5-fold and 182 > 2-fold were found in the invading subpopulation (Figure 3.12 A).

To test for similarities between groups of the whole transcriptome replicate analysis, hierarchical clustering was performed with R scripts (hclust) and illustrated in a dendrogram. Effective clustering was validated for the arrays of non-treated (n.t.) MLg fibroblasts, conducted after 72 hours and 96 hours of invasion (72 h n.t. inv., 72 h n.t. non-inv., 96 h n.t. inv., 96 h n.t. non-inv.).

The two main clusters separated into invading and non-invading fibroblasts, while sub-clustering into the two different time-points (72 hours and 96 hours) (Figure 3.12B).

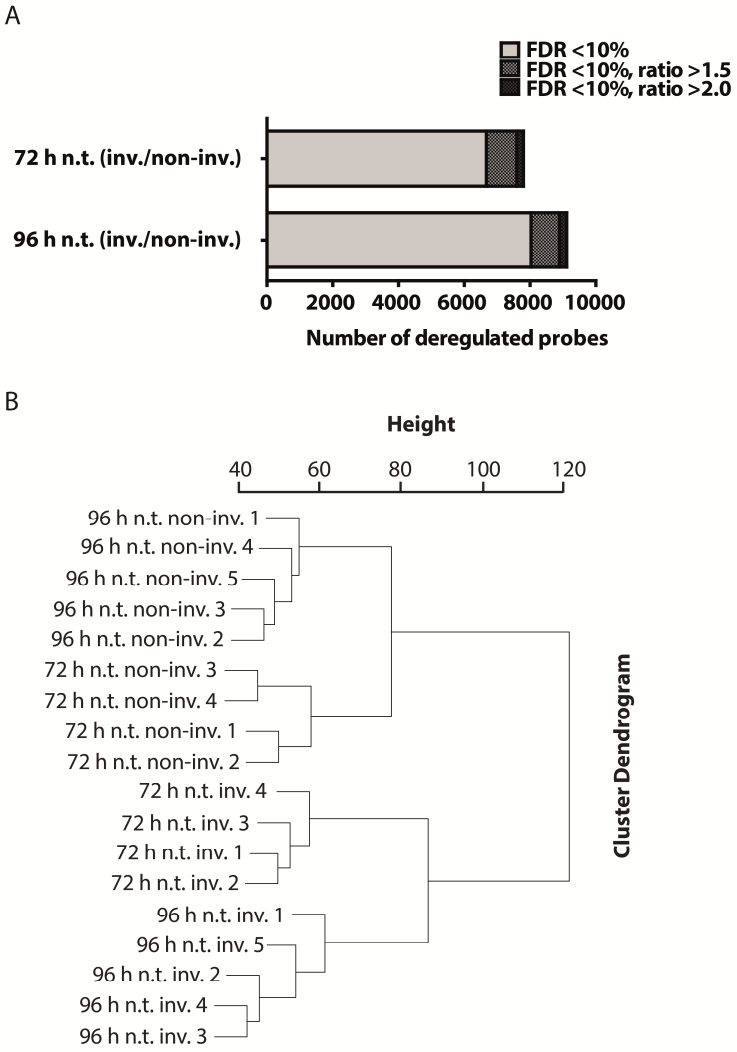

Figure 3.12: Differential gene expression numbers of conducted microarrays and hierarchical clustering.
Graphical representation of differentially expressed genes with a FDR < 10%. Genes that had an expression ratio of 1 <> 1.5 between invading (inv.) and non-invading (non-inv.) phenotypes are depicted in light grey. Probesets with a ratio of > 1.5 and > 2 are represented in dark grey and black, respectively **(A)**. Cluster dendrogram, conducted with R using the script hclust, on RMA data filtered for expression values higher than 100 in at least one sample reveals effective clustering of invading and non-invading fibroblasts at 72 and 96 hours **(B)**. Inv. = invading, non-inv. = non-invading. (Published in (Oehrle, Burgstaller et al. 2015) *(in press) - modified*).

For visualization of differentially regulated transcripts with expression ratio > 2-fold, heatmaps were generated with CARMAweb. Heatmaps of invasion signatures at 72 and 96 hours are depicted in Figure 3.13 A and B, respectively.

Probesets with transcript variations of > 1.5-fold upon invasion were further graphically represented by means of volcano plots (Figure 3.13 C and D). Of note, regulation of transcripts in both, up- and down-regulated groups, increased over time, with a concomitant rising statistical

significance. By literature research, both signatures were found to comprise transcripts, which are highly interesting in the context of fibroblast invasion and/or ILD and are described in detail in the text below (For complete gene expression lists see section 6.2 and GEO (GSE55322)).

For a more systematic approach on target selection, the invasion signatures at 72 and 96 hours were analyzed for correlating gene regulation. The invasion induced transcriptome signature was enriched for commonly regulated genes at 72 and 96 hours of invasion. In this comparative analysis approach, targets with a fold induction of > 1.5 fold were included. With a total number of 621 overlapping genes, 166 of which in the up- and 455 in the down-regulated group, the expression profiles of the invading fibroblasts at 72 hours and 96 hours were highly equal (Figure 3.14 A). This result verified reproducibility and robustness of the 3D collagen separation system and substantiated the invasion induced gene expression profile. By plotting logarithmical expression values of the gene profiles at 96 hours against 72 hours, overlapping genes were assigned. Of note, no target was found to be up-regulated in one and down-regulated in the other group, demonstrating a consistency between time-points (Figure 3.14 B).

Of interest, several proteins, involved in matrix degradation were differently regulated upon invasion. Overlapping up-regulated genes included Matrix metalloprotease (MMP) 13, which was the highest up-regulated transcript after 72 (4.5-fold) and 96 hours (9.4-fold) of invasion. Interestingly, besides MMP13, with MMP3 (4.0-fold / 72 hours; 7.6-fold / 96 hours) and MMP10 (2.8-fold / 72 hours; 3.4-fold / 96 hours), two further MMPs were found up-regulated in the invasion induced transcriptome signatures. In addition, the MMP inhibitor tissue inhibitor of metalloproteinases (Timp) 3 was significantly down-regulated in the invading fibroblast phenotype at 72 hours (1.7-fold) and 96 hours (1.6-fold). This finding indicates a pivotal role of matrix degradation in the profile of the invading fibroblast phenotype. Thus, likely ECM degradation assists in the process of fibroblast invasion.

Furthermore, Ectonucleotide Pyrophosphatase/Phosphodiesterase 2 (Enpp2), also named autotaxin, an enzyme recently reported as pathogenic contributor of IPF (Oikonomou, Mouratis et al. 2012), (Tager, LaCamera et al. 2008) was significantly up-regulated upon 72 (2.9-fold) and 96 hours (5.1-fold) of invasion.

Importantly, TGFβ1 was found to be significantly up-regulated in the invasion signature at 96 hours (3.3-fold). At 72 hours of invasion the up-regulation accounted 2.4-fold. With TGFβ1, the invasion induced transcriptome signature included one key mediator of fibrogenesis. Within this study, TGFβ1 was found to significantly induce fibroblast invasion in the established 3D collagen invasion assay (Figure 3.11 A).

With bone morphogenic protein 4 (BMP4), one further member of the TGFβ-superfamily was significantly differentially regulated upon invasion with a down-regulation of 3.7-fold (72 hours)

and 3.5-fold (96 hours). Strikingly, the inhibitor of BMP4 signaling, Gremlin 2 (Grem2), was found to be upregulated upon invasion with 1.6-fold at 72 hours and 2.4-fold at 96 hours.

Osteoglycin (Ogn), also called mimican, is one further TGFβ associated small proteoglycan that was consistently down-regulated at 72 and 96 hours of invasion with 4.5-fold and 3.7-fold, respectively.

Collagen invasion also affected, by a significant down-regulation of CTGF (connective tissue growth factor or CCN2) (2.0-fold at 72 hours and 2.4-fold at 96 hours), WISP1 (WNT1 inducible signaling pathway protein (WISP) 1) (1.6-fold / 72 hours and 1.6-fold / 96 hours), Cyr61 (cysteine-rich angiogenic protein 61 or CCN1) (2.0-fold / 72 hours and 1.9-fold / 96 hours) and an up-regulation of NOV (nephroblastoma overexpressed or CCN3) (1.7-fold / 72 hours and 2.7-fold / 96 hours) members of the matricellular protein cluster of CCN proteins, which in part has been recognized in fibrogenesis (Konigshoff, Kramer et al. 2009), (Kono, Nakamura et al. 2011), (Zhang, Li et al. 2014).

Intriguingly, Pten was significantly decreased by 2.9-fold in the invasion induced transcriptome signature at 72 hours and 3.3-fold at 96 hours. These reduced expression levels of Pten were considered as an important corroborative finding for the invasion signature, as a loss of function for Pten is widely associated with fibrosis, cancer, and cellular invasion (White, Thannickal et al. 2003), (Tamura, Gu et al. 1998).

Secreted frizzled-related protein 1 (Sfrp1) is one further remarkable target found in the present study on the invading fibroblast phenotype in lung disease. Sfrp1, which acts mainly as inhibitor of canonical and non-canonical Wnt-signaling pathways, was found to be strongly down-regulated upon invasion with 2.7-fold at 72 hours and 2.1-fold at 96 hours.

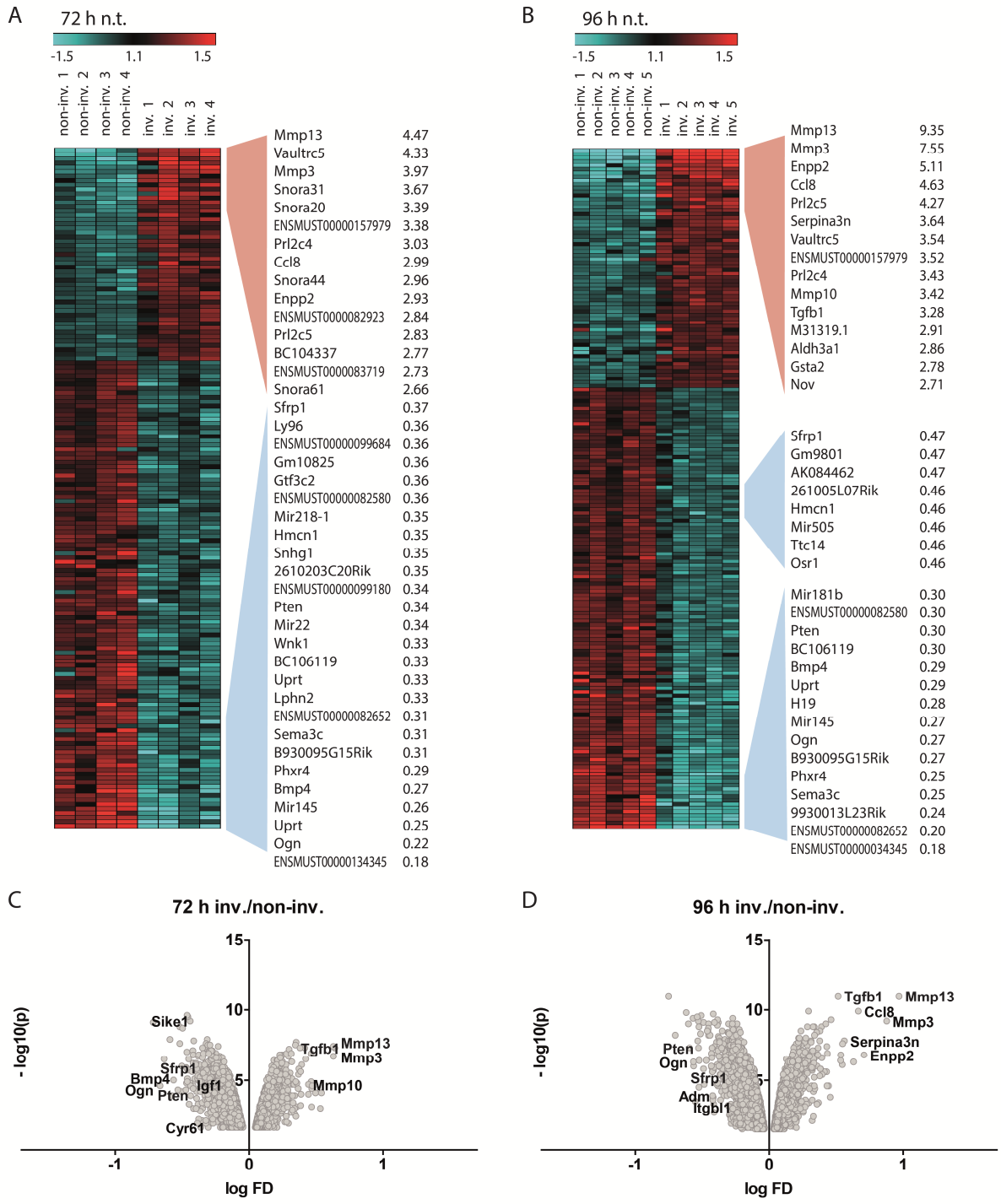

Figure 3.13: Heatmaps and Volcano plots for transcript expression of the invasion signatures at 72 and 96 hours. Separation and RNA extraction of invading (inv.) and non-invading (non-inv.) cell fractions was accomplished 72 **(A)** and 96 hours **(B)** after initial plating. The presented heatmaps depict the top > 2-fold differentially regulated targets found in the microarray analyses (Affymetrix Mouse Gene 1.0 ST array). High and low expressed targets of the inv. compared to non-inv. cell fraction are illustrated in the heatmaps in red and blue, respectively. Each column represents one independent experiment. Expression profile of fibroblast invasion at 72 hours **(C)** and 96 hours of > 1.5-fold regulated targets **(D)**. P-values are plotted against fold-difference (FD) values in a logarithmic scale. n.t. = non-treated, inv. = invading, non-inv. = non-invading. (Published in (Oehrle, Burgstaller et al. 2015) *(in press) - modified*).

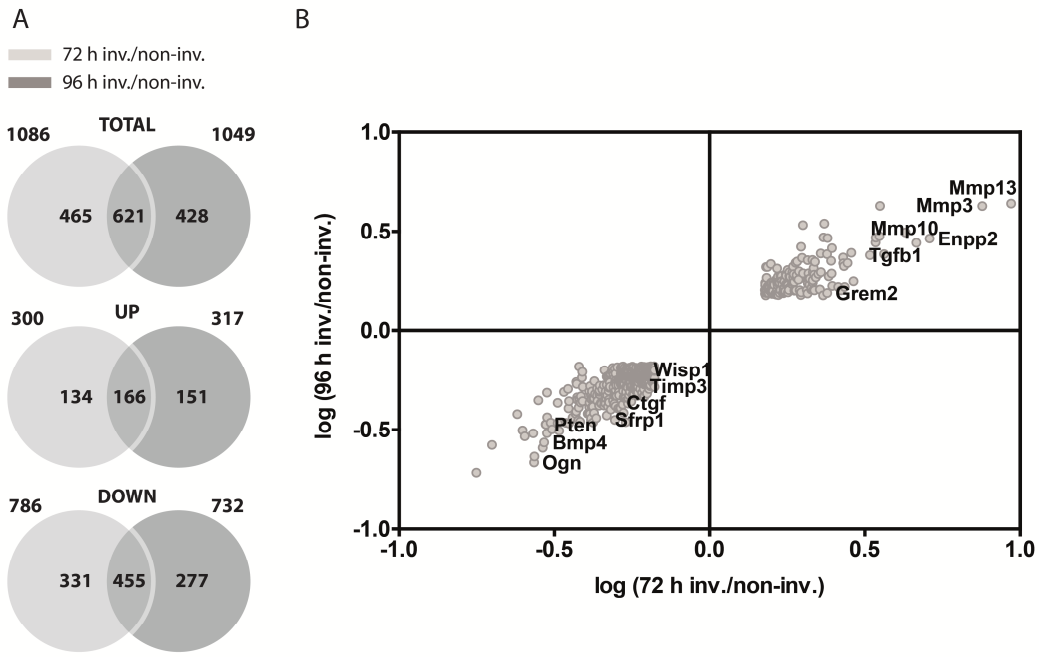

Figure 3.14: Overlap of gene expression in the conducted transcriptome analyses at 72 and 96 hours.
The expression overlap is depicted in Venn diagrams comparing expression ratios of invading (inv.) and non-invading (non-inv.) fibroblasts at 72 and 96 hours of invasion. The overlap accounted 621 probesets; 166 in the up-, and 455 in the down-regulated group **(A)**. Dotplot, representing gene expression ratios at 96 hours against 72 hours in a logarithmic scale **(B)**. Targets, associated with invasion/ILD are highlighted in the dotplot by their name. Inv. = invading, non-inv. = non-invading. (Figure A published in (Oehrle, Burgstaller et al. 2015) *(in press) - modified*).

To narrow down promising targets, the overlapping signature of fibroblast invasion was analyzed in detail with the Ingenuity® Pathway Analysis (IPA) software. Heatmaps were generated for the ten most significantly over-represented "disease processes" and "biological function" by using the transcript profiles with fold induction of > 1.5 for both time-points. Strikingly, the clusters "invasion of cells", "idiopathic pulmonary fibrosis", and "metastasis" were most significantly affected upon 72 and 96 hours of invasion. This finding once more validated the significance of the generated transcriptome signature and implied a role of the invasion profile in disease.

From the top three enriched clusters, "invasion of cells", "idiopathic pulmonary fibrosis", and "metastasis" underlying molecular networks were generated. Importantly, from the most significantly regulated transcripts, described in Figure 3.14 B, TGFβ1, MMP13, MMP3, Grem2, Enpp2, Bmp4, Pten, and Sfrp1 appeared in the generated network. TGFβ1 was identified as being connected with all three clusters. Additionally, MMP3, MMP9, Pten, BMP4, and ENPP2 were associated with both "invasion of cells" and "metastasis". A cluster of micro RNA precursors, including miR-10, miR-130, miR-143, miR-145, miR-181*, and let-7 was found to be down-

regulated in the invasion signature. These miRNAs were either linked to “metastasis”, “invasion of cells”, and/or “idiopathic pulmonary fibrosis” (Figure 3.15).

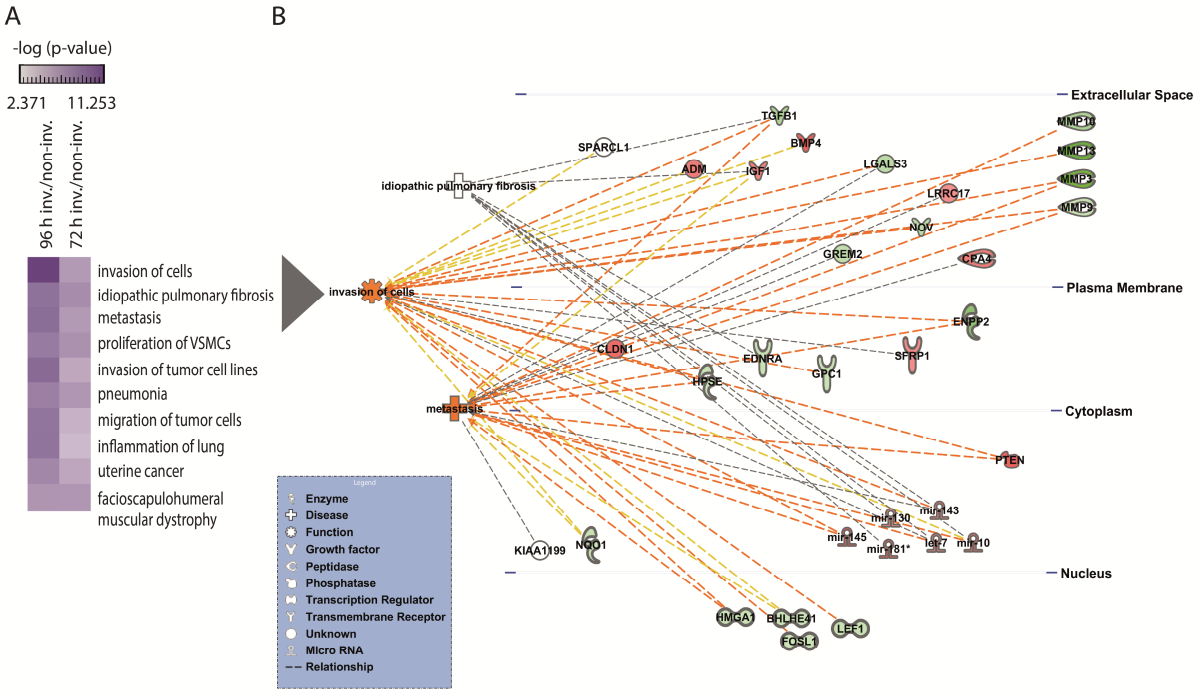

Figure 3.15: Analysis of functional gene cluster enrichment in the invasion induced transcriptome signature with the Ingenuity® pathway analysis platform (IPA).
The ten most significantly over-represented “disease processes” and “biological function” are represented in a heatmap. Of note, the clusters “invasion of cells”, “idiopathic pulmonary fibrosis”, and “metastasis” were found to be most significantly enriched in the invasion induced transcriptome signature **(A)**. From the top three enriched clusters, “invasion of cells”, “idiopathic pulmonary fibrosis” and “metastasis” underlying molecular networks were generated. Targets, significantly up-, or down-regulated in the invading fibroblast phenotype are represented in green and red, respectively. Dashed orange lines illustrate activating relationships, yellow lines findings that are inconsistent with the state of downstream molecules, and grey lines that the mode of effect is not defined **(B)**. (Published in (Oehrle, Burgstaller et al. 2015) *(in press).*

3.3.2 Identification of TGFβ1-mediated transcriptomic invasion signature

With TGFβ1, one pro-invasive regulator was identified in the overlapping fibroblast invasion transcriptome signature. As this target is of particular interest in the context of ILD and was linked to the clusters “invasion of cells”, “idiopathic pulmonary fibrosis”, and “metastasis” in the generated networks presented in section 3.3.1 (Figure 3.15), the gene expression pattern of TGFβ1-modulated fibroblast invasion was profiled next.

Invasion of MLg lung fibroblasts was induced by TGFβ1 (5 ng/ml) stimulation in the 3D separation system, 24 hours after plating. After 72 hours, the invading fibroblast subpopulations were separated from the non-invading and RNA probed by whole transcriptome analysis. Microarrays and data processing were performed under equal terms as described in 3.3.1 (collaboration with Dr. Martin Irmler from the Institute of Experimental Genetics, Helmholtz-Zentrum München).

Within the invading and non-invading fibroblast fractions, gene expression induced by TGFβ1 treatment was revealed by comparing the gene profile of TGFβ1-treated to non-treated controls. In the non-invading fraction 1013 probesets were significantly regulated upon TGFβ1 treatment with a fold-change of > 1.5 and 310 with a fold-change of > 2. In the invading fibroblast fraction, 679 probesets with expression ratios of >1.5-fold and 202 with expression ratios of > 2-fold, were differentially expressed between treatment groups (Figure 3.16 A). Hierarchical clustering, as illustrated in a dedrogram generated with R scripts (hclust), revealed that array data mainly clustered in invading and non-invading groups and subdivided into non-treated and TGFβ1-treated on the second hierarchical level. Of note, two samples (96 h TGFβ1 non-inv. 5 and 96 h TGFβ1 inv. 5) were identified as outliers and excluded from further analyses (Figure 3.16 B).

The TGFβ1-induced gene expression profile in the invading fibroblast fraction was of particular interest and was used in the subsequent experiments to more precisely define the molecular basis of fibroblast invasion in the context of ILD.

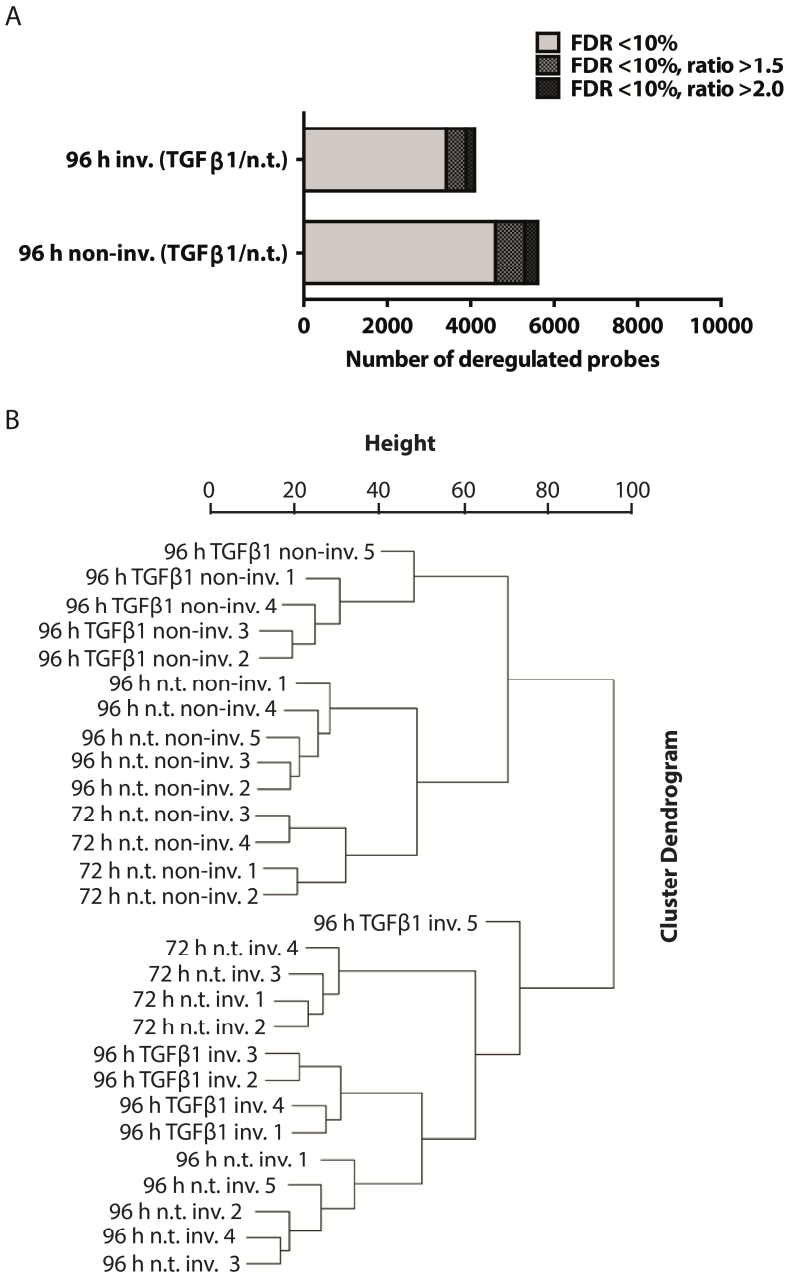

Figure 3.16: Differential gene expression numbers of conducted microarrays (TGFβ1-treated groups) and hierarchical clustering.

Graphical representation of differentially expressed genes with a FDR < 10%. Genes that had an expression ratio of 1 - 1.5 between invading (inv.) and non-invading (non-inv.) or non-treated (n.t.) and TGFβ1-treated are depicted in light grey. Probesets with a ratio of > 1.5 and > 2 are represented in dark grey and black, respectively **(A)**. Cluster dendrogram, conducted with R using the script hclust, on RMA data filtered for expression values higher than 100 in at least one sample. Two samples (96 h TGFβ1 non-inv. 5 and 96 h TGFβ1 inv. 5) were identified as outliers and excluded from further analyses **(B)**. n.t. = non-treated; inv. = invading, non-inv. = non-invading.

For a complete description of TGFβ1-induced transcript variations two heatmaps were created for differentially regulated transcripts with expression ratio > 2-fold. First, for the non-invading group, the TGFβ1-induced gene profile was compared to the gene profile of the non-treated control group (Figure 3.17 A). Secondly, for the invading fibroblast fraction, TGFβ1 and non-treated groups were compared (Figure 3.17 B).

Comparing microarrays of non-invading TGFβ1-stimulated (5 ng/ml) with non-invading untreated fibroblasts, C1q and tumor necrosis factor related protein 3 (C1qtnf3) was found to be the highest up-regulated transcript (34.7-fold), as shown in the heatmap of Figure 3.17 A. Focusing on the group of genes associated with matrix degradation, Disintegrin and Metalloproteinase domain-containing protein 12 (Adam12) and Metallopeptidase with Thrombospondin Type 1 Motif, 16 (Adamts16) were significantly up-regulated upon TGFβ1 treatment with 5.4-, and 4.3-fold, respectively. In the group of significantly down-regulated targets, with Bmp4 (8.3-fold), Ogn (6.7-fold), and Sfrp1 (2.0-fold) targets associated with the invasion signature were identified.

Of interest, in line with the generated heatmap of non-invading TGFβ1-stimulated versus non-invading untreated fibroblasts, comparison of invading TGFβ1-stimulated with invading untreated fibroblasts revealed C1qtnf3 as most highly up-regulated target (12.0-fold) (Figure 3.17 B). Mmp12 was furthermore significantly up-regulated (3.3-fold) and Ogn down-regulated (4.4-fold) in the invading fibroblast fraction upon TGFβ1 stimulation. Unexpectedly, Enpp2, one target found to be significantly up-regulated in the invasion signature, was highly down-regulated in the TGFβ1-treated invading cells (7.1-fold).

For an extended analysis on TGFβ1-induced gene regulation in invading and non-invading fibroblast phenotypes, volcano plots were generated for transcription profiles with > 1.5-fold induction. In the invading compared to non-invading TGFβ1-treated transcript profile, TGFβ1 (1.9-fold), Enpp2 (1.8-fold), and Ogn (2.4-fold) were identified (Figure 3.18 A).

In the analysis of invading TGFβ1-treated compared to non-treated fibroblasts, Sfrp1 was one target identified to be significantly down-regulated in the invading fibroblast phenotype upon stimulation (1.5-fold).

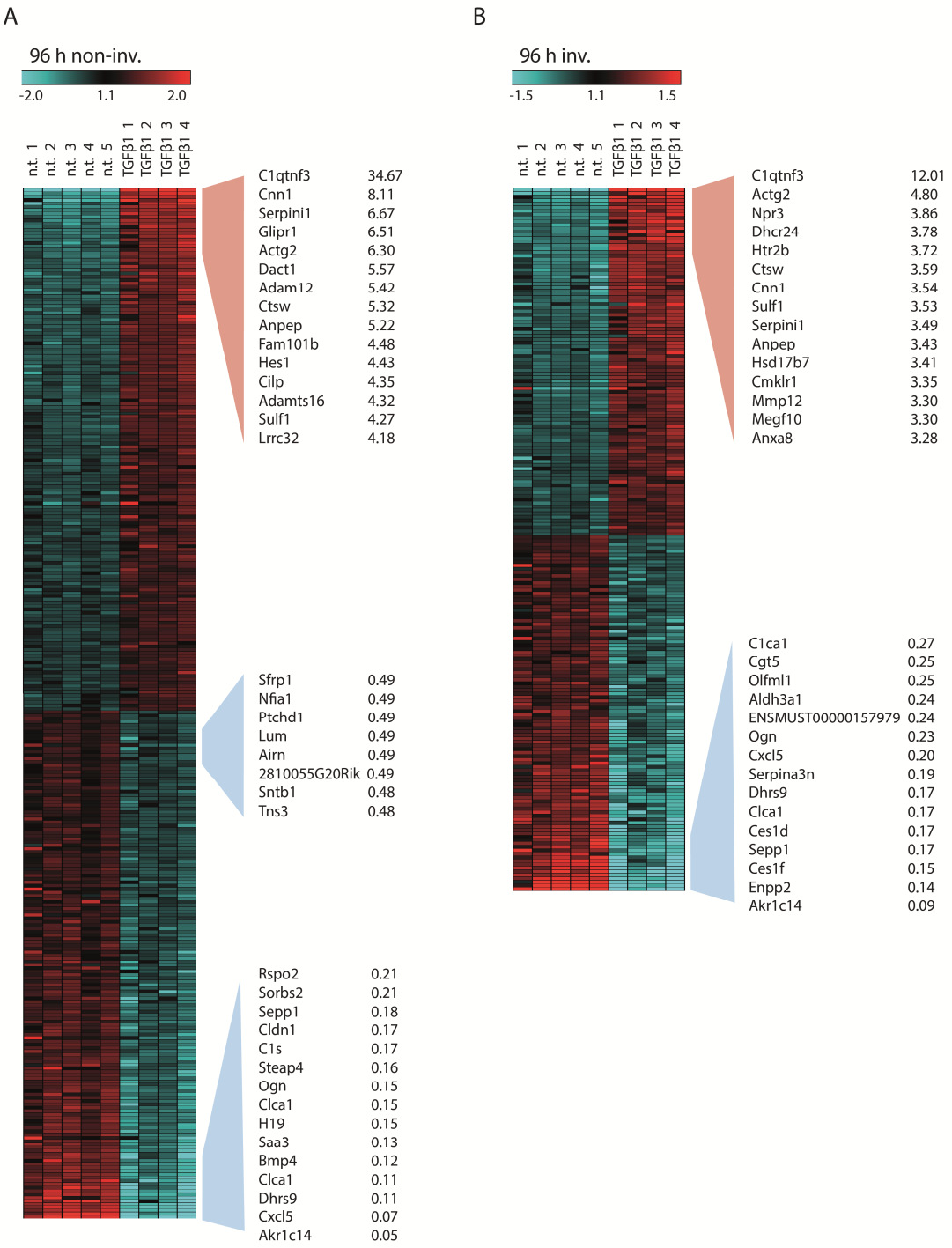

Figure 3.17: Heatmaps visualizing differential gene expression of TGFβ1-treated compared to non-treated non-invading and invading fibroblasts.
Heatmap representing differential gene expression (> 2-fold) of non-invading (non-inv.) and non-treated compared to non-inv. TGFβ1-treated fibroblasts at 96 hours of invasion and 72 hours of treatment, respectively **(A)**. Differential TGFβ1-induced gene expression (> 2-fold) in invading (inv.) fibroblast subpopulation **(B)**. High and low expressed probesets of the inv. compared to non-inv. cell fraction are illustrated in the heatmaps in red and blue, respectively. Each column represents one independent experiment. Inv. = invading, non-inv. = non-invading.

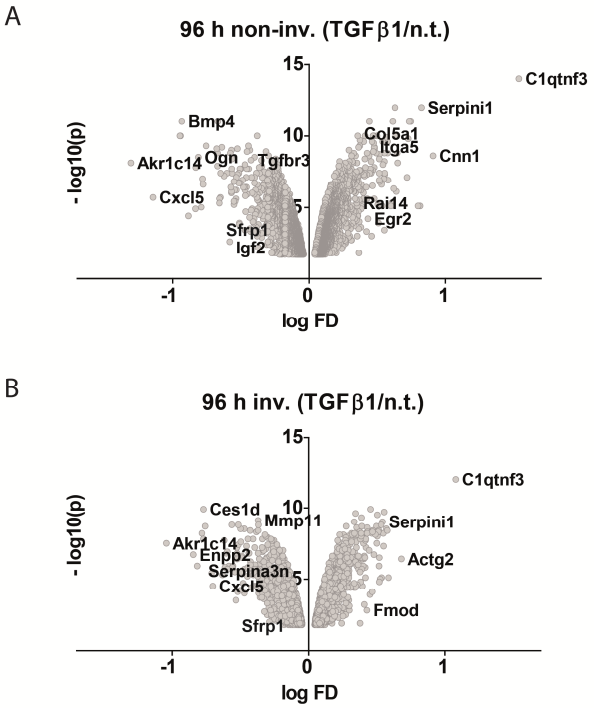

Figure 3.18: Volcano plots for TGFβ1-induced variation in transcript expression levels.
Volcano plots representing logarithmic gene expression ratios of TGFβ1-treated compared to n.t. fibroblasts at 96 hours. P-values are plotted against fold-difference (FD) values in a logarithmic scale. TGFβ1-induced (5 ng/ml) changes in expression levels in non-invading (non-inv) **(A)** and invading (inv) **(B)** MLg fibroblast. Inv. = invading, non-inv. = non-invading.

Subsequently, in order to further enrich the invasion transcriptome signature, the expression profile of invading fibroblasts was compared with the identified signature of TGFβ1-induced invasion. With that, the focus was set on genes that were both, regulated by TGFβ1 and related to the invading capacity of the cells. In total, 193 targets were found in the overlap of invading compared to non-invading and invading TGFβ1-treated compared to untreated profiles with > 1.5-fold induction. This overlap itemized in 27 consistently up-, and 40 down-regulated transcripts (Figure 3.19 A). Thus 129 probesets were inversely regulated between groups, as depicted in clear circles in Figure 3.19 B. As targets of interest in the context of fibroblast invasion were considered those, which showed aligned regulation between groups, as depicted in grey circles in Figure 3.19 B. Consequently, these targets were represented in the heatmap shown in Figure 3.21 B.

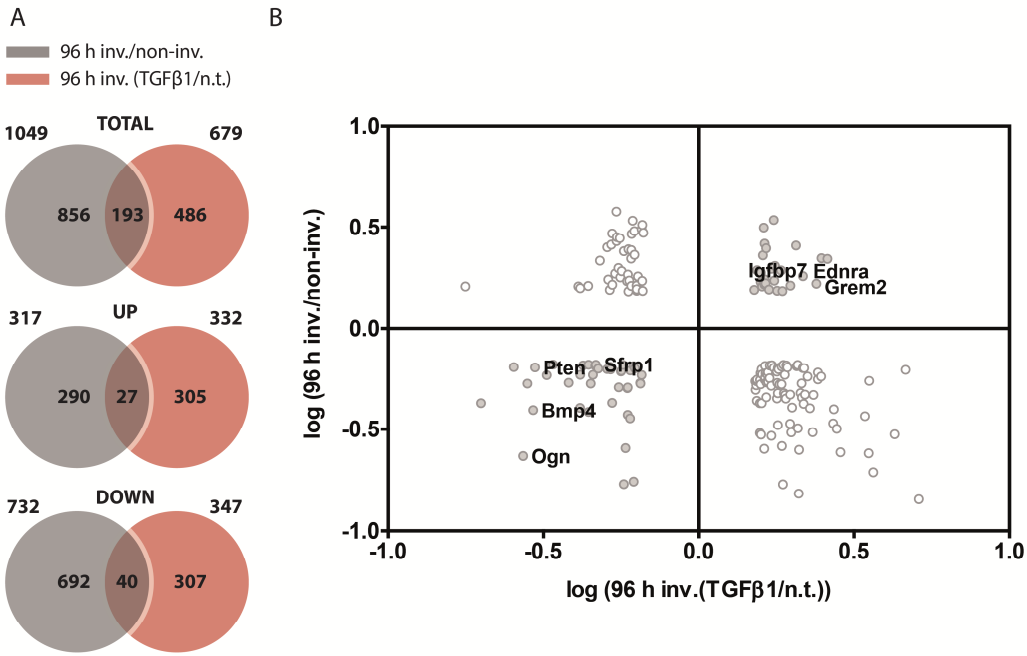

Figure 3.19 Overlap of gene expression in the conducted transcriptome analyses at 96 hours invading/non-invading with invading TGFβ1/non-treated.
The expression overlap is depicted in Venn diagrams comparing expression ratios of invading (inv.) and non-invading (non-inv.) fibroblasts at 96 hours with TGFβ1-treated and non-treated (n.t.) inv. fibroblasts. The overlap accounted 193 probesets; 27 equally regulated in the up-, and 40 in the down-regulated group **(A)**. Dotplot representing logarithmic gene expression ratios of inv. compared to non-inv. fibroblasts against TGFβ1-treated/ n.t. fibroblasts at 96 hours **(B)**. Clear circles: targets, with opposing regulation between groups. Grey circles: Targets, consistently up-, or down-regulated in both groups. Inv. = invading, non-inv. = non-invading.

The overlapping signature of targets, regulated upon invasion and in the invading subpopulation by TGFβ1 stimulation, was designated as TGFβ1-mediated transcriptomic invasion signature. IPA analysis revealed that both groups showed gene cluster enrichments in invasion, morphogenesis, and carcinogenesis-related pathways (Figure 3.20). The heatmap of the TGFβ1-mediated transcriptomic invasion signature revealed among others, Grem2 (2.4-, 1.7-fold up-regulated), Bmp4 (3.5-, 2.6-fold down-regulated), Ogn (3.7-, 4.4-fold down-regulated), Pten (3.3-, 1.6-fold down-regulated), and Sfrp1 (2.1-, 1.5-fold down-regulated) as invasion critical targets (Figure 3.20).

Taken together these data provide for the first time a detailed description of invasion induced gene regulation in fibroblasts with the extension to TGFβ1-mediated invasion.

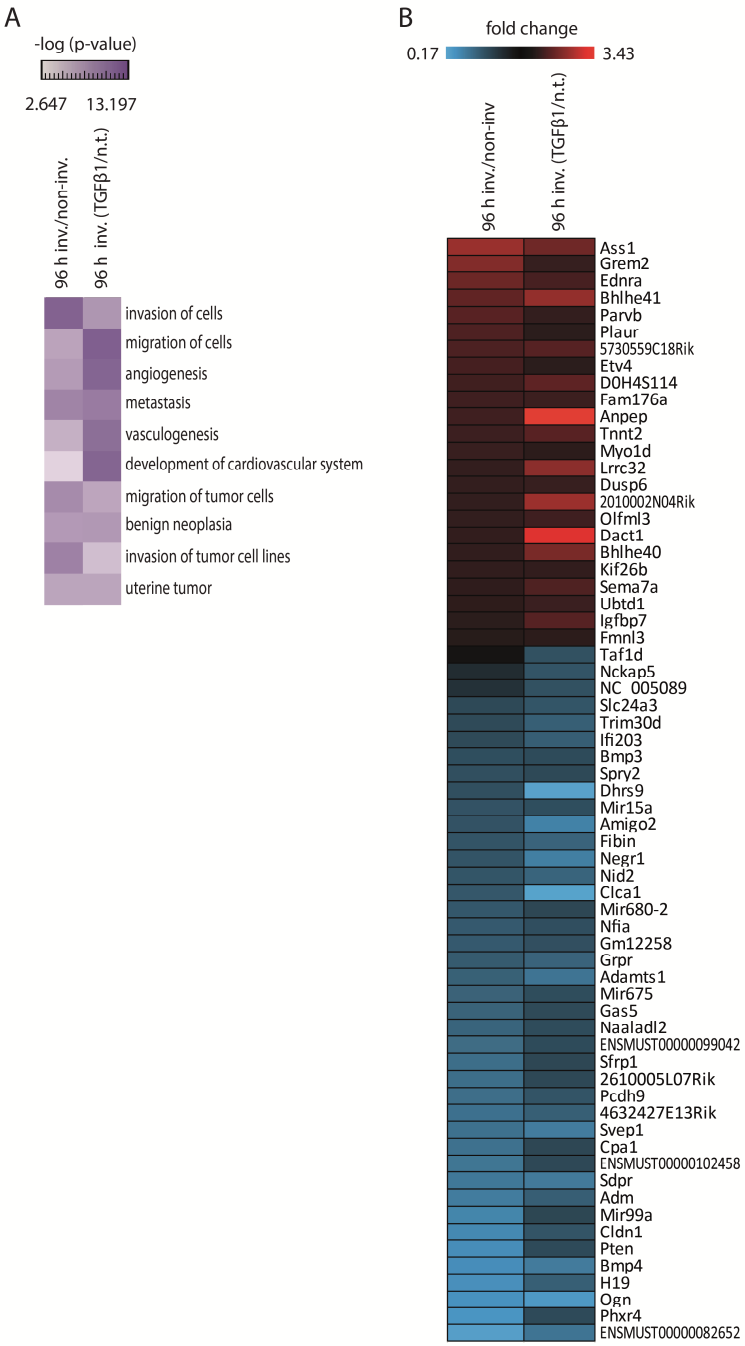

Figure 3.20: Heatmaps of the TGFβ1-mediated transcriptomic invasion signature.
The 10 most significantly over-represented "disease processes" and "biological functions" in inv. compared to non-inv. fibroblasts, and inv. TGFβ1-treated (5 ng/ml) compared to non-treated (n.t.) fibroblasts at 96 hours are represented in a heatmap. These "disease processes" and "biological functions" include "invasion of cells", "migration of cells", and "metastasis" **(A)**. TGFβ1-mediated transcriptomic invasion signature depicted as heatmap of the consistently up- and down-regulated genes in the analyzed overlap of inv. compared to non-inv. fibroblasts, and inv. TGFβ1-treated (5 ng/ml) compared to n.t. fibroblasts. Low and high expressed targets in the heatmap are depicted in blue and red, respectively **(B).** Inv. = invading, non-inv. = non-invading.

3.3.3 Gene array verification

The gene expression profiling approach, presented in section 3.3.1, was validated by confirmative expression analysis using qRT-PCR, surveying expression changes of several invasion-associated target genes: MMP13 (Lederle, Hartenstein et al. 2010), (Sabeh, Li et al. 2009), TGFβ1 (Zolak, Jagirdar et al. 2013), Caveolin 1 (Cav1) (Lino Cardenas, Henaoui et al. 2013), and Phosphatase and Tensin Homolog (Pten) (White, Thannickal et al. 2003). Control qRT-PCR analysis was performed for all microarrays and is exemplified for the 96 hour samples in Figure 3.21. Whole transcriptome analysis revealed an induction of 9.4-fold for MMP13 ($p = 8.2x10^{-8}$), 3.3-fold for TGFβ1 ($p = 8.2x10^{-8}$), and a reduction of 1.3-fold for Cav1 ($p = 2.3x10^{-2}$) and Pten 3.3-fold ($p = 1.1x10^{-5}$) in the invading fibroblasts 96 hours after plating (Figure 3.21 A). Accordingly, in the qRT-PCR data MMP13 and TGFβ1 were found significantly higher expressed in the invading fibroblast subpopulation with 6.02- and 1.85-fold induction, respectively. Furthermore, Cav1 was significantly down-regulated by 3.48-fold and Pten by 2.61-fold (Figure 3.21 B), corroborating the microarray data. Thus, the qRT-PCR data confirmed the robustness of the applied microarray analysis and validated the described fibroblast invasion transcriptome signature.

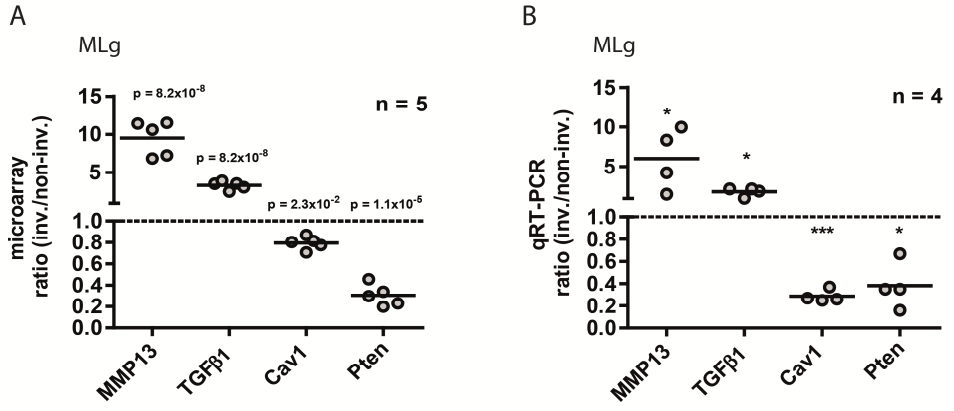

Figure 3.21: Validation of transcriptome analysis for selected invasion-associated genes.
Separation of MLg fibroblasts was accomplished at 96 hours of invasion and selected invasion-associated genes (MMP13, TGFβ1, Cav1, and Pten) were probed. Original microarray data for five independent experiments. Data are represented with Benjamini-Hochberg (BH)-adjusted p-values. Genewise testing for differential expression was done employing the limma t-test and Benjamini-Hochberg multiple testing correction (FDR < 10%) **(A)**. Confirmative qRT-PCR analysis **(B)** of the selected group of genes (n = 4). Data are represented with p-values. Inv. = invading, non-inv. = non-invading. Statistical analysis: paired t-test *p<0.05 and ***p<0.001. (Published in (Oehrle, Burgstaller et al. 2015) *(in press) - modified*).

In a next step, regulation of two of the chosen invasion-associated transcripts, MMP13 and Cav1 in the invading fibroblasts was analyzed on protein level. Protein samples extracted from invading

and non-invading fibroblasts after physical separation were probed by immunoblotting. While MMP13 was strongly up-regulated in the invading fibroblast phenotype, Cav1 expression was negatively affected as shown in Figure 3.22. Consequently, protein expression data went in line with mRNA expression as revealed by microarray and qRT-PCR analysis (Figure 3.21).

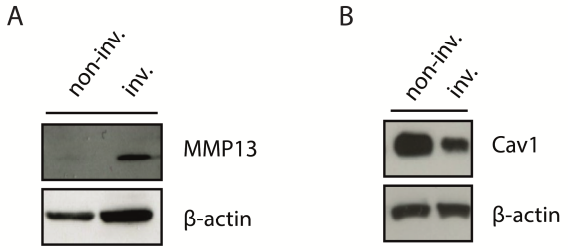

Figure 3.22: MMP13 and Cav1 protein expression in invading MLg fibroblasts.
Representative immunoblots illustrating up-regulation of MMP13 **(A)** and down-regulation of Cav1 **(B)** in invading mouse lung fibroblasts. Inv. = invading, non-inv. = non-invading. (Figure A published in (Burgstaller, Oehrle et al. 2013)- *modified*), Figure B published in (Oehrle, Burgstaller et al. 2015) *(in press)*).

To rule out any cell line (MLg) restricted effects and to validate the results from murine in human cells, separation and subsequent analysis of the chosen targets on mRNA level was performed for primary human lung fibroblasts (phF). Corroborating the findings in MLg fibroblasts, MMP13 and TGFβ1 were up-regulated on mRNA level upon invasion, with 2.26-fold and 1.14-fold, respectively (Figure 3.20). Additionally, Cav1 was 2.42-fold and Pten 3.17-fold down-regulated in invading phF. In conclusion, selected invasion relevant target genes were uniformly differentially regulated in murine and human fibroblasts upon invasion.

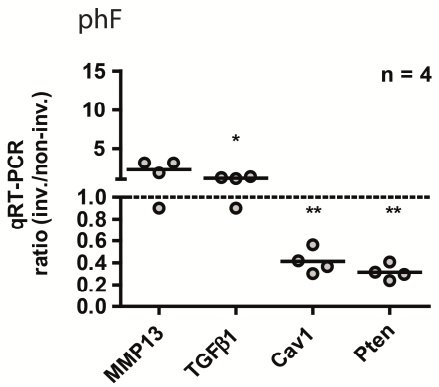

Figure 3.23: Expression of invasion-associated target genes in invading phF.
qRT-PCR analysis of invading (inv.) compared to non-invading (non-inv.) fibroblasts after 96 hours of invasion. Data are represented as mean values from four independent experiments (n = 4). Inv. = invading, non-inv. = non-invading. Statistical analysis: paired t-test *p<0.05 and **p<0.01. published in (Oehrle, Burgstaller et al. 2015) *(in press)* - *modified*).

3.4 Secreted frizzled-related protein 1 (Sfrp1)

In search of novel potential regulators of fibroblasts invasion, by applying a systematic comparative analysis of invasion of transcriptomic profiles (section 3.3.1 - 3.3.2) Sfrp1 emerged as an interesting target for in-depth functional analysis. Sfrp1 belongs to a family of secreted glycoproteins that triggers Wnt-signaling cascades by binding to Wnt ligands or Frizzled receptors (Esteve and Bovolenta 2010). Thereby, Sfrps act inhibitory on the Wnt-signaling pathways that potentially play an important role in IPF pathogenesis (Konigshoff, Kramer et al. 2009) (Vuga, Ben-Yehudah et al. 2009).

As part of the present study, the role of Sfrp1 expression in the context of fibroblast invasion and interstitial lung disease was investigated.

3.4.1 Sfrp1 within the molecular signature of invading fibroblasts

The resulting invasion-related expression signature (section 3.3.2) was screened for functional targets and novel regulators of fibroblast invasion. In this process, Sfrp1 was identified to be uniformly down-regulated after both, 72 and 96 hours of invasion as well as in the TGFβ1-induced invasion signature. Down-regulation of Sfrp1 in invading MLg fibroblasts was first verified on mRNA and protein level. With a mean ddCt-value of 1.23 (≡ 2.35-fold) between invading and non-invading cells, Sfrp1 mRNA expression was significantly reduced upon invasion (Figure 3.24 A). To verify this on protein level, immunoblot analysis demonstrated a strong Sfrp1 protein down-regulation in the invading MLg fibroblasts (Figure 3.24 B). Thereupon, together with the microarray data reduced Sfrp1 levels were considered as a consistent feature of the molecular signature of invading lung fibroblasts.

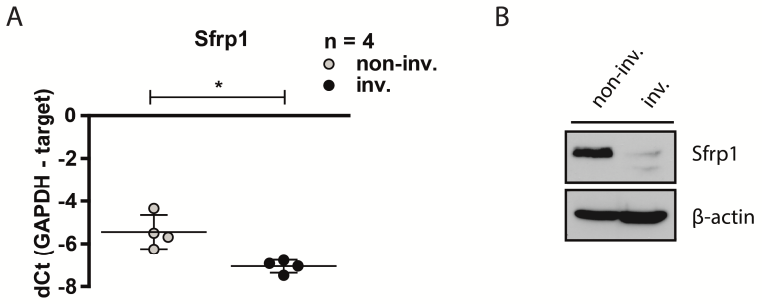

Figure 3.24: Sfrp1 expression in invading MLg fibroblasts.
Sfrp1 transcript levels are significantly reduced in invading compared to non-invading MLg fibroblasts, as revealed by qRT-PCR of four independent experiments (n = 4) **(A)**. Data are shown as dCt-values in relation to GAPDH. Down-regulation of Sfrp1 on protein level was confirmed by immunoblotting **(B)**. Inv = invading, non-inv. = non-invading. Statistical analysis: paired t-test *p<0.05. Published in (Oehrle, Burgstaller et al. 2015) *(in press) - modified*).

Sfrp1 belongs to the family of secreted frizzled-related proteins that consist of five members namely Sfrp1, Sfrp2, Frzb (Sfrp3), Sfrp4, and Sfrp5. To investigate specificity of Sfrp1 down-regulation, gene expression data sets were scanned for all members of the Sfrp family. In the microarray data at 96 hours, Sfrp1 showed a significant decrease during invasion from 1268.0 ± 239.1 relative fluorescence units (RFU) in non-invading to 592.0 ± 125.7 RFU in invading MLg fibroblasts. Expression levels of Sfrp2 thru Sfrp5 however, were near the lower detection limit and with exception of Frzb not substantially affected by invasion. Expression of Frzb was significantly increased in the process of invasion from 31.80 ± 2.05 RFU to 34.60 ± 0.89 RFU (Figure 3.25).

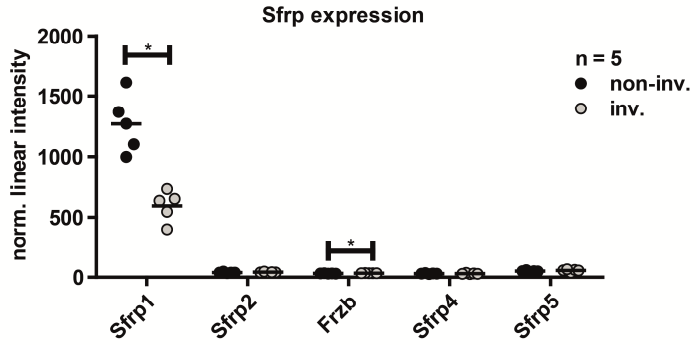

Figure 3.25: Transcript levels of Sfrp isoforms.
Various expression levels of the Sfrp isoforms Sfrp1-5 in Affymetrix Mouse Gene 1.0 ST array data set at 96 hours. Data are represented as mean linear relative fluorescence units (RFU) from five independent experiments (n = 5). Inv. = invading, non-inv. = non-invading. Statistical analysis: paired t-test. *p<0.05.

To verify down-regulation of Sfrp1 in a disease-related context, differential expression of Sfrp1 in response to invasion was further investigated in patient-derived fibroblasts. On transcript levels, Sfrp1 was significantly down-regulated in the invading fraction of fibroblast lines isolated from eight different patient-derived lung biopsy samples, with a mean ddCt value of 2.44 (≡ 5.43-fold) (Figure 3.26 A). Sfrp1 expression on protein level was investigated in three different patient lines (P1, P2, P3) by immunoblot analysis (Figure 3.26 B). These data confirmed the differential expression of Sfrp1 upon 3D collagen invasion found in MLg fibroblasts.

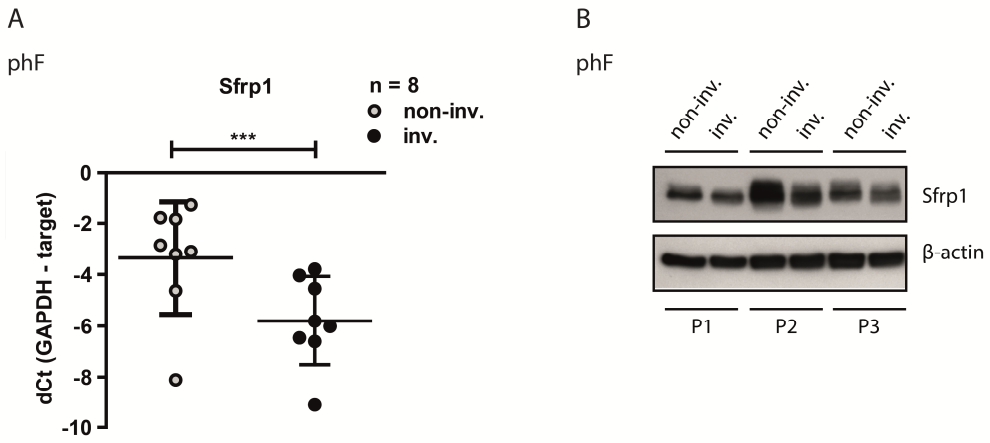

Figure 3.26: Differential expression of Sfrp1 in phF upon invasion.
phF show a significant down-regulation of Sfrp1 transcript levels upon invasion (96 hours), as detected in eight different fibroblast lines derived from lung biopsies/explants (n = 8) **(A)**. Three phF lines were probed with Western blot analysis (n = 3) and a strong reduction of Sfrp1 expression was detected in the invading (inv.) compared to non-invading (non-inv.) subpopulation (**B**). (P = patient). Statistical analysis: paired t-test. ***p<0.001.

3.4.2 Growth factor induced regulation of Sfrp1

Due to the fact that Sfrp1 was identified in the inherent and the TGFβ1-induced transcriptomic invasion signature, it was hypothesized that Sfrp1 might function as an initial trigger for fibroblast invasion. To address this hypothesis, the regulation of Sfrp1 expression by TGFβ1 was analyzed in more detail. Besides TGFβ1, EGF was identified as a pro-invasive growth factor (Figure 3.11) and therefore included in the studies on growth factor regulated Sfrp1 expression dynamics. MLg fibroblasts were cultured for 4, 8 and 24 hours in conventional 2D plastic dishes in the presence or absence of TGFβ1 (5 ng/ml) or EGF (50 ng/ml). The Sfrp1 expression was monitored on mRNA level by qRT-PCR. Sfrp1 transcripts were significantly down-regulated 24 hours after treatment with TGFβ1 (ddCt value of -1.79 ≡ 3.45-fold) and EGF (ddCt value of -2.43 ≡ 5.38-fold) (Figure 3.27).

As Sfrp1 transcript levels were gradually reduced over time in MLg fibroblasts after stimulation with TGFβ1 (5 ng/ml) and EGF (50 ng/ml), the correlation on protein level was analyzed next. Using Enzyme-linked immunosorbent assays (ELISAs), the amount of secreted Sfrp1 was determined in the fibroblasts' supernatants. Baseline secretion ranged at 326.13 ± 133.48 pg/ml and was significantly lowered to 44.81 ± 27.88% and 34.24 ± 22.89% 24 hours after TGFβ1 and EGF stimulation, respectively. In the total cell lysate, Sfrp1 expression was substantially reduced. Coinciding with the mRNA data, down-regulation of Sfrp1 on protein level occurred earlier in response to EGF than to TGFβ1. Three independent experiments demonstrated

that Sfrp1 expression in the EGF-treated fibroblasts was reduced 8 hours after stimulation, whereas TGFβ1-treated fibroblasts lagged behind showing first signs of reduced protein expression after 48 hours of treatment (Figure 3.28 B). The more efficient Sfrp1 down-regulation upon EGF than TGFβ1 treatment might be reflected in the higher pro-invasive efficiency of EGF compared to TGFβ1 as shown in Figure 3.11

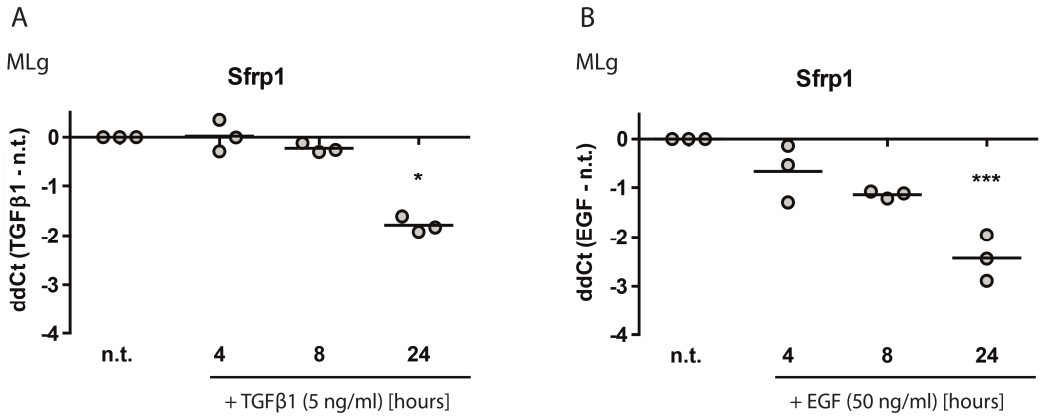

Figure 3.27: Down-regulation of Sfrp1 transcript upon TGFβ1 and EGF stimulation.
Dynamics of TGFβ1-, (5 ng/ml) **(A)** and EGF (50 ng/ml) -induced **(B)** Sfrp1 down-regulation on mRNA level. Data are shown as ddCt-values of three independent (n =3) experiments at the indicated time-points. Statistical analysis: One way ANOVA with Dunnett's multiple comparison test. (n.t. = non-treated). *p<0.05, ***p<0.001.

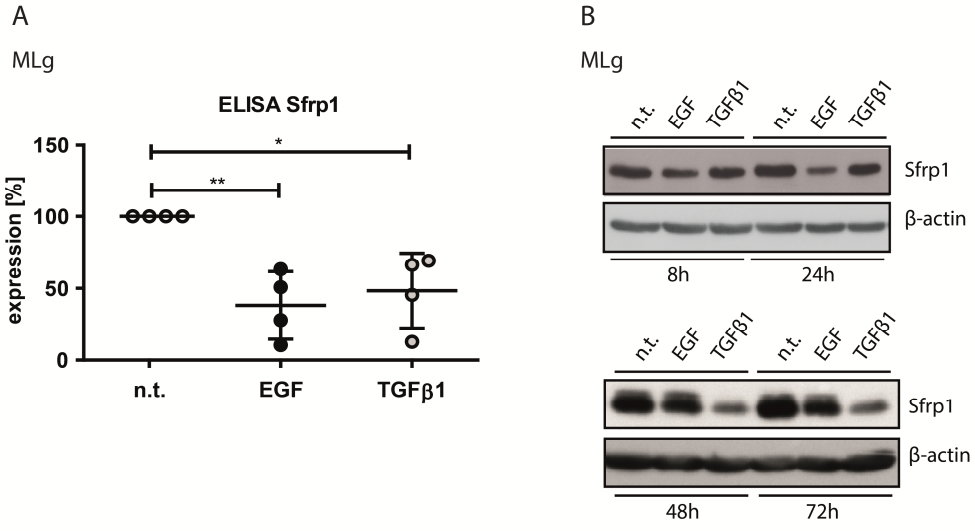

Figure 3.28: TGFβ1 and EGF induced reduction of Sfrp1 protein expression.
Significant reduction of secreted Sfrp1 was detected by ELISA 24 hours after stimulation with TGFβ1 (5 ng/ml) or EGF (50 ng/ml) **(A)**. In MLg cell lysates, EGF (50 ng/ml) induced a strong reduction of Sfrp1 protein expression already 8 hours and TGFβ1 (5 ng/ml) 48 hours after treatment **(B)**. Data are shown as relative expression (±SD) of 4 independent experiments Statistical analysis: One way ANOVA with Dunnett's multiple comparison test. (n.t. = non-treated). *p<0.05, **p<0.01.

3.4.3 Sfrp1 expression in interstitial lung disease (ILD)

Sfrp1 is significantly down-regulated in invading lung fibroblasts as observed in the 3D cell culture invasion assay. Moreover, growth factors like TGFβ1 and EGF that play a major role in interstitial lung diseases down-regulated Sfrp1 expression in a conventional 2D cell culture system. After this extensive characterization of Sfrp1 expression in MLg fibroblasts, the aim was to investigate the relevance of Sfrp1 down-regulation in ILD. Therefore, Sfrp1 mRNA expression was investigated in fibroblast lines of ILD patients compared to controls. While no significant difference was identified between groups, a trend to lower expression levels in ILD-lines was apparent (mean ddCT 1.7 ≡ 3.25-fold).

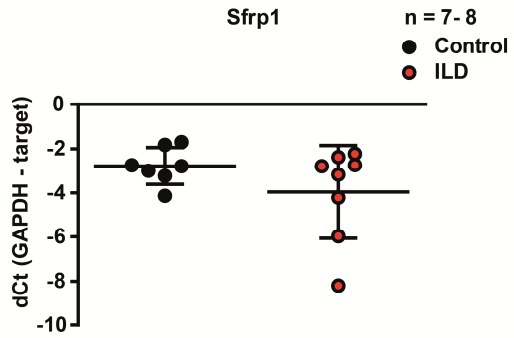

Figure 3.29: Sfrp1 mRNA expression in phF derived from ILD patients.
Seven control and eight ILD lines were probed for Sfrp1 mRNA expression with qRT-PCR. ILD lines showed a trend to lower Sfrp1 transcript levels (n = 7-8). Data are shown as relative expression (±SD).

Subsequently, Western blot analysis of in total eight different ILD lung fibroblast lines and seven control lines, isolated from lung transplant donors, was performed. Figure 3.30 A depicts a representative immunoblot of four control and five ILD lines and Figure 3.30 B densitometric quantification, normalized to β-actin, of all eight ILD and seven control lines tested. Importantly, Sfrp1 showed overall a trend to be lower expressed in fibroblasts derived from ILD patients compared to controls. As control for the degree of fibrosis, the well accepted fibrotic markers Col1a1 (Eickelberg and Laurent 2010) and αSMA (Fernandez and Eickelberg 2012a) were probed and a slight overall induction of both markers was found in the diseased cells.

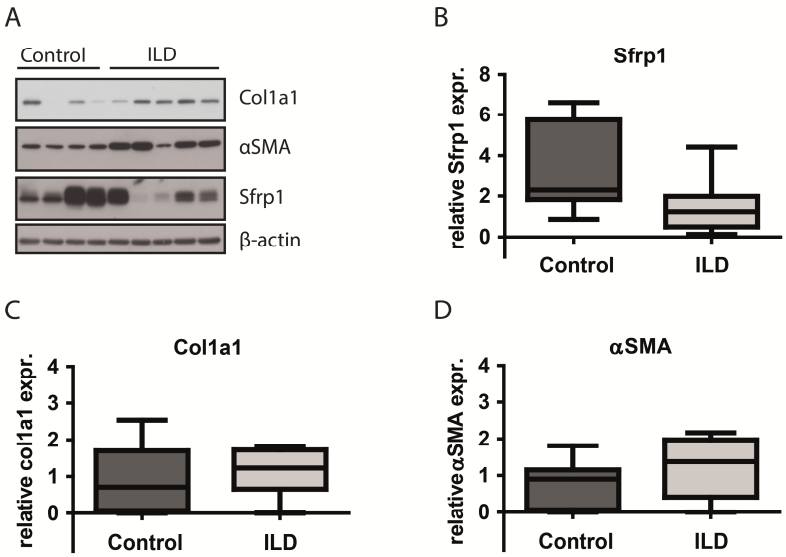

Figure 3.30: Sfrp1 protein expression in phF derived from ILD patients.
Representative Western blot of four control and five ILD-derived fibroblast lines. Samples were probed for Sfrp1, αSMA and Col1a1 **(A)**. Densitometric quantification of Sfrp1 **(B)**, Col1a1 **(C)**, and αSMA **(D)**, normalized to β-actin expression of all phF lines tested (control: n = 7, ILD: n = 8).

Next, differences in the invasion capacity of ILD-derived compared to control fibroblasts were investigated. Seven ILD (red) and seven control fibroblast lines (grey) were subjected to the 3D collagen invasion assay (72 hours) in the absence and presence of EGF (50 ng/ml) for 48 hours. In both groups, EGF significantly induced invasion. However, fibrotic and control lines did not differ in the invasion capacity. Of note, invasion capacity of single lines within the different groups was highly variable (Figure 3.31).

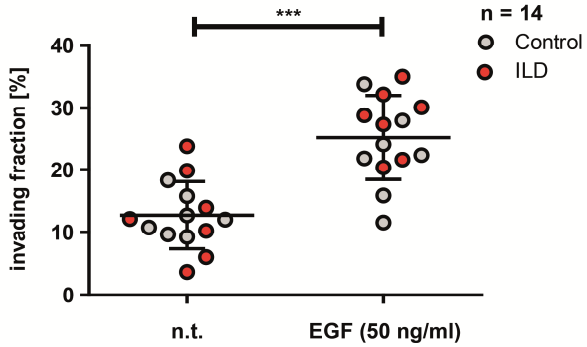

Figure 3.31: Induction of phF invasion upon EGF stimulation.
Software-based quantification of fibroblast invasion by means of 3D reconstructed confocal z-stacks. EGF (50 ng/ml) significantly induced fibroblast invasion as assessed 48 hours after treatment. Data-points derived from fibroblasts of interstitial lung disease (ILD) patients are highlighted in red circles, control lines in grey circles. Statistical analysis: Paired t-test. (n.t. = non-treated). ***p<0.001.

Due to these two major observations, first, that Sfrp1 was down-regulated in some, but not all ILD-derived fibroblast lines and second, that the invasion capacity between different fibroblast lines varied strongly, it was further investigated whether Sfrp1 expression affected the invasion capacity of the different lines. Therefore, a correlation analysis of Sfrp1 expression and the invasion capacity was performed. Interestingly, Sfrp1 expression negatively correlated with the invasion capacity of the different lines only for EGF-induced invasion. This observation was made for Sfrp1 mRNA expression, as revealed by qRT-PCR (linear regression; F-value = 5.51 and p-value = 0.0369 of slope; R^2 = 0.316) (Figure 3.32 A) and on protein level, from normalized Western blot signals (linear regression; F-value = 13.72 and p-value = 0.0035 of slope; R^2 = 0.555) (Figure 3.32 B). In conclusion, reduced Sfrp1 expression levels went in line with increased EGF-induced invasion. Thus, down-regulation of Sfrp1 may be a central event in the process of fibroblast invasion.

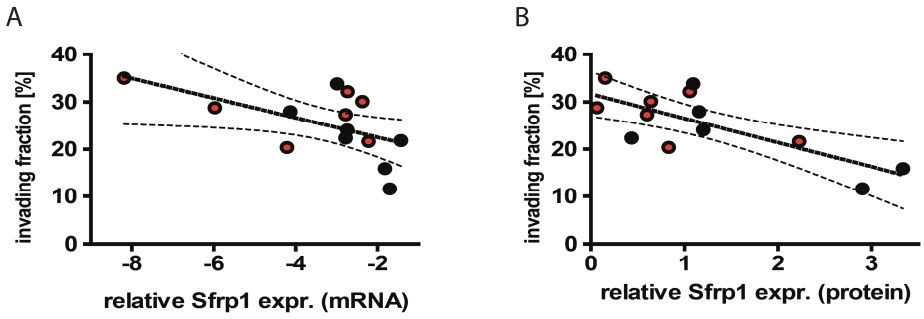

Figure 3.32: Correlation of Sfrp1 expression and EGF-induced fibroblast invasion.
PhF lines from 14 individual patients were analyzed for Sfrp1 expression and EGF-induced invasion capacity. A strong negative correlation between Sfrp1 expression was found on mRNA level (Statistical analysis: linear regression; F-value = 5.51 and p-value =0.0369 of slope; R^2 = 0.316) **(A)** and protein level (Statistical analysis: linear regression; F-value = 13.72 and p-value =0.0035 of slope; R2 = 0.555) **(B)**. Dashed lines represent the linear regression and a confidence interval of 95%, respectively. Data points for ILD-derived lines are represented in red.

In conventional 2D cell culture systems, MLg fibroblasts showed a significant reduction in Sfrp1 expression upon TGFβ1 and EGF treatment (Figure 3.27 and Figure 3.28). To verify this regulation in phF, Sfrp1 immunofluorescence stainings were performed. Both growth factors, EGF (50 ng/ml) and TGFβ1 (5 ng/ml), induced a strong reduction of Sfrp1 expression 24 hours after treatment (Figure 3.33). Of note, co-staining with the fibrotic marker αSMA revealed a mutual exclusion of Sfrp1 and αSMA positive cells (Figure 3.33 B). This result indicates that Sfrp1 expression may prevent fibroblast activation *in vitro*. Expectedly, the content of αSMA positive cells in TGFβ1-treated samples was strongly higher than in the non-treated controls.

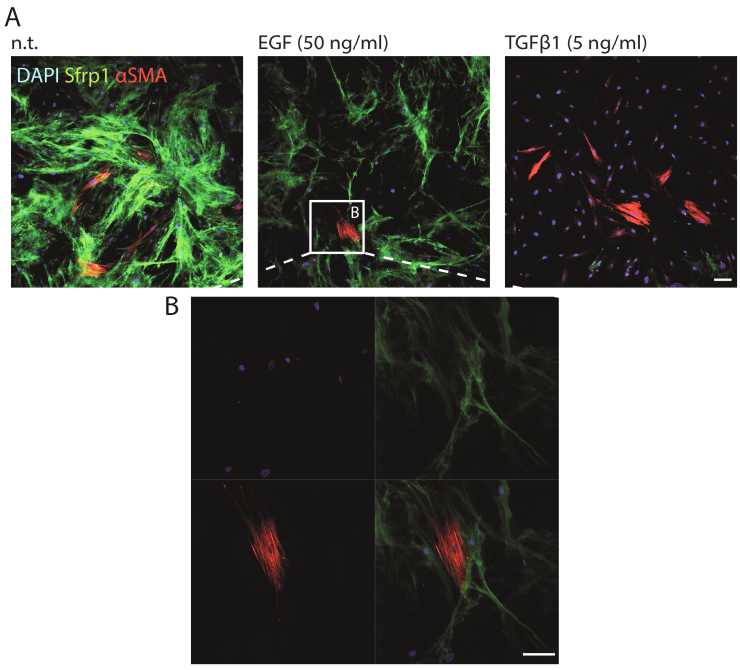

Figure 3.33: TGFβ1 and EGF reduced Sfrp1 protein expression in phF.
Representative immunofluorescence stainings for Sfrp1 (green) in phF revealed a strong reduction of Sfrp1 expression 24 hours after treatment with EGF (50 ng/ml) **(middle panel)** and TGFβ1 (5 ng/ml) **(right panel)** compared to non-treated (n.t.) control **(left panel)**. Content of αSMA positive fibroblasts was increased in TGFβ1-treated samples **(right panel) (A)**. Co-staining with αSMA (red) discloses a mutual exclusion of Sfrp1 and αSMA, as visualized in the higher magnified image **(B)**. Nuclei are stained with DAPI (blue). Scale bar, 100 µm.

Subsequently, phF, which were left untreated or stimulated with either EGF (50 ng/ml) or TGFβ1 (5 ng/ml) were stained for Sfrp1 and for the fibrotic marker Col1a1. For the assessment of cell density and morphology, F-actin was visualized with phalloidin. In contrast to the myofibroblast marker αSMA, staining of Col1a1 did not reveal a clear exclusion with the Sfrp1 signal in neither of the treatment groups (Figure 3.34).

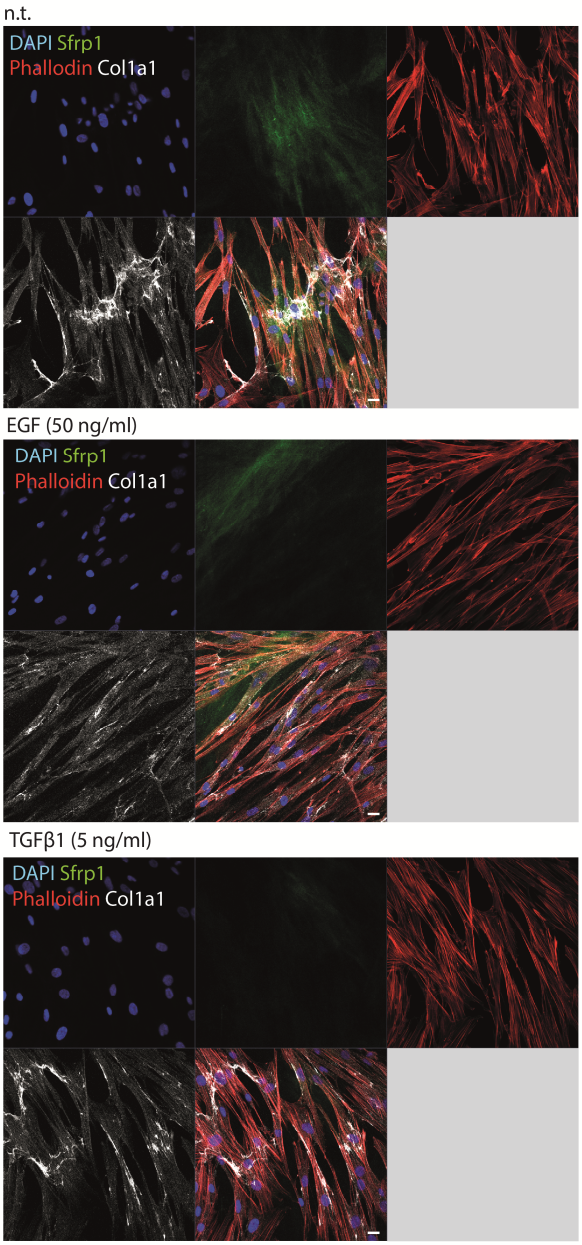

Figure 3.34: Co-staining of Sfrp1 and col1a1 in phF.
Representative images of immunofluorescence stainings for Sfrp1 (green) and Col1a1 (white), phalloidin (red) in non-treated (n.t.) **(upper panel)**, EGF-, (50 ng/ml) **(middle panel)** or TGFβ1-treated (5 ng/ml) phF samples **(lower panel)**. Nuclei are stained with DAPI (blue). Scale bar, 20 µm.

As Sfrp1 is a secreted glycoprotein, it mainly acts extracellular. Thus, besides regulation of Sfrp1, localization of the protein in human lung fibroblasts was further assessed. Therefore, fibroblasts were stained for Sfrp1 and F-actin in a 2D cell culture system. Z-stacks were acquired by means of confocal immunofluorescence microscopy 48 hours after plating the cells. Thereupon, signals for Sfrp1 in images of each plane from the upper to the lower side of the cell were evaluated. A

maximum intensity projection of a x-z orthoview indicated that phF secreted Sfrp1 on the side of the cell contact with the culture dish.

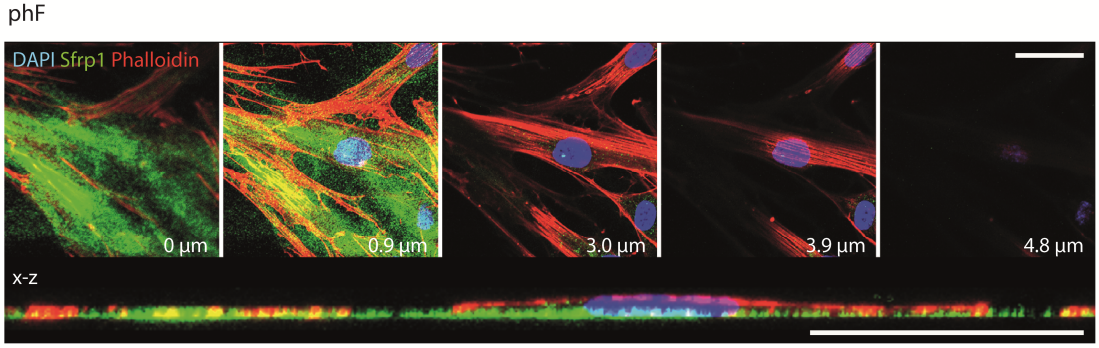

Figure 3.35: Localization of Sfrp1 in phF.
Confocal immunofluorescence microscopy showed a deposition of secreted Sfrp1 (green) on the basal side of fibroblasts. Five images of a z-stack are depicted starting from the basal (0 µm) to the apical (4.9 µm) side of the cell **(upper panel)**. The maximum intensity projection of a x-z orthoview is shown in the **lower panel**. F-actin was stained with phalloidin (red) and nuclei with DAPI (blue). Scale bars, 20 µm.

3.4.4 Functional characterization of Sfrp1 in invading fibroblasts

For the functional characterization of Sfrp1 in the context of fibroblast invasion, a specific Sfrp1 inhibitor, the diarylsulfone sulfonamide derivate 5-(benzenesulfonyl)-N-[3-(dimethylamino)propyl]-2-ethylbenzenesulfonamide, (CHEMBL473916) (EC50 = 1.27 µm (Gopalsamy, Shi et al. 2008)) was utilized. First, activation of the canonical Wnt-signaling pathway by the inhibitor was monitored and thus the working concentration of the inhibitor titrated in the presence of recombinant Wnt3a by means of a TCF luciferase reporter (TOP/FOP) assay. For the assay, MLg fibroblasts were transfected with TOPFLASH or FOPFLASH reporter plasmids. Cells were treated with Wnt3a (100 ng/ml), recombinant human (rh) Sfrp1 (1 µg/ml), or CHEMBL473916 (10 µM, 30 µM) five hours after transfection and subsequently luminescence as read-out for luciferase activity was measured. A significant reporter activity induction was detected after Wnt3a (100 ng/ml) stimulation, which was counteracted by the co-treatment with rh-Sfrp1. Co-stimulation with the Sfrp1-inhibitor CHEMBL473916 potentiated the Wnt3a induced luciferase activity. Thereby, CHEMBL473916 showed highest effects when used in a concentration of 30 µM. Consequently, CHEMBL473916 was used in a dose of 30 µM in all further experiments (Figure 3.36).

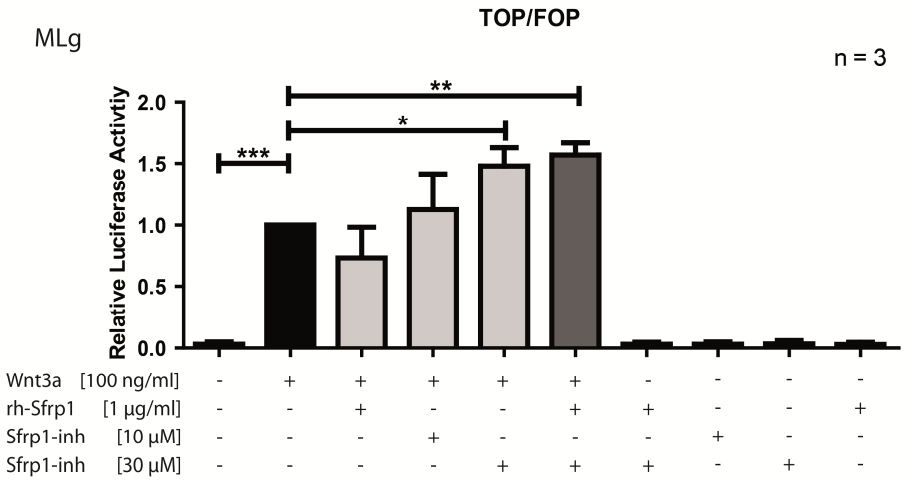

Figure 3.36: Titration of the Sfrp1-inhibitor CHEMBL473916 with TCF luciferase (TOP/FOP) assay.
MLg fibroblasts were transfected with TOP/FOPFLASH reporter constructs and treated with Wnt3a (100 ng/ml), rh-Sfrp1 (1 µg/ml) and/or Sfrp1-inhibitor (10 µM, 30 µM). Luciferase activity was assessed by means of luminescence measurement of TOP-transfected cells and normalized to the respective FOP-transfected counterparts. Data are shown in relation to Wnt3a treated group for three independent (n = 3) experiments (±SD). Statistical analysis: One way ANOVA with Dunnett's multiple comparison test. (n.t. = non-treated). *p<0.05, **p<0.01, ***p<0.001.

To study whether the inhibition of Sfrp1 by CHEMBL473916 induces fibroblast invasion, MLg cells were treated with the inhibitor (30 µM) in the 3D collagen invasion system. Invasion capacity was assessed 48 hours after treatment. Inhibition of Sfrp1 significantly augmented invasion from 10.78 ± 3.20% to 16.41 ± 3.46%. In combination with the pro-invasive growth factor EGF (50 ng/ml) this effect was further enhanced to 26.41 ± 5.29%, which might be explained by a synergistic effect of Sfrp1 down-regulation by EGF and functional inhibition of Sfrp1 with CHEMBL473916 (Figure 3.37 A). Of note, CHEMBL473916 (30 µM) did not induce cell toxicity in the MLg cells, as assessed by total cell counts (Figure 3.37 B).

To assess whether Sfrp1 inhibition specifically modified 3D invasion or whether the effects seen resulted from increased cell motility in general, 2D migration assays were performed. Fibroblasts were treated with CHEMBL473916 (10 µM, 30 µM) in a conventional 2D cell culture system. Live cell imaging was conducted 24 hours after stimulation for 48 hours. The assay did not reveal an impact of Sfrp1 inhibition on 2D motility with a mean baseline motility rate of 0.29 ± 0.04 µm/min and 0.27 ± 0.04 µm/min (10 µm), 0.26 ± 0.01 µm/min (30 µM) after Sfrp1 inhibition (Figure 3.38). Therefore, inhibition of Sfrp1 might exclusively alter fibroblast invading migration behavior in a 3D environment, as mimicked by the collagen-based invasion assay but not migration on 2D surfaces.

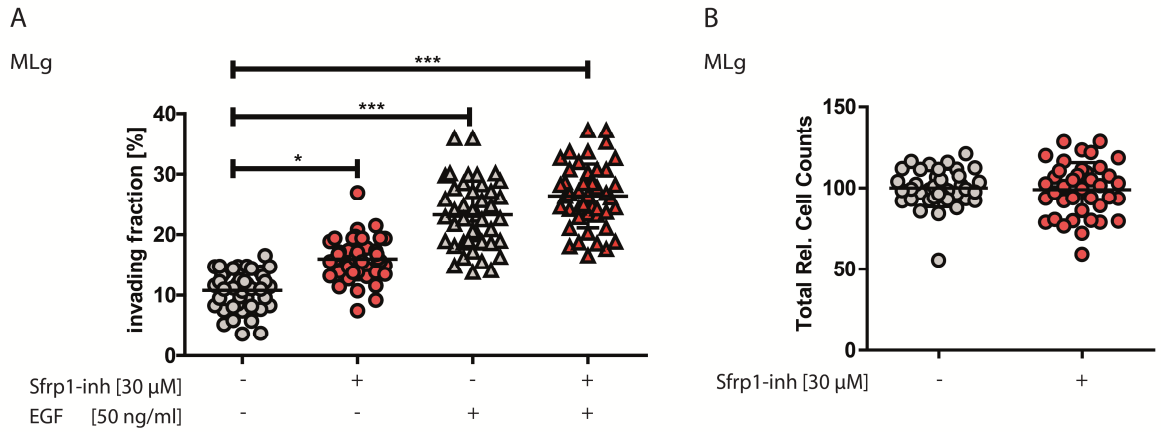

Figure 3.37: Induction of fibroblast invasion by Sfrp1 inhibition.
Sfrp1 was specifically inhibited by CHEMBL473916 (30 µM) in MLg fibroblasts (red circle) and invasion capacity measured in the 3D collagen invasion assay compared to control (open circles). The inhibitor significantly enhanced invasion to 16.41 ± 3.46% compared to 10.78 ± 3.20% in the non-treated control. Invasion was monitored 72 hours after plating and 48 hours after treatment. In addition cells were either only treated with EGF (50 ng/ml) (grey triangles) or a combination of EGF and the inhibitor (red triangle). Total relative cell counts, normalized to the mean of the untreated control **(B)**. Data are shown in five technical replicates per each of eight independent experiment (n = 8) (±SD). Statistical analysis: One way ANOVA with Dunnett's multiple comparison test. (n.t. = non-treated). *p<0.05, ***p<0.001.

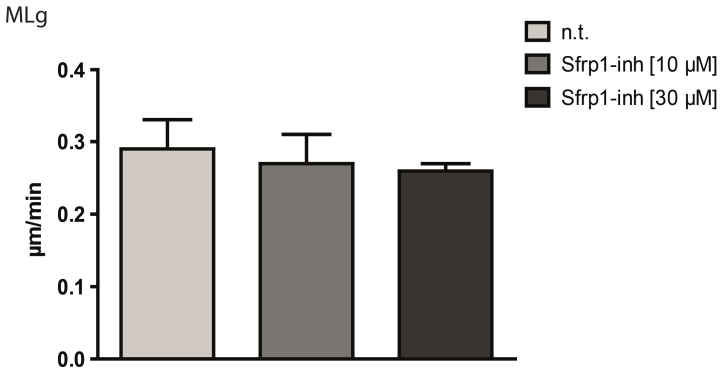

Figure 3.38: Assessment of 2D motility of MLg fibroblasts after Sfrp1 inhibition CHEMBL473916.
Inhibition of Sfrp1 with CHEMBL473916 (10 µM, 30 µM) did not significantly alter 2D motility of MLg fibroblasts 24 hours after treatment. Data are shown as mean motility (±SD) of 3 independent experiments (n = 3).

In summary, within this study, 3D collagen-based invasion assays were established and validated. On hand of these 3D cell culturing models, the whole transcriptome profile of fibroblast invasion was unraveled. This signature was furthermore extended to TGFβ1-mediated cell invasion. In search of novel target genes associated with fibroblast invasion, Sfrp1 was identified in the inherent and TGFβ1-mediated transcriptomic signature. Subsequently, a connection between ILD and fibrogenic growth factor signaling with low Sfrp1 expression levels in phF was established.

Thereupon, Sfrp1 was validated as a protective functional target for fibroblast invasion in the established 3D collagen-based invasion assay.

These data provide strong evidence that Sfrp1 acts as modifier of fibroblast invasion in general and in the context of fatal lung diseases, such as ILD.

4. DISCUSSION

Tissue repair that takes place as a physiological dynamic response to lung injury is highly dependent on a versatile and active fibroblast phenotype that eventually restores the lung architecture. When fibroblasts become aberrantly activated, tissue repair processes cumulate in excessive lung remodeling, as seen in IPF. In the fibrotic lung, activated fibroblasts infiltrate the lung interstitium, form fibroblastic foci, and deposit high amounts of ECM.

The current study concentrated on one essential feature of activated fibroblasts, their tissue invasion capacity. Although, this invasive fibroblast phenotype in IPF has frequently been reported in scientific literature (Suganuma, Sato et al. 1995), (Li, Jiang et al. 2011), (White, Thannickal et al. 2003), it has not comprehensively been characterized thus far.

Using the herein established 3D invasion models, invading fibroblasts were extensively profiled. Microarray analysis of invading and non-invading fibroblast phenotypes resulted in a transcriptome signature of cellular invasion. Confirmative for the model approach, this invasion signature included several markers reported to be involved in cellular invasion and/or fibrosis i.e. TGFβ1, MMP13, Caveolin 1 (Cav1), and Phosphatase and tensin homologue deleted on chromosome 10 (Pten). Applying the invasion signature to system biological analysis with the help of Ingenuity® Pathway Analysis (IPA) software, a significant enrichment of the biological processes “invasion of cells”, “IPF”, and “metastasis” was further unraveled.

In order to specify fibroblast invasion in the context of IPF, effects of profibrotic growth factors, in particular TGFβ1, were analyzed with the 3D invasion model. In line with the literature, TGFβ1 was identified as a pro-invasive cytokine (Zolak, Jagirdar et al. 2013). Thereupon, the gene expression profile of invading fibroblasts was extended to TGFβ1-mediated invasion. The overlapping signature of base-line and TGFβ1-mediated invasion comprised 193 genes, including Sfrp1. Sfrp1 was significantly down-regulated upon invasion and growth factor treatment, as assessed on mRNA and protein level. A connection of Sfrp1 expression levels and invasion was not only elaborated for TGFβ1 but moreover Sfrp1 expression and EGF induced invasion correlated negatively in primary human fibroblasts from different patients.

These data delineate for the first time a comprehensive description of the whole transcriptome profile of fibroblast invasion assessed by means of a novel collagen-based 3D high-throughput invasion assay.

4.1 3D ECM model systems for extensive profiling of invasive cell types

The first goal of this current thesis was to establish valid 3D cell culture models, enabling the extensive characterization of fibroblast invasion. The first model, termed *invasion assay*, a

collagen-based 3D cell culture model in 96-well format, was developed using MLg fibroblasts. This model allowed an assessment of cellular invasion capacity in a high-throughput manner. Collagen type I matrices were chosen as model ECM structure as collagen is one of the most abundant ECM proteins and collagen type I is heavily deposited in fibrotic diseases such as pulmonary fibrosis (Vasaturo, Caserta et al. 2012), (Wolf, Alexander et al. 2009), (Chien, Richards et al. 2014). Furthermore, according to the literature, polymerized collagen type I used in a concentration of 3.2 mg/ml was expected to give rise to an environment of comparable stiffness to healthy lung parenchymal tissue (Liu, Mih et al. 2010), (Harjanto, Maffei et al. 2011).

To date, cell motility has widely been studied in 2D cell culture systems. Prevailing 2D migration assays are wound healing or scratch assays, transwell migration assays, capillary chamber or tube assays or time-lapse cell tracking (reviewed in (Kramer, Walzl et al. 2013)). However, there is a fast-growing body of literature indicating that the migratory behavior of mesenchymal cells, which physiologically reside in the ECM, should be studied in a physiologically more relevant 3D environment rather than on 2D plastic surfaces (Cukierman, Pankov et al. 2002). Moreover, dimensionality and structure of the cell culture system were reported to influence signaling of mechanoregulatory growth factors, such as TGFβ1 (Grinnell and Ho 2002), (Brown, Sethi et al. 2002) and the mode of cellular adhesion (Cukierman, Pankov et al. 2001). Based on this knowledge, several 3D invasion assays have been developed in the past. These assays range from 3D cell tracking assays using time-lapse microscopy to spheroid gel invasion assays. Spheroid-based assays have mainly been used to assess tumor outgrowth and metastasis behavior of neoplastic epithelial cells. Another invasion assay, commercialized by Platypus (Oris™) works with assessment of cellular infiltration into a cell exclusion zone (Joy, Vollmer et al. 2014).

The invasion assay, established here, can be seen as a variant form of organotypic skin models or vertical gel invasion assays. Vertical invasion assays have been used over a long period of time to assess for example lymphocyte migration (Schor, Allen et al. 1983) or behavior of carcinoma cells in a 3D co-culture system in the presence of stromal fibroblasts (Timpson, McGhee et al. 2011). In those studies, evaluation of invasion behavior was accomplished by counting extracted cells, scintillation counting of radioactive labeled cells, or immunohistochemical stainings (Kramer, Walzl et al. 2013). This current study extended the applicability of the vertical invasion assay by implementing an automated analysis method resulting in, to my knowledge, an unprecedented modified high-throughput invasion assay.

Resulting from the high-throughput format of the established invasion assay, this model potentially enables also the screening for compounds interfering with the invasion capacity of cells. In the course of this study, compounds resulting from a bioinformatical approach on the

identified invasion signature (see section 3.3.1) and the proteasome inhibitor oprozomib (ONX 0912) were tested. Selected compounds investigated in the course of this study did not include effective candidates and were therefore not further elaborated in this thesis.

The second 3D cell culture model, termed *separation assay*, that was established, allowed the physical separation of invading and non-invading fibroblasts by the combination of a porous polyethyleneterephthalate (PET) membrane and a collagen I matrix. This setup enabled the systematic identification of the molecular signature of fibroblast invasion by whole transcriptome analysis of invading and non-invading cell fractions following their physical separation. Thus far, conventional invasion assays described before were solely deployed to assess cellular invasion, but were not used for a detailed molecular profiling of the invading cellular phenotype.

Altogether, the two newly established assays may be superior to former published assays, as they are easily performed and most importantly can be applied for measuring the invasion capacity in combination with a concomitant extensive molecular and biochemical profiling.

4.2 Growth factor mediated fibroblast invasion

The parenchymal invasion of activated lung fibroblasts is a central event in IPF, a disease highly driven by growth factors. Therefore, the relation between growth factor signaling and fibroblast invasion was of particular interest. TGFβ1 and EGF were found to significantly induce fibroblast invasion *in vitro*, suggesting a pivotal role of these growth factors in fibroblast activation.

As reported, the pleiotropic fibrogenic cytokine TGFβ1 is a key regulator of IPF (Fernandez and Eickelberg 2012a). With respect to mesenchymal activation, TGFβ1 was found to induce proliferation, as well as synthesis and deposition of ECM, specifically collagen type I (Cutroneo, White et al. 2007). Furthermore, TGFβ1 was shown to elicit the transformation of several cell types into activated fibroblasts, including epithelial, endothelial cells and pleural mesothelial cells (PMCs) (Gao, Yan et al. 2015), (Nasreen, Mohammed et al. 2009), (Montorfano, Becerra et al. 2014).

The role of TGFβ1 for PMC-mesenchymal transition, as well as dissemination of fibrotic lesions in the lung interstitium was recently demonstrated by Zolak *et al.*. By tracking PMCs after intratracheal TGFβ1 instillation in mice, expressing green fluorescence protein exclusively in PMCs through the control of the Wilms tumor-1 promoter, the authors could verify TGFβ1-induced infiltration of PMCs into the lung interstitium with a concomitant mesenchymal transition (Zolak, Jagirdar et al. 2013). These data highlight the importance of TGFβ1-induced interstitial invasion of mesenchymal cells in IPF pathogenesis.

Moreover, in cancerous diseases, TGFβ has been linked to tumor invasiveness and dissemination (Massague 2008). In this context, paracrine crosstalk between cancer cells and cancer associated fibroblasts (CAF) from the neoplastic stroma by TGFβ1 has recently been recognized as an important contributor for an aggressive phenotype of breast cancer (Yu, Xiao et al. 2014).

In addition to TGFβ1, a second growth factor, EGF; was tested for its capacity to induce fibroblast invasion. EGF was chosen as it represents a noted pro-invasive cytokine for cancer cells (Lu, Jiang et al. 2001) and dermal fibroblasts (Gobin and West 2003). In the established 3D invasion assay, EGF was found to strongly increase fibroblast invasion, thus verifying the model approach and providing a potent positive control for cellular invasion.

In summary, in the present study TGFβ1 and EGF were successfully demonstrated to be positive effectors of fibroblastic invasion in the newly established 3D cell culture model.

4.3 Phenotypic characterization of fibroblasts cultured in 3D

For mesenchymal cells that physiologically reside in the lung interstitium, adaptive and reciprocal interactions between cells and surrounding matrix are well recognized (Cukierman, Pankov et al. 2002). The 3D environment may trigger cellular responses, such as adhesion or migration status of the cells. These changes may be reflected in the cellular morphology. Accordingly, Hakkinen and colleagues compared effects of different environments on the cell morphology and could identify matrix-dependent influences (Hakkinen, Harunaga et al. 2011), (Rhee 2009). Here, we used the assessment of fibroblast morphology as a measure to describe the invading fibroblast phenotype in the established 3D invasion assay. Fibroblasts that spontaneously invaded the collagen matrix had a distinct morphology compared to fibroblasts that remained on top of the matrix in the course of the culturing period. The invading fraction had a highly elongated or cylindrical phenotype as determined by length/width ratios and their significant low sphericity values. Invading fibroblasts further seemed to exhibit fewer lateral protrusions, which may indicate persistent directionality of cell orientation. Thus, fibroblasts within the 3D collagen matrix were found elongated and polarized, indicating that the cell is in the active process of 3D invasion (Friedl and Wolf 2003). Additionally, both cell fractions, invading and non-invading, outlined against fibroblasts cultured in 2D, which had a highly spread morphology. These findings are in line with previous studies, where comparable significant changes in cell morphology between fibroblasts cultured in 2D and 3D were reported (Hakkinen, Harunaga et al. 2011). As integrins are the main adhesion receptors responsible for the bi-directional signal transduction between ECM and embedded cells (Arnaout, Mahalingam et al. 2005), integrin assembly and activation status for cells cultured in the invasion model remain intriguing open questions. In the course of to current study, thin fibrillar adhesion-

like structures, which stained positive for integrin β1 (CD29) were visualized along F-actin fibres of fibroblast embedded in the collagen matrix.

In order to exclude effects of the collagen type I matrix on cell viability as stated previously (Xia, Diebold et al. 2008), intact cell cycle turnover for collagen-embedded fibroblasts was verified by nuclear Ki67 staining. Subsequently, completing the characterization of fibroblasts cultured in the invasion assay, fibroblasts embedded in collagen were found to secrete high amounts of fibronectin. Accordingly, embedded fibroblasts maintained their function as ECM producing cells and may refine the composition of the surrounding ECM structure. Furthermore, substantial expression of vimentin, a major intermediate filament and important component of motile mesenchymal cells, provided evidence for intact cellular mechanical integrity of fibroblasts in the 3D collagen-based cell culture system (Mendez, Restle et al. 2014), (Shabbir, Cleland et al. 2014).

In conclusion, fibroblasts embedded in collagen matrix exhibit a distinct morphological phenotype, are proliferative, and express characteristic mesenchymal markers.

4.4 Analysis of the gene profile of fibroblast invasion

To date, studies investigating invasion capacity of cells have mainly focused on single factors (White, Thannickal et al. 2003), (Li, Jiang et al. 2011), (Goetz, Minguet et al. 2011), (Sabeh, Li et al. 2009) and have not implemented a systems biology approach. Here, using the established 3D separation assay, the whole transcriptome signature of the invading fibroblast phenotype was unraveled by microarray analysis.

Initially, arrays were conducted at two different time-points of invasion. A systematic comparative analysis (IPA) was performed to substantiate the fibroblast invasion signature and narrow down the number of promising targets. The pathway analysis of the overlapping invasion signature of both time-points identified a significant enrichment for the biological processes “invasion of cells”, “idiopathic pulmonary fibrosis”, and “metastasis”. As outlined in section 3.3.1, the underlying molecular networks of these functional clusters revealed that the invasion signature featured a profile of matrix degradation, several prevailing IPF-associated transcripts, as well as members of the CCN and TGFβ-superfamilies.

Regarding the functional cluster of matrix degradation, the Matrix Metallo-proteinases (MMPs), MMP13, MMP3, and MMP10 were found to be up-regulated in the invading cellular subpopulation at both time-points. These zinc-dependent endopeptidases may assist in the protease dependent process of interstitial migration. However, as in a very recent study MMPs were found

to also regulate cancer amoeboid migration (Orgaz, Pandya et al. 2014), these findings do not implicitly imply a mesenchymal rather than amoeboid mode of migration in the invasion model.

Interestingly, in the context of pulmonary fibrosis, an up-regulation of MMP13 along with MMP1 and MMP7 in IPF lung homogenates, was reported in the past (Rosas, Richards et al. 2008), (Bauer, Tedrow et al. 2015), whereby the lung epithelium and interstitial space featured as their main source (Nkyimbeng, Ruppert et al. 2013). Furthermore, as reasoned from studies showing an increased MMP13 expression in subsets of cancer associated fibroblasts (CAFs), MMP13 expression in invading fibroblasts may not solely trigger their own invasion capacity but also induce invasion of carcinoma cells (Lederle, Hartenstein et al. 2010), (Lecomte, Masset et al. 2012). Recently, MMP3 has been reported as a potential systemic biomarker for IPF as disease severity was found to be reflected in augmented serum MMP3 levels (DePianto, Chandriani et al. 2015). In addition, MMP10 was found to be increased in IPF lung tissue (Bauer, Tedrow et al. 2015). Apart from its role in cellular invasion, MMP overexpression in the disease might further indicate ongoing ECM remodeling processes, accomplished by activated fibroblasts. An association of this profile of matrix degradation to the clusters “metastasis” and/or “invasion of cells” was predicted by IPA.

Importantly, confirming literature reports, the invasion signature comprised Phosphatase and tensin homologue deleted on chromosome 10 (Pten) as down-regulated target at both time-points analyzed. As dual protein/lipid phosphatase, Pten dephosphorylates phosphatidylinositol (3,4,5)-trisphosphate, which leads to an inhibition of the AKT/mTOR pathway (Maehama and Dixon 1998). Pten has widely been studied in the context of cellular invasion, cancer and fibrosis. Accordingly, activated fibroblasts in IPF exhibit decreased Pten expression which correlates with increased αSMA expression (White, Atrasz et al. 2006). Moreover, reactivation of Pten activity by α4β1 integrin was reported to interfere with an α5β1 integrin-induced invasive phenotype of lung fibroblasts (White, Thannickal et al. 2003). In epithelial kidney cells, Pten was described as a stabilizer of junctional complexes, thereby preventing transformation to an invasive phenotype (Kotelevets, van Hengel et al. 2005). In addition, in the context of IPF, Xia et al. identified that the down-regulation of Pten in fibroblastic foci is accompanied by decreased Caveolin 1 (Cav1) levels. They postulated that depletion of the integral membrane protein Cav1 reduces membrane-associated Pten, which in turn favors the activation of PI3K/Akt signal pathway (Xia, Khalil et al. 2010). The scaffolding protein Cav1 is an important component of the plasma membranes’ caveolae, which can assist in triggering a large number of signaling pathways, such as TGFβ, EGF, Src, Rho GTPases, and β integrins (reviewed in (Gvaramia, Blaauboer et al. 2013) and (Okamoto, Schlegel et al. 1998). Although not included in the list of strongest down-regulated transcripts upon invasion, Cav1 showed consistently lower expression in invading fibroblasts. Despite the fact

that down-regulation of Cav1 has repeatedly been reported in IPF (Xia, Khalil et al. 2010), (Wang, Zhang et al. 2006), literature survey reveals a double-edged role of differential expressed Cav1 in the context of cellular invasion and pulmonary fibrosis. Thus, in CAFs elevated levels of Cav1 favor tumor invasion and metastasis (Goetz, Minguet et al. 2011). In pulmonary fibrosis activation of fibroblasts was demonstrated to go along with a decreased Cav1 expression mediated by TGFβ1 (Shivshankar, Brampton et al. 2012), however Cav1 deficiency has a protective impact in experimental fibrosis (Shivshankar, Brampton et al. 2012).

In addition to Pten and Cav1, the invasion signature featured with autotaxin (ENPP2) one further target that has recently been described in pulmonary fibrosis (Oikonomou, Mouratis et al. 2012), (Tager, LaCamera et al. 2008). This enzyme is mostly responsible for extracellular lysophosphatidic acid (LPA) production, which is a potent mitogen. In IPF patients increased LPA levels were detected in the alveolar space, with a direct link to pathogenesis. Subsequently, increased LPA concentrations could be traced back to elevated autotaxin expression and pharmacological inhibition of autotaxin attenuated bleomycin induced fibrosis. In the invasion signature, autotaxin ranked among the most significantly up-regulated transcripts and an association to the clusters “metastasis” and “invasion of cells” was predicted.

Collagen invasion also affected members of the CCN protein family which comprises Cyr61, CTGF, NOV, and WISP 1-3 (CCN 4-6) (Holbourn, Acharya et al. 2008). While NOV was found to be up-regulated upon invasion, expression of CTGF, Cyr61, and WISP1 was negatively affected. Thus, collagen invasion significantly regulated the expression of four out of six members of this matricellular protein cluster. Considering that CCN proteins play a crucial role in cellular processes, such as proliferation, apoptosis, cell adhesion, ECM production and migration (Leask and Abraham 2006) as well as in pulmonary fibrosis (Konigshoff, Kramer et al. 2009), collective regulation of this cluster upon cellular invasion may pose an interesting finding in the generated invasion signature.

Of interest, TGFβ1 was found differentially regulated in the invading fibroblasts, hence the invasion induced transcriptome signature included the key mediator of fibrogenesis. Considering the pro-invasive property of TGFβ1, up-regulation of this growth factor in the invading fibroblast phenotype might be of particular interest as increased TGFβ1 levels potentially induce a feed-forward loop of fibroblast activation. TGFβ1 was associated with all three enriched clusters “invasion of cells”, “idiopathic pulmonary fibrosis”, and “metastasis”. Notably, two further members of the TGFβ-superfamily, bone morphogenic protein 4 (BMP4) and osteoglycin (Ogn) were found to be differentially regulated in the invading fibroblasts. BMP4 mainly functions in skeletal repair, regeneration and kidney formation and was identified to be involved in the pathogenesis of pulmonary hypertension (Bragdon, Moseychuk et al. 2011) (Frank, Johnson et al.

2005). Strikingly, while BMP4 was significantly down-regulated, the inhibitor of BMP4 signaling, gremlin 2 (Grem2), was found to be upregulated upon invasion. Moreover, Gremlin is known to be overexpressed in IPF (Koli, Myllarniemi et al. 2006). Most recently, BMP4 was identified in a genomic IPF signature albeit an up-regulation was reported here (Bauer, Tedrow et al. 2015).

In summary, these molecular changes highlight the potential relevance of the generated invasion signature in IPF pathogenesis.

4.5 TGFβ1-induced invasion gene profile and strategy for target selection

In the course of this thesis, the key fibrogenic cytokine TGFβ1 was verified as a pro-invasive mediator. Remarkably, expression of TGFβ1 was found to be increased in fibroblasts upon collagen invasion at both time-points tested. As outlined in section 4.4, this might indicate that via TGFβ1 invading fibroblasts initiate a feed-forward loop of fibroblast activation. Therefore, we sought to profile the TGFβ1-mediated invasion signature. Interestingly, overall expression data clustered on the first hierarchical level in invading and non-invading groups, which subdivided into non-treated and TGFβ1-treated on the second hierarchical level, indicating a very distinct invasion dependent gene profile.

In the TGFβ1-induced gene profiles, differential expression between 1) non-invading treated and untreated, as well as 2) invading treated and untreated was monitored. A proof for effective stimulation by TGFβ1 was found in both signatures, as for example TGFβ1 strongly induced expression of C1q and tumor necrosis factor related protein 3 (C1qtnf3), which is in line with the literature. Accordingly, Hoyles *et al.* reported an TGFβ1 dependent induction of C1qtnf3 in primary mouse fibroblasts which was less pronounced in fibroblasts of TGFRII knockout animals (Hoyles, Derrett-Smith et al. 2011).

As in the context of IPF pathogenesis TGFβ1-mediated cellular invasion might be of specific interest, congruently regulated genes in the baseline invasion signature and TGFβ1-mediated invasion signature were considered in particular for subsequent functional investigations. In order to filter relevant candidates for TGFβ1-regulated invasion, the overlap of the baseline invasion signature and the TGFβ1-induced signature in invading fibroblasts was revealed by systematic comparative analysis. IPA analysis showed that both gene profiles integrated in functional clusters of invasion, morphogenesis, and carcinogenesis-related pathways. The molecular basis of the overlapping signature comprised among others Grem2, BMP4, Ogn, Pten, and Sfrp1. This strategy not only allowed for enrichment of invasion relevant targets but also for the exclusion of targets found with reversed regulation. Thus, TGFβ1 for example strongly down-regulated Enpp2, one target found to be highly up-regulated upon invasion. Additionally, members of the CCN protein

family (CTGF, WISP1, Cyr61), which were found repressed in the invasion signature, were induced by TGFβ1.

Of note, aligning the invasion signature to TGFβ1-induced invasion was one approach used to screen for targets of interest. Nevertheless, since TGFβ1 is not considered as the exclusive regulator of fibroblast invasion, the baseline invasion signature harbors numerous further targets of interest in the context of fibroblast invasion as described in section 3.3.1.

4.6 Sfrp1 as functional target for fibroblast invasion

With the strategy on target selection described above, several potential invasion critical candidates were extracted from the invasion signature including Sfrp1. Sfrps belong with the Dickkopf protein family (DKK), Wnt inhibitory factor-1 (WIF-1), Nemo-like kinase (NLK), and β-catenin binding inhibitors to a group of endogenously expressed Wnt-signaling modulators. Thereby, Sfrps antagonize Wnt-signaling by preventing binding of Wnt ligands to their receptors, Frizzled (FZD), either by direct binding of Wnt or the formation of non-functional complexes with FZD (Baarsma, Konigshoff et al. 2013). In mammals, the Sfrp family of secreted glycoproteins comprises five members: Sfrp1 thru Sfrp5 (Surana, Sikka et al. 2014). Of these members, Sfrp1 was exclusively found to be down-regulated in the invasion signature. In the current study, Sfrp1 attracted particular interest as in the context of ILD, Wnt-signaling pathways have widely been shown to be up-regulated. (Konigshoff, Kramer et al. 2009), (Vuga, Ben-Yehudah et al. 2009). However, the potential role of Sfrp1 in this context is not known in detail. In regards to Wnt pathway involvement in pulmonary fibrosis, Königshoff *et al.* revealed an activation of the canonical Wnt/β-catenin pathway in experimental fibrosis (Konigshoff, Balsara et al. 2008). In addition, Vuga *et al.* identified an induction of the non-canonical Wnt pathway ligand Wnt5a in fibroblasts derived from UIP compared to healthy lungs in a gene expression study (Vuga, Ben-Yehudah et al. 2009).

Corroborative incidence for Wnt-signaling in IPF currently arose from further large gene expression studies. Accordingly, Bauer and colleagues reported a regulation of Wnt/β-catenin pathway associated molecules in the genomic signature of IPF lungs. Interestingly, this signature included an up-regulation of Sfrp2 (Bauer, Tedrow et al. 2015), which was not observed in the present study.

Here, not only was a significant down-regulation of Sfrp1 on mRNA and protein levels in invading MLg and phF demonstrated, but correlation studies also manifested a significant association of Sfrp1 expression and the invasion capacity of phF. Accordingly, low Sfrp1 levels in phF indicated a high EGF-induced invasion capacity and vice versa. However, the baseline

invasion capacity of phF lines could not be predicted by Sfrp1 expression levels. This might indicate that low Sfrp1 expression levels in phF provide a pro-invasive environment on which a second trigger may act.

In various cancerous diseases, including lung cancer, silencing of Sfrp1 has frequently been reported, thus assigning Sfrp1 to well established tumor suppressor genes. In the context of carcinogenesis, a tumor-suppressive role through mediation of apoptosis by p53 has been ascribed to Sfrp1 (Gauger and Schneider 2014). Furthermore, Sfrp1 was suggested as a potential marker for breast cancer progression, as silencing of Sfrp1 was found to be associated with adverse tumor progression (Veeck, Niederacher et al. 2006). Interestingly, regarding cellular invasion, ectopic expression of Sfrp1 in invasive human derived MDA-MB-231 adenocarcinoma cells attenuated tumor outgrowth and lung metastases by reducing the migratory potential of the cells (Matsuda, Schlange et al. 2009). Additionally, Sfrp1 along with Sfrp2 was reported to prevent transition of cervical cancer cells and concomitant invasion through Wnt-signaling (Chung, Lai et al. 2009). In the established invasion model, inhibition of Sfrp1 by a diarylsulfone sulfonamide derivate significantly increased invasion of MLg fibroblasts. The concentration of the Sfrp1 inhibitor was titrated by means of the TCF/LEF luciferase reporter assay and thus adjusted to the canonical Wnt-signaling pathway. Invasion, induced by Sfrp1 inhibition was further enhanced by EGF stimulation, which may be explained by a synergistic effect of functional inhibition of Sfrp1 and pro-invasive EGF activity. Due to limitations in cell viability upon lipotransfection of small interfering RNAs in the 3D cell culture models, effects of Sfrp1 knock-down on the invasion capacity could not be studied.

Interestingly 2D migration, as assessed by automatic cell tracking, was not affected by functional inhibition of Sfrp1. Altogether, Sfrp1 was found to be more highly expressed in non-invading fibroblasts on the collagen surface than in invading fibroblast within the matrix and functional inhibition of Sfrp1 induced an invading fibroblast phenotype without affecting lateral 2D migration (Figure 4.1).

One could speculate that Sfrp1 might particularly affect cellular processes exclusively important for cell invasion, such as matrix degradation and reciprocal cell matrix effects. Remarkably, *in silico* analysis (IPA) revealed an interaction of Sfrp1 and MMPs, which is detailed below.

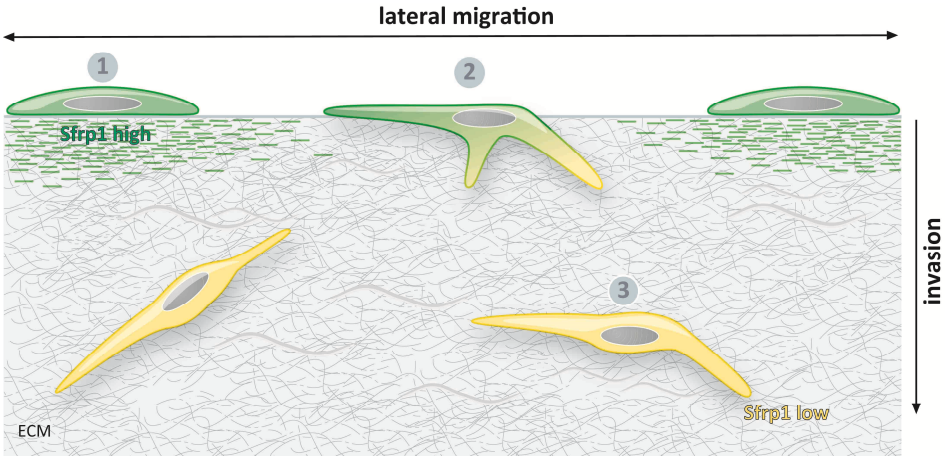

Figure 4.1: Schematical illustration of Sfrp1 expression in fibroblasts upon collagen invasion.
In vitro, fibroblasts that remained on the collagen surface exhibit high Sfrp1 expression levels (green) (1). Down-regulation of Sfrp1 induces fibroblast invasion (2). Invading fibroblasts exhibit low Sfrp1 levels (yellow) (3). Lateral migration might not be affected by Sfrp1 expression.

Although, a detailed analysis of downstream effects of Sfrp1 was beyond the scope of this thesis the transcriptome invasion signature was used to create a Sfrp1-referred molecular network to delineate future research directions around Sfrp1 in the context of fibroblast invasion (Figure 4.2). Based on the IPA knowledgebase, low expression levels of Pten, as found in the invasion signature, may favor low Sfrp1 expression (Bronisz, Godlewski et al. 2012). Furthermore, down-regulation of Sfrp1 is predicted to contribute to higher expression and activation of MMP9 and MMP3. Based on this prediction, it might be highly promising to investigate expression and activity of MMPs in light of the fact that the inhibition of Sfrp1 increases cellular invasion without affecting 2D motility (Figure 4.1).

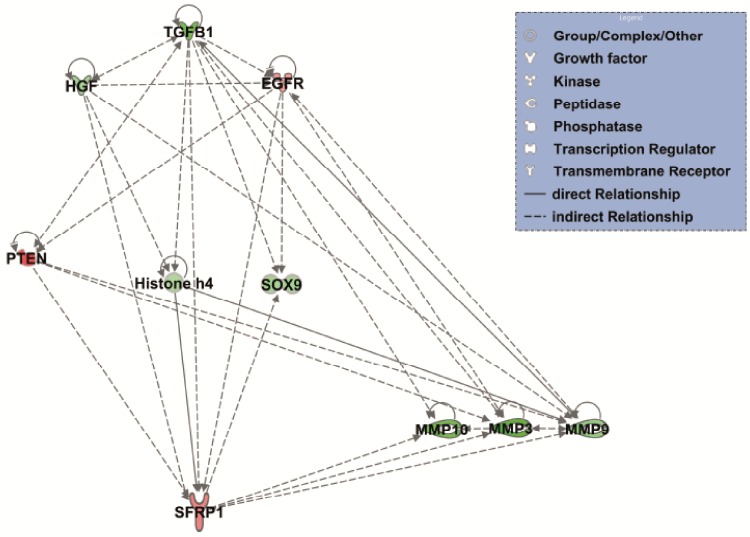

Figure 4.2: Prediction on up- and down-stream effects of Sfrp1 in the conducted invasion signature.
A molecular network around the invasion transcriptome signature (> 1.5-fold, 96 hours) was generated using the up- and down-stream function algorithm (IPA). Hepatocyte growth factor (HGF), TGFβ1 and Epidermal growth factor receptor (EGFR), histone H4, and Pten were found upstream of Sfrp1. Predicted downstream targets of Sfrp1 were MMP10, MMP3, MMP9, and SRY (sex determining region Y)-box 9 (SOX9).

4.7 Regulation of Sfrp1 in interstitial lung disease (ILD)-related environments

In the course of the current study, the pro-invasive cytokines TGFβ1 and EGF were found to significantly diminish Sfrp1 expression in fibroblasts while functional inhibition of Sfrp1 induced an invading phenotype. This might indicate that pro-invasive effects of these growth factors might in part be mediated by down-regulation of Sfrp1 although further studies, including for example overexpression of Sfrp1, are needed to prove this hypothesis.

As outlined in the previous section, Sfrp1 acts as a tumor suppressor gene. Accordingly, aberrantly low expression of Sfrps has frequently been observed in cancer, such as lung, kidney, ovarian or breast tumors (Surana, Sikka et al. 2014). Additional, studies furthermore provided evidence that this down-regulation is caused by epigenetic silencing, primarily promoter hypermethylation. Accordingly, Sfrp1, Sfrp2, and Sfrp4 promoter hypermethylation were reported in cervical cancer (Chung, Lai et al. 2009). Notably, Zhu *et al.* could demonstrate a negative correlation of Sfrp1 and Sfrp5 promoter methylation with EGFR mutation (Zhu, Wang et al. 2012), indicating EGF-induced Sfrp promoter hyper-methylation. In human A549 lung adenocarcinoma cell line, diminished Sfrp1 expression has recently been reported upon TGFβ1

stimulation with a concomitant induction of cell migration and invasion (Ren, Wang et al. 2013). However, in the context of mesenchymal invasion in ILD, the mode of Sfrp1 silencing still remains elusive.

As highlighted above, Sfrp1 represents a secreted inhibitor of canonical and non-canonical Wnt-signaling pathways, which are involved in pathogenesis of several cancers and fibroproliferative diseases in different organs (Clevers 2006), (Yeang, McCormick et al. 2008). Taking into consideration that TGFβ1 potentially activates both Wnt-signaling pathways (Carre, James et al. 2010), (Kumawat, Menzen et al. 2013), down-regulation of Sfrp1 by TGFβ1 might represent a link for cross-activation of Wnt-signaling by TGFβ1. Interestingly, an interchanged relationship has also been reported by Gauger *et al.* as they identified an increased sensitivity to TGFβ1 signaling upon Sfrp1 reduction in mammary epithelial cells (Gauger, Chenausky et al. 2011). Therefore, it might be worth to further investigate the role of Sfrp1 in TGFβ1 Wnt-signaling crosstalk especially in the background of pulmonary fibrosis.

In summary, TGFβ1 and EGF were found to diminish Sfrp1 expression and secretion in MLg fibroblasts as well as Sfrp1 deposition by primary human fibroblasts. Cytokine-induced Sfrp1 depletion in fibroblasts may represent an initiating event for invasion. Additionally, invading fibroblasts were found to express higher levels of TGFβ1, which might in turn initiate activation of adjacent cells (Figure 4.3).

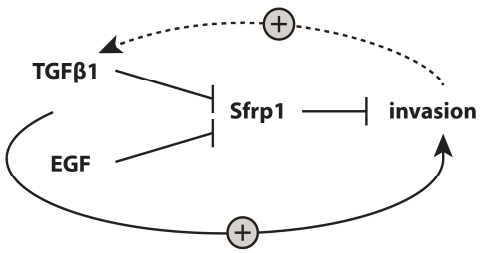

Figure 4.3: Suppression of Sfrp1 expression by TGFβ1 and EGF.
TGFβ1 and EGF inhibit expression and secretion of Sfrp1 whereupon fibroblasts acquire an invading phenotpye. Activated, invading fibroblasts in turn secrete higher levels of TGFβ1 thus theoretically activating adjacent fibroblasts.

The final part of this thesis aimed to establish a link between Sfrp1 expression and interstitial lung disease (ILD). For this purpose, fibroblasts derived from ILD patients were probed for Sfrp1 expression. Although no significant down-regulation of Sfrp1 in ILD compared to non-ILD fibroblasts could be proven, a clear trend towards lower Sfrp1 levels in diseased fibroblasts

emerged. However, as discussed above, an overall significant correlation between Sfrp1 expression and EGF-induced invasion capacity was found in phF.

Interestingly, transcriptional silencing was recently discovered in fibroblasts derived from keloid lesions (Russell, Russell et al. 2010), Systemic Sclerosis (Dees, Schlottmann et al. 2014), and IPF fibrotic lungs (Hsu, Shi et al. 2011). Further, Sfrps were reported to inhibit collagen synthesis and improve tissue function in experimental tissue injury models. Thus, Sfrp4 administration following unilateral ureteral obstruction ameliorated experimental renal fibrosis (Surendran, Schiavi et al. 2005). Along with these findings, exogenously administered Sfrp2 prevented right ventricle fibrosis in an experimental myocardial infarction model with a significant reduction in collagen type 1 deposition (He, Zhang et al. 2010). Hence, Sfrp silencing in fibrotic fibroblasts was predominantly linked to increased ECM deposition and not to the invasive behavior of the cells, as elaborated in the current study. Regarding this perspective of the disease, increased invasion capacity of fibroblasts, derived from fibrotic lungs has frequently been reported in the literature (Suganuma, Sato et al. 1995), (Li, Jiang et al. 2011), (White, Thannickal et al. 2003). Although, this coherence could not be verified in the current study, which might be due to limitations in patient numbers, a significant correlation of low Sfrp1 expression levels in ILD-derived fibroblasts with an elevated invasion capacity was found.

Therefore in conclusion, our findings may add a new aspect of the impact of Sfrp1 silencing in fibrotic diseases, especially ILD.

4.8 Conclusion and future directions

Two novel 3D collagen-based invasion models emerged from this study. Using these 3D models, a transcriptome-wide signature of fibroblast invasion was elaborated that delineates this complex cellular phenotype to unprecedented detail. The relevance of this signature was validated by an *in silico* (IPA) systemic analysis. With Sfrp1, one invasion relevant target was extracted from the invasion signature and analyzed in the context of fibrotic lung disease. A significant down-regulation of Sfrp1 in response to the cytokines TGFβ1 and EGF was demonstrated. Expression of Sfrp1 was further substantially diminished in ILD compared to control derived fibroblasts. Importantly, a strong negative correlation between Sfrp1 expression and EGF-induced invasion capacity could be shown. In summary, strong evidence was provided for a significant role of the established invasion signature in the course of fibrogenesis in ILD. Furthermore Sfrp1 was validated as a functional target within the invasion signature and further *in vitro* studies strongly indicated a substantial role of Sfrp1 silencing in fibrogenesis.

In the course of the current study, several potential future research directions emerged with regards to the invasion signature and Sfrp1 function in pulmonary fibrosis.

As stated above, besides Sfrp1 the invasion signature harbors several further potential targets worth elaborating in the context of fibroblast invasion. These targets include several MMPs, Enpp2, BMP4, Ogn and the CCN protein family. Furthermore, a different strategy for target selection might be chosen to enrich the invasion signature for targets of interest. For example enrichment of the signature by comparative analysis with reported gene profiles of experimental or clinical pulmonary fibrosis might reveal further invasion and disease relevant targets (e.g. (Bauer, Tedrow et al. 2015)).

Regarding Sfrp1, the mode of down-regulation was not investigated in the current study. Considering frequent reports on promoter hypermethylation as the underlying mechanism for aberrant Sfrp silencing in cancer and fibrotic diseases, the methylation status of Sfrp1 upon invasion in the 3D collagen matrix might be of further interest.

As outlined above, detailed analyses on downstream effects of Sfrp1 were beyond the scope of this thesis. Nevertheless, the Sfrp1-referred molecular network (Figure 4.2), described in section 4.6 might assist to delineate future research directions around Sfrp1 in the context of fibroblast invasion that include Pten, MMP9, and MMP3.

Furthermore, it remains an intriguing open question, whether downstream effects of Sfrp1 are primarily mediated by the canonical or non-canonical Wnt-signaling pathway. In particular, non-canonical Wnt-signaling, comprising among others the Wnt/planar cell polarity (PCP), the Wnt-cGMP/Ca^{2+}, and the Wnt/receptor tyrosine kinase-like orphan receptor 2 (ROR2), is highly associated with cell adhesion, formation of filopodia, and migration (Gomez-Orte, Saenz-Narciso et al. 2013). These signaling cascades interact with cell division cycle 42 protein (Cdc42), Ras-related C3 botulinum toxin substrate 1 (Rac1), and Ras homologous A (RhoA) members of the small GTPases Rho family, as down-stream effectors, which regulate actin cytoskeleton rearrangement. Therefore, one can speculate that the effect of Sfrp1 might potentially be triggered by the non-canonical Wnt pathways.

5. REFERENCES

Abbott, A. (2003). "Cell culture: biology's new dimension." Nature **424**(6951): 870-872.

Andersson-Sjoland, A., de Alba, C. G., Nihlberg, K., Becerril, C., Ramirez, R., Pardo, A., Westergren-Thorsson, G. and Selman, M. (2008). "Fibrocytes are a potential source of lung fibroblasts in idiopathic pulmonary fibrosis." Int J Biochem Cell Biol **40**(10): 2129-2140.

Antoniou, K. M., Margaritopoulos, G. A., Tomassetti, S., Bonella, F., Costabel, U. and Poletti, V. (2014). "Interstitial lung disease." Eur Respir Rev **23**(131): 40-54.

Arnaout, M. A., Mahalingam, B. and Xiong, J. P. (2005). "Integrin structure, allostery, and bidirectional signaling." Annu Rev Cell Dev Biol **21**: 381-410.

Baarsma, H. A., Konigshoff, M. and Gosens, R. (2013). "The WNT signaling pathway from ligand secretion to gene transcription: molecular mechanisms and pharmacological targets." Pharmacol Ther **138**(1): 66-83.

Baker, B. M. and Chen, C. S. (2012). "Deconstructing the third dimension: how 3D culture microenvironments alter cellular cues." J Cell Sci **125**(Pt 13): 3015-3024.

Bauer, Y., Tedrow, J., de Bernard, S., Birker-Robaczewska, M., Gibson, K. F., Guardela, B. J., Hess, P., Klenk, A., Lindell, K. O., Poirey, S., Renault, B., Rey, M., Weber, E., Nayler, O. and Kaminski, N. (2015). "A novel genomic signature with translational significance for human idiopathic pulmonary fibrosis." Am J Respir Cell Mol Biol **52**(2): 217-231.

Baughman, R. P., Lower, E. E., Miller, M. A., Bejarano, P. A. and Heffelfinger, S. C. (1999). "Overexpression of transforming growth factor-alpha and epidermal growth factor-receptor in idiopathic pulmonary fibrosis." Sarcoidosis Vasc Diffuse Lung Dis **16**(1): 57-61.

Bjermer, L., Lundgren, R. and Hallgren, R. (1989). "Hyaluronan and type III procollagen peptide concentrations in bronchoalveolar lavage fluid in idiopathic pulmonary fibrosis." Thorax **44**(2): 126-131.

Bonniaud, P., Margetts, P. J., Kolb, M., Schroeder, J. A., Kapoun, A. M., Damm, D., Murphy, A., Chakravarty, S., Dugar, S., Higgins, L., Protter, A. A. and Gauldie, J. (2005). "Progressive transforming growth factor beta1-induced lung fibrosis is blocked by an orally active ALK5 kinase inhibitor." Am J Respir Crit Care Med **171**(8): 889-898.

Booth, A. J., Hadley, R., Cornett, A. M., Dreffs, A. A., Matthes, S. A., Tsui, J. L., Weiss, K., Horowitz, J. C., Fiore, V. F., Barker, T. H., Moore, B. B., Martinez, F. J., Niklason, L. E. and White, E. S. (2012). "Acellular normal and fibrotic human lung matrices as a culture system for in vitro investigation." Am J Respir Crit Care Med **186**(9): 866-876.

Bragdon, B., Moseychuk, O., Saldanha, S., King, D., Julian, J. and Nohe, A. (2011). "Bone morphogenetic proteins: a critical review." Cell Signal **23**(4): 609-620.

Bronisz, A., Godlewski, J., Wallace, J. A., Merchant, A. S., Nowicki, M. O., Mathsyaraja, H., Srinivasan, R., Trimboli, A. J., Martin, C. K., Li, F., Yu, L., Fernandez, S. A., Pecot, T., Rosol, T. J., Cory, S., Hallett, M., Park, M., Piper, M. G., Marsh, C. B., Yee, L. D., Jimenez, R. E., Nuovo, G., Lawler, S. E., Chiocca, E. A., Leone, G. and Ostrowski, M. C. (2012). "Reprogramming of the tumour microenvironment by stromal PTEN-regulated miR-320." Nat Cell Biol **14**(2): 159-167.

Brown, R. A., Sethi, K. K., Gwanmesia, I., Raemdonck, D., Eastwood, M. and Mudera, V. (2002). "Enhanced fibroblast contraction of 3D collagen lattices and integrin expression by TGF-beta1 and -beta3: mechanoregulatory growth factors?" Exp Cell Res **274**(2): 310-322.

Burgstaller, G., Oehrle, B., Koch, I., Lindner, M. and Eickelberg, O. (2013). "Multiplex profiling of cellular invasion in 3D cell culture models." PLoS One **8**(5): e63121.

Cabrera, S., Selman, M., Lonzano-Bolanos, A., Konishi, K., Richards, T. J., Kaminski, N. and Pardo, A. (2013). "Gene expression profiles reveal molecular mechanisms involved in the progression and resolution of bleomycin-induced lung fibrosis." Am J Physiol Lung Cell Mol Physiol **304**(9): L593-601.

Carre, A. L., James, A. W., MacLeod, L., Kong, W., Kawai, K., Longaker, M. T. and Lorenz, H. P. (2010). "Interaction of wingless protein (Wnt), transforming growth factor-beta1, and hyaluronan production in fetal and postnatal fibroblasts." Plast Reconstr Surg **125**(1): 74-88.

Cavazza, A., Rossi, G., Carbonelli, C., Spaggiari, L., Paci, M. and Roggeri, A. (2010). "The role of histology in idiopathic pulmonary fibrosis: an update." Respir Med **104 Suppl 1**: S11-22.

Chien, J. W., Richards, T. J., Gibson, K. F., Zhang, Y., Lindell, K. O., Shao, L., Lyman, S. K., Adamkewicz, J. I., Smith, V., Kaminski, N. and O'Riordan, T. (2014). "Serum lysyl oxidase-like 2 levels and idiopathic pulmonary fibrosis disease progression." Eur Respir J **43**(5): 1430-1438.

Chung, M. T., Lai, H. C., Sytwu, H. K., Yan, M. D., Shih, Y. L., Chang, C. C., Yu, M. H., Liu, H. S., Chu, D. W. and Lin, Y. W. (2009). "SFRP1 and SFRP2 suppress the transformation and invasion abilities of cervical cancer cells through Wnt signal pathway." Gynecol Oncol **112**(3): 646-653.

Clark, R. A., McCoy, G. A., Folkvord, J. M. and McPherson, J. M. (1997). "TGF-beta 1 stimulates cultured human fibroblasts to proliferate and produce tissue-like fibroplasia: a fibronectin matrix-dependent event." J Cell Physiol **170**(1): 69-80.

Clarke, D. L., Carruthers, A. M., Mustelin, T. and Murray, L. A. (2013). "Matrix regulation of idiopathic pulmonary fibrosis: the role of enzymes." Fibrogenesis Tissue Repair **6**(1): 20.

Clevers, H. (2006). "Wnt/beta-catenin signaling in development and disease." Cell **127**(3): 469-480.

Coker, R. K., Laurent, G. J., Jeffery, P. K., du Bois, R. M., Black, C. M. and McAnulty, R. J. (2001). "Localisation of transforming growth factor beta1 and beta3 mRNA transcripts in normal and fibrotic human lung." Thorax **56**(7): 549-556.

Cool, C. D., Groshong, S. D., Rai, P. R., Henson, P. M., Stewart, J. S. and Brown, K. K. (2006). "Fibroblast foci are not discrete sites of lung injury or repair: the fibroblast reticulum." Am J Respir Crit Care Med **174**(6): 654-658.

Cukierman, E., Pankov, R., Stevens, D. R. and Yamada, K. M. (2001). "Taking cell-matrix adhesions to the third dimension." Science **294**(5547): 1708-1712.

Cukierman, E., Pankov, R. and Yamada, K. M. (2002). "Cell interactions with three-dimensional matrices." Curr Opin Cell Biol **14**(5): 633-639.

Cutroneo, K. R., White, S. L., Phan, S. H. and Ehrlich, H. P. (2007). "Therapies for bleomycin induced lung fibrosis through regulation of TGF-beta1 induced collagen gene expression." J Cell Physiol **211**(3): 585-589.

Dees, C., Schlottmann, I., Funke, R., Distler, A., Palumbo-Zerr, K., Zerr, P., Lin, N. Y., Beyer, C., Distler, O., Schett, G. and Distler, J. H. (2014). "The Wnt antagonists DKK1 and SFRP1 are downregulated by promoter hypermethylation in systemic sclerosis." Ann Rheum Dis **73**(6): 1232-1239.

DePianto, D. J., Chandriani, S., Abbas, A. R., Jia, G., N'Diaye, E. N., Caplazi, P., Kauder, S. E., Biswas, S., Karnik, S. K., Ha, C., Modrusan, Z., Matthay, M. A., Kukreja, J., Collard, H. R., Egen, J. G., Wolters, P. J. and Arron, J. R. (2015). "Heterogeneous gene expression signatures correspond to distinct lung pathologies and biomarkers of disease severity in idiopathic pulmonary fibrosis." Thorax **70**(1): 48-56.

du Bois, R. M. (2010). "Strategies for treating idiopathic pulmonary fibrosis." Nat Rev Drug Discov **9**(2): 129-140.

Eickelberg, O. and Laurent, G. J. (2010). "The quest for the initial lesion in idiopathic pulmonary fibrosis: gene expression differences in IPF fibroblasts." Am J Respir Cell Mol Biol **42**(1): 1-2.

Eickelberg, O. and Selman, M. (2010). "Update in diffuse parenchymal lung disease 2009." Am J Respir Crit Care Med **181**(9): 883-888.

Esteve, P. and Bovolenta, P. (2010). "The advantages and disadvantages of sfrp1 and sfrp2 expression in pathological events." Tohoku J Exp Med **221**(1): 11-17.

Fan, D., Creemers, E. E. and Kassiri, Z. (2014). "Matrix as an interstitial transport system." Circ Res **114**(5): 889-902.

Fernandez, I. E. and Eickelberg, O. (2012a). "The impact of TGF-beta on lung fibrosis: from targeting to biomarkers." Proc Am Thorac Soc **9**(3): 111-116.

Fernandez, I. E. and Eickelberg, O. (2012b). "New cellular and molecular mechanisms of lung injury and fibrosis in idiopathic pulmonary fibrosis." Lancet **380**(9842): 680-688.

Frank, D., Johnson, J. and de Caestecker, M. (2005). "Bone morphogenetic protein 4 promotes vascular remodeling in hypoxic pulmonary hypertension." Chest **128**(6 Suppl): 590s-591s.

Frantz, C., Stewart, K. M. and Weaver, V. M. (2010). "The extracellular matrix at a glance." J Cell Sci **123**(Pt 24): 4195-4200.

Friedl, P. and Wolf, K. (2003). "Tumour-cell invasion and migration: diversity and escape mechanisms." Nat Rev Cancer **3**(5): 362-374.

Gao, J., Yan, Q., Wang, J., Liu, S. and Yang, X. (2015). "Epithelial-to-mesenchymal transition induced by TGF-beta1 is mediated by AP1-dependent EpCAM expression in MCF-7 cells." J Cell Physiol **230**(4): 775-782.

Gauger, K. J., Chenausky, K. L., Murray, M. E. and Schneider, S. S. (2011). "SFRP1 reduction results in an increased sensitivity to TGF-beta signaling." BMC Cancer **11**: 59.

Gauger, K. J. and Schneider, S. S. (2014). "Tumour supressor secreted frizzled related protein 1 regulates p53-mediated apoptosis." Cell Biol Int **38**(1): 124-130.

Gobin, A. S. and West, J. L. (2003). "Effects of epidermal growth factor on fibroblast migration through biomimetic hydrogels." Biotechnol Prog **19**(6): 1781-1785.

Goetz, J. G., Minguet, S., Navarro-Lerida, I., Lazcano, J. J., Samaniego, R., Calvo, E., Tello, M., Osteso-Ibanez, T., Pellinen, T., Echarri, A., Cerezo, A., Klein-Szanto, A. J., Garcia, R., Keely, P. J., Sanchez-Mateos, P., Cukierman, E. and Del Pozo, M. A. (2011). "Biomechanical remodeling of the microenvironment by stromal caveolin-1 favors tumor invasion and metastasis." Cell **146**(1): 148-163.

Gomez-Orte, E., Saenz-Narciso, B., Moreno, S. and Cabello, J. (2013). "Multiple functions of the noncanonical Wnt pathway." Trends Genet **29**(9): 545-553.

Gopalsamy, A., Shi, M., Stauffer, B., Bahat, R., Billiard, J., Ponce-de-Leon, H., Seestaller-Wehr, L., Fukayama, S., Mangine, A., Moran, R., Krishnamurthy, G. and Bodine, P. (2008). "Identification of diarylsulfone sulfonamides as secreted frizzled related protein-1 (sFRP-1) inhibitors." J Med Chem **51**(24): 7670-7672.

Green, J. A. and Yamada, K. M. (2007). "Three-dimensional microenvironments modulate fibroblast signaling responses." Adv Drug Deliv Rev **59**(13): 1293-1298.

Grinnell, F. and Ho, C. H. (2002). "Transforming growth factor beta stimulates fibroblast-collagen matrix contraction by different mechanisms in mechanically loaded and unloaded matrices." Exp Cell Res **273**(2): 248-255.

Gross, T. J. and Hunninghake, G. W. (2001). "Idiopathic pulmonary fibrosis." N Engl J Med **345**(7): 517-525.

Gvaramia, D., Blaauboer, M. E., Hanemaaijer, R. and Everts, V. (2013). "Role of caveolin-1 in fibrotic diseases." Matrix Biol **32**(6): 307-315.

Hafemann, B., Ensslen, S., Erdmann, C., Niedballa, R., Zuhlke, A., Ghofrani, K. and Kirkpatrick, C. J. (1999). "Use of a collagen/elastin-membrane for the tissue engineering of dermis." Burns **25**(5): 373-384.

Hakkinen, K. M., Harunaga, J. S., Doyle, A. D. and Yamada, K. M. (2011). "Direct comparisons of the morphology, migration, cell adhesions, and actin cytoskeleton of fibroblasts in four different three-dimensional extracellular matrices." Tissue Eng Part A **17**(5-6): 713-724.

Hall, D. M. and Brooks, S. A. (2014). "In vitro invasion assay using matrigel: a reconstituted basement membrane preparation." Methods Mol Biol **1070**: 1-11.

Harburger, D. S. and Calderwood, D. A. (2009). "Integrin signalling at a glance." J Cell Sci **122**(Pt 2): 159-163.

Harjanto, D., Maffei, J. S. and Zaman, M. H. (2011). "Quantitative analysis of the effect of cancer invasiveness and collagen concentration on 3D matrix remodeling." PLoS One **6**(9): e24891.

Hayen, W., Goebeler, M., Kumar, S., Riessen, R. and Nehls, V. (1999). "Hyaluronan stimulates tumor cell migration by modulating the fibrin fiber architecture." J Cell Sci **112 (Pt 13)**: 2241-2251.

He, W., Zhang, L., Ni, A., Zhang, Z., Mirotsou, M., Mao, L., Pratt, R. E. and Dzau, V. J. (2010). "Exogenously administered secreted frizzled related protein 2 (Sfrp2) reduces fibrosis and improves cardiac function in a rat model of myocardial infarction." Proc Natl Acad Sci U S A **107**(49): 21110-21115.

Hinz, B. (2009). "Tissue stiffness, latent TGF-beta1 activation, and mechanical signal transduction: implications for the pathogenesis and treatment of fibrosis." Curr Rheumatol Rep **11**(2): 120-126.

Hinz, B., Phan, S. H., Thannickal, V. J., Prunotto, M., Desmouliere, A., Varga, J., De Wever, O., Mareel, M. and Gabbiani, G. (2012). "Recent developments in myofibroblast biology: paradigms for connective tissue remodeling." Am J Pathol **180**(4): 1340-1355.

Holbourn, K. P., Acharya, K. R. and Perbal, B. (2008). "The CCN family of proteins: structure-function relationships." Trends Biochem Sci **33**(10): 461-473.

Hoyles, R. K., Derrett-Smith, E. C., Khan, K., Shiwen, X., Howat, S. L., Wells, A. U., Abraham, D. J. and Denton, C. P. (2011). "An essential role for resident fibroblasts in experimental lung fibrosis is defined by lineage-specific deletion of high-affinity type II transforming growth factor beta receptor." Am J Respir Crit Care Med **183**(2): 249-261.

Hsu, E., Shi, H., Jordan, R. M., Lyons-Weiler, J., Pilewski, J. M. and Feghali-Bostwick, C. A. (2011). "Lung tissues in patients with systemic sclerosis have gene expression patterns unique to pulmonary fibrosis and pulmonary hypertension." Arthritis Rheum **63**(3): 783-794.

Huang, C. and Ogawa, R. (2012). "Fibroproliferative disorders and their mechanobiology." Connect Tissue Res **53**(3): 187-196.

Hung, C., Linn, G., Chow, Y. H., Kobayashi, A., Mittelsteadt, K., Altemeier, W. A., Gharib, S. A., Schnapp, L. M. and Duffield, J. S. (2013). "Role of lung pericytes and resident fibroblasts in the pathogenesis of pulmonary fibrosis." Am J Respir Crit Care Med **188**(7): 820-830.

Hynes, R. O. and Naba, A. (2012). "Overview of the matrisome--an inventory of extracellular matrix constituents and functions." Cold Spring Harb Perspect Biol **4**(1): a004903.

Johannson, K. A., Vittinghoff, E., Lee, K., Balmes, J. R., Ji, W., Kaplan, G. G., Kim, D. S. and Collard, H. R. (2014). "Acute exacerbation of idiopathic pulmonary fibrosis associated with air pollution exposure." Eur Respir J **43**(4): 1124-1131.

Joy, M. E., Vollmer, L. L., Hulkower, K., Stern, A. M., Peterson, C. K., Boltz, R. C., Roy, P. and Vogt, A. (2014). "A high-content, multiplexed screen in human breast cancer cells identifies profilin-1 inducers with anti-migratory activities." PLoS One **9**(2): e88350.

Kage, H. and Borok, Z. (2012). "EMT and interstitial lung disease: a mysterious relationship." Curr Opin Pulm Med **18**(5): 517-523.

Kalluri, R. and Neilson, E. G. (2003). "Epithelial-mesenchymal transition and its implications for fibrosis." J Clin Invest **112**(12): 1776-1784.

Kalluri, R. and Zeisberg, M. (2006). "Fibroblasts in cancer." Nat Rev Cancer **6**(5): 392-401.

Kendall, R. T. and Feghali-Bostwick, C. A. (2014). "Fibroblasts in fibrosis: novel roles and mediators." Front Pharmacol **5**: 123.

Kim, K. K., Kugler, M. C., Wolters, P. J., Robillard, L., Galvez, M. G., Brumwell, A. N., Sheppard, D. and Chapman, H. A. (2006). "Alveolar epithelial cell mesenchymal transition develops in vivo during pulmonary fibrosis and is regulated by the extracellular matrix." Proc Natl Acad Sci U S A **103**(35): 13180-13185.

King, T. E., Jr., Pardo, A. and Selman, M. (2011). "Idiopathic pulmonary fibrosis." Lancet **378**(9807): 1949-1961.

King, T. E., Jr., Schwarz, M. I., Brown, K., Tooze, J. A., Colby, T. V., Waldron, J. A., Jr., Flint, A., Thurlbeck, W. and Cherniack, R. M. (2001). "Idiopathic pulmonary fibrosis: relationship between histopathologic features and mortality." Am J Respir Crit Care Med **164**(6): 1025-1032.

Knight, S. D., Presto, J., Linse, S. and Johansson, J. (2013). "The BRICHOS domain, amyloid fibril formation, and their relationship." Biochemistry **52**(43): 7523-7531.

Koli, K., Myllarniemi, M., Vuorinen, K., Salmenkivi, K., Ryynanen, M. J., Kinnula, V. L. and Keski-Oja, J. (2006). "Bone morphogenetic protein-4 inhibitor gremlin is overexpressed in idiopathic pulmonary fibrosis." Am J Pathol **169**(1): 61-71.

Konigshoff, M., Balsara, N., Pfaff, E. M., Kramer, M., Chrobak, I., Seeger, W. and Eickelberg, O. (2008). "Functional Wnt signaling is increased in idiopathic pulmonary fibrosis." PLoS One **3**(5): e2142.

Konigshoff, M., Kramer, M., Balsara, N., Wilhelm, J., Amarie, O. V., Jahn, A., Rose, F., Fink, L., Seeger, W., Schaefer, L., Gunther, A. and Eickelberg, O. (2009). "WNT1-inducible signaling protein-1 mediates pulmonary fibrosis in mice and is upregulated in humans with idiopathic pulmonary fibrosis." J Clin Invest **119**(4): 772-787.

Kono, M., Nakamura, Y., Suda, T., Kato, M., Kaida, Y., Hashimoto, D., Inui, N., Hamada, E., Miyazaki, O., Kurashita, S., Fukamachi, I., Endo, K., Ng, P. S., Takehara, K., Nakamura, H., Maekawa, M. and Chida, K. (2011). "Plasma CCN2 (connective tissue growth factor; CTGF) is a potential biomarker in idiopathic pulmonary fibrosis (IPF)." Clin Chim Acta **412**(23-24): 2211-2215.

Kotelevets, L., van Hengel, J., Bruyneel, E., Mareel, M., van Roy, F. and Chastre, E. (2005). "Implication of the MAGI-1b/PTEN signalosome in stabilization of adherens junctions and suppression of invasiveness." Faseb j **19**(1): 115-117.

Kramer, N., Walzl, A., Unger, C., Rosner, M., Krupitza, G., Hengstschlager, M. and Dolznig, H. (2013). "In vitro cell migration and invasion assays." Mutat Res **752**(1): 10-24.

Kumawat, K., Menzen, M. H., Bos, I. S., Baarsma, H. A., Borger, P., Roth, M., Tamm, M., Halayko, A. J., Simoons, M., Prins, A., Postma, D. S., Schmidt, M. and Gosens, R. (2013). "Noncanonical WNT-5A signaling regulates TGF-beta-induced extracellular matrix production by airway smooth muscle cells." Faseb j **27**(4): 1631-1643.

Laurent, G. J., McAnulty, R. J., Hill, M. and Chambers, R. (2008). "Escape from the matrix: multiple mechanisms for fibroblast activation in pulmonary fibrosis." Proc Am Thorac Soc **5**(3): 311-315.

Lawson, W. E., Cheng, D. S., Degryse, A. L., Tanjore, H., Polosukhin, V. V., Xu, X. C., Newcomb, D. C., Jones, B. R., Roldan, J., Lane, K. B., Morrisey, E. E., Beers, M. F., Yull, F. E. and Blackwell, T. S. (2011). "Endoplasmic reticulum stress enhances fibrotic remodeling in the lungs." Proc Natl Acad Sci U S A **108**(26): 10562-10567.

Leask, A. and Abraham, D. J. (2004). "TGF-beta signaling and the fibrotic response." Faseb j **18**(7): 816-827.

Leask, A. and Abraham, D. J. (2006). "All in the CCN family: essential matricellular signaling modulators emerge from the bunker." J Cell Sci **119**(Pt 23): 4803-4810.

Lecomte, J., Masset, A., Blacher, S., Maertens, L., Gothot, A., Delgaudine, M., Bruyere, F., Carnet, O., Paupert, J., Illemann, M., Foidart, J. M., Lund, I. K., Hoyer-Hansen, G. and Noel, A. (2012). "Bone marrow-derived myofibroblasts are the providers of pro-invasive matrix metalloproteinase 13 in primary tumor." Neoplasia **14**(10): 943-951.

Lederle, W., Hartenstein, B., Meides, A., Kunzelmann, H., Werb, Z., Angel, P. and Mueller, M. M. (2010). "MMP13 as a stromal mediator in controlling persistent angiogenesis in skin carcinoma." Carcinogenesis **31**(7): 1175-1184.

Lee, J., Reddy, R., Barsky, L., Scholes, J., Chen, H., Shi, W. and Driscoll, B. (2009). "Lung alveolar integrity is compromised by telomere shortening in telomerase-null mice." Am J Physiol Lung Cell Mol Physiol **296**(1): L57-70.

Lee, J. S., Song, J. W., Wolters, P. J., Elicker, B. M., King, T. E., Jr., Kim, D. S. and Collard, H. R. (2012). "Bronchoalveolar lavage pepsin in acute exacerbation of idiopathic pulmonary fibrosis." Eur Respir J **39**(2): 352-358.

Li, M., Krishnaveni, M. S., Li, C., Zhou, B., Xing, Y., Banfalvi, A., Li, A., Lombardi, V., Akbari, O., Borok, Z. and Minoo, P. (2011). "Epithelium-specific deletion of TGF-beta receptor type II protects mice from bleomycin-induced pulmonary fibrosis." J Clin Invest **121**(1): 277-287.

Li, M. O., Wan, Y. Y., Sanjabi, S., Robertson, A. K. and Flavell, R. A. (2006). "Transforming growth factor-beta regulation of immune responses." Annu Rev Immunol **24**: 99-146.

Li, Y., Jiang, D., Liang, J., Meltzer, E. B., Gray, A., Miura, R., Wogensen, L., Yamaguchi, Y. and Noble, P. W. (2011). "Severe lung fibrosis requires an invasive fibroblast phenotype regulated by hyaluronan and CD44." J Exp Med **208**(7): 1459-1471.

Lindahl, G. E., Chambers, R. C., Papakrivopoulou, J., Dawson, S. J., Jacobsen, M. C., Bishop, J. E. and Laurent, G. J. (2002). "Activation of fibroblast procollagen alpha 1(I) transcription by mechanical strain is transforming growth factor-beta-dependent and involves increased binding of CCAAT-binding factor (CBF/NF-Y) at the proximal promoter." J Biol Chem **277**(8): 6153-6161.

Lino Cardenas, C. L., Henaoui, I. S., Courcot, E., Roderburg, C., Cauffiez, C., Aubert, S., Copin, M. C., Wallaert, B., Glowacki, F., Dewaeles, E., Milosevic, J., Maurizio, J., Tedrow, J., Marcet, B., Lo-Guidice, J. M., Kaminski, N., Barbry, P., Luedde, T., Perrais, M., Mari, B. and Pottier, N. (2013). "miR-199a-5p Is upregulated during fibrogenic response to tissue injury and mediates TGFbeta-induced lung fibroblast activation by targeting caveolin-1." PLoS Genet **9**(2): e1003291.

Liu, F., Mih, J. D., Shea, B. S., Kho, A. T., Sharif, A. S., Tager, A. M. and Tschumperlin, D. J. (2010). "Feedback amplification of fibrosis through matrix stiffening and COX-2 suppression." J Cell Biol **190**(4): 693-706.

Liu, T., Ullenbruch, M., Young Choi, Y., Yu, H., Ding, L., Xaubet, A., Pereda, J., Feghali-Bostwick, C. A., Bitterman, P. B., Henke, C. A., Pardo, A., Selman, M. and Phan, S. H. (2013). "Telomerase and telomere length in pulmonary fibrosis." Am J Respir Cell Mol Biol **49**(2): 260-268.

Lu, Z., Jiang, G., Blume-Jensen, P. and Hunter, T. (2001). "Epidermal growth factor-induced tumor cell invasion and metastasis initiated by dephosphorylation and downregulation of focal adhesion kinase." Mol Cell Biol **21**(12): 4016-4031.

Maehama, T. and Dixon, J. E. (1998). "The tumor suppressor, PTEN/MMAC1, dephosphorylates the lipid second messenger, phosphatidylinositol 3,4,5-trisphosphate." J Biol Chem **273**(22): 13375-13378.

Maher, T. M., Evans, I. C., Bottoms, S. E., Mercer, P. F., Thorley, A. J., Nicholson, A. G., Laurent, G. J., Tetley, T. D., Chambers, R. C. and McAnulty, R. J. (2010). "Diminished prostaglandin E2 contributes to the apoptosis paradox in idiopathic pulmonary fibrosis." Am J Respir Crit Care Med **182**(1): 73-82.

Marmai, C., Sutherland, R. E., Kim, K. K., Dolganov, G. M., Fang, X., Kim, S. S., Jiang, S., Golden, J. A., Hoopes, C. W., Matthay, M. A., Chapman, H. A. and Wolters, P. J. (2011). "Alveolar epithelial cells express mesenchymal proteins in patients with idiopathic pulmonary fibrosis." Am J Physiol Lung Cell Mol Physiol **301**(1): L71-78.

Massague, J. (2008). "TGFbeta in Cancer." Cell **134**(2): 215-230.

Massague, J. (2012). "TGFbeta signalling in context." Nat Rev Mol Cell Biol **13**(10): 616-630.

Matsuda, Y., Schlange, T., Oakeley, E. J., Boulay, A. and Hynes, N. E. (2009). "WNT signaling enhances breast cancer cell motility and blockade of the WNT pathway by sFRP1 suppresses MDA-MB-231 xenograft growth." Breast Cancer Res **11**(3): R32.

McAnulty, R. J., Campa, J. S., Cambrey, A. D. and Laurent, G. J. (1991). "The effect of transforming growth factor beta on rates of procollagen synthesis and degradation in vitro." Biochim Biophys Acta **1091**(2): 231-235.

Mendez, M. G., Restle, D. and Janmey, P. A. (2014). "Vimentin enhances cell elastic behavior and protects against compressive stress." Biophys J **107**(2): 314-323.

Montorfano, I., Becerra, A., Cerro, R., Echeverria, C., Saez, E., Morales, M. G., Fernandez, R., Cabello-Verrugio, C. and Simon, F. (2014). "Oxidative stress mediates the conversion of endothelial cells into myofibroblasts via a TGF-beta1 and TGF-beta2-dependent pathway." Lab Invest **94**(10): 1068-1082.

Mubarak, K. K., Montes-Worboys, A., Regev, D., Nasreen, N., Mohammed, K. A., Faruqi, I., Hensel, E., Baz, M. A., Akindipe, O. A., Fernandez-Bussy, S., Nathan, S. D. and Antony, V. B. (2012). "Parenchymal trafficking of pleural mesothelial cells in idiopathic pulmonary fibrosis." Eur Respir J **39**(1): 133-140.

Naba, A., Clauser, K. R., Hoersch, S., Liu, H., Carr, S. A. and Hynes, R. O. (2012). "The matrisome: in silico definition and in vivo characterization by proteomics of normal and tumor extracellular matrices." Mol Cell Proteomics **11**(4): M111.014647.

Nalysnyk, L., Cid-Ruzafa, J., Rotella, P. and Esser, D. (2012). "Incidence and prevalence of idiopathic pulmonary fibrosis: review of the literature." Eur Respir Rev **21**(126): 355-361.

Nasreen, N., Mohammed, K. A., Mubarak, K. K., Baz, M. A., Akindipe, O. A., Fernandez-Bussy, S. and Antony, V. B. (2009). "Pleural mesothelial cell transformation into myofibroblasts and haptotactic migration in response to TGF-beta1 in vitro." Am J Physiol Lung Cell Mol Physiol **297**(1): L115-124.

Nho, R. S., Hergert, P., Kahm, J., Jessurun, J. and Henke, C. (2011). "Pathological alteration of FoxO3a activity promotes idiopathic pulmonary fibrosis fibroblast proliferation on type i collagen matrix." Am J Pathol **179**(5): 2420-2430.

Nkyimbeng, T., Ruppert, C., Shiomi, T., Dahal, B., Lang, G., Seeger, W., Okada, Y., D'Armiento, J. and Gunther, A. (2013). "Pivotal role of matrix metalloproteinase 13 in extracellular matrix turnover in idiopathic pulmonary fibrosis." PLoS One **8**(9): e73279.

Nogee, L. M., Dunbar, A. E., 3rd, Wert, S. E., Askin, F., Hamvas, A. and Whitsett, J. A. (2001). "A mutation in the surfactant protein C gene associated with familial interstitial lung disease." N Engl J Med **344**(8): 573-579.

Oehrle, B., Burgstaller, G., Irmler, M., Dehmel, S., Gruen, J., Hwang, T., Krauss-Etschmann, S., Beckers, J., Meiners, S. and Eickelberg, O. (2015). "Validated prediction of pro-invasive growth factors using a transcriptome-wide invasion signature derived from a complex 3D invasion assay." Sci Rep.: - *in press*.

Oikonomou, N., Mouratis, M. A., Tzouvelekis, A., Kaffe, E., Valavanis, C., Vilaras, G., Karameris, A., Prestwich, G. D., Bouros, D. and Aidinis, V. (2012). "Pulmonary autotaxin expression contributes to the pathogenesis of pulmonary fibrosis." Am J Respir Cell Mol Biol **47**(5): 566-574.

Okamoto, T., Schlegel, A., Scherer, P. E. and Lisanti, M. P. (1998). "Caveolins, a family of scaffolding proteins for organizing "preassembled signaling complexes" at the plasma membrane." J Biol Chem **273**(10): 5419-5422.

Orgaz, J. L., Pandya, P., Dalmeida, R., Karagiannis, P., Sanchez-Laorden, B., Viros, A., Albrengues, J., Nestle, F. O., Ridley, A. J., Gaggioli, C., Marais, R., Karagiannis, S. N. and Sanz-Moreno, V. (2014). "Diverse matrix metalloproteinase functions regulate cancer amoeboid migration." Nat Commun **5**: 4255.

Overall, C. M. (2002). "Molecular determinants of metalloproteinase substrate specificity: matrix metalloproteinase substrate binding domains, modules, and exosites." Mol Biotechnol **22**(1): 51-86.

Pandit, K. V., Milosevic, J. and Kaminski, N. (2011). "MicroRNAs in idiopathic pulmonary fibrosis." Transl Res **157**(4): 191-199.

Pardo, A., Selman, M. and Kaminski, N. (2008). "Approaching the degradome in idiopathic pulmonary fibrosis." Int J Biochem Cell Biol **40**(6-7): 1141-1155.

Parker, M. W., Rossi, D., Peterson, M., Smith, K., Sikstrom, K., White, E. S., Connett, J. E., Henke, C. A., Larsson, O. and Bitterman, P. B. (2014). "Fibrotic extracellular matrix activates a profibrotic positive feedback loop." J Clin Invest **124**(4): 1622-1635.

Patel, P., West-Mays, J., Kolb, M., Rodrigues, J. C., Hoff, C. M. and Margetts, P. J. (2010). "Platelet derived growth factor B and epithelial mesenchymal transition of peritoneal mesothelial cells." Matrix Biol **29**(2): 97-106.

Pathak, A. and Kumar, S. (2011). "Biophysical regulation of tumor cell invasion: moving beyond matrix stiffness." Integr Biol (Camb) **3**(4): 267-278.

Pechkovsky, D. V., Hackett, T. L., An, S. S., Shaheen, F., Murray, L. A. and Knight, D. A. (2010). "Human lung parenchyma but not proximal bronchi produces fibroblasts with enhanced TGF-beta signaling and alpha-SMA expression." Am J Respir Cell Mol Biol **43**(6): 641-651.

Phan, S. H. (2008). "Biology of fibroblasts and myofibroblasts." Proc Am Thorac Soc **5**(3): 334-337.

Potts, J. and Yogaratnam, D. (2013). "Pirfenidone: a novel agent for the treatment of idiopathic pulmonary fibrosis." Ann Pharmacother **47**(3): 361-367.

Rabinovich, E. I., Kapetanaki, M. G., Steinfeld, I., Gibson, K. F., Pandit, K. V., Yu, G., Yakhini, Z. and Kaminski, N. (2012). "Global methylation patterns in idiopathic pulmonary fibrosis." PLoS One **7**(4): e33770.

Raeber, G. P., Lutolf, M. P. and Hubbell, J. A. (2005). "Molecularly engineered PEG hydrogels: a novel model system for proteolytically mediated cell migration." Biophys J **89**(2): 1374-1388.

Rafii, R., Juarez, M. M., Albertson, T. E. and Chan, A. L. (2013). "A review of current and novel therapies for idiopathic pulmonary fibrosis." J Thorac Dis **5**(1): 48-73.

Raghu, G., Collard, H. R., Egan, J. J., Martinez, F. J., Behr, J., Brown, K. K., Colby, T. V., Cordier, J. F., Flaherty, K. R., Lasky, J. A., Lynch, D. A., Ryu, J. H., Swigris, J. J., Wells, A. U., Ancochea, J., Bouros, D., Carvalho, C., Costabel, U., Ebina, M., Hansell, D. M., Johkoh, T., Kim, D. S., King, T. E., Jr., Kondoh, Y., Myers, J., Muller, N. L., Nicholson, A. G., Richeldi, L., Selman, M., Dudden, R. F., Griss, B. S., Protzko, S. L. and Schunemann, H. J. (2011). "An official ATS/ERS/JRS/ALAT statement: idiopathic pulmonary fibrosis: evidence-based guidelines for diagnosis and management." Am J Respir Crit Care Med **183**(6): 788-824.

Rainer, J., Sanchez-Cabo, F., Stocker, G., Sturn, A. and Trajanoski, Z. (2006). "CARMAweb: comprehensive R- and bioconductor-based web service for microarray data analysis." Nucleic Acids Res **34**(Web Server issue): W498-503.

Ren, J., Wang, R., Huang, G., Song, H., Chen, Y. and Chen, L. (2013). "sFRP1 Inhibits Epithelial-Mesenchymal Transition in A549 Human Lung Adenocarcinoma Cell Line." Cancer Biother Radiopharm **28**(7): 565-571.

Rhee, S. (2009). "Fibroblasts in three dimensional matrices: cell migration and matrix remodeling." Exp Mol Med **41**(12): 858-865.

Ricard-Blum, S. (2011). "The collagen family." Cold Spring Harb Perspect Biol **3**(1): a004978.

Richeldi, L., du Bois, R. M., Raghu, G., Azuma, A., Brown, K. K., Costabel, U., Cottin, V., Flaherty, K. R., Hansell, D. M., Inoue, Y., Kim, D. S., Kolb, M., Nicholson, A. G., Noble, P. W., Selman, M., Taniguchi, H., Brun, M., Le Maulf, F., Girard, M., Stowasser, S., Schlenker-Herceg, R., Disse, B. and Collard, H. R. (2014). "Efficacy and safety of nintedanib in idiopathic pulmonary fibrosis." N Engl J Med **370**(22): 2071-2082.

Ridley, A. J., Schwartz, M. A., Burridge, K., Firtel, R. A., Ginsberg, M. H., Borisy, G., Parsons, J. T. and Horwitz, A. R. (2003). "Cell migration: integrating signals from front to back." Science **302**(5651): 1704-1709.

Rock, J. R., Barkauskas, C. E., Cronce, M. J., Xue, Y., Harris, J. R., Liang, J., Noble, P. W. and Hogan, B. L. (2011). "Multiple stromal populations contribute to pulmonary fibrosis without evidence for epithelial to mesenchymal transition." Proc Natl Acad Sci U S A **108**(52): E1475-1483.

Rodin, S., Antonsson, L., Niaudet, C., Simonson, O. E., Salmela, E., Hansson, E. M., Domogatskaya, A., Xiao, Z., Damdimopoulou, P., Sheikhi, M., Inzunza, J., Nilsson, A. S., Baker, D., Kuiper, R., Sun, Y., Blennow, E., Nordenskjold, M., Grinnemo, K. H., Kere, J., Betsholtz, C., Hovatta, O. and Tryggvason, K. (2014). "Clonal culturing of human embryonic stem cells on laminin-521/E-cadherin matrix in defined and xeno-free environment." Nat Commun **5**: 3195.

Rosas, I. O., Richards, T. J., Konishi, K., Zhang, Y., Gibson, K., Lokshin, A. E., Lindell, K. O., Cisneros, J., Macdonald, S. D., Pardo, A., Sciurba, F., Dauber, J., Selman, M., Gochuico, B. R. and Kaminski, N. (2008). "MMP1 and MMP7 as potential peripheral blood biomarkers in idiopathic pulmonary fibrosis." PLoS Med **5**(4): e93.

Rudolph, K. L., Chang, S., Lee, H. W., Blasco, M., Gottlieb, G. J., Greider, C. and DePinho, R. A. (1999). "Longevity, stress response, and cancer in aging telomerase-deficient mice." Cell **96**(5): 701-712.

Russell, S. B., Russell, J. D., Trupin, K. M., Gayden, A. E., Opalenik, S. R., Nanney, L. B., Broquist, A. H., Raju, L. and Williams, S. M. (2010). "Epigenetically altered wound healing in keloid fibroblasts." J Invest Dermatol **130**(10): 2489-2496.

Sabeh, F., Li, X. Y., Saunders, T. L., Rowe, R. G. and Weiss, S. J. (2009). "Secreted versus membrane-anchored collagenases: relative roles in fibroblast-dependent collagenolysis and invasion." J Biol Chem **284**(34): 23001-23011.

Sand, J. M., Larsen, L., Hogaboam, C., Martinez, F., Han, M., Rossel Larsen, M., Nawrocki, A., Zheng, Q., Karsdal, M. A. and Leeming, D. J. (2013). "MMP mediated degradation of type IV collagen alpha 1 and alpha 3 chains reflects basement membrane remodeling in experimental and clinical fibrosis--validation of two novel biomarker assays." PLoS One **8**(12): e84934.

Sanders, Y. Y., Ambalavanan, N., Halloran, B., Zhang, X., Liu, H., Crossman, D. K., Bray, M., Zhang, K., Thannickal, V. J. and Hagood, J. S. (2012). "Altered DNA methylation profile in idiopathic pulmonary fibrosis." Am J Respir Crit Care Med **186**(6): 525-535.

Santibanez, J. F., Quintanilla, M. and Bernabeu, C. (2011). "TGF-beta/TGF-beta receptor system and its role in physiological and pathological conditions." Clin Sci (Lond) **121**(6): 233-251.

Saums, M. K., Wang, W., Han, B., Madhavan, L., Han, L., Lee, D. and Wells, R. G. (2014). "Mechanically and chemically tunable cell culture system for studying the myofibroblast phenotype." Langmuir **30**(19): 5481-5487.

Schor, S. L., Allen, T. D. and Winn, B. (1983). "Lymphocyte migration into three-dimensional collagen matrices: a quantitative study." J Cell Biol **96**(4): 1089-1096.

Selman, M., King, T. E. and Pardo, A. (2001). "Idiopathic pulmonary fibrosis: prevailing and evolving hypotheses about its pathogenesis and implications for therapy." Ann Intern Med **134**(2): 136-151.

Selman, M., Pardo, A. and Kaminski, N. (2008). "Idiopathic pulmonary fibrosis: aberrant recapitulation of developmental programs?" PLoS Med **5**(3): e62.

Shabbir, S. H., Cleland, M. M., Goldman, R. D. and Mrksich, M. (2014). "Geometric control of vimentin intermediate filaments." Biomaterials **35**(5): 1359-1366.

Shivshankar, P., Brampton, C., Miyasato, S., Kasper, M., Thannickal, V. J. and Le Saux, C. J. (2012). "Caveolin-1 deficiency protects from pulmonary fibrosis by modulating epithelial cell senescence in mice." Am J Respir Cell Mol Biol **47**(1): 28-36.

Siegel, P. M. and Massague, J. (2003). "Cytostatic and apoptotic actions of TGF-beta in homeostasis and cancer." Nat Rev Cancer **3**(11): 807-821.

Silver, F. H. and Pins, G. (1992). "Cell growth on collagen: a review of tissue engineering using scaffolds containing extracellular matrix." J Long Term Eff Med Implants **2**(1): 67-80.

Sime, P. J., Xing, Z., Graham, F. L., Csaky, K. G. and Gauldie, J. (1997). "Adenovector-mediated gene transfer of active transforming growth factor-beta1 induces prolonged severe fibrosis in rat lung." J Clin Invest **100**(4): 768-776.

Studer, S. M. and Kaminski, N. (2007). "Towards systems biology of human pulmonary fibrosis." Proc Am Thorac Soc **4**(1): 85-91.

Sueblinvong, V., Neujahr, D. C., Mills, S. T., Roser-Page, S., Ritzenthaler, J. D., Guidot, D., Rojas, M. and Roman, J. (2012). "Predisposition for disrepair in the aged lung." Am J Med Sci **344**(1): 41-51.

Suganuma, H., Sato, A., Tamura, R. and Chida, K. (1995). "Enhanced migration of fibroblasts derived from lungs with fibrotic lesions." Thorax **50**(9): 984-989.

Surana, R., Sikka, S., Cai, W., Shin, E. M., Warrier, S. R., Tan, H. J., Arfuso, F., Fox, S. A., Dharmarajan, A. M. and Kumar, A. P. (2014). "Secreted frizzled related proteins: Implications in cancers." Biochim Biophys Acta **1845**(1): 53-65.

Surendran, K., Schiavi, S. and Hruska, K. A. (2005). "Wnt-dependent beta-catenin signaling is activated after unilateral ureteral obstruction, and recombinant secreted frizzled-related protein 4 alters the progression of renal fibrosis." J Am Soc Nephrol **16**(8): 2373-2384.

Tager, A. M., LaCamera, P., Shea, B. S., Campanella, G. S., Selman, M., Zhao, Z., Polosukhin, V., Wain, J., Karimi-Shah, B. A., Kim, N. D., Hart, W. K., Pardo, A., Blackwell, T. S., Xu, Y., Chun, J. and Luster, A. D. (2008). "The lysophosphatidic acid receptor LPA1 links pulmonary fibrosis to lung injury by mediating fibroblast recruitment and vascular leak." Nat Med **14**(1): 45-54.

Tamura, M., Gu, J., Matsumoto, K., Aota, S., Parsons, R. and Yamada, K. M. (1998). "Inhibition of cell migration, spreading, and focal adhesions by tumor suppressor PTEN." Science **280**(5369): 1614-1617.

Thannickal, V. J., Henke, C. A., Horowitz, J. C., Noble, P. W., Roman, J., Sime, P. J., Zhou, Y., Wells, R. G., White, E. S. and Tschumperlin, D. J. (2014). "Matrix biology of idiopathic pulmonary fibrosis: a workshop report of the national heart, lung, and blood institute." Am J Pathol **184**(6): 1643-1651.

Thomas, A. Q., Lane, K., Phillips, J., 3rd, Prince, M., Markin, C., Speer, M., Schwartz, D. A., Gaddipati, R., Marney, A., Johnson, J., Roberts, R., Haines, J., Stahlman, M. and Loyd, J. E. (2002). "Heterozygosity for a surfactant protein C gene mutation associated with usual interstitial pneumonitis and cellular nonspecific interstitial pneumonitis in one kindred." Am J Respir Crit Care Med **165**(9): 1322-1328.

Timpson, P., McGhee, E. J., Erami, Z., Nobis, M., Quinn, J. A., Edward, M. and Anderson, K. I. (2011). "Organotypic collagen I assay: a malleable platform to assess cell behaviour in a 3-dimensional context." J Vis Exp(56): e3089.

Vasaturo, A., Caserta, S., Russo, I., Preziosi, V., Ciacci, C. and Guido, S. (2012). "A novel chemotaxis assay in 3-D collagen gels by time-lapse microscopy." PLoS One **7**(12): e52251.

Veeck, J., Niederacher, D., An, H., Klopocki, E., Wiesmann, F., Betz, B., Galm, O., Camara, O., Durst, M., Kristiansen, G., Huszka, C., Knuchel, R. and Dahl, E. (2006). "Aberrant methylation of

the Wnt antagonist SFRP1 in breast cancer is associated with unfavourable prognosis." Oncogene **25**(24): 3479-3488.

Vuga, L. J., Ben-Yehudah, A., Kovkarova-Naumovski, E., Oriss, T., Gibson, K. F., Feghali-Bostwick, C. and Kaminski, N. (2009). "WNT5A is a regulator of fibroblast proliferation and resistance to apoptosis." Am J Respir Cell Mol Biol **41**(5): 583-589.

Wang, X. M., Zhang, Y., Kim, H. P., Zhou, Z., Feghali-Bostwick, C. A., Liu, F., Ifedigbo, E., Xu, X., Oury, T. D., Kaminski, N. and Choi, A. M. (2006). "Caveolin-1: a critical regulator of lung fibrosis in idiopathic pulmonary fibrosis." J Exp Med **203**(13): 2895-2906.

Wang, Y., Kuan, P. J., Xing, C., Cronkhite, J. T., Torres, F., Rosenblatt, R. L., DiMaio, J. M., Kinch, L. N., Grishin, N. V. and Garcia, C. K. (2009). "Genetic defects in surfactant protein A2 are associated with pulmonary fibrosis and lung cancer." Am J Hum Genet **84**(1): 52-59.

Wells, A. U. (2013). "The revised ATS/ERS/JRS/ALAT diagnostic criteria for idiopathic pulmonary fibrosis (IPF)--practical implications." Respir Res **14 Suppl 1**: S2.

White, E. S., Atrasz, R. G., Hu, B., Phan, S. H., Stambolic, V., Mak, T. W., Hogaboam, C. M., Flaherty, K. R., Martinez, F. J., Kontos, C. D. and Toews, G. B. (2006). "Negative regulation of myofibroblast differentiation by PTEN (Phosphatase and Tensin Homolog Deleted on chromosome 10)." Am J Respir Crit Care Med **173**(1): 112-121.

White, E. S., Thannickal, V. J., Carskadon, S. L., Dickie, E. G., Livant, D. L., Markwart, S., Toews, G. B. and Arenberg, D. A. (2003). "Integrin alpha4beta1 regulates migration across basement membranes by lung fibroblasts: a role for phosphatase and tensin homologue deleted on chromosome 10." Am J Respir Crit Care Med **168**(4): 436-442.

Wilborn, J., Crofford, L. J., Burdick, M. D., Kunkel, S. L., Strieter, R. M. and Peters-Golden, M. (1995). "Cultured lung fibroblasts isolated from patients with idiopathic pulmonary fibrosis have a diminished capacity to synthesize prostaglandin E2 and to express cyclooxygenase-2." J Clin Invest **95**(4): 1861-1868.

Willenbrock, F., Crabbe, T., Slocombe, P. M., Sutton, C. W., Docherty, A. J., Cockett, M. I., O'Shea, M., Brocklehurst, K., Phillips, I. R. and Murphy, G. (1993). "The activity of the tissue inhibitors of metalloproteinases is regulated by C-terminal domain interactions: a kinetic analysis of the inhibition of gelatinase A." Biochemistry **32**(16): 4330-4337.

Willis, B. C. and Borok, Z. (2007). "TGF-beta-induced EMT: mechanisms and implications for fibrotic lung disease." Am J Physiol Lung Cell Mol Physiol **293**(3): L525-534.

Willis, B. C., Liebler, J. M., Luby-Phelps, K., Nicholson, A. G., Crandall, E. D., du Bois, R. M. and Borok, Z. (2005). "Induction of epithelial-mesenchymal transition in alveolar epithelial cells by transforming growth factor-beta1: potential role in idiopathic pulmonary fibrosis." Am J Pathol **166**(5): 1321-1332.

Wipff, P. J., Rifkin, D. B., Meister, J. J. and Hinz, B. (2007). "Myofibroblast contraction activates latent TGF-beta1 from the extracellular matrix." J Cell Biol **179**(6): 1311-1323.

Wolf, K., Alexander, S., Schacht, V., Coussens, L. M., von Andrian, U. H., van Rheenen, J., Deryugina, E. and Friedl, P. (2009). "Collagen-based cell migration models in vitro and in vivo." Semin Cell Dev Biol **20**(8): 931-941.

Wolters, P. J., Collard, H. R. and Jones, K. D. (2014). "Pathogenesis of idiopathic pulmonary fibrosis." Annu Rev Pathol **9**: 157-179.

Wootton, S. C., Kim, D. S., Kondoh, Y., Chen, E., Lee, J. S., Song, J. W., Huh, J. W., Taniguchi, H., Chiu, C., Boushey, H., Lancaster, L. H., Wolters, P. J., DeRisi, J., Ganem, D. and Collard, H. R. (2011). "Viral infection in acute exacerbation of idiopathic pulmonary fibrosis." Am J Respir Crit Care Med **183**(12): 1698-1702.

Wu, M. Y. and Hill, C. S. (2009). "Tgf-beta superfamily signaling in embryonic development and homeostasis." Dev Cell **16**(3): 329-343.

Xaubet, A., Marin-Arguedas, A., Lario, S., Ancochea, J., Morell, F., Ruiz-Manzano, J., Rodriguez-Becerra, E., Rodriguez-Arias, J. M., Inigo, P., Sanz, S., Campistol, J. M., Mullol, J. and Picado, C. (2003). "Transforming growth factor-beta1 gene polymorphisms are associated with disease progression in idiopathic pulmonary fibrosis." Am J Respir Crit Care Med **168**(4): 431-435.

Xia, H., Diebold, D., Nho, R., Perlman, D., Kleidon, J., Kahm, J., Avdulov, S., Peterson, M., Nerva, J., Bitterman, P. and Henke, C. (2008). "Pathological integrin signaling enhances proliferation of primary lung fibroblasts from patients with idiopathic pulmonary fibrosis." J Exp Med **205**(7): 1659-1672.

Xia, H., Khalil, W., Kahm, J., Jessurun, J., Kleidon, J. and Henke, C. A. (2010). "Pathologic caveolin-1 regulation of PTEN in idiopathic pulmonary fibrosis." Am J Pathol **176**(6): 2626-2637.

Yeang, C. H., McCormick, F. and Levine, A. (2008). "Combinatorial patterns of somatic gene mutations in cancer." Faseb j **22**(8): 2605-2622.

Yu, Y., Xiao, C. H., Tan, L. D., Wang, Q. S., Li, X. Q. and Feng, Y. M. (2014). "Cancer-associated fibroblasts induce epithelial-mesenchymal transition of breast cancer cells through paracrine TGF-beta signalling." Br J Cancer **110**(3): 724-732.

Zhang, K., Rekhter, M. D., Gordon, D. and Phan, S. H. (1994). "Myofibroblasts and their role in lung collagen gene expression during pulmonary fibrosis. A combined immunohistochemical and in situ hybridization study." Am J Pathol **145**(1): 114-125.

Zhang, L., Li, Y., Liang, C. and Yang, W. (2014). "CCN5 overexpression inhibits profibrotic phenotypes via the PI3K/Akt signaling pathway in lung fibroblasts isolated from patients with idiopathic pulmonary fibrosis and in an in vivo model of lung fibrosis." Int J Mol Med **33**(2): 478-486.

Zhu, J., Wang, Y., Duan, J., Bai, H., Wang, Z., Wei, L., Zhao, J., Zhuo, M., Wang, S., Yang, L., An, T., Wu, M. and Wang, J. (2012). "DNA Methylation status of Wnt antagonist SFRP5 can predict the response to the EGFR-tyrosine kinase inhibitor therapy in non-small cell lung cancer." J Exp Clin Cancer Res **31**: 80.

Zi, Z., Chapnick, D. A. and Liu, X. (2012). "Dynamics of TGF-beta/Smad signaling." FEBS Lett **586**(14): 1921-1928.

Zolak, J. S., Jagirdar, R., Surolia, R., Karki, S., Oliva, O., Hock, T., Guroji, P., Ding, Q., Liu, R. M., Bolisetty, S., Agarwal, A., Thannickal, V. J. and Antony, V. B. (2013). "Pleural mesothelial cell differentiation and invasion in fibrogenic lung injury." Am J Pathol **182**(4): 1239-1247.

List of Tables

Table 1.1: Diagnosis of IPF in absence of surgical lung biopsy (2000). (Wells 2013) – *modified.* ..2
Table 1.2: Selected ongoing clinical trials for IPF (Rafii, Juarez et al. 2013) – *modified.* 3
Table 2.1: Primary antibodies for Western blot.....17
Table 2.2: Secondary antibodies for Western blot.....17
Table 2.3: Primary antibodies for immunofluorescence stainings.....17
Table 2.4: Secondary antibodies for immunofluorescence stainings.....17
Table 2.5: Murine cell line.....20
Table 2.6: Human cell line.....21
Table 2.7: Primary human fibroblast lines.....21
Table 2.8: Laboratory equipment.....22
Table 2.9: Software.....23
Table 2.10: Chemicals 24
Table 2.11: Consumables.....25
Table 2.12: Enzymes 25
Table 2.13: Oligonucleotides.....26
Table 2.14: quantitative human qPCR primer. 26
Table 2.15: quantitative mouse qPCR primer.....26
Table 2.16: Standards 27
Table 2.17: Kits 27
Table 2.18: Cell type specific culturing conditions 29
Table 2.19: Transfection protocol for one well of a 6-well plate 29
Table 2.20: Preparation of collagen G matrices.....31
Table 2.21: Culturing conditions for invasion assay 32
Table 2.22: Pipet scheme for reverse transcription.....34
Table 2.23: Reaction scheme qRT-PCR 34
Table 6.1: Up-regulated probesets in invading/non-invading fibroblasts.....121
Table 6.2: Down-regulated probesets in invading/non-invading fibroblasts.....133
Table 6.3: Up-regulated probesets in invading and non-invading TGFβ1-treated fibroblasts. 138
Table 6.4: Down-regulated probesets in invading and non-invading TGFβ1-treated fibroblasts..143

List of Figures

Figure 1.1: Histopathological appearance of UIP. 4
Figure 1.2: Cellular transition. 10
Figure 1.3: Mode of mesenchymal migration. 12
Figure 3.1: Confocal image of an invading MLg fibroblast, embedded in collagen matrix. 42
Figure 3.2: Experimental set-up and analysis of 3D collagen-based invasion assay. 43
Figure 3.3: Quantification of the maximal invasion distance of MLg and A549 cells. 43
Figure 3.4: Live cell imaging showing fibroblast invasion over time. 44
Figure 3.5: Assessment of the morphological plasticity of MLg fibroblasts. 46
Figure 3.6: Assessment of the geometry of MLg fibroblasts in different microenvironments. 47
Figure 3.7: Immunofluorescence staining for integrin β1 (CD29) in invading MLg fibroblasts..... 47
Figure 3.8: Immunofluorescence staining for Ki67. 48
Figure 3.9: Immunofluorescence staining fibronectin and vimentin in invading MLg fibroblasts. 49
Figure 3.10: Experimental set-up of 3D collagen-based separation assay. 50
Figure 3.11: TGFβ1 and EGF induce MLg fibroblast invasion. 51
Figure 3.12: Differential gene expression numbers of conducted microarrays and hierarchical clustering. 53
Figure 3.13: Heatmaps and Volcano plots for transcript expression of the invasion signatures at 72 and 96 hours. 56
Figure 3.14: Overlap of gene expression in the conducted transcriptome analyses at 72 and 96 hours. 57
Figure 3.15: Analysis of functional gene cluster enrichment in the invasion induced transcriptome signature with the Ingenuity® pathway analysis platform (IPA). 58
Figure 3.16: Differential gene expression numbers of conducted microarrays (TGFβ1-treated groups) and hierarchical clustering. 60
Figure 3.17: Heatmaps visualizing differential gene expression of TGFβ1-treated compared to non-treated non-invading and invading fibroblasts. 62
Figure 3.18: Volcano plots for TGFβ1-induced variation in transcript expression levels. 63
Figure 3.19 Overlap of gene expression in the conducted transcriptome analyses at 96 hours invading/non-invading with invading TGFβ1/non-treated. 64
Figure 3.20: Heatmaps of the TGFβ1-mediated transcriptomic invasion signature. 65
Figure 3.21: Validation of transcriptome analysis for selected invasion-associated genes. 66
Figure 3.22: MMP13 and Cav1 protein expression in invading MLg fibroblasts. 67
Figure 3.23: Expression of invasion-associated target genes in invading phF. 67
Figure 3.24: Sfrp1 expression in invading MLg fibroblasts. 68

Figure 3.25: Transcript levels of Sfrp isoforms. 69
Figure 3.26: Differential expression of Sfrp1 in phF upon invasion. 70
Figure 3.27: Down-regulation of Sfrp1 transcript upon TGFβ1 and EGF stimulation..... 71
Figure 3.28: TGFβ1 and EGF induced reduction of Sfrp1 protein expression. 71
Figure 3.29: Sfrp1 mRNA expression in phF derived from ILD patients. 72
Figure 3.30: Sfrp1 protein expression in phF derived from ILD patients..... 73
Figure 3.31: Induction of phF invasion upon EGF stimulation. 73
Figure 3.32: Correlation of Sfrp1 expression and EGF-induced fibroblast invasion. 74
Figure 3.33: TGFβ1 and EGF reduced Sfrp1 protein expression in phF. 75
Figure 3.34: Co-staining of Sfrp1 and col1a1 in phF. 76
Figure 3.35: Localization of Sfrp1 in phF. 77
Figure 3.36: Titration of the Sfrp1-inhibitor CHEMBL473916 with TCF luciferase (TOP/FOP) assay..... 78
Figure 3.37: Induction of fibroblast invasion by Sfrp1 inhibition. 79
Figure 3.38: Assessment of 2D motility of MLg fibroblasts after Sfrp1 inhibition CHEMBL473916..... 79
Figure 4.1: Schematical illustration of Sfrp1 expression in fibroblasts upon collagen invasion. 91
Figure 4.2: Prediction on up- and down-stream effects of Sfrp1 in the conducted invasion signature..... 92
Figure 4.3: Suppression of Sfrp1 expression by TGFβ1 and EGF. 93
Figure 6.1: Overview on prolate and oblate Spheroids..... 116

6. APPENDIX

6.1 Scheme for cell morphology quantification

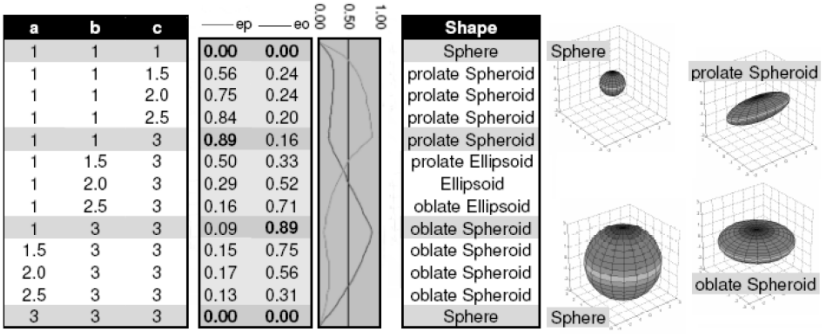

a	b	c	ep	eo	Shape
1	1	1	**0.00**	**0.00**	Sphere
1	1	1.5	0.56	0.24	prolate Spheroid
1	1	2.0	0.75	0.24	prolate Spheroid
1	1	2.5	0.84	0.20	prolate Spheroid
1	1	3	**0.89**	0.16	prolate Spheroid
1	1.5	3	0.50	0.33	prolate Ellipsoid
1	2.0	3	0.29	0.52	Ellipsoid
1	2.5	3	0.16	0.71	oblate Ellipsoid
1	3	3	0.09	**0.89**	oblate Spheroid
1.5	3	3	0.15	0.75	oblate Spheroid
2.0	3	3	0.17	0.56	oblate Spheroid
2.5	3	3	0.13	0.31	oblate Spheroid
3	3	3	**0.00**	**0.00**	Sphere

Figure 6.1: Overview on prolate and oblate Spheroids.

Decision criteria for prolate and oblate cell shape. Imaris V6.0 Reference Manual (Bitplane 2007), (Reprinted with permission of Bitplane (Bitplane AG, Zurich; Switzerland)).

6.2 Gene expression lists

Up-regulated probesets in invading/non-invading fibroblasts

				72 h n.t. (inv./non-inv.) Statistical analysis, limma t-test, BH			96 h n.t. (inv./non-inv.) Statistical analysis, limma t-test, BH		
Probe_set	Gene symbol or ID	Entrez	Unclear annotation	rawp	BH	Ratio (G/M), significant FDR<10%, ratio>1.5x (1086)	rawp	BH	Ratio (G/M), significant FDR<10%, ratio>1.5x (1049)
10583044	Mmp13	17386		5.4E-08	4.7E-05	4.37	8.7E-12	8.2E-08	9.35
10455015	Vaultrc5	378472		3.8E-08	3.9E-05	4.26	2.7E-08	8.1E-06	3.54
10583071	Mmp3	17392		1.9E-07	7.7E-05	4.25	7.1E-10	1.3E-06	7.55
10416503	Snora31	100303751		8.0E-05	2.0E-03	3.47	3.7E-04	3.5E-03	2.34
10441813	Snora20	100303746		8.9E-04	9.4E-03	3.41	3.6E-05	6.6E-04	2.00
10403579	Prl2c5	107849	*	8.0E-05	2.0E-03	3.13	5.3E-07	4.8E-05	4.27
10493307	ENSMUST00000157979			3.0E-05	1.1E-03	2.99	8.4E-07	6.4E-05	3.52
10508721	Snora44	100217418		2.5E-05	9.8E-04	2.95	5.5E-08	1.2E-05	2.32
10407797	Prl2c4	26421	*	3.6E-05	1.3E-03	2.94	1.6E-07	2.2E-05	3.43
10454731	ENSMUST00000082923			8.2E-04	8.9E-03	2.93	2.9E-09	2.2E-06	2.40
10428619	Enpp2	18606		1.4E-05	7.0E-04	2.91	1.7E-07	2.3E-05	5.11
10598085	BC104337			1.1E-07	6.9E-05	2.90	1.5E-03	1.0E-02	1.41
10583090	Mmp10	17384		1.9E-05	8.4E-04	2.78	4.2E-07	4.2E-05	3.42
10379535	Ccl8	20307		1.0E-04	2.3E-03	2.77	1.2E-10	7.8E-07	4.63
10508723	Snora61	100217440		3.3E-07	1.1E-04	2.65	2.2E-07	2.7E-05	1.97
10366275	ENSMUST00000083719			5.6E-08	4.7E-05	2.60	2.6E-07	3.1E-05	2.48
10376765	Aldh3a1	11670		7.5E-07	1.6E-04	2.46	1.4E-04	1.8E-03	2.86
10384396	ENSMUST00000157365			8.9E-05	2.1E-03	2.44	1.1E-06	7.2E-05	2.28
10398075	Serpina3n	20716		2.7E-06	3.1E-04	2.43	1.5E-08	6.4E-06	3.64
10345527	ENSMUST00000093691			6.9E-04	7.9E-03	2.42	1.7E-08	6.4E-06	2.39
10551185	Tgfb1	21803		4.9E-08	4.3E-05	2.40	7.0E-12	8.2E-08	3.28
10387557	ENSMUST00000142348			1.6E-06	2.4E-04	2.35	7.6E-01	8.6E-01	
10398859	Adssl1	11565		3.8E-06	3.7E-04	2.33	2.4E-06	1.2E-04	2.69
10560624	Apoe	11816		4.4E-05	1.4E-03	2.33	3.9E-04	3.7E-03	1.98
10466712	Mamdc2	71738		1.4E-05	7.2E-04	2.27	3.7E-03	1.9E-02	2.14
10445741	ENSMUST00000082814			8.2E-04	8.8E-03	2.26	1.6E-07	2.2E-05	2.07
10409508	Ddx41	72935		2.1E-08	3.0E-05	2.25	1.7E-09	1.6E-06	2.46
10356329	Snora75	100303740		3.8E-03	2.5E-02	2.23	8.9E-01	9.4E-01	
10362674	Rnu3a	19850		1.2E-05	6.6E-04	2.23	2.4E-06	1.2E-04	1.91
10471424	Fam102a	98952		3.1E-08	3.3E-05	2.22	5.7E-09	3.2E-06	2.18
10368277	Rps12	20042		2.4E-03	1.8E-02	2.19	2.8E-05	5.7E-04	1.89
10587323	Gsta2	14858	*	1.1E-04	2.5E-03	2.19	2.7E-05	5.5E-04	2.78
10544523	Rny1	19872		9.2E-04	9.6E-03	2.18	4.1E-08	1.0E-05	2.69
10507872	ENSMUST00000083844			1.8E-05	8.2E-04	2.16	4.9E-06	1.8E-04	1.57
10425799	Rnu12	104307		4.3E-04	5.8E-03	2.13	9.0E-06	2.7E-04	1.49
10587331	Gsta2	14858	*	1.3E-04	2.6E-03	2.11	2.5E-05	5.3E-04	2.71
10505071	Tmem38b	52076		1.1E-03	1.1E-02	2.10	9.4E-08	1.6E-05	1.86
10409014	ENSMUST00000082624			7.2E-06	5.0E-04	2.09	4.1E-06	1.7E-04	1.54
10507870	ENSMUST00000082721			2.0E-05	8.6E-04	2.09	9.8E-06	2.9E-04	1.52
10355105	AF362573			5.1E-07	1.3E-04	2.08	5.4E-04	4.7E-03	1.39
10516908	Snora73a	100306944		1.3E-07	6.9E-05	2.06	6.7E-07	5.5E-05	2.16
10525041	ENSMUST00000082683			2.2E-03	1.7E-02	2.06	1.4E-04	1.7E-03	1.65
10598087	ND6	17722		3.0E-06	3.3E-04	2.02	1.7E-05	4.2E-04	1.78
10434105	Scarf2	224024		6.8E-08	5.2E-05	1.99	3.9E-07	4.0E-05	1.94
10378438	ENSMUST00000093668			9.5E-05	2.2E-03	1.97	2.2E-07	2.7E-05	2.28
10528455	ENSMUST00000083726			2.0E-04	3.5E-03	1.97	1.4E-04	1.7E-03	1.46
10459768	ENSMUST00000158610			4.2E-06	3.8E-04	1.97	1.0E-07	1.7E-05	1.81
10405189	ENSMUST00000082738			1.4E-02	6.1E-02	1.97	9.2E-08	1.6E-05	2.15
10525185	ENSMUST00000082907			2.2E-07	8.3E-05	1.97	2.2E-08	7.2E-06	1.85
10565813	Snord15a	449630		4.6E-05	1.4E-03	1.95	3.4E-03	1.8E-02	1.37
10431635	ENSMUST00000082986			2.1E-05	8.8E-04	1.95	9.2E-03	3.9E-02	1.28
10516906	Snora73b	100306945		5.8E-06	4.5E-04	1.94	1.2E-06	7.6E-05	2.08
10592084	St3gal4	20443		1.2E-05	6.6E-04	1.94	2.0E-07	2.6E-05	2.00
10538791	Tnip3	414084		8.3E-04	8.9E-03	1.94	2.8E-07	3.3E-05	2.47
10489235	9430008C03Rik	68108		2.3E-04	3.8E-03	1.93	3.0E-05	6.0E-04	1.45
10565811	Snord15b	449631		2.1E-04	3.6E-03	1.93	6.9E-07	5.6E-05	1.76
10487595	ENSMUST00000083123			1.7E-04	3.2E-03	1.93	5.1E-04	4.5E-03	1.40
10581538	Nqo1	18104		4.6E-06	4.0E-04	1.93	7.6E-08	1.4E-05	2.24
10580635	Ces1d	104158		4.2E-04	5.7E-03	1.92	2.6E-04	2.8E-03	1.87
10346114	ENSMUST00000093689			4.4E-06	3.9E-04	1.91	1.6E-09	1.6E-06	2.17
10432178	Snora2b	100217416		9.8E-03	4.8E-02	1.90	2.9E-05	5.8E-04	1.43

10517677	**Nbl1**	17965		1.2E-07	6.9E-05	1.90	1.8E-07	2.3E-05	1.91
10514219	**Scarna8**	100217448		3.6E-03	2.4E-02	1.89	2.5E-01	4.2E-01	
10582556	**ENSMUST00000102009**			7.2E-05	1.8E-03	1.89	1.3E-07	2.0E-05	1.76
10582558	**ENSMUST00000102009**			7.2E-05	1.8E-03	1.89	1.3E-07	2.0E-05	1.76
10582564	**ENSMUST00000102009**			7.2E-05	1.8E-03	1.89	1.3E-07	2.0E-05	1.76
10582568	**ENSMUST00000102009**			7.2E-05	1.8E-03	1.89	1.3E-07	2.0E-05	1.76
10582574	**ENSMUST00000102009**			7.2E-05	1.8E-03	1.89	1.3E-07	2.0E-05	1.76
10582578	**ENSMUST00000102009**			7.2E-05	1.8E-03	1.89	1.3E-07	2.0E-05	1.76
10572647	**Slc27a1**	26457		8.5E-07	1.7E-04	1.88	1.0E-07	1.7E-05	1.69
10508719	**Snora16a**	100310813		1.3E-04	2.7E-03	1.88	9.4E-06	2.8E-04	1.70
10454807	**Snora74a**	436583		1.9E-06	2.6E-04	1.88	6.4E-06	2.2E-04	1.80
10530536	**Tec**	21682		4.0E-06	3.8E-04	1.87	1.8E-06	9.6E-05	2.42
10481101	**Snhg7**	72091	*	1.4E-05	7.1E-04	1.87	1.0E-05	2.9E-04	1.66
10523161	**Mthfd2l**	665563		2.3E-05	9.5E-04	1.86	6.0E-06	2.1E-04	1.82
10381211	**Naglu**	27419		1.2E-06	2.1E-04	1.86	3.8E-07	4.0E-05	1.86
10587339	**Gsta2**	14858	*	5.4E-05	1.6E-03	1.85	4.0E-05	7.1E-04	2.20
10374197	**Ramp3**	56089		1.1E-02	5.2E-02	1.85	4.7E-04	4.3E-03	1.91
10375065	**Sh3pxd2b**	268396		1.4E-06	2.3E-04	1.84	4.6E-08	1.1E-05	1.52
10348653	**Gpc1**	14733		3.2E-05	1.2E-03	1.83	1.9E-06	9.9E-05	2.10
10450482	**ENSMUST00000082919**			1.0E-05	6.1E-04	1.82	4.5E-06	1.7E-04	1.65
10542518	**ENSMUST00000083948**			1.2E-05	6.5E-04	1.82	9.7E-07	6.9E-05	2.09
10461162	**Snord22**	100127111		1.0E-03	1.0E-02	1.82	1.7E-03	1.1E-02	1.41
10489239	**ENSMUST00000154030**			1.2E-05	6.6E-04	1.81	2.1E-04	2.4E-03	1.50
10601549	**ENSMUST00000157893**			4.7E-05	1.5E-03	1.81	2.5E-06	1.2E-04	1.64
10427045	**9430023L20Rik**	68118		2.4E-06	2.9E-04	1.81	3.5E-08	9.6E-06	1.93
10587778	**ENSMUST00000083947**			7.3E-04	8.2E-03	1.80	2.4E-05	5.1E-04	1.64
10380059	**Rnu3b4**	19861	*	5.9E-05	1.6E-03	1.80	1.7E-06	9.5E-05	1.46
10380061	**Rnu3b4**	19861	*	5.9E-05	1.6E-03	1.80	1.7E-06	9.5E-05	1.46
10380063	**Rnu3b4**	19861	*	5.9E-05	1.6E-03	1.80	1.7E-06	9.5E-05	1.46
10380065	**Rnu3b4**	19861	*	5.9E-05	1.6E-03	1.80	1.7E-06	9.5E-05	1.46
10556611	**ENSMUST00000083940**			5.6E-05	1.6E-03	1.80	9.6E-05	1.3E-03	1.37
10595148	**Gsta1**	14857	*	2.3E-04	3.8E-03	1.80	6.6E-05	1.0E-03	2.15
10590267	**Snora62**	104433		1.7E-04	3.2E-03	1.78	1.3E-05	3.5E-04	1.50
10576795	**Cd209a**			7.4E-07	1.6E-04	1.78	2.8E-07	3.2E-05	1.74
10608136	**ENSMUST00000101925**			2.5E-05	9.8E-04	1.78	1.8E-08	6.6E-06	2.06
10448441	**Amdhd2**	245847		1.7E-07	7.3E-05	1.78	5.0E-07	4.7E-05	1.71
10597513	**ENSMUST00000083215**			2.5E-06	3.0E-04	1.77	1.1E-03	8.0E-03	1.31
10602733	**ENSMUST00000083907**			3.1E-06	3.3E-04	1.77	3.0E-01	4.7E-01	
10608693	**M31319.1**			5.5E-04	6.8E-03	1.77	5.2E-10	1.1E-06	2.91
10491058	**Rprl2**	19784		4.6E-07	1.3E-04	1.77	2.2E-07	2.7E-05	1.74
10512949	**Abca1**	11303		1.5E-03	1.3E-02	1.76	6.0E-07	5.1E-05	1.87
10398665	**Tnfaip2**	21928		6.6E-07	1.5E-04	1.76	1.0E-08	4.6E-06	1.66
10562812	**Spib**	272382		9.7E-06	5.8E-04	1.75	7.9E-04	6.1E-03	1.85
10464601	**ENSMUST00000082466**			3.6E-06	3.7E-04	1.75	7.3E-06	2.4E-04	1.39
10351504	**FJ556972**			9.4E-06	5.8E-04	1.75	7.9E-03	3.4E-02	1.60
10496091	**Lef1**	16842		1.4E-04	2.9E-03	1.75	3.4E-07	3.7E-05	2.15
10592983	**Atp5l**	27425	*	2.4E-06	2.9E-04	1.75	5.4E-05	8.9E-04	1.45
10435787	**ENSMUST00000093651**			1.7E-03	1.4E-02	1.75	2.9E-03	1.6E-02	1.58
10498024	**Slc7a11**	26570		3.2E-04	4.8E-03	1.74	4.2E-02	1.2E-01	
10445434	**Mrps18a**	68565		2.0E-07	7.7E-05	1.74	2.3E-07	2.9E-05	1.65
10424894	**Heatr7a**	223658		1.7E-07	7.3E-05	1.74	5.6E-06	2.0E-04	1.51
10389025	**Myo1d**	338367		4.1E-06	3.8E-04	1.74	3.9E-05	7.0E-04	1.68
10571312	**Dusp4**	319520		7.6E-04	8.4E-03	1.73	9.6E-08	1.6E-05	2.07
10370037	**Mmp11**	17385		1.1E-05	6.2E-04	1.73	1.7E-05	4.2E-04	1.57
10380589	**ENSMUST00000082873**			2.6E-06	3.0E-04	1.73	4.3E-02	1.2E-01	
10577315	**Angpt2**	11601		1.3E-04	2.7E-03	1.73	9.0E-06	2.7E-04	1.67
10358177	**5730559C18Rik**	67313		4.2E-06	3.8E-04	1.72	2.4E-06	1.2E-04	1.84
10525365	**Hvcn1**	74096	*	9.8E-06	5.9E-04	1.71	7.7E-07	6.1E-05	1.77
10492953	**ENSMUST00000082933**			2.8E-04	4.3E-03	1.71	2.3E-05	5.0E-04	1.51
10526853	**Fam20c**	80752		3.1E-05	1.1E-03	1.71	4.1E-06	1.7E-04	1.45
10603700	**ENSMUST00000083879**			2.6E-03	1.9E-02	1.71	8.6E-05	1.2E-03	1.72
10528662	**Atp5l**	27425		1.6E-06	2.4E-04	1.71	3.7E-05	6.8E-04	1.45
10480714	**Uap1l1**	227620		2.8E-07	9.6E-05	1.71	1.3E-06	8.0E-05	1.61
10595680	**Tbc1d2b**	67016		3.9E-06	3.7E-04	1.71	3.6E-07	3.8E-05	1.49
10580663	**Ces1f**	234564		2.6E-03	1.9E-02	1.71	8.2E-03	3.6E-02	2.10
10356406	**Ngef**	53972		1.1E-03	1.1E-02	1.71	6.7E-05	1.0E-03	1.40
10583056	**Mmp12**	17381		2.2E-04	3.7E-03	1.70	8.1E-05	1.2E-03	1.47
10389022	**Myo1d**	338367		5.5E-06	4.5E-04	1.70	9.2E-05	1.3E-03	1.61

10545192	**Rprl1**	19783		1.5E-07	7.0E-05	1.69	8.0E-08	1.5E-05	1.78
10465354	**1110014N23Rik**	68505		1.0E-06	1.9E-04	1.69	3.8E-06	1.6E-04	1.51
10387890	**Cxcl16**	66102		3.1E-06	3.3E-04	1.69	3.6E-05	6.6E-04	1.79
10543065	**ENSMUST00000083836**			1.5E-05	7.2E-04	1.69	8.6E-05	1.2E-03	1.46
10453688	**ENSMUST00000158575**			1.1E-03	1.1E-02	1.69	5.3E-04	4.6E-03	1.28
10500345	**Terc**	21748		1.0E-05	6.1E-04	1.68	1.1E-04	1.4E-03	1.66
10471154	**Ass1**	11898	*	1.2E-04	2.5E-03	1.68	4.4E-06	1.7E-04	2.48
10413014	**Chchd1**	66121		1.4E-04	2.9E-03	1.67	2.6E-04	2.8E-03	1.38
10523672	**ENSMUST00000082695**			1.3E-05	6.9E-04	1.67	1.1E-06	7.4E-05	1.54
10590263	**ENSMUST00000083107**			2.5E-04	4.1E-03	1.67	1.3E-02	5.0E-02	1.21
10347860	**ENSMUST00000083121**			2.4E-04	3.9E-03	1.66	1.6E-06	9.1E-05	1.50
10424119	**Nov**	18133		8.2E-04	8.8E-03	1.66	1.4E-07	2.0E-05	2.72
10598083	**LOC100503984**	100503984	*	5.0E-06	4.2E-04	1.66	1.3E-01	2.6E-01	
10363541	**Ass1**	11898	*	1.0E-04	2.3E-03	1.66	2.6E-06	1.2E-04	2.59
10354739	**Atp5l**	27425		6.1E-06	4.6E-04	1.66	5.9E-05	9.5E-04	1.40
10572048	**ENSMUST00000082971**			3.2E-04	4.8E-03	1.65	2.5E-04	2.7E-03	1.33
10556244	**Snora23**	100379145		1.4E-05	7.0E-04	1.65	3.7E-01	5.4E-01	
10545200	**ENSMUST00000101325**			2.5E-04	4.1E-03	1.65	1.6E-01	3.1E-01	
10424555	**ENSMUST00000083234**			8.3E-04	8.9E-03	1.65	8.2E-01	9.0E-01	
10489463	**Slpi**	20568		1.5E-04	3.0E-03	1.65	5.8E-05	9.4E-04	1.55
10582572	**ENSMUST00000101907**			6.9E-03	3.8E-02	1.65	1.6E-09	1.6E-06	2.13
10499748	**Rps27**	57294	*	1.1E-05	6.3E-04	1.65	1.1E-06	7.5E-05	1.56
10413874	**Ogdhl**	239017		3.6E-06	3.7E-04	1.65	2.3E-04	2.5E-03	1.40
10391431	**Aarsd1**	69684		1.1E-05	6.2E-04	1.65	3.0E-06	1.4E-04	1.54
10380871	**Stard3**	59045		8.3E-06	5.4E-04	1.64	3.5E-07	3.8E-05	1.59
10503835	**Rragd**	52187		2.0E-05	8.7E-04	1.64	3.0E-04	3.0E-03	1.74
10424860	**Heatr7a**	223658		4.2E-07	1.2E-04	1.64	6.4E-06	2.2E-04	1.44
10383025	**C1qtnf1**	56745		2.3E-05	9.5E-04	1.63	1.4E-05	3.7E-04	1.80
10550320	**ENSMUST00000083959**			3.6E-04	5.2E-03	1.63	2.9E-08	8.5E-06	1.73
10390560	**Stac2**	217154		9.2E-06	5.7E-04	1.63	5.5E-04	4.8E-03	1.42
10391577	**Hdac5**	15184		1.2E-05	6.6E-04	1.63	9.4E-03	3.9E-02	1.25
10599333	**Atp5l**	27425		3.7E-06	3.7E-04	1.62	8.2E-05	1.2E-03	1.40
10563110	**Rpl13a**	22121	*	9.6E-06	5.8E-04	1.62	4.8E-04	4.3E-03	1.36
10465831	**5730408K05Rik**	67531		4.0E-05	1.3E-03	1.62	4.2E-04	3.9E-03	1.46
10482793	**ENSMUST00000157339**			3.9E-07	1.2E-04	1.62	2.0E-03	1.3E-02	1.31
10526838	**Got2**	14719	*	2.1E-06	2.7E-04	1.62	4.9E-05	8.3E-04	1.35
10587748	**Adamts7**	108153		4.3E-04	5.8E-03	1.62	7.2E-05	1.1E-03	1.38
10560247	**Ccdc9**	243846		6.2E-06	4.7E-04	1.62	7.2E-08	1.4E-05	1.68
10488804	**ENSMUST00000118495**			5.5E-03	3.2E-02	1.61	6.0E-02	1.6E-01	
10380821	**Atp5l**	27425		4.6E-07	1.3E-04	1.61	5.4E-05	8.9E-04	1.42
10416732	**Snora30**	100217442		2.0E-03	1.6E-02	1.61	6.5E-01	7.8E-01	
10557703	**Snora30**	100217442		2.0E-03	1.6E-02	1.61	6.5E-01	7.8E-01	
10579812	**Ednra**	13617		2.5E-03	1.9E-02	1.61	3.0E-07	3.4E-05	2.16
10510580	**Tnfrsf9**	21942		6.7E-04	7.8E-03	1.61	7.4E-08	1.4E-05	2.12
10582582	**ENSMUST00000093696**			5.5E-03	3.2E-02	1.61	4.0E-09	2.5E-06	2.26
10582584	**ENSMUST00000093696**			5.5E-03	3.2E-02	1.61	4.0E-09	2.5E-06	2.26
10553475	**Rps27a**	78294		5.9E-06	4.6E-04	1.61	2.4E-05	5.2E-04	1.48
10527961	**ENSMUST00000157506**			2.3E-02	8.7E-02	1.61	3.3E-02	1.0E-01	1.20
10427026	**Grasp**	56149		4.1E-05	1.3E-03	1.61	1.2E-03	8.4E-03	1.45
10388451	**Wdr81**	192652		2.5E-06	3.0E-04	1.60	5.4E-05	8.8E-04	1.43
10489204	**Tgm2**	21817		2.5E-06	3.0E-04	1.60	4.0E-07	4.0E-05	1.69
10379630	**Slfn2**	20556		1.3E-05	6.9E-04	1.60	1.4E-07	2.1E-05	1.80
10549276	**Bhlhe41**	79362		1.0E-04	2.3E-03	1.60	1.6E-08	6.4E-06	2.06
10469906	**Nelf**	56876		7.3E-07	1.6E-04	1.60	3.3E-07	3.7E-05	1.51
10384208	**ENSMUST00000082561**			1.3E-02	6.0E-02	1.60	1.5E-01	3.0E-01	
10528036	**ENSMUST00000082917**			1.1E-05	6.3E-04	1.60	6.2E-03	2.9E-02	1.33
10466353	**ENSMUST00000082890**			9.8E-04	1.0E-02	1.60	7.6E-02	1.8E-01	
10538704	**ENSMUST00000082581**			4.7E-04	6.1E-03	1.60	1.4E-07	2.0E-05	1.95
10414360	**Lgals3**	16854		1.4E-04	2.8E-03	1.60	1.1E-09	1.3E-06	2.65
10531737	**Hpse**	15442		2.5E-04	4.0E-03	1.60	6.8E-06	2.3E-04	2.18
10503334	**Gem**	14579		9.0E-05	2.1E-03	1.60	9.4E-06	2.8E-04	1.90
10496438	**Adh1**	11522		1.5E-04	2.9E-03	1.60	8.7E-06	2.6E-04	1.59
10425078	**Mpst**	246221		7.8E-06	5.3E-04	1.60	4.3E-07	4.2E-05	1.58
10498992	**Tlr2**	24088		1.5E-04	2.9E-03	1.59	1.5E-03	1.0E-02	1.32
10608701	**NM_025584.2**			1.9E-06	2.6E-04	1.59	4.6E-07	4.4E-05	1.68
10555174	**Lrrc32**	434215		5.4E-04	6.7E-03	1.59	1.1E-06	7.5E-05	1.65
10548892	**Arhgdib**	11857		1.6E-05	7.7E-04	1.59	1.0E-06	7.0E-05	1.88
10501922	**Snhg8**	69895	*	2.5E-03	1.9E-02	1.59	5.0E-05	8.4E-04	1.50

10461038	**Macrod1**	107227		7.1E-06	5.0E-04	1.59	1.7E-04	2.0E-03	1.38
10585874	**Hexa**	15211		1.3E-05	6.8E-04	1.58	6.2E-07	5.2E-05	1.60
10425335	**Syngr1**	20972		3.9E-06	3.7E-04	1.58	5.8E-05	9.4E-04	1.57
10561063	**Bckdha**	12039		9.8E-07	1.9E-04	1.58	4.8E-06	1.8E-04	1.44
10597490	**Rps27**	57294	*	3.2E-05	1.2E-03	1.58	1.7E-06	9.5E-05	1.57
10494413	**Rnu1b1**	19844	*	4.4E-03	2.8E-02	1.58	2.4E-05	5.1E-04	1.47
10494421	**Rnu1b1**	19844	*	4.4E-03	2.8E-02	1.58	2.4E-05	5.1E-04	1.47
10500343	**Rnu1b1**	19844	*	4.4E-03	2.8E-02	1.58	2.4E-05	5.1E-04	1.47
10500358	**Rnu1b1**	19844	*	4.4E-03	2.8E-02	1.58	2.4E-05	5.1E-04	1.47
10512937	**Rnu1b1**	19844	*	4.4E-03	2.8E-02	1.58	2.4E-05	5.1E-04	1.47
10561461	**Samd4b**	233033		1.8E-05	8.1E-04	1.58	2.2E-06	1.1E-04	1.52
10435185	**ENSMUST00000093713**			5.6E-03	3.3E-02	1.58	8.4E-07	6.4E-05	1.75
10352234	**Itpkb**	320404		3.1E-04	4.7E-03	1.58	7.8E-05	1.2E-03	1.28
10492426	**Acsf2**	264895		1.5E-05	7.2E-04	1.58	3.0E-04	3.0E-03	1.37
10545130	**Gadd45a**	13197		7.9E-05	2.0E-03	1.58	2.3E-06	1.1E-04	1.58
10401665	**ENSMUST00000102019**			4.4E-04	5.9E-03	1.58	2.4E-04	2.6E-03	1.29
10548857	**Hist4h4**	320332		2.0E-04	3.5E-03	1.58	9.7E-07	6.9E-05	1.53
10527327	**Bri3**	55950		2.6E-06	3.0E-04	1.57	2.4E-05	5.1E-04	1.37
10587315	**Gsta4**	14860		3.1E-04	4.6E-03	1.57	2.3E-04	2.5E-03	1.42
10525406	**Anapc7**	56317		2.0E-06	2.7E-04	1.57	1.3E-05	3.5E-04	1.38
10352150	**ENSMUST00000083033**			5.7E-05	1.6E-03	1.57	8.1E-05	1.2E-03	1.44
10546349	**Xpc**	22591		3.4E-04	5.0E-03	1.57	5.0E-05	8.4E-04	1.39
10574415	**1700047G07Rik**	73323		1.6E-05	7.5E-04	1.57	2.4E-03	1.4E-02	1.42
10346374	**Aox1**	11761		5.3E-04	6.7E-03	1.56	4.9E-02	1.3E-01	
10390032	**Acsf2**	264895		1.7E-05	8.0E-04	1.56	1.1E-04	1.4E-03	1.39
10377605	**1810027O10Rik**	69186		2.3E-05	9.4E-04	1.56	1.0E-06	7.2E-05	1.74
10439989	**ENSMUST00000083060**			1.3E-02	5.9E-02	1.56	6.4E-05	1.0E-03	1.38
10425852	**Parvb**	170736		1.5E-03	1.3E-02	1.56	1.4E-10	7.8E-07	1.97
10391490	**Etv4**	18612		1.3E-03	1.2E-02	1.56	2.7E-05	5.6E-04	1.79
10356170	**ENSMUST00000116749**			1.9E-05	8.4E-04	1.55	1.3E-02	5.1E-02	1.27
10361152	**Gstp2**	14869	*	7.4E-06	5.1E-04	1.55	2.6E-06	1.2E-04	1.45
10430006	**Slc39a4**	72027		1.6E-03	1.4E-02	1.55	7.6E-05	1.1E-03	1.41
10506330	**ENSMUST00000075999**			9.9E-06	5.9E-04	1.55	8.7E-01	9.3E-01	
10430660	**Pdgfb**	18591		2.3E-04	3.9E-03	1.55	1.3E-04	1.6E-03	1.44
10565689	**Capn5**	12337		1.0E-06	1.9E-04	1.55	1.8E-06	9.7E-05	1.45
10533345	**Aldh2**	11669		1.8E-06	2.6E-04	1.55	2.3E-04	2.5E-03	1.50
10541721	**Spsb2**	14794		6.5E-05	1.7E-03	1.55	1.1E-07	1.8E-05	1.52
10588201	**ENSMUST00000083173**			1.8E-05	8.1E-04	1.55	3.0E-04	3.0E-03	1.52
10359859	**ENSMUST00000102176**			2.9E-05	1.1E-03	1.55	5.2E-06	1.9E-04	1.45
10450920	**AY036118**	170798		7.5E-06	5.1E-04	1.55	1.3E-01	2.7E-01	
10397275	**Ltbp2**	16997	*	2.6E-05	1.0E-03	1.55	3.1E-06	1.4E-04	1.68
10463625	**Fbxl15**	68431	*	1.1E-06	2.0E-04	1.55	1.7E-06	9.5E-05	1.54
10515427	**ENSMUST00000140226**			1.6E-02	6.9E-02	1.55	8.8E-05	1.3E-03	1.41
10376239	**Gm12238**	100303747		4.1E-03	2.6E-02	1.55	2.9E-01	4.7E-01	
10489246	**Mafb**	16658		2.5E-04	4.0E-03	1.55	1.5E-05	3.8E-04	1.59
10360415	**Grem2**	23893		1.2E-02	5.5E-02	1.55	4.9E-06	1.8E-04	2.39
10408200	**Hist1h4f**	319157		7.9E-04	8.7E-03	1.55	4.3E-07	4.2E-05	1.96
10378870	**Git1**	216963		1.2E-05	6.6E-04	1.55	9.1E-07	6.7E-05	1.44
10545812	**Sfxn5**	94282		1.7E-05	8.0E-04	1.55	1.5E-06	8.9E-05	1.55
10494411	**Rnu1b1**	19844	*	1.6E-03	1.4E-02	1.55	2.1E-05	4.8E-04	1.47
10494417	**Rnu1b1**	19844	*	1.6E-03	1.4E-02	1.55	2.1E-05	4.8E-04	1.47
10500356	**Rnu1b1**	19844	*	1.6E-03	1.4E-02	1.55	2.1E-05	4.8E-04	1.47
10358879	**Npl**	74091		3.3E-05	1.2E-03	1.54	1.9E-06	1.0E-04	1.72
10585097	**Gm5617**	434402		1.6E-05	7.7E-04	1.54	6.5E-06	2.2E-04	1.58
10566993	**Galntl4**	233733		9.9E-05	2.3E-03	1.54	7.7E-01	8.7E-01	
10380566	**Phospho1**	237928	*	3.0E-04	4.5E-03	1.54	3.0E-09	2.2E-06	1.73
10512063	**ENSMUST00000083410**			3.2E-05	1.2E-03	1.54	8.1E-05	1.2E-03	1.39
10464586	**Gstp2**	14869	*	1.5E-05	7.4E-04	1.54	2.0E-06	1.0E-04	1.44
10456001	**Rps14**	20044		1.8E-05	8.1E-04	1.54	2.1E-08	7.2E-06	1.65
10553840	**Atp5l**	27425		9.6E-07	1.8E-04	1.54	1.3E-04	1.6E-03	1.37
10444665	**Ddah2**	51793		2.7E-05	1.0E-03	1.54	2.2E-05	4.9E-04	1.47
10383479	**Hmga1-rs1**	111241	*	7.6E-03	4.0E-02	1.54	1.0E-06	7.2E-05	2.07
10370259	**Col18a1**	12822		8.7E-04	9.3E-03	1.54	4.7E-05	8.1E-04	1.38
10520211	**Agap3**	213990		1.4E-05	7.0E-04	1.54	1.5E-06	8.8E-05	1.39
10466680	**Klf9**	16601	*	1.9E-04	3.4E-03	1.54	3.3E-03	1.8E-02	1.22
10432439	**Fmnl3**	22379		8.0E-05	2.0E-03	1.53	2.7E-05	5.5E-04	1.51
10427369	**Pde1b**	18574		9.8E-06	5.9E-04	1.53	2.5E-06	1.2E-04	1.59
10577025	**Rab20**	19332		2.4E-04	3.9E-03	1.53	2.3E-05	5.1E-04	1.29

10541494	**Rps27a**	78294	8.5E-06	5.4E-04	1.53	1.6E-04	1.9E-03	1.38
10533529	**Camkk2**	207565	4.2E-07	1.2E-04	1.53	2.9E-05	5.8E-04	1.36
10596637	**Mapkapk3**	102626	2.2E-04	3.7E-03	1.53	5.5E-04	4.7E-03	1.30
10598238	**ENSMUST00000101968**		4.6E-05	1.4E-03	1.53	6.7E-06	2.2E-04	1.47
10478890	**Cebpb**	12608	4.6E-05	1.4E-03	1.53	2.7E-05	5.5E-04	1.35
10476102	**ENSMUST00000160976**		2.4E-02	8.9E-02	1.53	7.0E-03	3.2E-02	1.24
10452485	**Rab31**	106572	1.4E-06	2.2E-04	1.53	8.9E-08	1.6E-05	1.62
10399470	**Trib2**	217410	2.5E-04	4.1E-03	1.53	2.7E-03	1.6E-02	1.47
10608721	**NM_009293.1**		4.4E-06	3.9E-04	1.53	9.8E-05	1.4E-03	1.42
10378649	**Slc43a2**	215113	1.2E-04	2.5E-03	1.52	1.8E-05	4.2E-04	1.39
10600403	**Fam50a**	108160	4.3E-05	1.4E-03	1.52	2.7E-05	5.6E-04	1.40
10497381	**Cyp7b1**	13123	7.0E-05	1.8E-03	1.52	1.1E-05	3.1E-04	1.63
10365290	**Chst11**	58250	8.1E-04	8.8E-03	1.52	3.9E-08	1.0E-05	1.66
10545862	**Cml3**	93674	5.1E-03	3.1E-02	1.52	4.6E-03	2.3E-02	1.39
10381809	**Itgb3**	16416	3.5E-05	1.2E-03	1.52	1.1E-05	3.0E-04	1.46
10433274	**Vasn**	246154	1.1E-05	6.5E-04	1.52	5.5E-06	2.0E-04	1.46
10444890	**Ier3**	15937	1.1E-04	2.4E-03	1.52	9.1E-07	6.7E-05	1.64
10442542	**Nthl1**	18207	2.7E-06	3.1E-04	1.52	6.6E-05	1.0E-03	1.40
10534854	**Mospd3**	68929	1.7E-05	7.8E-04	1.52	5.0E-07	4.7E-05	1.44
10364056	**Ggt1**	14598	5.9E-05	1.7E-03	1.52	3.8E-06	1.6E-04	1.39
10555233	**ENSMUST00000083377**		3.2E-03	2.2E-02	1.52	1.1E-06	7.5E-05	1.66
10572897	**Hmox1**	15368	6.7E-05	1.8E-03	1.51	6.1E-04	5.1E-03	1.41
10543939	**Fam180a**	208164	9.1E-05	2.1E-03	1.51	5.7E-07	5.1E-05	1.97
10570068	**Col4a2**	12827	7.1E-04	8.1E-03	1.51	4.1E-06	1.7E-04	1.40
10354205	**GENSCAN00000024165**		3.4E-05	1.2E-03	1.51	1.7E-03	1.1E-02	1.41
10605181	**Renbp**	19703	6.6E-05	1.8E-03	1.51	9.6E-06	2.8E-04	1.66
10402266	**ENSMUST00000082842**		2.8E-06	3.1E-04	1.51	2.2E-04	2.4E-03	1.37
10419563	**Rnase1**	19752	6.0E-05	1.7E-03	1.51	9.5E-05	1.3E-03	1.44
10419160	**ENSMUST00000159783**		6.8E-04	7.9E-03	1.51	2.8E-01	4.6E-01	
10481383	**Wdr34**	71820	5.2E-05	1.5E-03	1.51	5.5E-07	5.0E-05	1.50
10448916	**Tpsab1**	17230	8.3E-04	8.9E-03	1.51	1.5E-07	2.1E-05	2.32
10370376	**Pfkl**	18641	1.1E-03	1.0E-02	1.51	8.4E-05	1.2E-03	1.46
10404024	**Hist1h4h**	69386	2.7E-04	4.2E-03	1.51	2.3E-05	5.0E-04	1.44
10451932	**Plin4**	57435	4.6E-04	6.0E-03	1.51	7.8E-06	2.5E-04	1.52
10400628	**ENSMUST00000083299**		4.8E-05	1.5E-03	1.51	1.3E-04	1.6E-03	1.35

Table 6.1: Up-regulated probesets in invading/non-invading fibroblasts.

Gene expression lists for microarrays conducted at 72 and 96 hours of MLg fibroblast invasion. Data are shown for up-regulated probesets with > 1.5-fold regulation. Data are sorted by 72 h n.t. (inv/non-inv). Statistical analysis: limma t-test and Benjamini-Hochberg multiple testing correction.(n.t. = non-treated, BH = Benjamini-Hochberg, FDR = False discovery rate, inv. = invading, non-inv. = non-invading).

Down-regulated probesets in invading/non-invading fibroblasts

				72 h n.t. (inv./non-inv.) Statistical analysis, limma t-test, BH			96 h n.t. (inv./non-inv.) Statistical analysis, limma t-test, BH		
Probe_set	Gene symbol or ID	Entrez	Unclear annotation	rawp	BH	Ratio (G/M), significant FDR<10%, ratio>1.5x (1086)	rawp	BH	Ratio (G/M), significant FDR<10%, ratio>1.5x (1049)
10378570	ENSMUST00000134345			7.5E-10	5.3E-06	0.19	4.0E-12	8.2E-08	0.18
10405063	Ogn	18295		2.7E-05	1.0E-03	0.22	5.0E-07	4.7E-05	0.27
10459225	Mir145	387163		3.5E-07	1.1E-04	0.23	1.1E-06	7.3E-05	0.27
10601328	Uprt	331487		1.2E-08	2.6E-05	0.26	3.5E-10	1.0E-06	0.29
10492165	ENSMUST00000082652			1.3E-04	2.7E-03	0.26	5.7E-09	3.2E-06	0.20
10419261	Bmp4	12159		9.5E-06	5.8E-04	0.27	1.7E-08	6.4E-06	0.29
10583203	Phxr4	18689		4.8E-05	1.5E-03	0.29	5.3E-08	1.2E-05	0.25
10417124	B930095G15Rik	320268		1.4E-09	8.2E-06	0.30	4.0E-10	1.0E-06	0.27
10586174	ENSMUST00000082580			2.2E-08	3.0E-05	0.30	1.7E-09	1.6E-06	0.30
10502770	Lphn2	99633		5.8E-05	1.6E-03	0.31	2.1E-05	4.8E-04	0.33
10519886	Sema3c	20348		9.3E-07	1.8E-04	0.31	9.9E-10	1.3E-06	0.25
10378568	Mir22	387141	*	1.8E-09	8.6E-06	0.32	2.7E-10	9.5E-07	0.31
10462535	Pten	19211		5.1E-05	1.5E-03	0.34	5.0E-08	1.1E-05	0.30
10384566	BC106119			1.2E-06	2.0E-04	0.34	6.2E-10	1.3E-06	0.30
10485633	Gm10796	100038694		1.7E-05	7.9E-04	0.34	6.6E-09	3.3E-06	0.35
10584595	2610203C20Rik	100042464		1.1E-07	6.9E-05	0.34	7.8E-10	1.3E-06	0.32
10601326	Uprt	331487		2.7E-10	4.1E-06	0.34	3.3E-09	2.3E-06	0.34
10362102	Gm10825	100038752		1.7E-06	2.5E-04	0.34	5.0E-09	2.9E-06	0.31
10547469	Wnk1	232341		1.2E-05	6.5E-04	0.34	1.9E-07	2.5E-05	0.42
10461158	Snhg1	83673		8.4E-06	5.4E-04	0.35	1.1E-03	7.8E-03	0.54
10494832	Sike1	66641		2.9E-10	4.1E-06	0.35	2.0E-10	8.0E-07	0.38
10358577	Hmcn1	545370		3.4E-07	1.1E-04	0.35	2.3E-06	1.1E-04	0.38
10344966	Ly96	17087		2.1E-06	2.8E-04	0.35	1.6E-07	2.1E-05	0.50
10430245	BC056623			5.5E-04	6.8E-03	0.36	2.6E-05	5.4E-04	0.41
10407122	ENSMUST00000099180			1.5E-05	7.4E-04	0.36	1.4E-06	8.4E-05	0.43
10367982	Gpr126	215798		6.2E-10	5.3E-06	0.36	1.1E-06	7.5E-05	0.42
10521796	Mir218-1	723822		1.1E-04	2.5E-03	0.37	6.1E-09	3.2E-06	0.36
10471880	Mir181b-2	723903		2.3E-05	9.3E-04	0.37	3.7E-07	3.9E-05	0.30
10570957	Sfrp1	20377		2.3E-06	2.9E-04	0.37	7.0E-06	2.3E-04	0.47
10565255	9930013L23Rik	80982		7.9E-08	5.6E-05	0.38	1.7E-10	7.9E-07	0.24
10459227	Mir143	387161		2.4E-05	9.6E-04	0.38	2.1E-05	4.8E-04	0.41
10442087	Ncrna00085	75202		1.6E-07	7.1E-05	0.38	4.6E-10	1.1E-06	0.41
10351111	Mir214	387210	*	3.7E-05	1.3E-03	0.38	9.3E-07	6.7E-05	0.37
10604505	6720401G13Rik	103012		6.8E-07	1.5E-04	0.38	2.1E-08	7.2E-06	0.41
10367475	ENSMUST00000102458			8.9E-04	9.4E-03	0.38	8.3E-07	6.4E-05	0.42
10489053	4930518I15Rik	74704		1.4E-08	2.6E-05	0.39	9.1E-06	2.7E-04	0.53
10586967	Gm7265	639396		8.9E-06	5.6E-04	0.39	1.3E-07	2.0E-05	0.37
10450904	Scoc	56367		7.2E-07	1.6E-04	0.40	6.1E-05	9.7E-04	0.71
10519998	Lrrc17	74511		5.9E-07	1.4E-04	0.40	3.4E-07	3.7E-05	0.48
10529091	Gtf3c2	71752		9.2E-04	9.6E-03	0.40	7.6E-04	6.0E-03	0.51
10388782	ENSMUST00000082606			6.6E-05	1.8E-03	0.41	2.3E-02	7.7E-02	0.70
10362201	Ctgf	14219		2.2E-04	3.7E-03	0.41	1.8E-05	4.4E-04	0.51
10454828	Pnet-ps	448986		1.4E-06	2.3E-04	0.41	2.0E-09	1.8E-06	0.35
10595211	Col12a1	12816		9.0E-06	5.6E-04	0.41	4.6E-04	4.2E-03	0.52
10474102	ENSMUST00000099684			1.1E-02	5.3E-02	0.41	1.2E-04	1.6E-03	0.38
10417371	Gm3696	100042149	*	3.1E-06	3.3E-04	0.41	8.6E-09	4.2E-06	0.42
10365559	Igf1	16000		7.3E-06	5.1E-04	0.41	8.7E-07	6.5E-05	0.41
10379996	Mir301	723834		5.5E-06	4.5E-04	0.41	2.2E-07	2.7E-05	0.42
10392010	1700081L11Rik	76719		5.6E-04	6.9E-03	0.42	6.9E-05	1.1E-03	0.47
10412260	Fst	14313	*	1.9E-07	7.7E-05	0.42	1.3E-07	2.0E-05	0.50
10555323	P4ha3	320452		1.5E-07	6.9E-05	0.42	7.0E-08	1.4E-05	0.44
10582896	ENSMUST00000099046			6.6E-03	3.7E-02	0.42	1.0E-05	3.0E-04	0.46
10599348	Gria3	53623		7.8E-07	1.6E-04	0.42	3.0E-06	1.4E-04	0.52
10495685	Arhgap29	214137		3.8E-05	1.3E-03	0.43	2.2E-07	2.7E-05	0.49
10484201	Ccdc141	545428		4.5E-06	3.9E-04	0.43	1.8E-08	6.5E-06	0.49
10565567	4632427E13Rik	666737		9.2E-06	5.7E-04	0.43	5.0E-08	1.1E-05	0.45
10491438	Ttc14	67120		1.3E-05	6.9E-04	0.43	5.2E-07	4.8E-05	0.46
10585988	Myo9a	270163		6.3E-06	4.7E-04	0.43	3.5E-05	6.6E-04	0.55
10406536	Tmem167	66074		5.7E-05	1.6E-03	0.43	2.9E-09	2.2E-06	0.45
10438769	Cldn1	12737		1.7E-03	1.4E-02	0.43	1.5E-06	8.8E-05	0.32
10412517	Gm3002	100040852	*	1.0E-06	1.9E-04	0.43	1.3E-09	1.5E-06	0.41

10537026	**Cpa4**	71791		1.5E-05	7.3E-04	0.44	4.7E-04	4.3E-03	0.38
10406982	**Adamts6**	108154		2.0E-06	2.7E-04	0.44	2.0E-07	2.5E-05	0.46
10582888	**ENSMUST00000099042**			2.5E-02	9.2E-02	0.44	6.4E-07	5.4E-05	0.47
10354203	**ENSMUST00000083002**			1.4E-06	2.3E-04	0.44	4.1E-05	7.3E-04	0.56
10417269	**AK084462**			2.2E-06	2.9E-04	0.44	3.6E-08	9.7E-06	0.39
10441787	**Airn**	104103		6.8E-05	1.8E-03	0.44	1.1E-09	1.3E-06	0.35
10430929	**Tbrg3**	21378		1.3E-05	6.8E-04	0.44	4.1E-06	1.7E-04	0.43
10582890	**ENSMUST00000099042**			8.9E-03	4.5E-02	0.44	5.2E-06	1.9E-04	0.49
10569335	**H19**	14955		3.6E-04	5.1E-03	0.45	3.3E-04	3.2E-03	0.28
10375501	**Snord95**	100216540		2.3E-07	8.4E-05	0.45	6.3E-06	2.2E-04	0.54
10503359	**C430048L16Rik**	77604		9.3E-04	9.6E-03	0.45	2.6E-06	1.2E-04	0.38
10519717	**Sema3a**	20346		4.8E-08	4.3E-05	0.45	4.0E-06	1.6E-04	0.47
10556297	**Adm**	11535		1.3E-06	2.1E-04	0.45	1.6E-04	1.9E-03	0.38
10421932	**Pcdh9**	211712		4.1E-06	3.8E-04	0.45	7.0E-08	1.4E-05	0.41
10560043	**Zfp329**	67230		3.5E-06	3.6E-04	0.45	9.2E-07	6.7E-05	0.42
10600597	**Tmem47**	192216		1.3E-07	6.9E-05	0.45	5.5E-08	1.2E-05	0.55
10604610	**Mir351**	723910		1.9E-06	2.6E-04	0.46	1.0E-08	4.6E-06	0.42
10570639	**2610005L07Rik**	381598		5.4E-06	4.4E-04	0.46	7.0E-08	1.4E-05	0.46
10448195	**3110048L19Rik**	73233		5.6E-04	6.9E-03	0.46	1.7E-06	9.5E-05	0.53
10603805	**Mir221**	723827		8.3E-06	5.4E-04	0.46	5.1E-06	1.9E-04	0.54
10585956	**Myo9a**	270163		2.3E-06	2.9E-04	0.46	1.2E-07	1.9E-05	0.53
10599213	**ENSMUST00000082596**			1.4E-07	6.9E-05	0.46	5.0E-08	1.1E-05	0.37
10607499	**Phex**	18675		4.1E-05	1.3E-03	0.46	8.4E-02	2.0E-01	
10463997	**Pdcd4**	18569		8.0E-07	1.6E-04	0.46	8.6E-07	6.5E-05	0.62
10359917	**Hsd17b7**	15490		1.4E-04	2.8E-03	0.47	6.4E-05	1.0E-03	0.61
10548727	**D230041D01Rik**	100038615	*	9.7E-07	1.8E-04	0.47	2.1E-06	1.1E-04	0.38
10353102	**Cpa6**	329093		1.0E-07	6.9E-05	0.47	4.3E-06	1.7E-04	0.53
10472538	**Dhrs9**	241452		5.6E-04	6.9E-03	0.47	6.5E-04	5.3E-03	0.62
10586880	**Zfp280d**	235469		6.7E-06	4.9E-04	0.47	5.1E-09	3.0E-06	0.50
10346164	**Sdpr**	20324		1.5E-05	7.5E-04	0.47	8.7E-08	1.5E-05	0.41
10482172	**Zbtb26**	320633	*	3.1E-06	3.3E-04	0.47	3.9E-06	1.6E-04	0.59
10442224	**BC049807**	381066		1.6E-05	7.5E-04	0.47	4.2E-09	2.5E-06	0.49
10434802	**Lpp**	210126		2.6E-04	4.1E-03	0.47	9.6E-06	2.8E-04	0.47
10440534	**Adamts5**	23794		6.3E-07	1.5E-04	0.47	2.2E-08	7.2E-06	0.43
10495993	**Elovl6**	170439		5.9E-07	1.4E-04	0.47	6.7E-07	5.5E-05	0.51
10582882	**ENSMUST00000147569**			8.7E-03	4.5E-02	0.47	5.6E-06	2.0E-04	0.55
10582884	**ENSMUST00000099046**			1.4E-02	6.0E-02	0.48	1.7E-06	9.5E-05	0.50
10467191	**Ankrd1**	107765		1.0E-04	2.3E-03	0.48	2.0E-04	2.3E-03	0.56
10394534	**Osr1**	23967		2.5E-08	3.1E-05	0.48	8.5E-08	1.5E-05	0.46
10487480	**Bub1**	12235		4.3E-08	4.0E-05	0.48	2.6E-02	8.5E-02	0.76
10484203	**Ccdc141**	545428		7.9E-07	1.6E-04	0.48	8.9E-07	6.6E-05	0.57
10537051	**Cpa1**	109697		6.1E-05	1.7E-03	0.48	6.1E-05	9.6E-04	0.44
10504499	**Zcchc7**	319885		1.9E-06	2.6E-04	0.48	1.9E-08	6.7E-06	0.43
10389795	**Stxbp4**	20913		1.4E-05	7.2E-04	0.48	5.6E-07	5.0E-05	0.63
10604616	**Plac1**	56096		5.2E-04	6.6E-03	0.49	4.2E-04	3.9E-03	0.61
10360745	**Lbr**	98386		1.3E-08	2.6E-05	0.49	5.9E-05	9.5E-04	0.71
10485622	**Qser1**	99003		9.7E-06	5.8E-04	0.49	8.9E-08	1.5E-05	0.59
10350341	**Mir181b-1**	723890		2.7E-04	4.3E-03	0.49	3.0E-05	5.9E-04	0.30
10354816	**Clk1**	12747		2.6E-03	1.9E-02	0.49	5.0E-07	4.7E-05	0.51
10598041	**NC_005089**			8.3E-05	2.0E-03	0.49	6.5E-09	3.3E-06	0.57
10442250	**Zfp229**	381067		1.1E-04	2.4E-03	0.49	5.9E-07	5.1E-05	0.50
10436600	**Mir99a**	387229		7.8E-05	1.9E-03	0.49	4.2E-07	4.2E-05	0.34
10475199	**Snap23**	20619		3.0E-08	3.3E-05	0.49	2.7E-09	2.2E-06	0.54
10513208	**Svep1**	64817		2.0E-05	8.5E-04	0.49	5.0E-06	1.8E-04	0.44
10592201	**Chek1**	12649		1.2E-07	6.9E-05	0.49	2.1E-01	3.7E-01	
10479979	**Slc25a36**	192287		3.5E-06	3.6E-04	0.49	8.3E-07	6.4E-05	0.55
10516221	**BC147505**			1.3E-06	2.1E-04	0.49	8.1E-10	1.3E-06	0.42
10604832	**Mir505**	751545		5.3E-05	1.5E-03	0.49	2.7E-05	5.5E-04	0.46
10497646	**Phc3**	241915		1.2E-05	6.5E-04	0.49	3.9E-02	1.1E-01	
10379344	**Gm10387**	100038730		4.6E-07	1.3E-04	0.50	1.2E-07	1.9E-05	0.41
10502655	**Cyr61**	16007		2.3E-02	8.7E-02	0.50	4.9E-03	2.4E-02	0.53
10606178	**Xist**	213742		1.9E-04	3.4E-03	0.50	1.9E-07	2.5E-05	0.47
10554419	**Vps33b**	233405		1.2E-07	6.9E-05	0.50	2.7E-07	3.1E-05	0.53
10416371	**Lpar6**	67168		1.1E-07	6.9E-05	0.50	3.7E-09	2.5E-06	0.58
10500847	**Magi3**	99470		2.8E-05	1.1E-03	0.50	2.7E-08	8.0E-06	0.44
10435789	**Zbtb20**	56490		1.9E-05	8.4E-04	0.50	1.6E-06	9.1E-05	0.50
10409059	**Mirlet7d**	387247		2.3E-05	9.5E-04	0.50	1.5E-06	8.7E-05	0.45
10410295	**Zfp595**	218314		7.4E-06	5.1E-04	0.51	2.1E-05	4.8E-04	0.61

10484197	**Ccdc141**	545428		1.3E-07	6.9E-05	0.51	3.8E-08	1.0E-05	0.60
10360542	**AI503316**	105860	*	1.4E-04	2.8E-03	0.51	3.2E-09	2.3E-06	0.35
10400589	**C79407**	217653		5.3E-07	1.3E-04	0.51	2.3E-04	2.5E-03	0.64
10585986	**Myo9a**	270163		2.2E-04	3.7E-03	0.51	1.2E-04	1.6E-03	0.57
10598079	**NC_005089**			2.1E-04	3.5E-03	0.51	1.0E-06	7.2E-05	0.58
10472289	**Tank**	21353		3.4E-08	3.6E-05	0.51	6.2E-08	1.3E-05	0.58
10582464	**ENSMUST00000083981**			9.7E-06	5.9E-04	0.51	4.1E-07	4.2E-05	0.43
10567412	**Eri2**	71151	*	1.1E-07	6.9E-05	0.51	2.9E-06	1.3E-04	0.69
10504912	**ENSMUST00000082848**			1.1E-03	1.1E-02	0.51	1.0E-01	2.2E-01	
10362387	**ENSMUST00000082681**			1.2E-04	2.6E-03	0.51	3.3E-05	6.4E-04	0.58
10482762	**Idi1**	319554		2.2E-03	1.7E-02	0.51	2.3E-03	1.4E-02	0.53
10421526	**Rb1**	19645		1.8E-06	2.6E-04	0.52	3.7E-05	6.8E-04	0.69
10403413	**Idi1**	319554		2.0E-03	1.6E-02	0.52	3.5E-03	1.9E-02	0.54
10442240	**Zfp760**	240034		1.7E-05	7.8E-04	0.52	4.0E-07	4.0E-05	0.48
10572024	**Spock3**	72902		8.7E-06	5.5E-04	0.52	4.7E-03	2.3E-02	0.54
10459643	**4930503L19Rik**	269033		3.2E-07	1.0E-04	0.52	5.2E-04	4.5E-03	0.69
10375820	**Clk4**	12750		2.0E-04	3.5E-03	0.52	2.5E-07	3.1E-05	0.58
10502565	**Clca1**	12722	*	9.2E-03	4.6E-02	0.52	7.1E-03	3.2E-02	0.58
10584578	**Hspa8**	15481	*	1.6E-04	3.0E-03	0.52	3.6E-05	6.7E-04	0.57
10448247	**Zfp40**	22700		5.2E-05	1.5E-03	0.52	9.1E-07	6.7E-05	0.49
10584576	**Hspa8**	15481	*	1.6E-04	3.0E-03	0.52	3.5E-05	6.6E-04	0.57
10411332	**Hmgcr**	15357		3.8E-07	1.2E-04	0.52	2.2E-06	1.1E-04	0.54
10520388	**Rbm33**	381626		5.4E-06	4.4E-04	0.52	7.1E-10	1.3E-06	0.39
10583297	**Taf1d**	75316		5.9E-06	4.6E-04	0.52	4.8E-06	1.8E-04	0.66
10595856	**Slc25a36**	192287		2.3E-05	9.5E-04	0.52	1.1E-06	7.4E-05	0.56
10501778	**Ptbp2**	56195		1.0E-05	6.0E-04	0.52	1.5E-07	2.1E-05	0.59
10586722	**F830001A07Rik**	320055		5.5E-03	3.2E-02	0.52	2.6E-06	1.2E-04	0.48
10408870	**Tbc1d7**	67046		7.3E-08	5.5E-05	0.52	9.8E-03	4.1E-02	0.75
10546834	**Rad18**	58186		1.6E-07	7.1E-05	0.52	3.4E-04	3.3E-03	0.71
10440881	**Gcfc1**	67367		2.2E-06	2.8E-04	0.52	8.5E-07	6.4E-05	0.56
10496485	**Eif4e**	13684		9.1E-07	1.8E-04	0.52	6.2E-03	2.9E-02	0.81
10502552	**Clca1**	12722		1.4E-02	6.1E-02	0.53	7.4E-04	5.9E-03	0.57
10542335	**Gprc5a**	232431		6.7E-05	1.8E-03	0.53	3.1E-04	3.1E-03	0.64
10360504	**Mir350**	723921		3.2E-04	4.7E-03	0.53	1.5E-05	3.8E-04	0.41
10483770	**Lnp**	69605		1.8E-06	2.5E-04	0.53	2.1E-06	1.1E-04	0.69
10608695	**NM_001024731.1**			7.3E-04	8.2E-03	0.53	1.4E-07	2.0E-05	0.54
10434806	**Lpp**	210126		3.3E-07	1.1E-04	0.53	3.8E-07	3.9E-05	0.56
10503570	**Sfrs18**	66625		9.1E-06	5.7E-04	0.53	4.8E-08	1.1E-05	0.44
10375002	**Cpeb4**	67579		7.1E-06	5.0E-04	0.53	3.2E-06	1.4E-04	0.54
10346722	**Nbeal1**	269198		9.1E-05	2.1E-03	0.53	4.7E-06	1.8E-04	0.50
10442270	**1300003B13Rik**	74149		1.2E-05	6.5E-04	0.53	8.4E-05	1.2E-03	0.69
10391744	**Gpatch8**	237943		9.2E-05	2.1E-03	0.53	2.5E-06	1.2E-04	0.51
10421924	**Pcdh9**	211712		6.8E-06	4.9E-04	0.53	2.6E-08	8.0E-06	0.46
10435704	**Cd80**	12519		7.2E-06	5.0E-04	0.53	6.4E-05	1.0E-03	0.71
10475990	**Slc20a1**	20515		8.5E-08	5.9E-05	0.53	1.1E-06	7.5E-05	0.64
10412491	**AK084462**			3.8E-06	3.7E-04	0.53	1.2E-08	5.0E-06	0.47
10374793	**Pnpt1**	71701		1.4E-07	6.9E-05	0.53	4.7E-05	8.1E-04	0.72
10546432	**Adamts9**	101401		1.9E-05	8.3E-04	0.53	3.9E-05	7.0E-04	0.57
10489018	**Rbm39**	170791		8.1E-06	5.3E-04	0.53	4.6E-08	1.1E-05	0.62
10350516	**Ptgs2**	19225		5.8E-03	3.4E-02	0.54	3.3E-03	1.8E-02	0.61
10395692	**Arhgap5**	11855		4.2E-06	3.8E-04	0.54	6.8E-06	2.3E-04	0.72
10385466	**Sgcd**	24052		1.7E-06	2.5E-04	0.54	2.9E-07	3.3E-05	0.52
10417264	**Gm3373**	100036568	*	1.4E-05	7.0E-04	0.54	1.6E-08	6.4E-06	0.52
10571241	**Purg**	75029		2.2E-05	9.3E-04	0.54	6.8E-07	5.6E-05	0.61
10498018	**Pcdh18**	73173		2.4E-06	2.9E-04	0.54	4.5E-06	1.7E-04	0.69
10606315	**Taf9b**	407786		1.4E-05	7.1E-04	0.54	3.6E-06	1.5E-04	0.70
10502791	**Ifi44**	99899		1.3E-02	5.8E-02	0.54	4.4E-04	4.0E-03	0.64
10544638	**Tra2a**	101214		6.4E-05	1.7E-03	0.54	2.4E-07	2.9E-05	0.37
10419676	**Rab2b**	76338		1.9E-07	7.7E-05	0.54	3.1E-07	3.5E-05	0.62
10557229	**LOC100134980**	100134980	*	9.5E-07	1.8E-04	0.54	1.0E-09	1.3E-06	0.53
10505630	**Snapc3**	77634		2.8E-06	3.1E-04	0.54	3.9E-09	2.5E-06	0.61
10580955	**ENSMUST00000083277**			1.7E-05	7.7E-04	0.54	4.5E-04	4.1E-03	0.66
10365003	**Snord37**	100217454		1.2E-03	1.1E-02	0.54	1.9E-04	2.2E-03	0.62
10344981	**Pi15**	94227		5.2E-06	4.3E-04	0.54	7.3E-06	2.4E-04	0.53
10491621	**4932438A13Rik**	229227		4.9E-04	6.4E-03	0.54	1.2E-06	7.6E-05	0.58
10408935	**Gm10786**	100038539		1.0E-05	6.0E-04	0.54	2.7E-04	2.8E-03	0.69
10502050	**Alpk1**	71481		1.9E-04	3.4E-03	0.54	9.4E-08	1.6E-05	0.52
10423568	**5730407I07Rik**	70515		7.4E-05	1.9E-03	0.54	3.3E-08	9.4E-06	0.50

10396008	**Prpf39**	328110	*	7.3E-05	1.9E-03	0.55	4.7E-07	4.5E-05	0.52
10485607	**Qser1**	99003		3.2E-06	3.4E-04	0.55	2.6E-07	3.1E-05	0.63
10603878	**Uxt**	22294		1.7E-06	2.5E-04	0.55	1.8E-05	4.2E-04	0.64
10366409	**Zfc3h1**	216345		6.7E-04	7.8E-03	0.55	9.7E-07	6.9E-05	0.50
10487033	**Myef2**	17876		7.6E-07	1.6E-04	0.55	4.4E-05	7.6E-04	0.71
10535894	**Hmgb1**	15289		2.2E-05	9.1E-04	0.55	3.8E-02	1.1E-01	
10410644	**Zfp72**	238722		1.6E-05	7.7E-04	0.55	2.7E-07	3.2E-05	0.60
10427290	**Hoxc8**	15426		2.8E-06	3.1E-04	0.55	9.9E-10	1.3E-06	0.50
10601610	**ENSMUST00000096331**			3.6E-04	5.1E-03	0.55	1.8E-07	2.3E-05	0.57
10585318	**9830163H01Rik**	414109	*	4.2E-06	3.8E-04	0.55	1.2E-06	7.6E-05	0.48
10491613	**4932438A13Rik**	229227		2.1E-03	1.7E-02	0.55	1.2E-05	3.3E-04	0.57
10420348	**Zmym5**	219105		1.6E-05	7.5E-04	0.55	3.4E-05	6.4E-04	0.68
10528015	**Steap1**	70358		3.9E-05	1.3E-03	0.55	2.0E-05	4.7E-04	0.59
10401822	**Gm4027**	100042776	*	9.7E-07	1.8E-04	0.55	4.9E-03	2.4E-02	0.86
10344658	**Rb1cc1**	12421		5.5E-05	1.6E-03	0.55	3.5E-06	1.5E-04	0.58
10375529	**Zfp62**	22720		7.5E-05	1.9E-03	0.55	3.9E-07	4.0E-05	0.59
10365286	**Eid3**	66341		5.7E-05	1.6E-03	0.55	1.3E-06	8.0E-05	0.37
10482177	**Strbp**	20744		2.5E-05	9.7E-04	0.55	4.1E-04	3.9E-03	0.65
10594800	**Fam63b**	235461		4.0E-05	1.3E-03	0.55	2.5E-05	5.4E-04	0.66
10446965	**Rasgrp3**	240168		9.8E-04	1.0E-02	0.55	1.3E-05	3.5E-04	0.56
10574456	**Cklf**	75458		2.4E-06	2.9E-04	0.55	4.2E-08	1.0E-05	0.59
10461152	**Snhg1**	83673		1.1E-03	1.1E-02	0.55	2.5E-03	1.5E-02	0.68
10401667	**0610007P14Rik**	58520		5.6E-06	4.5E-04	0.55	9.2E-07	6.7E-05	0.67
10491627	**4932438A13Rik**	229227		3.6E-04	5.2E-03	0.55	2.9E-05	5.8E-04	0.60
10370544	**2610008E11Rik**	72128		4.0E-04	5.5E-03	0.55	1.8E-06	9.8E-05	0.55
10608667	**NM_010852.1**			2.3E-06	2.9E-04	0.56	1.2E-04	1.5E-03	0.73
10346695	**Nbeal1**	269198		3.2E-04	4.7E-03	0.56	5.9E-05	9.4E-04	0.54
10412537	**Gm3373**	100036568	*	8.1E-06	5.4E-04	0.56	4.1E-09	2.5E-06	0.50
10435791	**Mir568**	100124467	*	5.4E-06	4.4E-04	0.56	1.5E-08	6.3E-06	0.43
10351026	**Gas5**	14455		9.6E-07	1.8E-04	0.56	6.1E-09	3.2E-06	0.52
10604542	**Hs6st2**	50786		2.9E-05	1.1E-03	0.56	4.8E-07	4.6E-05	0.61
10352905	**Cd34**	12490		1.2E-03	1.1E-02	0.56	7.8E-02	1.9E-01	
10446986	**Crim1**	50766		1.3E-05	6.7E-04	0.56	2.1E-08	7.2E-06	0.51
10355893	**Epha4**	13838		1.1E-06	1.9E-04	0.56	4.4E-08	1.0E-05	0.57
10507885	**Mycbp**	56309		7.5E-06	5.1E-04	0.56	2.0E-05	4.6E-04	0.68
10476297	**Mir103-2**	723825		7.0E-05	1.8E-03	0.56	1.3E-05	3.5E-04	0.50
10354792	**1110034B05Rik**	68736	*	2.7E-07	9.4E-05	0.56	4.5E-07	4.3E-05	0.61
10474381	**Kif18a**	228421		1.8E-05	8.2E-04	0.56	1.9E-03	1.2E-02	0.79
10439798	**Dzip3**	224170		1.5E-04	3.0E-03	0.56	5.5E-05	9.0E-04	0.61
10546450	**Adamts9**	101401		1.3E-04	2.6E-03	0.56	3.9E-05	7.1E-04	0.51
10490794	**Pkia**	18767		5.6E-04	6.9E-03	0.56	4.6E-04	4.2E-03	0.57
10350838	**2810417H13Rik**	68026		5.0E-06	4.2E-04	0.56	3.1E-03	1.7E-02	0.72
10403743	**Inhba**	16323		3.1E-03	2.1E-02	0.56	2.6E-04	2.8E-03	0.57
10590433	**1700048O20Rik**	69430		8.8E-06	5.5E-04	0.56	1.4E-07	2.0E-05	0.63
10417461	**Gm3558**	100041874	*	3.4E-06	3.6E-04	0.56	7.8E-09	3.8E-06	0.54
10496822	**Gng5**	14707		6.5E-04	7.6E-03	0.56	2.6E-03	1.5E-02	0.77
10379363	**Atad5**	237877		5.9E-06	4.6E-04	0.56	7.7E-05	1.1E-03	0.65
10428707	**Has2**	15117		2.6E-04	4.2E-03	0.56	3.5E-01	5.3E-01	
10407211	**Ppap2a**	19012		1.4E-07	6.9E-05	0.56	9.4E-07	6.7E-05	0.57
10455146	**3222401L13Rik**	320513		3.6E-06	3.7E-04	0.56	4.2E-04	3.9E-03	0.58
10543145	**Thsd7a**	330267		1.5E-06	2.3E-04	0.57	3.4E-08	9.4E-06	0.54
10579799	**Tmem184c**	234463		1.5E-06	2.4E-04	0.57	7.2E-08	1.4E-05	0.62
10465244	**Malat1**	72289		2.3E-05	9.5E-04	0.57	5.9E-06	2.1E-04	0.60
10523746	**BC005561**	100042165		1.4E-04	2.8E-03	0.57	2.9E-06	1.3E-04	0.51
10428837	**ENSMUST00000083115**			9.4E-05	2.2E-03	0.57	1.4E-05	3.6E-04	0.57
10462866	**Cep55**	74107		7.8E-06	5.2E-04	0.57	1.1E-01	2.4E-01	
10344674	**Fam150a**	620393		1.8E-04	3.3E-03	0.57	1.6E-03	1.1E-02	0.60
10397145	**Acot2**	171210		1.9E-05	8.4E-04	0.57	2.8E-03	1.6E-02	0.77
10604424	**Zfp280c**	208968		1.6E-06	2.4E-04	0.57	6.6E-07	5.5E-05	0.62
10432263	**BC147361**			7.5E-05	1.9E-03	0.57	1.4E-06	8.5E-05	0.51
10505187	**Ugcg**	22234		1.1E-06	1.9E-04	0.57	7.3E-05	1.1E-03	0.69
10399087	**Ncapg2**	76044		3.4E-05	1.2E-03	0.57	3.5E-02	1.0E-01	
10497520	**Ect2**	13605		1.1E-05	6.4E-04	0.57	3.7E-01	5.5E-01	
10604944	**Gabre**	14404		5.3E-07	1.3E-04	0.57	4.2E-08	1.0E-05	0.58
10501567	**Rnpc3**	67225		5.3E-05	1.5E-03	0.57	1.6E-07	2.2E-05	0.60
10591228	**Zfp26**	22688		2.7E-07	9.4E-05	0.57	6.4E-07	5.4E-05	0.66
10488449	**ENSMUST00000063463**			2.5E-05	9.9E-04	0.57	5.8E-06	2.0E-04	0.60
10505270	**Slc31a2**	20530		1.6E-05	7.7E-04	0.57	1.3E-07	2.0E-05	0.53

10502359	**Dapp1**	26377		2.8E-06	3.1E-04	0.57	5.7E-07	5.1E-05	0.55
10412495	**Gm3002**			4.5E-06	3.9E-04	0.57	1.6E-08	6.4E-06	0.51
10591035	**5830418K08Rik**	319675		2.7E-06	3.1E-04	0.57	1.9E-06	9.9E-05	0.62
10417421	**Gm3468**	100041678	*	8.0E-06	5.3E-04	0.57	1.5E-08	6.4E-06	0.53
10554599	**Adamtsl3**	269959		8.2E-05	2.0E-03	0.57	7.1E-03	3.2E-02	0.64
10437236	**B230307C23Rik**	245305		1.4E-05	7.0E-04	0.57	4.7E-05	8.0E-04	0.68
10449999	**Zfp101**	22643		1.1E-05	6.4E-04	0.57	2.2E-05	5.0E-04	0.63
10417226	**Gm3002**			6.9E-06	5.0E-04	0.57	1.6E-08	6.4E-06	0.52
10417286	**Gm3002**			2.3E-05	9.4E-04	0.57	5.6E-08	1.2E-05	0.53
10442231	**3110052M02Rik**	73229		6.9E-05	1.8E-03	0.57	7.9E-05	1.2E-03	0.70
10350594	**Ivns1abp**	117198		1.8E-05	8.2E-04	0.57	5.2E-02	1.4E-01	
10470320	**ENSMUST00000137376**			1.1E-02	5.1E-02	0.57	4.6E-01	6.3E-01	
10439895	**Alcam**	11658		3.1E-04	4.6E-03	0.57	1.1E-01	2.4E-01	
10536505	**Met**	17295		3.9E-06	3.7E-04	0.57	1.5E-04	1.8E-03	0.69
10418927	**Bmpr1a**	12166		2.4E-06	2.9E-04	0.57	3.4E-05	6.5E-04	0.71
10353010	**Mybl1**	17864		1.3E-04	2.7E-03	0.57	1.1E-02	4.3E-02	0.72
10354868	**Fam126b**	213056		4.7E-05	1.5E-03	0.57	1.3E-05	3.5E-04	0.63
10600082	**Nsdhl**	18194		9.3E-05	2.2E-03	0.58	6.5E-06	2.2E-04	0.61
10502284	**Tet2**	214133		1.4E-05	7.0E-04	0.58	6.9E-08	1.4E-05	0.55
10604620	**Fam122b**	78755		3.2E-07	1.0E-04	0.58	1.9E-05	4.5E-04	0.58
10401829	**BB287469**	544881	*	6.4E-07	1.5E-04	0.58	3.0E-04	3.0E-03	0.81
10521731	**Ncapg**	54392		5.2E-05	1.5E-03	0.58	1.0E+00	1.0E+00	
10576403	**Urb2**	382038		9.8E-06	5.9E-04	0.58	6.2E-06	2.2E-04	0.66
10451004	**Cd2ap**	12488		1.1E-05	6.4E-04	0.58	3.4E-05	6.5E-04	0.67
10607089	**Acsl4**	50790		2.6E-06	3.1E-04	0.58	3.0E-02	9.3E-02	0.83
10503410	**Tmem64**	100201		4.8E-07	1.3E-04	0.58	3.9E-04	3.7E-03	0.70
10385248	**Hmmr**	15366		1.8E-05	8.1E-04	0.58	5.0E-02	1.4E-01	
10429568	**Ly6c2**	100041546	*	6.8E-06	4.9E-04	0.58	3.2E-01	4.9E-01	
10583314	**Taf1d**	75316		4.6E-06	4.0E-04	0.58	1.2E-03	8.4E-03	0.71
10424349	**Sqle**	20775		3.8E-05	1.3E-03	0.58	5.7E-05	9.2E-04	0.56
10569344	**Igf2**	16002		7.3E-04	8.2E-03	0.58	3.0E-01	4.7E-01	
10400155	**Nova1**	664883		2.6E-06	3.0E-04	0.58	1.8E-03	1.1E-02	0.39
10467979	**Scd1**	20249		3.0E-05	1.1E-03	0.58	1.1E-03	8.2E-03	0.66
10496204	**Cenpe**	229841		5.7E-06	4.5E-04	0.58	1.5E-02	5.5E-02	0.78
10442238	**Zfp51**	22709	*	1.4E-05	7.0E-04	0.58	7.6E-08	1.4E-05	0.58
10440238	**Nsun3**	106338		4.3E-05	1.4E-03	0.58	2.1E-04	2.3E-03	0.63
10422194	**Rbm26**	74213		1.9E-05	8.5E-04	0.58	2.8E-06	1.3E-04	0.61
10352125	**Gm9982**	791357		1.1E-05	6.4E-04	0.58	1.4E-05	3.6E-04	0.56
10600566	**ENSMUST00000157653**			1.2E-04	2.5E-03	0.58	5.4E-06	2.0E-04	0.47
10417212	**Itgbl1**	223272		9.0E-06	5.6E-04	0.58	5.6E-04	4.8E-03	0.49
10397543	**Eif1a**	13664	*	1.3E-06	2.2E-04	0.58	5.4E-04	4.7E-03	0.81
10488108	**Esf1**	66580		5.5E-05	1.6E-03	0.58	5.2E-05	8.6E-04	0.64
10585990	**Myo9a**	270163		8.5E-04	9.1E-03	0.58	7.6E-05	1.1E-03	0.62
10603135	**Fancb**	237211		3.6E-06	3.7E-04	0.58	3.9E-02	1.1E-01	
10539710	**Tia1**	21841		1.8E-05	8.1E-04	0.58	3.8E-06	1.6E-04	0.58
10395612	**G2e3**	217558		7.4E-06	5.1E-04	0.58	2.8E-04	2.9E-03	0.74
10537494	**Ssbp1**	381760		1.0E-03	1.0E-02	0.58	3.9E-05	7.0E-04	0.63
10397633	**Flrt2**	399558		2.4E-06	2.9E-04	0.58	2.0E-06	1.0E-04	0.53
10514128	**Ttc39b**	69863		1.1E-06	1.9E-04	0.58	1.9E-05	4.5E-04	0.70
10549536	**Amn1**	232566		1.5E-05	7.4E-04	0.58	5.8E-07	5.1E-05	0.60
10605493	**Prrg1**	546336		2.3E-05	9.5E-04	0.59	7.0E-05	1.1E-03	0.72
10491623	**4932438A13Rik**	229227		2.7E-03	1.9E-02	0.59	1.0E-05	2.9E-04	0.62
10367422	**Sarnp**	66118		4.7E-06	4.1E-04	0.59	4.2E-03	2.1E-02	0.88
10554895	**Crebzf**	233490		3.9E-07	1.2E-04	0.59	7.7E-06	2.4E-04	0.61
10491732	**Fat4**	329628		7.3E-05	1.9E-03	0.59	4.8E-06	1.8E-04	0.58
10400095	**Ifrd1**	15982	*	1.1E-04	2.5E-03	0.59	5.5E-02	1.5E-01	
10350377	**Zbtb41**	226470		1.8E-04	3.2E-03	0.59	2.8E-03	1.6E-02	0.73
10564237	**Gm9801**	330552		2.0E-04	3.5E-03	0.59	2.6E-06	1.2E-04	0.47
10462100	**Sarnp**	66118		5.0E-06	4.2E-04	0.59	3.0E-03	1.7E-02	0.88
10384150	**Purb**	19291		5.1E-05	1.5E-03	0.59	4.4E-03	2.2E-02	0.79
10571384	**Efha2**	78506		1.1E-03	1.0E-02	0.59	2.2E-05	5.0E-04	0.58
10579049	**Gm10033**	378466		2.4E-04	3.9E-03	0.59	4.3E-05	7.6E-04	0.55
10454512	**Sft2d3**	67158		1.2E-05	6.5E-04	0.59	4.6E-06	1.8E-04	0.69
10379215	**Ift20**	55978		4.0E-08	3.9E-05	0.59	1.7E-06	9.5E-05	0.72
10525733	**Setd8**	67956		6.1E-07	1.4E-04	0.59	3.9E-06	1.6E-04	0.67
10599686	**Zfp449**	78619		1.1E-05	6.2E-04	0.59	1.2E-05	3.3E-04	0.67
10361375	**Fbxo5**	67141		9.0E-06	5.6E-04	0.59	7.8E-02	1.9E-01	
10432471	**ENSMUST00000082789**			6.4E-04	7.5E-03	0.59	6.1E-05	9.6E-04	0.57

10462237	**Smarca2**	67155		9.5E-06	5.8E-04	0.59	1.4E-07	2.0E-05	0.58
10586773	**Gtf2a2**	235459	*	9.4E-06	5.8E-04	0.59	1.4E-03	9.4E-03	0.82
10514072	**Zdhhc21**	68268		2.7E-07	9.4E-05	0.59	3.6E-05	6.7E-04	0.71
10396795	**Eif2s1**	13665		5.9E-06	4.6E-04	0.59	8.1E-03	3.5E-02	0.82
10386219	**Zfp39**	22698		5.5E-06	4.5E-04	0.59	2.1E-07	2.7E-05	0.62
10436106	**C330027C09Rik**	224171		6.1E-06	4.6E-04	0.59	3.7E-02	1.1E-01	
10505109	**BC026590**	230234		1.2E-06	2.0E-04	0.59	9.1E-05	1.3E-03	0.78
10492558	**Smc4**	70099		5.5E-05	1.6E-03	0.59	9.4E-06	2.8E-04	0.63
10479973	**Gm10115**	791270		8.7E-04	9.2E-03	0.59	5.5E-05	9.0E-04	0.47
10593293	**Ncam1**	17967		1.7E-05	7.9E-04	0.59	3.7E-05	6.8E-04	0.75
10427606	**Skp2**	27401		2.6E-05	1.0E-03	0.59	5.3E-07	4.8E-05	0.68
10443459	**Srsf3**	20383		5.4E-04	6.8E-03	0.59	1.2E-02	4.6E-02	0.82
10365482	**Timp3**	21859		3.7E-06	3.7E-04	0.59	1.5E-06	8.8E-05	0.62
10578241	**Dlc1**	50768	*	1.5E-05	7.2E-04	0.59	2.3E-05	5.0E-04	0.61
10400395	**Ppp2r3c**	59032		4.2E-06	3.8E-04	0.59	1.2E-02	4.8E-02	0.83
10468275	**Pcgf6**	71041		3.4E-07	1.1E-04	0.59	6.4E-06	2.2E-04	0.69
10530733	**Clock**	12753		1.3E-05	6.8E-04	0.59	3.2E-06	1.4E-04	0.64
10542911	**Samd9l**	209086		1.9E-04	3.4E-03	0.59	3.2E-08	9.0E-06	0.59
10459183	**Slc26a2**	13521		8.5E-06	5.5E-04	0.59	2.0E-05	4.7E-04	0.69
10384725	**Rel**	19696		1.9E-06	2.6E-04	0.59	1.1E-05	3.0E-04	0.71
10491564	**4932438A13Rik**	229227		1.3E-03	1.2E-02	0.59	1.6E-06	9.2E-05	0.58
10405779	**Mir23b**	387217		1.1E-03	1.1E-02	0.59	1.5E-05	3.8E-04	0.58
10604612	**Mir503**	723879		3.6E-05	1.3E-03	0.59	1.3E-06	7.9E-05	0.47
10497831	**Ccna2**	12428		1.3E-04	2.6E-03	0.59	7.5E-02	1.8E-01	
10491611	**4932438A13Rik**	229227		8.1E-03	4.2E-02	0.59	5.0E-06	1.8E-04	0.59
10587655	**4930422I07Rik**	71640		3.2E-04	4.7E-03	0.59	4.6E-05	7.9E-04	0.62
10455118	**Pcdhb18**	93889		6.7E-04	7.8E-03	0.60	4.2E-06	1.7E-04	0.57
10391985	**Taf1d**	75316		8.6E-05	2.0E-03	0.60	3.5E-05	6.6E-04	0.55
10405739	**Taf1d**	75316		8.6E-05	2.0E-03	0.60	3.5E-05	6.6E-04	0.55
10409988	**Taf1d**	75316		8.6E-05	2.0E-03	0.60	3.5E-05	6.6E-04	0.55
10583318	**Taf1d**	75316		8.6E-05	2.0E-03	0.60	3.5E-05	6.6E-04	0.55
10607712	**Grpr**	14829		4.6E-04	6.0E-03	0.60	3.1E-03	1.7E-02	0.55
10555041	**Alg8**	381903		2.0E-07	7.7E-05	0.60	4.8E-05	8.2E-04	0.75
10578572	**Stox2**	71069		2.3E-04	3.8E-03	0.60	1.7E-06	9.5E-05	0.49
10497399	**Pde7a**	18583		1.4E-06	2.2E-04	0.60	5.3E-06	1.9E-04	0.64
10368616	**Zufsp**	72580		3.9E-04	5.4E-03	0.60	6.6E-08	1.3E-05	0.56
10455108	**Pcdhb16**	93887		5.1E-04	6.5E-03	0.60	3.1E-04	3.1E-03	0.72
10417326	**Gm10406**	100038847	*	3.2E-05	1.2E-03	0.60	7.6E-08	1.4E-05	0.57
10471550	**Rpl12**	269261		1.9E-04	3.4E-03	0.60	1.5E-05	3.9E-04	0.61
10400649	**Pole2**	18974		4.4E-05	1.4E-03	0.60	1.6E-01	3.1E-01	
10417359	**Gm3373**	100036568	*	1.4E-04	2.8E-03	0.60	9.9E-09	4.6E-06	0.54
10417258	**Gm8348**	666890	*	9.0E-05	2.1E-03	0.60	1.9E-08	6.7E-06	0.54
10445071	**Zfp57**	22715		3.5E-06	3.6E-04	0.60	4.2E-08	1.0E-05	0.59
10455602	**Dmxl1**	240283		6.7E-05	1.8E-03	0.60	7.3E-06	2.4E-04	0.63
10344789	**Cspp1**	211660		5.6E-05	1.6E-03	0.60	4.0E-04	3.8E-03	0.71
10544148	**Jhdm1d**	338523		1.7E-04	3.2E-03	0.60	1.2E-06	7.6E-05	0.58
10605421	**Mtcp1**	17763		2.4E-05	9.6E-04	0.60	1.3E-06	8.0E-05	0.57
10454039	**Impact**	16210		6.9E-06	5.0E-04	0.60	2.6E-07	3.1E-05	0.56
10491619	**4932438A13Rik**	229227		2.2E-03	1.7E-02	0.60	3.1E-05	6.1E-04	0.59
10455123	**Pcdhb19**	93890		1.1E-04	2.5E-03	0.60	1.1E-05	3.1E-04	0.65
10395273	**Gdap10**	14546		2.1E-05	8.9E-04	0.60	3.4E-06	1.5E-04	0.56
10556456	**Tead1**	21676		6.5E-07	1.5E-04	0.60	1.3E-06	7.9E-05	0.67
10585976	**Myo9a**	270163		3.7E-04	5.2E-03	0.60	2.6E-03	1.5E-02	0.58
10491629	**4932438A13Rik**	229227		1.2E-03	1.1E-02	0.60	1.1E-05	3.2E-04	0.62
10531415	**Cxcl10**	15945		3.4E-04	4.9E-03	0.60	4.4E-03	2.2E-02	0.75
10412520	**Gm3002**			4.5E-05	1.4E-03	0.60	4.2E-08	1.0E-05	0.55
10424485	**Phf20l1**	239510		2.0E-04	3.5E-03	0.60	2.4E-05	5.2E-04	0.67
10448307	**Tnfrsf12a**	27279		5.2E-06	4.3E-04	0.60	4.2E-04	3.9E-03	0.69
10353989	**AK089564**			7.6E-06	5.2E-04	0.60	7.7E-07	6.1E-05	0.60
10428522	**Csmd3**	239420		4.6E-04	6.0E-03	0.60	1.4E-06	8.5E-05	0.48
10423917	**GENSCAN00000035335**			7.9E-04	8.7E-03	0.60	1.8E-05	4.4E-04	0.48
10417302	**Gm3373**	100036568	*	2.9E-05	1.1E-03	0.60	3.7E-09	2.5E-06	0.53
10491601	**4932438A13Rik**	229227		3.5E-04	5.0E-03	0.60	8.1E-04	6.3E-03	0.67
10368409	**Lama2**	16773		8.5E-05	2.0E-03	0.60	9.6E-06	2.8E-04	0.57
10575160	**Nfat5**	54446		1.8E-04	3.2E-03	0.60	1.9E-06	1.0E-04	0.59
10454298	**Zfp397**	69256		1.7E-04	3.1E-03	0.60	1.2E-05	3.2E-04	0.64
10437942	**Ube2v2**	70620		1.5E-04	3.0E-03	0.60	1.9E-04	2.2E-03	0.74
10497077	**Mir186**	387181		2.7E-04	4.2E-03	0.60	7.2E-08	1.4E-05	0.53

10608720	**NM_025534.2**			1.2E-05	6.6E-04	0.60	4.1E-06	1.7E-04	0.66
10395984	**Fam179b**	328108		1.7E-05	7.9E-04	0.60	2.8E-03	1.6E-02	0.80
10468881	**Zfp826**	414758		4.5E-04	6.0E-03	0.60	8.2E-08	1.5E-05	0.54
10396383	**Slc38a6**	625098		2.3E-06	2.9E-04	0.60	4.2E-07	4.2E-05	0.62
10383758	**Tug1**	544752		1.7E-06	2.5E-04	0.60	7.3E-05	1.1E-03	0.71
10497051	**Negr1**	320840		1.6E-04	3.1E-03	0.60	3.2E-05	6.1E-04	0.59
10592585	**Sc5d**	235293		3.5E-04	5.1E-03	0.60	1.5E-07	2.1E-05	0.59
10448094	**Lnpep**	240028		5.1E-05	1.5E-03	0.60	4.9E-06	1.8E-04	0.64
10353878	**Ankrd23**	78321	*	1.9E-07	7.7E-05	0.61	9.3E-07	6.7E-05	0.60
10393395	**Srsf2**	20382		1.1E-06	1.9E-04	0.61	4.0E-05	7.1E-04	0.74
10495935	**4930422G04Rik**	71643		3.1E-06	3.3E-04	0.61	6.2E-04	5.2E-03	0.72
10412921	**Nid2**	18074	*	7.6E-06	5.2E-04	0.61	3.5E-07	3.7E-05	0.59
10557233	**Tnrc6a**	233833		5.1E-05	1.5E-03	0.61	6.3E-07	5.3E-05	0.63
10356084	**Irs1**	16367		9.1E-05	2.1E-03	0.61	3.0E-07	3.4E-05	0.52
10593123	**Tagln**	21345		8.9E-04	9.3E-03	0.61	5.0E-05	8.4E-04	0.66
10400413	**Ralgapa1**	56784		8.1E-06	5.3E-04	0.61	1.0E-05	3.0E-04	0.63
10586448	**2810417H13Rik**	68026		4.9E-04	6.4E-03	0.61	1.1E-01	2.4E-01	
10578916	**Sc4mol**	66234		9.5E-04	9.8E-03	0.61	3.9E-05	7.0E-04	0.52
10352194	**Cdc42bpa**	226751		5.9E-05	1.6E-03	0.61	2.6E-05	5.4E-04	0.70
10472398	**Scn2a1**	110876		2.5E-05	1.0E-03	0.61	2.8E-05	5.6E-04	0.64
10522303	**Guf1**	231279		2.1E-04	3.6E-03	0.61	3.8E-08	1.0E-05	0.55
10371770	**Gas2l3**	237436		2.0E-04	3.5E-03	0.61	1.7E-02	6.3E-02	0.81
10491721	**Spry1**	24063		5.2E-04	6.7E-03	0.61	5.3E-05	8.8E-04	0.59
10592531	**ENSMUST00000082975**			7.2E-04	8.2E-03	0.61	2.1E-04	2.3E-03	0.67
10485580	**Cstf3**	228410		2.9E-04	4.4E-03	0.61	2.2E-05	5.0E-04	0.50
10604735	**Rbmx**	19655		1.9E-06	2.6E-04	0.61	2.4E-09	2.0E-06	0.60
10397541	**Gm8300**	666806	*	4.3E-07	1.2E-04	0.61	3.3E-04	3.3E-03	0.83
10585974	**Myo9a**	270163		4.2E-04	5.7E-03	0.61	5.1E-04	4.5E-03	0.66
10492195	**Tsc22d2**	72033		3.8E-06	3.7E-04	0.61	3.6E-06	1.6E-04	0.64
10402444	**Dicer1**	192119		2.5E-06	3.0E-04	0.61	2.0E-04	2.3E-03	0.72
10485711	**Fibin**	67606		2.8E-05	1.1E-03	0.61	8.1E-06	2.5E-04	0.59
10506571	**Dhcr24**	74754		1.5E-04	2.9E-03	0.61	1.1E-04	1.5E-03	0.54
10563780	**E2f8**	108961		5.4E-03	3.2E-02	0.61	5.2E-02	1.4E-01	
10379989	**Fam33a**	66140		4.7E-05	1.5E-03	0.61	3.4E-04	3.3E-03	0.79
10603809	**ENSMUST00000143129**			2.6E-02	9.4E-02	0.61	2.8E-03	1.6E-02	0.63
10476443	**Plcb4**	18798		1.9E-05	8.4E-04	0.61	1.4E-05	3.7E-04	0.66
10502240	**Npnt**	114249		9.0E-04	9.4E-03	0.61	2.4E-03	1.4E-02	0.76
10523021	**Slc4a4**	54403		1.7E-03	1.5E-02	0.61	1.5E-01	3.0E-01	
10424467	**Phf20l1**	239510		5.5E-05	1.6E-03	0.61	2.5E-05	5.3E-04	0.65
10400170	**Prkd1**	18760		4.7E-06	4.1E-04	0.61	7.4E-05	1.1E-03	0.72
10491617	**4932438A13Rik**	229227		2.8E-03	2.0E-02	0.61	1.5E-05	3.8E-04	0.59
10374590	**Xpo1**	103573		1.9E-06	2.6E-04	0.61	3.9E-04	3.7E-03	0.77
10417235	**Gm3373**	100036568	*	1.0E-04	2.3E-03	0.61	2.7E-08	8.0E-06	0.52
10417315	**Gm3373**	100036568	*	1.0E-04	2.3E-03	0.61	2.7E-08	8.0E-06	0.52
10458808	**Fem1c**	240263		1.1E-05	6.2E-04	0.61	3.3E-05	6.4E-04	0.71
10607486	**Ptchd1**	211612		5.7E-05	1.6E-03	0.61	1.4E-02	5.2E-02	0.67
10494821	**Tspan2**	70747		1.8E-04	3.2E-03	0.61	8.3E-06	2.6E-04	0.71
10595614	**2810026P18Rik**	72655		1.6E-06	2.5E-04	0.61	3.2E-06	1.4E-04	0.65
10405783	**Mir24-1**	387142		1.8E-05	8.2E-04	0.61	6.7E-06	2.2E-04	0.53
10412298	**Itga1**	109700		7.1E-03	3.8E-02	0.61	9.2E-05	1.3E-03	0.62
10449000	**Msln**	56047		1.0E-03	1.0E-02	0.61	1.3E-03	9.1E-03	0.64
10590389	**Nktr**	18087		4.5E-05	1.4E-03	0.61	1.6E-06	9.0E-05	0.66
10556487	**BC150970**			3.6E-05	1.3E-03	0.61	1.2E-06	7.7E-05	0.59
10532989	**Gatc**	384281		9.0E-06	5.6E-04	0.61	3.3E-06	1.4E-04	0.66
10571922	**Nek1**	18004		8.2E-05	2.0E-03	0.61	6.2E-04	5.2E-03	0.74
10419082	**5730469M10Rik**	70564		1.4E-04	2.8E-03	0.61	7.0E-03	3.2E-02	0.68
10523451	**Anxa3**	11745		1.2E-04	2.6E-03	0.62	4.0E-05	7.2E-04	0.63
10374621	**Usp34**	17847	*	1.9E-04	3.4E-03	0.62	9.7E-06	2.8E-04	0.67
10528332	**Napepld**	242864		4.1E-06	3.8E-04	0.62	8.9E-04	6.7E-03	0.69
10389505	**Gm9975**	327988		7.2E-05	1.8E-03	0.62	1.5E-04	1.8E-03	0.69
10491615	**4932438A13Rik**	229227		6.9E-05	1.8E-03	0.62	6.4E-05	1.0E-03	0.66
10534056	**Hpvc-ps**	15456		4.2E-06	3.8E-04	0.62	1.7E-09	1.6E-06	0.53
10400668	**Sdccag1**	66244		3.8E-05	1.3E-03	0.62	1.9E-05	4.5E-04	0.67
10457778	**Gm10551**	100126206		3.2E-05	1.2E-03	0.62	5.1E-07	4.7E-05	0.49
10574985	**Slc7a6**	330836		7.0E-07	1.6E-04	0.62	3.7E-07	3.9E-05	0.67
10417053	**Mbnl2**	105559		6.9E-06	5.0E-04	0.62	1.1E-05	3.0E-04	0.68
10551215	**Rnf170**	77733		3.0E-05	1.1E-03	0.62	6.7E-05	1.0E-03	0.75
10374821	**Smek2**	104570		4.7E-05	1.5E-03	0.62	9.1E-05	1.3E-03	0.74

10462973	**Hells**	15201		2.2E-06	2.9E-04	0.62	2.2E-01	3.8E-01	
10590968	**Ankrd49**	56503		1.3E-05	6.9E-04	0.62	1.7E-05	4.2E-04	0.70
10556581	**Gm10589**	100037281		1.4E-03	1.3E-02	0.62	5.9E-08	1.2E-05	0.52
10556640	**6330503K22Rik**	101565		6.1E-07	1.4E-04	0.62	5.3E-05	8.8E-04	0.72
10506680	**Tmem48**	72787		1.1E-05	6.4E-04	0.62	1.1E-03	8.0E-03	0.80
10475051	**Mga**	29808		3.1E-04	4.6E-03	0.62	9.5E-06	2.8E-04	0.67
10515836	**Ccnb1**	268697		2.5E-04	4.0E-03	0.62	5.8E-01	7.3E-01	
10465342	**Tm7sf2**	73166		1.4E-03	1.2E-02	0.62	5.8E-05	9.4E-04	0.72
10468653	**A630007B06Rik**	213993		4.7E-06	4.1E-04	0.62	2.5E-04	2.7E-03	0.74
10491625	**4932438A13Rik**	229227		4.2E-03	2.7E-02	0.62	2.5E-04	2.7E-03	0.67
10586920	**Rfx7**	319758		1.2E-05	6.6E-04	0.62	2.2E-05	4.9E-04	0.70
10469425	**Arl5b**	75869		1.3E-06	2.1E-04	0.62	2.8E-05	5.7E-04	0.69
10468795	**Rab11fip2**	74998		1.7E-04	3.2E-03	0.62	4.1E-05	7.3E-04	0.66
10501690	**Slc35a3**	229782		6.7E-05	1.8E-03	0.62	5.1E-02	1.4E-01	
10463121	**Zfp518a**	72672		6.0E-03	3.5E-02	0.62	4.0E-05	7.1E-04	0.69
10397085	**Rbm25**	67039		5.5E-05	1.6E-03	0.62	1.3E-05	3.5E-04	0.69
10606609	**Tspan6**	56496		1.5E-06	2.4E-04	0.62	3.2E-05	6.2E-04	0.77
10471878	**Mir181a-2**	387176		1.2E-05	6.5E-04	0.62	1.2E-06	7.8E-05	0.39
10607950	**G530011O06Rik**	654820		1.7E-03	1.4E-02	0.62	1.8E-04	2.1E-03	0.72
10407126	**Plk2**	20620		7.4E-05	1.9E-03	0.62	4.5E-06	1.7E-04	0.60
10569707	**Myadm**	50918		5.3E-07	1.3E-04	0.62	4.9E-07	4.7E-05	0.72
10488860	**ENSMUST00000116491**			1.1E-04	2.3E-03	0.62	2.7E-06	1.3E-04	0.59
10583228	**Fam76b**	72826		1.2E-05	6.6E-04	0.62	2.1E-05	4.8E-04	0.72
10482059	**Ggta1**	14594		6.0E-07	1.4E-04	0.62	2.2E-06	1.1E-04	0.68
10418004	**Ap3m1**	55946		2.6E-05	1.0E-03	0.62	1.1E-04	1.4E-03	0.75
10542264	**2700089E24Rik**	381820		1.0E-04	2.3E-03	0.62	1.3E-02	5.0E-02	0.84
10356997	**AK048760**			1.1E-04	2.4E-03	0.62	2.8E-06	1.3E-04	0.52
10389882	**Luc7l3**	67684		4.4E-05	1.4E-03	0.62	2.1E-04	2.3E-03	0.77
10466682	**Smc5**	226026		4.6E-05	1.4E-03	0.62	3.1E-04	3.1E-03	0.72
10412466	**Hmgcs1**	208715		4.6E-03	2.8E-02	0.62	5.2E-04	4.6E-03	0.62
10474169	**AK082647**			2.3E-04	3.9E-03	0.62	7.0E-06	2.3E-04	0.63
10417373	**2610042L04Rik**	554327	*	2.4E-05	9.6E-04	0.62	5.6E-08	1.2E-05	0.56
10361270	**Cd46**	17221		2.4E-03	1.8E-02	0.62	1.0E-06	7.0E-05	0.55
10527649	**6330406I15Rik**	70717		1.6E-04	3.1E-03	0.62	4.8E-07	4.5E-05	0.59
10422781	**Rictor**	78757		9.2E-05	2.1E-03	0.62	3.4E-05	6.5E-04	0.68
10529567	**D5Ertd579e**	320661		1.6E-05	7.5E-04	0.62	1.2E-04	1.6E-03	0.63
10555087	**ENSMUST00000083426**			6.6E-04	7.7E-03	0.62	6.7E-09	3.3E-06	0.56
10469712	**Pdss1**	56075		1.4E-04	2.8E-03	0.62	3.9E-03	2.0E-02	0.74
10601980	**Mum1l1**	245631		4.5E-06	3.9E-04	0.63	1.3E-04	1.6E-03	0.72
10394699	**Rock2**	19878		5.1E-05	1.5E-03	0.63	1.4E-05	3.6E-04	0.69
10433088	**Cbx5**	12419		1.0E-06	1.9E-04	0.63	6.2E-04	5.2E-03	0.82
10495574	**Sass6**	72776	*	3.2E-05	1.2E-03	0.63	2.3E-02	7.7E-02	0.80
10364402	**Slc1a6**	20513		8.9E-04	9.4E-03	0.63	1.0E-05	2.9E-04	0.56
10488291	**Rbbp9**	26450		2.4E-06	2.9E-04	0.63	2.6E-05	5.5E-04	0.77
10446425	**ENSMUST00000083372**			6.1E-04	7.3E-03	0.63	1.3E-06	8.2E-05	0.53
10524079	**2310001H12Rik**	69504		1.5E-03	1.3E-02	0.63	2.6E-06	1.2E-04	0.65
10582275	**Slc7a5**	20539		4.5E-04	6.0E-03	0.63	3.8E-05	6.9E-04	0.63
10346365	**Sgol2**	68549		1.2E-06	2.0E-04	0.63	2.2E-02	7.6E-02	0.80
10358432	**Zfp825**	235956		6.2E-05	1.7E-03	0.63	7.6E-07	6.0E-05	0.70
10435712	**Cd80**	12519		4.2E-04	5.7E-03	0.63	2.0E-05	4.7E-04	0.65
10472400	**Scn2a1**	110876		1.2E-03	1.1E-02	0.63	4.5E-04	4.1E-03	0.60
10521927	**Tbc1d19**	67249		1.6E-05	7.5E-04	0.63	2.6E-07	3.1E-05	0.69
10362426	**Trdn**	76757		2.4E-03	1.8E-02	0.63	2.8E-01	4.5E-01	
10582899	**ENSMUST00000099056**			2.1E-02	8.1E-02	0.63	5.5E-04	4.7E-03	0.69
10603911	**ENSMUST00000134724**			5.3E-03	3.1E-02	0.63	4.6E-06	1.8E-04	0.56
10407392	**BC016423**	105203		7.7E-05	1.9E-03	0.63	5.8E-05	9.4E-04	0.66
10588226	**Amotl2**	56332		2.5E-04	4.1E-03	0.63	6.0E-07	5.1E-05	0.48
10410756	**Ankrd32**	105377		2.3E-03	1.7E-02	0.63	6.8E-04	5.5E-03	0.75
10588419	**Aste1**	66595		4.6E-06	4.0E-04	0.63	3.2E-07	3.6E-05	0.64
10384691	**0610010F05Rik**	71675		3.8E-06	3.7E-04	0.63	4.6E-05	8.0E-04	0.68
10487577	**Ckap2l**	70466		2.1E-04	3.6E-03	0.63	1.2E-02	4.6E-02	0.81
10404496	**Nqo2**	18105		2.1E-05	8.9E-04	0.63	1.0E-06	7.2E-05	0.62
10462796	**Kif11**	16551		1.2E-05	6.5E-04	0.63	2.7E-01	4.5E-01	
10354649	**Pgap1**	241062		9.3E-05	2.2E-03	0.63	4.8E-05	8.2E-04	0.71
10603807	**Mir222**	723828		2.2E-04	3.7E-03	0.63	3.3E-04	3.2E-03	0.69
10420877	**Esco2**	71988		8.5E-05	2.0E-03	0.63	4.5E-02	1.2E-01	
10511368	**Impad1**	242291		3.7E-06	3.7E-04	0.63	6.4E-05	1.0E-03	0.69
10541695	**Lpcat3**	14792		4.8E-07	1.3E-04	0.63	3.8E-05	7.0E-04	0.77

10577395	**2610005L07Rik**	381598	*	4.4E-05	1.4E-03	0.63	7.8E-07	6.1E-05	0.61
10516103	**Macf1**	11426		2.9E-04	4.5E-03	0.63	3.1E-06	1.4E-04	0.54
10501676	**Hiat1**	15247		2.8E-06	3.1E-04	0.63	3.8E-06	1.6E-04	0.74
10598839	**Rp2h**	19889		9.1E-07	1.8E-04	0.63	1.1E-05	3.1E-04	0.71
10412773	**Slc4a7**	218756		2.5E-07	9.0E-05	0.63	8.7E-05	1.2E-03	0.69
10589087	**Prkar2a**	19087		1.2E-05	6.6E-04	0.63	1.8E-03	1.1E-02	0.82
10446376	**Man2a1**	17158		8.4E-05	2.0E-03	0.63	6.7E-07	5.5E-05	0.66
10388784	**Rpl23a**	268449		1.8E-04	3.2E-03	0.63	1.6E-05	4.0E-04	0.74
10518679	**Nmnat1**	66454		3.7E-04	5.2E-03	0.63	2.1E-05	4.7E-04	0.69
10458340	**Hbegf**	15200		2.4E-02	9.0E-02	0.63	5.4E-02	1.4E-01	
10530492	**Nfxl1**	100978		4.4E-04	5.9E-03	0.63	1.3E-05	3.4E-04	0.64
10453544	**Mettl4**	76781		1.5E-04	2.9E-03	0.63	4.6E-06	1.8E-04	0.73
10527920	**Cyp51**	13121		7.0E-04	8.0E-03	0.63	1.8E-01	3.4E-01	
10502780	**Lphn2**	99633		1.4E-05	7.0E-04	0.63	2.0E-05	4.6E-04	0.63
10490838	**Fabp5**	16592	*	1.2E-03	1.2E-02	0.63	3.1E-03	1.7E-02	0.63
10578810	**Clcn3**	12725		1.7E-06	2.5E-04	0.63	1.7E-05	4.1E-04	0.69
10579052	**Gm10033**	378466		6.1E-05	1.7E-03	0.63	1.2E-03	8.3E-03	0.63
10419370	**Exoc5**	105504		7.8E-06	5.2E-04	0.63	2.3E-04	2.5E-03	0.70
10554129	**B130024G19Rik**	434198		4.4E-04	5.9E-03	0.63	2.3E-09	2.0E-06	0.57
10532301	**ENSMUST00000092720**			4.0E-03	2.6E-02	0.63	6.2E-04	5.2E-03	0.66
10588192	**Msl2**	77853		6.5E-06	4.8E-04	0.63	1.4E-03	9.5E-03	0.77
10555116	**Gm9990**	791341		6.4E-05	1.7E-03	0.63	2.8E-08	8.1E-06	0.56
10575619	**Terf2ip**	57321		4.0E-06	3.8E-04	0.63	1.1E-05	3.2E-04	0.71
10394789	**B430203G13Rik**	791400		2.3E-04	3.8E-03	0.63	3.9E-06	1.6E-04	0.63
10582918	**ENSMUST00000099037**			6.3E-03	3.5E-02	0.63	1.9E-04	2.2E-03	0.65
10445428	**ENSMUST00000083809**			1.6E-03	1.4E-02	0.63	1.3E-04	1.7E-03	0.46
10491605	**4932438A13Rik**	229227		3.6E-03	2.4E-02	0.63	2.2E-04	2.4E-03	0.66
10535852	**Slc7a1**	11987		7.1E-05	1.8E-03	0.63	6.3E-06	2.2E-04	0.66
10422980	**Lmbrd2**	320506		2.0E-05	8.7E-04	0.63	9.1E-05	1.3E-03	0.70
10455483	**Ythdc2**	240255		6.4E-05	1.7E-03	0.63	7.1E-03	3.2E-02	0.79
10607679	**Txlng**	353170		6.2E-05	1.7E-03	0.63	5.1E-05	8.6E-04	0.73
10495359	**Clcc1**	229725		5.9E-07	1.4E-04	0.63	1.2E-06	7.6E-05	0.73
10557853	**B230325K18Rik**	319527		4.9E-05	1.5E-03	0.63	1.7E-05	4.2E-04	0.53
10439710	**Phldb2**	208177		3.8E-05	1.3E-03	0.63	7.7E-07	6.1E-05	0.59
10431732	**Zcrb1**	67197		1.4E-06	2.3E-04	0.64	1.6E-05	4.1E-04	0.74
10457331	**Mzt1**	76789		3.8E-05	1.3E-03	0.64	7.6E-03	3.3E-02	0.87
10578287	**Cnot7**	18983		3.9E-05	1.3E-03	0.64	1.2E-05	3.3E-04	0.75
10456423	**Seh1l**	72124		6.3E-06	4.7E-04	0.64	1.5E-02	5.5E-02	0.85
10491599	**4932438A13Rik**	229227		5.0E-03	3.0E-02	0.64	7.7E-04	6.0E-03	0.63
10495945	**4930422G04Rik**	71643		3.2E-06	3.4E-04	0.64	5.3E-04	4.6E-03	0.73
10415784	**Trim13**	66597		2.0E-05	8.6E-04	0.64	1.6E-04	1.9E-03	0.78
10455112	**Pcdhb17**	93888		5.2E-03	3.1E-02	0.64	6.1E-03	2.8E-02	0.77
10502766	**Lphn2**	99633		8.8E-04	9.3E-03	0.64	1.1E-06	7.2E-05	0.55
10480432	**Mastl**	67121		2.8E-06	3.1E-04	0.64	2.7E-01	4.5E-01	
10404429	**Serpinb9**	20723		5.7E-06	4.5E-04	0.64	1.3E-02	5.0E-02	0.82
10431935	**Amigo2**	105827	*	1.1E-06	1.9E-04	0.64	1.0E-07	1.7E-05	0.60
10371271	**Zfp781**	331188		4.4E-03	2.8E-02	0.64	7.8E-06	2.5E-04	0.65
10516007	**Zmpste24**	230709		1.0E-05	6.1E-04	0.64	7.0E-05	1.1E-03	0.82
10399038	**Zfp386**	56220		5.6E-06	4.5E-04	0.64	5.3E-08	1.2E-05	0.60
10503534	**Ccnc**	51813		1.2E-05	6.6E-04	0.64	9.4E-03	3.9E-02	0.85
10563649	**Uevld**	54122		5.7E-05	1.6E-03	0.64	1.3E-05	3.4E-04	0.72
10404538	**Prpf4b**	19134		3.2E-05	1.2E-03	0.64	8.7E-08	1.5E-05	0.59
10483401	**Spc25**	66442		3.1E-04	4.6E-03	0.64	4.4E-01	6.2E-01	
10594426	**Zwilch**	68014	*	2.8E-06	3.1E-04	0.64	3.0E-02	9.4E-02	0.81
10428755	**Zhx1**	22770		6.0E-04	7.2E-03	0.64	6.1E-07	5.2E-05	0.66
10354472	**Gls**	14660		8.3E-05	2.0E-03	0.64	1.1E-04	1.5E-03	0.70
10450363	**Snord52**	100217427		2.3E-02	8.7E-02	0.64	9.9E-01	9.9E-01	
10375497	**ENSMUST00000142269**			5.7E-06	4.5E-04	0.64	6.4E-05	1.0E-03	0.70
10457644	**Cdh2**	12558		1.1E-05	6.3E-04	0.64	9.4E-09	4.4E-06	0.59
10373577	**Ormdl2**	66844	*	1.4E-05	7.1E-04	0.64	1.5E-02	5.5E-02	0.84
10424543	**Wisp1**	22402		6.5E-06	4.8E-04	0.64	2.6E-04	2.7E-03	0.62
10483719	**Chn1**	108699		1.6E-05	7.5E-04	0.64	6.7E-02	1.7E-01	
10464084	**Tcf7l2**	21416		1.4E-05	7.1E-04	0.64	1.5E-07	2.1E-05	0.60
10347036	**Mtap2**	17756		1.8E-04	3.3E-03	0.64	1.8E-07	2.3E-05	0.60
10585992	**Myo9a**	270163		3.7E-04	5.2E-03	0.64	4.8E-05	8.2E-04	0.66
10425333	**Apobec3**	80287		1.7E-06	2.5E-04	0.64	1.1E-06	7.5E-05	0.62
10413695	**Pbrm1**	66923		6.2E-05	1.7E-03	0.64	5.0E-05	8.4E-04	0.67
10427904	**Fbxl7**	448987		2.8E-03	2.0E-02	0.64	4.9E-04	4.4E-03	0.58

10544219	**Braf**	109880		9.8E-05	2.2E-03	0.64	5.0E-06	1.9E-04	0.66
10372383	**Zdhhc17**	320150		6.2E-04	7.3E-03	0.64	3.3E-04	3.2E-03	0.71
10367434	**AK086046**			4.6E-06	4.0E-04	0.64	1.3E-07	2.0E-05	0.50
10567173	**Pik3c2a**	18704		8.1E-05	2.0E-03	0.64	1.9E-05	4.5E-04	0.66
10406968	**Cenpk**	60411	*	4.4E-04	5.9E-03	0.64	7.7E-02	1.9E-01	
10361882	**Nhsl1**	215819		2.9E-04	4.5E-03	0.64	3.8E-05	6.9E-04	0.66
10459590	**Ptpn2**	19255		5.4E-06	4.4E-04	0.64	4.0E-04	3.7E-03	0.79
10490931	**Ythdf3**	229096		8.2E-06	5.4E-04	0.64	1.5E-04	1.8E-03	0.77
10514049	**Nfib**	18028		2.0E-03	1.6E-02	0.64	2.0E-02	6.9E-02	0.79
10408049	**Zfp192**	93681		3.1E-06	3.3E-04	0.64	1.4E-05	3.6E-04	0.64
10536369	**C1galt1**	94192		4.4E-05	1.4E-03	0.64	2.5E-02	8.3E-02	0.88
10482144	**Rc3h2**	319817		9.7E-06	5.9E-04	0.64	1.1E-04	1.5E-03	0.71
10511881	**Manea**	242362		3.4E-05	1.2E-03	0.64	5.6E-06	2.0E-04	0.69
10595529	**4922501C03Rik**	382090		1.2E-04	2.5E-03	0.64	1.5E-06	8.7E-05	0.63
10488459	**Zfp442**	668923		1.3E-03	1.2E-02	0.64	1.1E-04	1.5E-03	0.65
10502778	**Lphn2**	99633		3.7E-04	5.3E-03	0.64	1.9E-04	2.2E-03	0.62
10604799	**Atp11c**	320940		2.5E-04	4.0E-03	0.65	3.1E-04	3.1E-03	0.74
10418991	**Gcap14**	72972		4.2E-06	3.8E-04	0.65	1.5E-06	8.9E-05	0.67
10472501	**Lass6**	241447		2.3E-06	2.9E-04	0.65	4.0E-06	1.6E-04	0.69
10466963	**9930021J03Rik**	240613		4.6E-04	6.0E-03	0.65	7.8E-06	2.5E-04	0.64
10411839	**Srsf12**	218543		4.2E-05	1.4E-03	0.65	2.0E-05	4.7E-04	0.64
10502830	**Nexn**	68810		9.4E-04	9.7E-03	0.65	3.9E-05	7.1E-04	0.62
10504957	**Smc2**	14211		5.1E-06	4.2E-04	0.65	1.7E-01	3.3E-01	
10428515	**Csmd3**	239420		5.6E-03	3.3E-02	0.65	5.8E-05	9.4E-04	0.54
10537397	**Luc7l2**	192196		1.5E-04	3.0E-03	0.65	8.6E-05	1.2E-03	0.72
10607619	**Cdkl5**	382253		5.1E-05	1.5E-03	0.65	2.8E-05	5.7E-04	0.58
10417446	**4930555G01Rik**	108978	*	2.9E-04	4.5E-03	0.65	8.3E-07	6.4E-05	0.56
10417452	**4930555G01Rik**	108978	*	2.9E-04	4.5E-03	0.65	8.3E-07	6.4E-05	0.56
10546567	**A130022J15Rik**	101351		5.9E-06	4.6E-04	0.65	1.7E-06	9.3E-05	0.63
10564573	**Chd2**	244059		8.9E-06	5.6E-04	0.65	2.4E-05	5.1E-04	0.72
10505028	**Slc44a1**	100434		8.5E-04	9.1E-03	0.65	2.6E-03	1.5E-02	1.41
10457959	**Sft2d3**	67158		2.5E-04	4.1E-03	0.65	9.8E-05	1.4E-03	0.72
10451851	**Armcx3**	71703		2.4E-04	3.9E-03	0.65	8.9E-03	3.8E-02	0.85
10355141	**Klf7**	93691		2.3E-05	9.4E-04	0.65	1.5E-03	1.0E-02	0.74
10468691	**Ablim1**	226251		1.8E-04	3.3E-03	0.65	2.8E-03	1.6E-02	0.77
10504491	**Zcchc7**	319885		2.1E-04	3.5E-03	0.65	3.9E-08	1.0E-05	0.54
10594774	**Ccnb2**	12442		2.1E-04	3.6E-03	0.65	3.2E-01	5.0E-01	
10540544	**Thumpd3**	14911		3.8E-04	5.3E-03	0.65	3.1E-02	9.6E-02	0.88
10568714	**Mki67**	17345		1.0E-04	2.3E-03	0.65	2.3E-03	1.4E-02	0.74
10540273	**Ube2v2**	70620	*	3.8E-05	1.3E-03	0.65	3.0E-05	6.0E-04	0.77
10428534	**Trps1**	83925		2.6E-04	4.1E-03	0.65	5.9E-03	2.8E-02	0.77
10409061	**Mirlet7f-1**	387252		1.2E-04	2.5E-03	0.65	3.4E-05	6.4E-04	0.70
10440288	**Zfp654**	72020		1.5E-03	1.4E-02	0.65	6.0E-04	5.0E-03	0.79
10532157	**Tmed5**	73130		1.7E-04	3.1E-03	0.65	4.7E-05	8.0E-04	0.71
10528723	**Mll3**	231051		1.7E-03	1.4E-02	0.65	6.2E-06	2.2E-04	0.65
10388938	**Wsb1**	78889		5.4E-06	4.4E-04	0.65	5.1E-04	4.5E-03	0.77
10428018	**Ube2v2**	70620	*	4.0E-05	1.3E-03	0.65	3.9E-05	7.0E-04	0.78
10461878	**Prune2**	353211		3.5E-05	1.2E-03	0.65	3.6E-02	1.1E-01	
10441359	**ENSMUST00000071832**			1.3E-04	2.7E-03	0.65	1.9E-06	1.0E-04	0.56
10538832	**Mad2l1**	56150		7.1E-06	5.0E-04	0.65	3.7E-02	1.1E-01	
10397267	**Isca2**	74316		1.7E-05	8.0E-04	0.65	9.3E-07	6.7E-05	0.65
10438911	**Atp13a3**	224088		1.5E-04	2.9E-03	0.65	4.4E-04	4.0E-03	0.74
10568529	**Ikzf5**	67143		7.2E-05	1.9E-03	0.65	2.2E-03	1.3E-02	0.70
10442083	**Mirlet7e**	387248		2.9E-05	1.1E-03	0.65	8.5E-08	1.5E-05	0.54
10361995	**Fam54a**	71804		2.3E-04	3.8E-03	0.65	5.9E-02	1.5E-01	
10429754	**Nrbp2**	223649		9.4E-04	9.7E-03	0.65	1.3E-05	3.4E-04	0.55
10547054	**ENSMUST00000119165**			1.1E-03	1.1E-02	0.65	2.2E-04	2.4E-03	0.78
10607250	**Apex2**	77622		2.9E-05	1.1E-03	0.65	1.1E-05	3.1E-04	0.68
10604248	**Thoc2**	331401		2.8E-03	2.0E-02	0.65	2.5E-05	5.3E-04	0.67
10410877	**Polr3g**	67486		2.1E-05	8.8E-04	0.65	5.9E-01	7.4E-01	
10507190	**4732418C07Rik**	230648		2.5E-06	3.0E-04	0.65	5.3E-05	8.8E-04	0.75
10479887	**Sec61a2**	57743		1.2E-05	6.5E-04	0.65	2.1E-08	7.2E-06	0.59
10441791	**Airn**	104103		1.1E-03	1.1E-02	0.65	3.4E-07	3.7E-05	0.49
10360406	**Ifi205**	226695		4.5E-04	6.0E-03	0.65	9.7E-01	9.8E-01	
10436487	**Vgll3**	73569		3.2E-03	2.2E-02	0.65	2.5E-06	1.2E-04	0.52
10506397	**Mier1**	71148		1.2E-05	6.5E-04	0.65	1.8E-03	1.1E-02	0.82
10543709	**Tmem209**	72649		4.8E-07	1.3E-04	0.65	3.8E-06	1.6E-04	0.77
10466441	**Vps13a**	271564		7.9E-04	8.6E-03	0.65	1.8E-05	4.4E-04	0.65

10552264	**9430025M13Rik**	233147		1.6E-04	3.1E-03	0.65	4.8E-04	4.3E-03	0.80
10535956	**Stard13**	243362		3.9E-04	5.4E-03	0.65	9.0E-07	6.6E-05	0.66
10565570	**4632434I11Rik**	74041		1.6E-04	3.1E-03	0.65	7.6E-01	8.6E-01	
10389214	**Ccl9**	20308		1.9E-02	7.6E-02	0.65	5.2E-02	1.4E-01	
10506050	**Nfia**	18027		3.7E-04	5.2E-03	0.65	4.8E-06	1.8E-04	0.56
10532305	**2310001H12Rik**	69504	*	2.4E-03	1.8E-02	0.65	1.8E-06	9.7E-05	0.69
10417411	**Gm3373**	100036568	*	4.4E-04	5.9E-03	0.65	3.1E-07	3.4E-05	0.58
10452404	**Nudt12**	67993		1.8E-04	3.3E-03	0.65	8.0E-06	2.5E-04	0.66
10351013	**Rc3h1**	381305		6.9E-04	7.9E-03	0.65	2.1E-04	2.3E-03	0.72
10449926	**Zfp799**	240064		2.0E-04	3.5E-03	0.65	1.2E-02	4.7E-02	0.81
10428453	**Csmd3**	239420		4.5E-04	6.0E-03	0.65	1.4E-05	3.7E-04	0.53
10523752	**Txlng**	353170		6.9E-05	1.8E-03	0.65	5.6E-05	9.1E-04	0.74
10475686	**Ap4e1**	108011		1.3E-04	2.7E-03	0.65	1.4E-06	8.3E-05	0.67
10380620	**Mir196a-1**	387191		8.7E-05	2.1E-03	0.65	1.5E-03	9.9E-03	0.66
10378902	**Nufip2**	68564		1.6E-04	3.1E-03	0.65	8.7E-04	6.6E-03	0.74
10371591	**4930547N16Rik**	75317	*	3.4E-05	1.2E-03	0.65	5.7E-03	2.7E-02	0.81
10435961	**Gm10808**	100038470		2.5E-04	4.0E-03	0.65	7.4E-04	5.9E-03	0.69
10463263	**Lztfl1**	93730		2.6E-05	1.0E-03	0.65	1.4E-05	3.6E-04	0.74
10476939	**Gm4979**	245174	*	3.4E-04	4.9E-03	0.65	4.0E-05	7.2E-04	0.64
10599335	**Mcts1**	68995		6.4E-05	1.7E-03	0.65	1.2E-06	7.6E-05	0.57
10490802	**Fam164a**	67306		1.3E-04	2.7E-03	0.65	1.3E-05	3.5E-04	0.70
10357191	**Ptpn4**	19258		6.3E-05	1.7E-03	0.65	7.1E-03	3.2E-02	0.78
10606301	**Magt1**	67075		1.5E-05	7.2E-04	0.65	4.4E-05	7.6E-04	0.76
10372121	**Tmtc3**	237500		1.5E-04	2.9E-03	0.65	2.7E-06	1.3E-04	0.63
10492888	**ENSMUST00000083913**			1.3E-04	2.7E-03	0.65	4.4E-08	1.0E-05	0.55
10557213	**Rbbp6**	19647		1.2E-04	2.5E-03	0.65	5.7E-06	2.0E-04	0.67
10429564	**Ly6a**	110454		2.2E-06	2.9E-04	0.65	2.5E-01	4.2E-01	
10494672	**Tbx15**	21384		1.3E-06	2.1E-04	0.65	3.8E-06	1.6E-04	0.68
10545707	**Actg2**	11468		2.9E-04	4.4E-03	0.65	1.5E-01	3.0E-01	
10442206	**Zfp51**	22709		2.6E-04	4.1E-03	0.65	2.3E-04	2.5E-03	0.72
10568363	**Armcx3**	71703		2.9E-04	4.5E-03	0.65	1.5E-03	1.0E-02	0.82
10439634	**Gtpbp8**	66067		4.0E-05	1.3E-03	0.66	3.1E-05	6.0E-04	0.74
10575153	**Cyb5b**	66427		3.2E-06	3.4E-04	0.66	2.9E-04	3.0E-03	0.81
10574962	**Nfatc3**	18021		2.8E-06	3.1E-04	0.66	1.4E-04	1.7E-03	0.77
10608422	**Rmi1**	74386	*	1.7E-05	8.0E-04	0.66	1.2E-03	8.7E-03	0.79
10479975	**ENSMUST00000083890**			2.2E-03	1.7E-02	0.66	1.5E-04	1.9E-03	0.63
10536499	**Cav1**	12389		6.1E-06	4.6E-04	0.66	4.7E-03	2.3E-02	0.79
10406614	**Mtx3**	382793		5.5E-04	6.8E-03	0.66	2.5E-07	3.1E-05	0.50
10344707	**Pcmtd1**	319263		4.5E-04	6.0E-03	0.66	1.6E-03	1.0E-02	0.76
10392410	**Gm10838**	100038581		7.3E-05	1.9E-03	0.66	1.8E-05	4.2E-04	0.62
10362633	**Rev3l**	19714		1.8E-03	1.5E-02	0.66	6.5E-06	2.2E-04	0.62
10536068	**Zfp788**	67607		2.5E-03	1.9E-02	0.66	4.6E-05	8.0E-04	0.70
10552320	**Zfp788**	67607		2.5E-03	1.9E-02	0.66	4.6E-05	8.0E-04	0.70
10571530	**Fat1**	14107		2.4E-04	3.9E-03	0.66	1.2E-06	7.6E-05	0.61
10559606	**Tmem86b**	68255		4.8E-05	1.5E-03	0.66	6.3E-04	5.2E-03	0.82
10356461	**Hjurp**	381280	*	1.4E-04	2.8E-03	0.66	1.3E-03	9.1E-03	0.77
10563657	**BC004639**			2.9E-04	4.5E-03	0.66	4.9E-08	1.1E-05	0.63
10523060	**Gm9958**	791294		1.6E-05	7.6E-04	0.66	2.5E-03	1.4E-02	0.78
10394366	**Atad2b**	320817		3.4E-04	5.0E-03	0.66	2.3E-05	5.0E-04	0.72
10428983	**Fam49b**	223601		7.6E-06	5.2E-04	0.66	8.0E-02	1.9E-01	
10594538	**Plekho2**	102595		2.9E-05	1.1E-03	0.66	4.8E-04	4.3E-03	0.63
10498531	**Ccnl1**	56706		8.4E-05	2.0E-03	0.66	8.7E-06	2.6E-04	0.68
10485963	**Arhgap11a**	228482		1.2E-04	2.6E-03	0.66	2.9E-02	9.1E-02	0.81
10472128	**Arl6ip6**	65103		3.9E-06	3.7E-04	0.66	1.4E-02	5.4E-02	1.23
10412421	**Zfp131**	72465		1.2E-05	6.5E-04	0.66	6.7E-04	5.5E-03	0.79
10497066	**Zranb2**	53861		1.5E-04	2.9E-03	0.66	1.2E-05	3.2E-04	0.70
10571093	**Rnf170**	77733		4.9E-05	1.5E-03	0.66	7.3E-06	2.4E-04	0.74
10474683	**Mir674**	732489		2.9E-04	4.5E-03	0.66	2.6E-05	5.4E-04	0.67
10400126	**Lrrn3**	16981		3.9E-05	1.3E-03	0.66	4.4E-06	1.7E-04	0.70
10451805	**Sgol1**	72415		3.8E-05	1.3E-03	0.66	3.6E-01	5.3E-01	
10530910	**Uba6**	231380		7.2E-05	1.8E-03	0.66	4.8E-03	2.4E-02	0.81
10571415	**Vps37a**	52348	*	4.0E-05	1.3E-03	0.66	2.7E-06	1.2E-04	0.66
10422227	**Spry2**	24064		2.1E-04	3.6E-03	0.66	5.5E-04	4.7E-03	0.62
10590654	**Aasdhppt**	67618		6.2E-06	4.6E-04	0.66	8.6E-05	1.2E-03	0.80
10414350	**Socs4**	67296		6.4E-05	1.7E-03	0.66	1.2E-04	1.6E-03	0.72
10416736	**6720463M24Rik**	77744		9.8E-04	1.0E-02	0.66	2.9E-03	1.6E-02	0.77
10467420	**Pdlim1**	54132		1.1E-04	2.4E-03	0.66	5.6E-05	9.2E-04	0.70
10495001	**Rsbn1**	229675		3.0E-05	1.1E-03	0.66	6.9E-05	1.1E-03	0.71

10363281	**Ranbp2**	19386		6.3E-04	7.4E-03	0.66	3.6E-05	6.7E-04	0.71
10490894	**E2f5**	13559		4.6E-05	1.4E-03	0.66	6.4E-04	5.3E-03	0.80
10599696	**Ddx26b**	236790		1.5E-03	1.3E-02	0.66	1.7E-05	4.1E-04	0.69
10442172	**Zfp160**	224585		4.8E-04	6.3E-03	0.66	2.1E-06	1.1E-04	0.61
10405185	**Cks2**	66197		8.5E-05	2.0E-03	0.66	1.0E-01	2.3E-01	
10585699	**Fabp5**	16592	*	3.0E-03	2.1E-02	0.66	3.6E-03	1.9E-02	0.64
10565547	**Pcf11**	74737		2.2E-04	3.7E-03	0.66	9.8E-04	7.3E-03	0.75
10400581	**Fkbp3**	30795	*	3.8E-06	3.7E-04	0.66	1.7E-03	1.1E-02	0.78
10601846	**2900062L11Rik**	76976		1.0E-04	2.3E-03	0.66	1.9E-03	1.2E-02	0.76
10412082	**Gpbp1**	73274		5.7E-05	1.6E-03	0.66	1.8E-04	2.1E-03	0.76
10414315	**Cdkn3**	72391		6.4E-05	1.7E-03	0.66	4.8E-01	6.5E-01	
10482301	**Scai**	320271		2.4E-05	9.6E-04	0.66	6.7E-08	1.3E-05	0.56
10443949	**Adamts10**	224697		2.7E-05	1.1E-03	0.66	6.0E-09	3.2E-06	0.52
10462507	**Papss2**	23972		2.1E-06	2.7E-04	0.66	6.8E-06	2.3E-04	0.71
10492310	**Mbnl1**	56758		1.1E-05	6.4E-04	0.66	7.5E-05	1.1E-03	0.70
10428509	**Csmd3**	239420		3.1E-03	2.2E-02	0.66	2.6E-04	2.7E-03	0.38
10472058	**Rif1**	51869		4.0E-04	5.5E-03	0.66	8.9E-05	1.3E-03	0.65
10346564	**Casp8**	12370		3.7E-06	3.7E-04	0.66	5.6E-04	4.8E-03	0.85
10429573	**Ly6c1**	17067	*	6.2E-06	4.6E-04	0.66	1.5E-01	3.0E-01	
10536494	**Cav2**	12390		2.1E-05	8.9E-04	0.66	9.6E-04	7.2E-03	0.76
10484283	**Pde1a**	18573		8.1E-05	2.0E-03	0.66	1.1E-05	3.0E-04	0.65
10447708	**Qk**	19317		3.9E-06	3.7E-04	0.66	2.2E-04	2.4E-03	0.74
10406953	**Trim23**	81003		1.5E-03	1.3E-02	0.66	8.5E-06	2.6E-04	0.74
10440522	**Adamts1**	11504		2.8E-05	1.1E-03	0.66	8.5E-08	1.5E-05	0.53
10603051	**Ap1s2**	108012		8.2E-06	5.4E-04	0.66	3.8E-03	2.0E-02	0.85
10475394	**Ctdspl2**	329506		1.8E-04	3.3E-03	0.66	1.1E-02	4.4E-02	0.84
10589587	**Setd2**	235626		2.5E-03	1.9E-02	0.66	8.9E-06	2.7E-04	0.69
10359377	**Zbtb37**	240869		4.0E-05	1.3E-03	0.66	4.5E-07	4.3E-05	0.60
10474243	**Cstf3**	228410		1.9E-05	8.4E-04	0.66	4.9E-03	2.4E-02	0.87
10468789	**Pdzd8**	107368		8.3E-05	2.0E-03	0.66	1.8E-05	4.3E-04	0.69
10601412	**Lpar4**	78134		1.0E-04	2.3E-03	0.66	5.2E-04	4.5E-03	0.71
10405927	**Zfp455**	218311		6.5E-04	7.6E-03	0.66	1.1E-01	2.4E-01	
10475362	**Wdr76**	241627		2.3E-04	3.9E-03	0.66	1.7E-02	6.3E-02	0.85
10484389	**Tfpi**	21788		6.0E-06	4.6E-04	0.66	6.5E-04	5.3E-03	0.80
10518167	**Trappc2**	66226		6.4E-04	7.5E-03	0.66	9.1E-03	3.8E-02	0.84
10587558	**Dopey1**	320615	*	2.0E-05	8.5E-04	0.66	3.6E-07	3.8E-05	0.66
10379342	**Mir365-2**	723853		8.4E-05	2.0E-03	0.66	6.4E-05	1.0E-03	0.65
10420823	**Hmbox1**	219150		1.9E-06	2.6E-04	0.66	1.8E-06	9.7E-05	0.68
10405911	**Zfp759**	268670		5.4E-03	3.2E-02	0.66	2.4E-05	5.1E-04	0.70
10543118	**Glcci1**	170772		3.0E-04	4.5E-03	0.66	4.8E-02	1.3E-01	
10353004	**Cks2**	66197		5.6E-05	1.6E-03	0.66	6.5E-02	1.6E-01	
10491603	**4932438A13Rik**	229227		1.3E-03	1.2E-02	0.66	1.8E-04	2.1E-03	0.69
10368011	**Vta1**	66201		2.6E-06	3.0E-04	0.66	8.2E-06	2.6E-04	0.75
10403229	**Itgb8**	320910		3.3E-04	4.8E-03	0.66	2.2E-02	7.4E-02	0.72
10600911	**Yipf6**	77929		2.3E-04	3.8E-03	0.66	1.5E-05	3.8E-04	0.71

Table 6.2: Down-regulated probesets in invading/non-invading fibroblasts.

Gene expression lists for microarrays conducted at 72 and 96 hours of MLg fibroblast invasion. Data are shown for down-regulated probesets with > 1.5-fold regulation. Data are sorted by 72 h n.t. (inv/non-inv). Statistical analysis: limma t-test and Benjamini-Hochberg multiple testing correction.(n.t. = non-treated, BH = Benjamini-Hochberg, FDR = False discovery rate, inv. = invading, non-inv. = non-invading).

Up-regulated probesets in TGFβ1/untreated

				96 h inv. (TGFβ1/n.t.) Statistical analysis, limma t-test, BH			96 h non-inv. (TGFβ1/n.t.) Statistical analysis, limma t-test, BH			96 h TGFβ1 (inv./non-inv.) Statistical analysis, limma t-test, BH		
Probe_set	Gene symbol or ID	Entrez	Unclear annotation	rawp	BH	Ratio (T/C), significant FDR<10%, ratio>1.5x (679)	rawp	BH	Ratio (T/C), significant FDR<10%, ratio>1.5x (1013)	rawp	BH	Ratio (G/M), significant FDR<10%, ratio>1.5x (620)
10423080	C1qtnf3	81799		1.1E-12	3.0E-08	12.01	2.0E-14	5.7E-10	34.67	1.3E-07	1.7E-04	0.43
10545707	Actg2	11468		4.2E-07	6.9E-05	4.80	8.9E-06	3.5E-04	6.30	1.4E-01	3.5E-01	
10427796	Npr3	18162		8.3E-06	5.4E-04	3.86	3.9E-08	8.6E-06	3.58	9.6E-02	2.8E-01	
10506571	Dhcr24	74754		4.0E-09	4.0E-06	3.78	3.0E-06	1.6E-04	2.22	2.5E-01	5.0E-01	
10356305	Htr2b	15559		3.4E-09	4.0E-06	3.72	1.6E-07	2.1E-05	3.30	2.3E-01	4.8E-01	
10465059	Ctsw	13041		2.0E-10	1.4E-06	3.59	1.6E-10	2.2E-07	5.32	2.3E-02	1.1E-01	
10583809	Cnn1	12797		4.9E-08	1.6E-05	3.54	2.7E-09	1.4E-06	8.11	2.9E-04	7.3E-03	0.43
10344897	Sulf1	240725		6.2E-09	4.8E-06	3.53	3.0E-12	2.9E-08	4.27	4.7E-02	1.8E-01	
10492628	Serpini1	20713		9.4E-10	2.8E-06	3.49	4.5E-13	6.3E-09	6.67	7.5E-05	3.4E-03	0.57
10564818	Anpep	16790		8.9E-06	5.7E-04	3.43	7.6E-08	1.3E-05	5.22	6.2E-01	8.0E-01	
10359917	Hsd17b7	15490		1.5E-09	3.3E-06	3.41	1.3E-10	1.9E-07	3.68	4.2E-08	8.5E-05	0.57
10532711	Cmklr1	14747		1.1E-05	6.8E-04	3.35	1.2E-04	2.2E-03	3.23	1.2E-01	3.2E-01	
10583056	Mmp12	17381		1.4E-05	8.0E-04	3.30	9.1E-04	1.0E-02	2.25	8.0E-03	5.7E-02	2.15
10455826	Megf10	70417		3.3E-07	5.9E-05	3.30	5.7E-06	2.5E-04	3.19	1.8E-01	4.1E-01	
10414065	Anxa8	11752		1.3E-06	1.5E-04	3.28	5.0E-06	2.3E-04	4.05	7.2E-01	8.6E-01	
10381809	Itgb3	16416		3.7E-09	4.0E-06	3.28	2.8E-10	3.1E-07	3.77	3.5E-02	1.5E-01	
10467979	Scd1	20249		4.9E-09	4.4E-06	3.25	2.7E-06	1.5E-04	2.51	1.5E-01	3.6E-01	
10388488	Fam101b	76566		9.7E-09	5.5E-06	3.19	7.8E-09	3.0E-06	4.48	4.6E-01	6.9E-01	
10410477	Adamts16	271127		3.0E-10	1.4E-06	3.19	7.4E-11	1.3E-07	4.32	2.7E-03	2.8E-02	0.74
10568668	Adam12	11489		3.4E-08	1.2E-05	3.17	8.0E-12	4.6E-08	5.42	3.3E-03	3.3E-02	0.70
10396270	Dact1	59036		2.0E-09	3.3E-06	3.14	1.8E-11	6.4E-08	5.57	7.3E-02	2.4E-01	
10365830	GENSCAN00000009003			8.0E-09	5.3E-06	3.09	5.7E-07	5.1E-05	2.01	9.8E-01	9.9E-01	
10412466	Hmgcs1	208715		2.2E-07	4.7E-05	3.02	1.7E-07	2.2E-05	1.95	4.1E-01	6.5E-01	
10593123	Tagln	21345		3.7E-09	4.0E-06	2.96	6.1E-09	2.5E-06	2.85	5.5E-04	1.0E-02	0.69
10364194	Lss	16987		4.9E-09	4.4E-06	2.95	2.1E-06	1.3E-04	1.85	1.1E-01	3.0E-01	
10482762	Idi1	319554		7.6E-05	2.6E-03	2.94	2.4E-04	3.8E-03	1.87	1.4E-01	3.5E-01	
10583732	Ldlr	16835		6.6E-09	4.8E-06	2.92	5.7E-09	2.4E-06	2.08	2.2E-02	1.1E-01	
10434925	Hes1	15205		1.3E-10	1.2E-06	2.85	1.7E-09	9.8E-07	4.43	1.3E-03	1.8E-02	0.78
10403413	Idi1	319554		1.2E-04	3.6E-03	2.82	1.6E-04	2.8E-03	1.90	9.3E-02	2.8E-01	
10424349	Sqle	20775		9.2E-08	2.5E-05	2.78	5.5E-06	2.5E-04	1.84	1.4E-02	8.4E-02	0.84
10369290	Ddit4	74747		4.6E-09	4.4E-06	2.71	4.4E-07	4.2E-05	2.62	2.5E-04	6.7E-03	1.48
10371332	Aldh1l2	216188		2.5E-09	3.8E-06	2.70	3.0E-07	3.2E-05	2.92	2.5E-03	2.7E-02	0.72
10411332	Hmgcr	15357		6.8E-09	4.8E-06	2.69	2.4E-07	2.8E-05	1.92	2.2E-04	6.3E-03	0.76
10349947	Fmod	14264		1.5E-03	2.1E-02	2.68	4.2E-04	5.9E-03	3.57	1.4E-01	3.5E-01	
10347748	Utp14b	195434	*	6.6E-09	4.8E-06	2.66	1.4E-09	9.3E-07	3.10	4.2E-04	9.0E-03	0.72
10586357	Cilp	214425		5.6E-08	1.7E-05	2.64	7.3E-07	5.9E-05	4.35	1.1E-01	3.1E-01	
10358091	Nav1	215690		1.6E-08	7.3E-06	2.63	3.7E-11	1.0E-07	3.16	7.5E-01	8.8E-01	
10459071	2010002N04Rik	106878		7.5E-06	5.0E-04	2.62	1.3E-07	1.8E-05	3.80	5.3E-01	7.4E-01	
10549222	Bcat1	12035		2.2E-08	8.3E-06	2.61	3.8E-08	8.5E-06	3.27	1.4E-01	3.6E-01	
10354191	Rnf149	67702		1.6E-06	1.7E-04	2.61	2.6E-10	3.0E-07	3.47	1.1E-01	3.0E-01	
10578916	Sc4mol	66234		3.5E-07	6.1E-05	2.59	2.0E-04	3.3E-03	1.71	2.2E-02	1.1E-01	
10527920	Cyp51	13121		2.4E-07	4.9E-05	2.56	2.1E-05	6.5E-04	2.18	9.3E-01	9.7E-01	
10549276	Bhlhe41	79362		6.1E-04	1.1E-02	2.56	7.4E-06	3.0E-04	3.98	3.5E-01	5.9E-01	
10428604	Tnfrsf11b	18383		1.2E-08	6.2E-06	2.56	1.1E-11	4.6E-08	4.12	4.4E-05	2.6E-03	0.63
10529515	Sorcs2	81840		4.2E-07	6.8E-05	2.54	1.4E-07	1.9E-05	3.27	9.1E-04	1.4E-02	0.70
10392464	Fam20a	208659		3.4E-08	1.2E-05	2.53	4.1E-09	1.9E-06	3.27	1.6E-01	3.8E-01	
10362201	Ctgf	14219		1.2E-06	1.5E-04	2.51	2.2E-08	6.1E-06	2.83	3.0E-07	2.4E-04	0.45
10555174	Lrrc32	434215		2.9E-05	1.3E-03	2.48	5.0E-07	4.6E-05	4.18	9.4E-01	9.7E-01	
10458033	Stard4	170459		3.2E-07	5.7E-05	2.46	2.3E-07	2.7E-05	2.06	4.1E-02	1.7E-01	
10451198	Vegfa	22339		4.4E-07	7.0E-05	2.46	2.6E-10	3.0E-07	2.90	2.0E-01	4.4E-01	
10593293	Ncam1	17967		1.9E-09	3.3E-06	2.46	1.1E-11	4.6E-08	2.76	1.4E-05	1.4E-03	0.67
10491721	Spry1	24063		2.0E-06	2.0E-04	2.45	6.2E-05	1.4E-03	2.17	2.0E-02	1.0E-01	
10578829	Palld	72333		5.3E-10	2.2E-06	2.45	7.8E-11	1.3E-07	2.97	1.3E-02	7.8E-02	0.86
10600082	Nsdhl	18194		6.1E-09	4.8E-06	2.43	5.0E-06	2.3E-04	1.68	4.9E-02	1.8E-01	
10499483	Fdps	110196		1.0E-08	5.5E-06	2.43	1.4E-06	9.5E-05	1.71	8.2E-01	9.1E-01	
10403743	Inhba	16323		1.6E-05	8.7E-04	2.41	7.7E-10	5.9E-07	3.02	4.1E-07	2.9E-04	0.46
10465342	Tm7sf2	73166		1.6E-08	7.3E-06	2.40	2.3E-08	6.1E-06	1.98	5.8E-02	2.1E-01	
10372410	Glipr1	73690	*	1.3E-02	9.2E-02	2.39	7.2E-06	3.0E-04	6.51	2.0E-02	1.0E-01	
10423109	Adamts12	239337		3.5E-07	6.1E-05	2.39	5.5E-08	1.0E-05	2.52	3.2E-02	1.4E-01	
10348580	Klhl30	70788		3.3E-06	2.8E-04	2.39	1.8E-04	3.1E-03	1.90	2.5E-03	2.7E-02	1.35
10535043	Pdgfa	18590		4.8E-09	4.4E-06	2.38	2.5E-10	3.0E-07	2.52	8.0E-01	9.0E-01	
10492689	Pdgfc	54635		7.5E-07	1.1E-04	2.36	9.1E-09	3.4E-06	3.48	4.2E-02	1.7E-01	
10585588	Cspg4	121021		2.1E-06	2.0E-04	2.33	1.5E-08	4.7E-06	2.59	1.2E-01	3.3E-01	
10555510	Pde2a	207728		2.8E-07	5.3E-05	2.32	3.3E-06	1.7E-04	1.82	7.1E-05	3.4E-03	1.70
10424543	Wisp1	22402		1.1E-06	1.3E-04	2.31	1.1E-07	1.6E-05	1.99	9.9E-06	1.2E-03	0.72
10540472	Bhlhe40	20893		9.9E-09	5.5E-06	2.29	6.1E-10	5.6E-07	3.01	1.2E-02	7.6E-02	1.23
10412909	Fdft1	14137		8.8E-09	5.4E-06	2.29	6.8E-07	5.7E-05	1.78	1.8E-01	4.0E-01	
10385526	9930111J21Rik2	245240	*	1.5E-08	7.3E-06	2.28	3.5E-08	8.2E-06	2.85	2.8E-04	7.2E-03	0.64

10589640	**Prss46**	74306		2.8E-05	1.3E-03	2.28	9.0E-07	7.0E-05	2.50	9.2E-01	9.6E-01	
10375614	**Gfpt2**	14584		2.5E-07	5.0E-05	2.27	5.0E-08	1.0E-05	3.59	3.0E-01	5.5E-01	
10505489	**Pappa**	18491		1.3E-06	1.5E-04	2.27	8.5E-06	3.3E-04	3.44	7.2E-02	2.4E-01	
10556381	**Mical2**	320878		2.8E-09	3.9E-06	2.25	1.2E-09	8.1E-07	2.97	3.5E-01	6.0E-01	
10385513	**9930111J21Rik2**	245240	*	2.0E-08	8.3E-06	2.25	5.3E-08	1.0E-05	2.65	1.0E-03	1.5E-02	0.68
10370303	**Adarb1**	110532		6.8E-08	1.9E-05	2.24	2.7E-08	6.9E-06	2.93	3.4E-02	1.5E-01	
10478884	**Snai1**	20613		2.2E-08	8.5E-06	2.24	3.8E-08	8.5E-06	2.23	9.1E-02	2.7E-01	
10371379	**Nuak1**	77976		2.2E-08	8.3E-06	2.22	2.1E-10	2.8E-07	2.36	2.2E-04	6.2E-03	0.72
10449452	**Fkbp5**	14229		1.1E-08	6.0E-06	2.22	6.2E-11	1.3E-07	2.58	1.2E-02	7.3E-02	1.20
10471154	**Ass1**	11898	*	3.4E-05	1.5E-03	2.22	6.9E-08	1.2E-05	2.27	1.8E-07	1.9E-04	2.43
10604616	**Plac1**	56096		6.4E-07	9.5E-05	2.21	9.7E-04	1.1E-02	1.99	3.1E-02	1.4E-01	
10518735	**Spsb1**	74646		2.7E-10	1.4E-06	2.21	2.6E-09	1.4E-06	2.05	5.2E-01	7.4E-01	
10363541	**Ass1**	11898	*	3.7E-05	1.5E-03	2.20	2.8E-08	7.2E-06	2.37	1.5E-07	1.7E-04	2.41
10513739	**Tnc**	21923		2.5E-05	1.2E-03	2.19	1.6E-08	5.0E-06	3.00	2.1E-01	4.5E-01	
10433114	**Itga5**	16402		1.4E-07	3.2E-05	2.17	3.1E-10	3.2E-07	2.97	1.1E-01	3.1E-01	
10582310	**Mvd**	192156		5.7E-09	4.8E-06	2.17	2.4E-06	1.4E-04	1.59	4.8E-06	8.6E-04	1.67
10519998	**Lrrc17**	74511		3.6E-05	1.5E-03	2.16	2.6E-04	4.1E-03	2.40	1.6E-03	2.0E-02	0.43
10548385	**Olr1**	108078		1.9E-05	9.9E-04	2.16	2.1E-04	3.4E-03	1.94	7.3E-03	5.4E-02	1.64
10463355	**Scd2**	20250		9.7E-10	2.8E-06	2.16	9.9E-08	1.5E-05	1.73	1.3E-01	3.4E-01	
10391103	**Jup**	16480		1.2E-07	2.9E-05	2.11	8.9E-08	1.4E-05	2.06	2.8E-02	1.3E-01	
10420730	**Fdft1**	14137	*	8.4E-09	5.4E-06	2.09	4.4E-06	2.1E-04	1.68	1.1E-01	3.0E-01	
10439895	**Alcam**	11658		3.2E-05	1.4E-03	2.07	3.0E-08	7.4E-06	2.41	3.0E-03	3.0E-02	0.73
10357833	**Atp2b4**	381290		7.7E-07	1.1E-04	2.07	5.8E-09	2.5E-06	3.57	7.5E-07	3.9E-04	0.47
10459944	**Nfatc1**	18018		7.0E-09	4.9E-06	2.07	1.0E-10	1.6E-07	2.94	5.3E-02	1.9E-01	
10525893	**Aacs**	78894		2.4E-08	8.8E-06	2.07	1.6E-06	1.1E-04	1.60	1.4E-02	8.3E-02	1.19
10406817	**Enc1**	13803		2.2E-08	8.3E-06	2.06	8.9E-09	3.3E-06	2.24	1.9E-03	2.2E-02	1.23
10545672	**Mthfd2**	17768		2.9E-07	5.4E-05	2.05	2.3E-06	1.3E-04	1.95	1.2E-01	3.3E-01	
10458046	**D0H4S114**	27528		5.1E-07	7.9E-05	2.04	1.6E-09	9.6E-07	3.76	5.2E-01	7.4E-01	
10350247	**Kif21b**	16565		2.8E-07	5.4E-05	2.03	5.7E-08	1.0E-05	2.32	9.7E-01	9.9E-01	
10563780	**E2f8**	108961		4.2E-05	1.7E-03	2.03	3.3E-05	8.9E-04	1.87	1.9E-01	4.2E-01	
10470462	**Col5a1**	12831		7.5E-07	1.1E-04	2.02	5.5E-11	1.3E-07	2.28	5.2E-03	4.3E-02	0.78
10505143	**Palm2**	242481	*	3.8E-07	6.3E-05	2.02	5.4E-07	5.0E-05	2.34	3.2E-01	5.7E-01	
10398121	**Bdkrb1**	12061		4.0E-08	1.4E-05	2.00	7.8E-11	1.3E-07	2.99	8.8E-04	1.4E-02	0.79
10367440	**Itga7**	16404		8.2E-04	1.3E-02	1.99	9.6E-02	2.7E-01		2.4E-01	4.8E-01	
10351551	**Adamts4**	240913		1.6E-03	2.2E-02	1.99	5.7E-04	7.3E-03	1.93	1.4E-01	3.6E-01	
10474972	**Chac1**	69065		2.5E-06	2.3E-04	1.98	2.3E-06	1.3E-04	2.17	4.2E-02	1.7E-01	
10493114	**Nes**	18008		7.2E-06	4.9E-04	1.98	2.0E-05	6.2E-04	2.13	2.0E-01	4.3E-01	
10364494	**Fstl3**	83554	*	4.6E-06	3.6E-04	1.98	2.6E-07	2.9E-05	2.41	6.0E-01	7.9E-01	
10532741	**Tmem119**	231633		1.2E-06	1.4E-04	1.98	3.3E-06	1.7E-04	2.57	9.2E-01	9.7E-01	
10350173	**Tnnt2**	21956		3.1E-04	6.8E-03	1.97	1.3E-05	4.6E-04	2.41	3.1E-02	1.4E-01	
10588836	**Gmppb**	331026	*	1.6E-07	3.6E-05	1.97	1.6E-07	2.1E-05	2.23	1.3E-01	3.3E-01	
10524555	**Mvk**	17855		5.7E-07	8.6E-05	1.97	2.7E-05	7.8E-04	1.53	1.6E-04	5.4E-03	1.52
10578880	**Tll1**	21892		4.3E-06	3.3E-04	1.97	1.9E-09	1.1E-06	3.27	1.3E-03	1.8E-02	0.66
10440258	**Epha3**	13837		2.0E-05	1.0E-03	1.96	2.5E-07	2.9E-05	3.40	1.0E-03	1.5E-02	0.56
10567735	**GENSCAN00000035518**			1.4E-06	1.6E-04	1.96	1.6E-09	9.6E-07	2.67	3.2E-03	3.2E-02	0.73
10451679	**Daam2**	76441		8.5E-04	1.4E-02	1.95	4.6E-03	3.4E-02	1.78	7.1E-01	8.5E-01	
10388880	**Tmem97**	69071		1.1E-07	2.8E-05	1.95	1.7E-05	5.6E-04	1.75	2.3E-01	4.8E-01	
10428707	**Has2**	15117		9.1E-06	5.8E-04	1.94	2.7E-06	1.5E-04	3.00	1.4E-04	5.0E-03	0.56
10408557	**Serpinb1a**	66222		2.0E-04	5.0E-03	1.94	4.8E-02	1.7E-01		7.5E-01	8.7E-01	
10560919	**Atp1a3**	232975		3.6E-05	1.5E-03	1.94	7.7E-06	3.1E-04	1.73	1.6E-02	9.0E-02	1.40
10530841	**Igfbp7**	29817		5.8E-04	1.1E-02	1.94	1.1E-03	1.2E-02	2.88	6.9E-01	8.4E-01	
10490159	**Pmepa1**	65112		9.4E-09	5.5E-06	1.94	3.9E-09	1.8E-06	2.56	1.1E-01	3.1E-01	
10358177	**5730559C18Rik**	67313		7.0E-08	2.0E-05	1.94	4.7E-06	2.2E-04	1.87	1.2E-07	1.7E-04	1.91
10430358	**C1qtnf6**	72709		2.3E-06	2.1E-04	1.93	1.3E-05	4.6E-04	2.04	3.0E-02	1.4E-01	
10409486	**Pdlim7**	67399		2.1E-08	8.3E-06	1.93	6.5E-08	1.1E-05	2.14	1.7E-01	4.0E-01	
10418898	**Ppyr1**	19065		4.3E-06	3.4E-04	1.92	9.9E-02	2.8E-01		2.3E-03	2.6E-02	1.47
10447891	**Acat2**	110460		2.9E-07	5.4E-05	1.92	2.0E-05	6.2E-04	1.47	7.0E-01	8.5E-01	
10467191	**Ankrd1**	107765		2.0E-07	4.2E-05	1.92	6.5E-04	8.0E-03	1.69	6.3E-05	3.1E-03	0.64
10459772	**Lipg**	16891		4.6E-04	9.0E-03	1.91	3.5E-04	5.2E-03	2.31	4.6E-01	6.9E-01	
10393887	**Pycr1**	209027		2.1E-06	2.0E-04	1.91	5.1E-06	2.3E-04	1.81	3.6E-01	6.1E-01	
10404053	**Hist1h2bc**	68024		1.1E-05	6.9E-04	1.90	1.9E-05	6.1E-04	2.29	6.1E-01	8.0E-01	
10369388	**Unc5b**	107449		6.8E-07	9.9E-05	1.89	2.3E-09	1.2E-06	2.76	9.3E-01	9.7E-01	
10456492	**D18Ertd653e**	52662		2.0E-09	3.3E-06	1.89	1.8E-09	9.8E-07	2.13	1.3E-04	4.6E-03	0.78
10388389	**Hic1**	15248		6.1E-06	4.4E-04	1.89	1.5E-03	1.5E-02	1.77	4.8E-01	7.1E-01	
10585778	**Sema7a**	20361		1.1E-03	1.7E-02	1.88	9.2E-05	1.9E-03	2.33	1.7E-01	4.0E-01	
10487890	**Erv3**	71995		4.9E-04	9.5E-03	1.88	5.9E-01	7.9E-01		2.3E-03	2.6E-02	1.77
10477644	**Trp53inp2**	68728		1.3E-08	6.5E-06	1.88	1.0E-09	7.3E-07	1.96	5.0E-02	1.9E-01	
10559312	**Dhcr7**	13360		2.9E-08	1.0E-05	1.88	1.6E-06	1.0E-04	1.62	3.0E-02	1.4E-01	
10393970	**Fasn**	14104		4.4E-07	7.0E-05	1.87	2.6E-06	1.5E-04	1.53	9.1E-04	1.4E-02	1.30
10572024	**Spock3**	72902		2.9E-03	3.2E-02	1.87	8.1E-03	5.1E-02	1.75	6.2E-03	4.8E-02	0.58
10465895	**Fads2**	56473		1.8E-08	8.1E-06	1.86	1.9E-07	2.3E-05	1.64	1.1E-01	3.0E-01	
10458340	**Hbegf**	15200		1.1E-06	1.3E-04	1.85	1.5E-09	9.5E-07	3.57	1.3E-06	5.0E-04	0.62
10427744	**Rai14**	75646		8.2E-06	5.4E-04	1.85	5.3E-06	2.4E-04	2.24	9.5E-02	2.8E-01	
10592585	**Sc5d**	235293		8.9E-08	2.4E-05	1.85	1.2E-05	4.2E-04	1.44	3.0E-04	7.5E-03	0.76
10363735	**Egr2**	13654		1.2E-03	1.8E-02	1.85	6.0E-05	1.4E-03	2.70	9.8E-01	9.9E-01	
10435704	**Cd80**	12519		2.8E-06	2.5E-04	1.84	2.9E-07	3.1E-05	1.95	4.0E-04	8.8E-03	0.67

10428579	**Ext1**	14042		1.2E-06	1.4E-04	1.84	1.4E-07	1.9E-05	2.12	2.4E-01	4.8E-01		
10383684	**Limk2**	16886		4.9E-08	1.6E-05	1.83	1.0E-07	1.5E-05	1.98	9.6E-01	9.8E-01		
10461629	**Ms4a4d**	66607		5.7E-06	4.1E-04	1.82	4.4E-02	1.6E-01		2.8E-03	2.9E-02	1.54	
10574226	**Ccl17**	20295		4.1E-05	1.7E-03	1.82	4.6E-03	3.4E-02	1.62	7.6E-01	8.8E-01		
10579812	**Ednra**	13617		1.0E-03	1.6E-02	1.81	5.2E-04	6.8E-03	2.65	8.3E-02	2.6E-01		
10523693	**Dmp1**	13406		1.4E-04	4.0E-03	1.81	2.6E-01	5.0E-01		7.9E-04	1.3E-02	1.70	
10554599	**Adamtsl3**	269959		1.4E-05	7.8E-04	1.81	1.3E-02	7.1E-02	1.55	2.8E-02	1.3E-01		
10569504	**Tnfrsf23**	79201		1.7E-06	1.8E-04	1.80	6.9E-10	5.8E-07	2.31	2.5E-01	5.0E-01		
10516064	**Mfsd2a**	76574		7.4E-09	5.0E-06	1.80	1.5E-07	2.1E-05	2.09	2.1E-02	1.1E-01		
10518147	**Pdpn**	14726		2.1E-05	1.1E-03	1.80	4.5E-04	6.2E-03	1.54	1.8E-03	2.2E-02	1.52	
10576088	**Gm22**	195209		2.7E-05	1.2E-03	1.80	2.2E-06	1.3E-04	1.79	3.6E-01	6.0E-01		
10394538	**Acaca**	107476		1.3E-06	1.5E-04	1.80	5.8E-07	5.1E-05	1.52	2.9E-01	5.4E-01		
10569707	**Myadm**	50918		5.0E-08	1.6E-05	1.80	4.2E-08	8.9E-06	1.57	3.4E-03	3.3E-02	0.82	
10607089	**Acsl4**	50790		1.7E-06	1.8E-04	1.79	3.5E-07	3.6E-05	1.97	3.1E-04	7.6E-03	0.75	
10487040	**Fbn1**	14118	*	3.9E-07	6.5E-05	1.79	3.0E-08	7.4E-06	1.63	8.0E-02	2.5E-01		
10361250	**Camk1g**	215303		4.4E-03	4.3E-02	1.79	2.6E-02	1.2E-01		6.7E-02	2.3E-01		
10586079	**Itga11**	319480		8.9E-05	2.9E-03	1.79	2.1E-03	1.9E-02	2.03	3.6E-01	6.1E-01		
10354203	**ENSMUST00000083002**			2.6E-03	3.0E-02	1.79	1.1E-07	1.6E-05	3.53	6.7E-06	9.9E-04	0.28	
10424905	**Scx**	20289		1.0E-03	1.6E-02	1.79	7.7E-05	1.6E-03	2.23	7.8E-01	8.9E-01		
10534667	**Serpine1**	18787		5.9E-05	2.2E-03	1.78	1.8E-08	5.4E-06	2.81	4.2E-08	8.5E-05	0.46	
10406777	**Gcnt4**	218476		2.7E-05	1.3E-03	1.78	6.4E-09	2.6E-06	1.97	4.7E-03	4.0E-02	0.79	
10576911	**Efnb2**	13642		3.8E-06	3.1E-04	1.77	6.4E-06	2.8E-04	1.86	2.9E-05	2.2E-03	0.71	
10417787	**Gng2**	14702		2.3E-05	1.1E-03	1.77	1.3E-07	1.8E-05	1.94	3.2E-05	2.2E-03	0.62	
10488608	**Trib3**	228775		8.7E-06	5.6E-04	1.77	1.7E-07	2.2E-05	2.07	7.8E-02	2.5E-01		
10543067	**Asns**	27053		3.2E-07	5.7E-05	1.77	1.9E-05	6.1E-04	1.61	9.0E-04	1.4E-02	0.76	
10441456	**Synj2**	20975		1.8E-06	1.8E-04	1.77	1.4E-07	1.9E-05	2.14	4.3E-01	6.6E-01		
10550660	**Ppp1r13l**	333654		5.7E-08	1.7E-05	1.77	3.5E-06	1.8E-04	1.78	1.3E-03	1.8E-02	1.32	
10366293	**Csrp2**	13008		1.2E-06	1.4E-04	1.76	1.1E-05	4.0E-04	1.99	3.6E-02	1.5E-01		
10425695	**Srebf2**	20788		9.5E-08	2.5E-05	1.76	2.7E-06	1.5E-04	1.45	3.8E-01	6.2E-01		
10434668	**Tmem97**	69071		6.6E-08	1.9E-05	1.76	4.8E-06	2.2E-04	1.70	6.6E-01	8.2E-01		
10562192	**Fxyd5**	18301		4.4E-07	7.0E-05	1.75	2.0E-07	2.5E-05	2.32	2.5E-03	2.7E-02	0.80	
10500808	**Olfml3**	99543		3.6E-06	3.0E-04	1.75	3.7E-08	8.5E-06	2.54	1.2E-01	3.2E-01		
10491300	**Skil**	20482		1.8E-05	9.7E-04	1.75	4.5E-10	4.4E-07	2.35	1.0E-03	1.5E-02	0.76	
10416406	**Htr2a**	15558		1.2E-02	8.5E-02	1.75	2.6E-03	2.3E-02	1.84	1.5E-03	1.9E-02	0.66	
10495993	**Elovl6**	170439		4.7E-05	1.9E-03	1.75	5.2E-04	6.8E-03	1.38	2.8E-04	7.1E-03	0.65	
10376074	**P4ha2**	18452		2.3E-04	5.5E-03	1.74	8.2E-08	1.3E-05	1.64	6.3E-02	2.2E-01		
10507908	**Fhl3**	14201		3.2E-07	5.7E-05	1.74	1.6E-06	1.0E-04	1.81	3.5E-02	1.5E-01		
10420957	**Ptk2b**	19229		1.8E-05	9.4E-04	1.74	8.7E-06	3.4E-04	2.41	7.9E-01	9.0E-01		
10554789	**Ctsc**	13032		1.5E-04	4.2E-03	1.73	3.3E-05	8.8E-04	1.94	8.0E-01	9.0E-01		
10585180	**Ncam1**	17967	*	3.1E-07	5.7E-05	1.73	1.9E-06	1.2E-04	1.86	7.8E-02	2.5E-01		
10564222	**A230006K03Rik**	27493		7.1E-06	4.9E-04	1.73	5.6E-05	1.3E-03	2.09	4.3E-03	3.8E-02	0.62	
10407126	**Plk2**	20620		5.6E-06	4.1E-04	1.73	1.6E-03	1.6E-02	1.26	4.8E-03	4.1E-02	0.82	
10368317	**Enpp3**	209558		2.2E-04	5.4E-03	1.72	3.2E-06	1.7E-04	2.33	9.7E-02	2.8E-01		
10539238	**Fam176a**	232146		3.6E-05	1.5E-03	1.72	6.3E-10	5.6E-07	3.03	8.7E-01	9.4E-01		
10555389	**Ucp2**	22228		6.9E-06	4.8E-04	1.72	7.8E-06	3.1E-04	2.06	1.6E-01	3.8E-01		
10535852	**Slc7a1**	11987		4.7E-06	3.6E-04	1.72	2.4E-05	7.2E-04	1.54	1.9E-03	2.3E-02	0.73	
10350136	**Csrp1**	13007		1.6E-07	3.6E-05	1.72	2.1E-08	6.0E-06	2.04	1.7E-01	3.9E-01		
10373918	**Lif**	16878		1.0E-06	1.3E-04	1.72	4.2E-08	8.9E-06	2.79	2.6E-02	1.2E-01		
10527649	**6330406I15Rik**	70717		3.5E-05	1.5E-03	1.71	3.4E-03	2.7E-02	1.36	1.6E-02	9.1E-02	0.74	
10487506	**Gm14005**	100043424		2.5E-07	5.0E-05	1.71	8.5E-07	6.7E-05	1.97	1.5E-03	2.0E-02	0.72	
10546725	**Pdzrn3**	55983		9.8E-08	2.5E-05	1.71	6.8E-07	5.7E-05	1.57	5.9E-03	4.7E-02	0.86	
10508392	**Rnf19b**	75234		1.2E-06	1.4E-04	1.70	6.8E-07	5.7E-05	1.98	4.5E-01	6.8E-01		
10393851	**Pcyt2**	68671		6.9E-07	9.9E-05	1.70	3.4E-05	9.2E-04	1.30	5.5E-01	7.6E-01		
10373407	**Esyt1**	23943		1.0E-05	6.5E-04	1.70	2.6E-08	6.8E-06	1.83	3.5E-02	1.5E-01		
10389022	**Myo1d**	338367		1.1E-06	1.4E-04	1.70	1.1E-04	2.2E-03	1.94	2.9E-03	2.9E-02	1.42	
10463185	**Ubtd1**	226122		3.8E-06	3.1E-04	1.70	2.2E-07	2.6E-05	2.11	1.1E-02	7.3E-02	1.27	
10505120	**Palm2**	242481	*	1.4E-06	1.6E-04	1.70	7.3E-07	5.9E-05	2.12	2.1E-01	4.5E-01		
10495781	**Bcar3**	29815		6.0E-07	8.9E-05	1.70	9.9E-08	1.5E-05	1.69	7.4E-02	2.4E-01		
10379820	**Acaca**	107476		2.5E-07	5.0E-05	1.70	1.5E-06	1.0E-04	1.57	8.7E-02	2.6E-01		
10517967	**Fblim1**	74202		8.8E-09	5.4E-06	1.69	1.1E-06	7.9E-05	1.59	7.7E-01	8.9E-01		
10520362	**Insig1**	231070		2.9E-06	2.5E-04	1.68	3.1E-05	8.5E-04	1.47	1.4E-01	3.5E-01		
10495596	**Frrs1**	20321		9.3E-06	5.9E-04	1.68	1.2E-06	8.9E-05	1.91	2.3E-01	4.8E-01		
10350864	**Sec16b**	89867		8.4E-08	2.3E-05	1.68	2.8E-06	1.5E-04	1.46	1.6E-02	9.1E-02	0.88	
10606016	**Il2rg**	16186		9.9E-04	1.5E-02	1.68	7.0E-04	8.5E-03	1.60	7.8E-01	8.9E-01		
10406464	**ENSMUST00000051524**			2.0E-04	5.1E-03	1.68	1.8E-02	8.8E-02	1.26	1.8E-02	9.7E-02	1.32	
10366043	**Dusp6**	67603		6.3E-05	2.3E-03	1.67	2.5E-05	7.3E-04	1.81	3.2E-04	7.8E-03	1.51	
10456400	**Tubb6**	67951		2.4E-08	8.8E-06	1.67	1.3E-04	2.5E-03	1.43	7.9E-01	9.0E-01		
10360415	**Grem2**	23893		4.4E-04	8.8E-03	1.67	1.8E-07	2.3E-05	3.41	1.6E-01	3.8E-01		
10595560	**Tbx18**	76365		8.7E-07	1.2E-04	1.67	1.7E-04	3.0E-03	1.54	9.2E-01	9.7E-01		
10477920	**Myl9**	98932		2.8E-06	2.5E-04	1.66	1.8E-07	2.2E-05	1.63	2.8E-01	5.3E-01		
10536483	**Tes**	21753		1.2E-06	1.5E-04	1.66	6.3E-07	5.5E-05	2.40	7.2E-02	2.3E-01		
10559667	**Il11**	16156		1.9E-06	1.9E-04	1.66	1.1E-06	8.2E-05	2.19	5.5E-02	2.0E-01		
10491699	**Fgf2**	14173		5.2E-05	2.0E-03	1.66	5.3E-04	6.9E-03	1.51	8.4E-01	9.2E-01		
10573319	**Podnl1**	244550		1.5E-05	8.1E-04	1.66	9.1E-06	3.5E-04	1.83	8.7E-01	9.4E-01		
10506714	**Lrp8**	16975		3.6E-05	1.5E-03	1.66	2.8E-05	7.9E-04	1.73	2.4E-01	4.8E-01		
10483353	**Scn7a**	20272		6.7E-06	4.7E-04	1.66	1.9E-04	3.3E-03	2.14	1.1E-01	3.1E-01		

10567564	Cdr2	12585		7.9E-07	1.1E-04	1.66	1.1E-08	3.9E-06	1.95	4.5E-04	9.4E-03	0.80
10352152	Kif26b	269152		3.2E-05	1.4E-03	1.65	6.3E-07	5.5E-05	2.32	2.3E-01	4.7E-01	
10355514	Tns1	21961		9.4E-07	1.3E-04	1.65	2.3E-08	6.1E-06	2.34	6.5E-02	2.2E-01	
10499904	Ivl	16447		5.5E-03	5.0E-02	1.65	1.0E-02	5.9E-02	1.17	3.2E-03	3.1E-02	1.80
10425287	Kdelr3	105785		2.7E-07	5.2E-05	1.65	1.1E-07	1.6E-05	1.82	7.6E-03	5.5E-02	0.84
10502655	Cyr61	16007		1.5E-03	2.1E-02	1.65	5.4E-02	1.9E-01		4.1E-04	8.9E-03	0.64
10564290	Klf13	50794		1.0E-05	6.4E-04	1.64	6.9E-08	1.2E-05	2.00	5.3E-01	7.4E-01	
10355534	Tns1	21961		4.1E-07	6.7E-05	1.64	5.7E-08	1.0E-05	2.31	9.1E-02	2.7E-01	
10539517	Dysf	26903		1.0E-07	2.6E-05	1.64	1.0E-08	3.6E-06	1.71	3.3E-01	5.7E-01	
10399725	Sox11	20666		7.3E-06	4.9E-04	1.64	4.2E-05	1.1E-03	2.28	7.2E-02	2.3E-01	
10346321	Gm10561	628004		9.5E-05	3.1E-03	1.64	2.4E-05	7.1E-04	1.55	6.6E-02	2.2E-01	
10542460	Dera	232449		2.1E-08	8.3E-06	1.64	4.0E-06	2.0E-04	1.41	2.3E-01	4.7E-01	
10432032	Vdr	22337		1.8E-04	4.8E-03	1.64	4.3E-05	1.1E-03	1.58	7.4E-02	2.4E-01	
10540085	Fbln2	14115		4.3E-07	7.0E-05	1.63	8.4E-09	3.2E-06	2.10	1.5E-01	3.7E-01	
10425852	Parvb	170736		2.2E-06	2.1E-04	1.63	6.4E-08	1.1E-05	1.86	1.0E-05	1.3E-03	1.73
10582275	Slc7a5	20539		6.5E-05	2.3E-03	1.63	3.1E-04	4.6E-03	1.40	1.2E-03	1.7E-02	0.73
10558496	Lrrc27	76612		1.1E-05	6.8E-04	1.63	1.4E-08	4.6E-06	1.65	6.5E-01	8.2E-01	
10584674	Mcam	84004		3.0E-05	1.3E-03	1.63	2.0E-07	2.4E-05	1.97	4.3E-04	9.2E-03	0.65
10355536	Tns1	21961		6.6E-06	4.7E-04	1.63	1.0E-07	1.5E-05	2.11	1.9E-01	4.3E-01	
10478258	Lpin3	64899		1.4E-06	1.6E-04	1.63	2.7E-09	1.4E-06	2.19	4.3E-01	6.6E-01	
10555323	P4ha3	320452		7.3E-05	2.5E-03	1.63	8.3E-04	9.6E-03	1.41	4.4E-06	8.1E-04	0.51
10350516	Ptgs2	19225		1.2E-03	1.8E-02	1.62	1.7E-05	5.5E-04	2.04	2.7E-08	6.9E-05	0.48
10537179	Bpgm	12183		6.4E-08	1.9E-05	1.62	9.9E-05	2.0E-03	1.57	8.3E-01	9.2E-01	
10541695	Lpcat3	14792		1.2E-07	2.9E-05	1.62	2.9E-07	3.1E-05	1.54	3.0E-04	7.5E-03	0.81
10365559	Igf1	16000		2.5E-04	5.8E-03	1.62	2.0E-01	4.4E-01		4.4E-06	8.1E-04	0.60
10352143	Kif26b	269152		4.5E-05	1.8E-03	1.61	4.3E-07	4.2E-05	2.29	3.0E-01	5.5E-01	
10461869	Prune2	353211		6.7E-04	1.2E-02	1.61	9.5E-04	1.1E-02	1.78	1.2E-01	3.2E-01	
10477042	Angpt4	11602		7.1E-04	1.2E-02	1.61	5.4E-04	7.0E-03	1.62	4.2E-01	6.6E-01	
10378570	ENSMUST00000134345			1.8E-04	4.8E-03	1.61	4.2E-02	1.6E-01		1.1E-09	3.1E-05	0.25
10408613	Tubb2b	73710		1.4E-05	7.8E-04	1.61	2.1E-03	1.9E-02	1.34	4.6E-01	6.9E-01	
10387689	Kctd11	216858	*	1.9E-07	4.1E-05	1.61	4.7E-07	4.4E-05	1.74	1.3E-01	3.4E-01	
10565958	P2ry6	233571		4.8E-06	3.6E-04	1.61	1.5E-03	1.5E-02	1.30	9.5E-05	4.0E-03	1.55
10541496	Mfap5	50530		1.5E-03	2.0E-02	1.61	3.9E-03	3.0E-02	1.65	1.6E-01	3.8E-01	
10384539	Slc1a4	55963		5.3E-06	3.9E-04	1.61	1.4E-08	4.6E-06	1.81	6.1E-03	4.8E-02	0.82
10399419	Tubb2b	73710	*	5.0E-06	3.7E-04	1.61	3.5E-04	5.2E-03	1.46	6.3E-01	8.1E-01	
10543219	Gpr85	64450		1.9E-04	4.9E-03	1.61	3.9E-06	2.0E-04	2.34	7.2E-04	1.2E-02	0.56
10598638	Mid1ip1	68041		8.5E-06	5.5E-04	1.61	9.6E-06	3.7E-04	1.34	2.5E-03	2.7E-02	1.24
10359235	Rasal2	226525		1.0E-04	3.2E-03	1.60	8.7E-09	3.3E-06	1.84	9.0E-04	1.4E-02	0.78
10441003	Runx1	12394		1.3E-04	3.8E-03	1.60	8.0E-08	1.3E-05	1.64	4.7E-05	2.7E-03	0.77
10560709	Pvr	52118		2.5E-06	2.3E-04	1.60	2.8E-08	7.2E-06	1.79	7.9E-04	1.3E-02	0.79
10389238	Dusp14	56405		1.4E-05	7.8E-04	1.60	3.8E-06	1.9E-04	1.57	1.1E-02	7.0E-02	0.85
10350592	3110040M04Rik	73176		4.4E-07	7.0E-05	1.60	1.1E-07	1.7E-05	2.29	2.2E-03	2.5E-02	0.74
10467470	Aldh18a1	56454		5.5E-06	4.0E-04	1.59	2.3E-06	1.4E-04	1.49	4.4E-01	6.7E-01	
10373452	Gm129	229599		1.3E-03	1.9E-02	1.59	2.5E-05	7.4E-04	1.70	7.2E-01	8.6E-01	
10375443	Havcr2	171285		1.4E-04	4.0E-03	1.59	3.1E-04	4.7E-03	1.46	3.5E-01	5.9E-01	
10462507	Papss2	23972		1.8E-07	4.0E-05	1.59	3.2E-06	1.7E-04	1.58	4.4E-05	2.6E-03	0.71
10467420	Pdlim1	54132		2.5E-06	2.3E-04	1.59	7.9E-05	1.7E-03	1.51	1.0E-03	1.5E-02	0.74
10370376	Pfkl	18641		2.6E-04	6.2E-03	1.59	1.3E-03	1.3E-02	1.56	7.3E-03	5.4E-02	1.49
10423274	Cdh18	320865		7.0E-05	2.4E-03	1.59	2.9E-07	3.1E-05	1.99	7.7E-04	1.3E-02	0.69
10367982	Gpr126	215798		2.0E-03	2.5E-02	1.58	5.4E-02	1.9E-01		1.4E-04	4.9E-03	0.52
10457359	Mpp7	75739		4.3E-03	4.3E-02	1.58	1.2E-03	1.3E-02	1.94	3.8E-02	1.6E-01	
10380419	Col1a1	12842		8.3E-06	5.4E-04	1.58	5.5E-07	5.1E-05	1.56	4.1E-02	1.6E-01	
10402708	Ckb	12709		8.5E-05	2.8E-03	1.58	1.3E-06	9.3E-05	1.78	6.9E-01	8.4E-01	
10608644	NM_177010.2			8.6E-06	5.6E-04	1.58	8.7E-04	9.9E-03	1.25	3.9E-04	8.6E-03	1.27
10587639	Nt5e	23959		4.9E-05	1.9E-03	1.58	2.7E-01	5.1E-01		1.3E-05	1.4E-03	1.66
10572398	Crlf1	12931		9.3E-04	1.5E-02	1.57	2.5E-03	2.2E-02	1.44	6.7E-01	8.3E-01	
10598976	Timp1	21857		2.1E-06	2.0E-04	1.57	1.5E-08	4.7E-06	1.93	2.4E-01	4.8E-01	
10374464	Spred2	114716		2.2E-05	1.1E-03	1.57	2.6E-05	7.4E-04	1.36	3.3E-01	5.8E-01	
10463173	Zdhhc16	74168	*	7.1E-06	4.9E-04	1.57	6.4E-07	5.6E-05	1.63	1.1E-01	3.1E-01	
10421361	Bmp1	12153		1.6E-05	8.5E-04	1.57	4.4E-05	1.1E-03	1.36	6.7E-01	8.3E-01	
10405211	Gadd45g	23882		1.5E-04	4.1E-03	1.57	1.1E-06	8.1E-05	1.73	1.1E-04	4.3E-03	0.61
10576854	Ctxn1	330695		5.1E-06	3.8E-04	1.57	5.2E-05	1.2E-03	1.46	1.3E-01	3.3E-01	
10503010	Fpgt	75540		1.2E-05	7.0E-04	1.57	1.4E-07	1.9E-05	1.77	9.7E-01	9.9E-01	
10345824	Il18rap	16174		2.9E-05	1.3E-03	1.57	5.7E-07	5.1E-05	2.01	4.8E-01	7.1E-01	
10354309	Col5a2	12832		2.1E-04	5.2E-03	1.57	6.3E-06	2.7E-04	1.57	2.7E-04	7.0E-03	0.63
10430871	Gm9855	624784	*	1.2E-05	7.2E-04	1.56	2.6E-05	7.4E-04	1.44	2.3E-01	4.7E-01	
10407481	Pfkp	56421		6.0E-06	4.3E-04	1.56	1.4E-06	9.4E-05	1.67	1.7E-01	4.0E-01	
10408870	Tbc1d7	67046		2.2E-04	5.4E-03	1.56	4.7E-01	7.0E-01		4.2E-01	6.6E-01	
10586433	Rbpms2	71973		2.8E-06	2.5E-04	1.56	2.2E-07	2.6E-05	1.79	1.1E-01	3.0E-01	
10389025	Myo1d	338367		1.0E-05	6.3E-04	1.56	9.5E-05	1.9E-03	1.78	2.9E-04	7.3E-03	1.47
10598138	Spry3	236576		2.0E-05	9.9E-04	1.56	3.6E-03	2.8E-02	1.34	9.7E-02	2.8E-01	
10357590	Dyrk3	226419		3.2E-03	3.5E-02	1.56	7.8E-05	1.7E-03	1.74	5.9E-01	7.8E-01	
10380660	Hoxb2	103889		5.6E-07	8.5E-05	1.56	3.3E-06	1.7E-04	1.75	9.3E-01	9.7E-01	
10569458	Cars	27267		3.9E-06	3.1E-04	1.56	6.9E-06	2.9E-04	1.46	1.6E-01	3.8E-01	
10524327	Mn1	433938		2.2E-05	1.1E-03	1.56	1.4E-07	1.9E-05	1.55	6.7E-01	8.3E-01	
10370946	Mobkl2a	208228		7.5E-06	5.0E-04	1.56	4.5E-05	1.1E-03	1.47	1.9E-03	2.2E-02	0.78

10607116	Ammecr1	56068		8.6E-05	2.9E-03	1.56	3.2E-07	3.4E-05	1.45	2.4E-01	4.8E-01	
10350697	Nmnat2	226518		1.2E-05	7.2E-04	1.55	3.8E-06	1.9E-04	1.61	3.2E-02	1.4E-01	
10595211	Col12a1	12816		3.9E-03	4.0E-02	1.55	2.0E-01	4.4E-01		8.9E-01	9.5E-01	
10432439	Fmnl3	22379		9.0E-07	1.2E-04	1.55	3.8E-06	1.9E-04	1.74	7.0E-05	3.3E-03	1.35
10373157	Mars	216443		2.7E-05	1.3E-03	1.55	2.3E-05	6.9E-04	1.46	2.0E-01	4.3E-01	
10478409	Pkig	18769		3.4E-06	2.9E-04	1.55	1.7E-03	1.6E-02	1.57	6.1E-03	4.8E-02	1.32
10401698	6430527G18Rik	238330		1.1E-05	6.7E-04	1.54	5.0E-06	2.3E-04	1.93	6.4E-01	8.1E-01	
10448307	Tnfrsf12a	27279		5.3E-04	1.0E-02	1.54	8.5E-05	1.8E-03	1.65	8.8E-04	1.4E-02	0.64
10461439	Fads1	76267		2.8E-07	5.4E-05	1.54	6.5E-06	2.8E-04	1.39	3.7E-01	6.1E-01	
10462005	Tmem2	83921		4.7E-06	3.6E-04	1.54	6.5E-06	2.8E-04	1.42	2.6E-03	2.8E-02	1.21
10595324	Htr1b	15551		3.9E-04	8.0E-03	1.54	1.9E-04	3.3E-03	1.34	4.7E-04	9.5E-03	0.73
10368883	Gm9855	624784	*	1.9E-05	9.7E-04	1.54	2.7E-05	7.6E-04	1.44	3.3E-01	5.8E-01	
10391490	Etv4	18612		3.5E-03	3.7E-02	1.54	3.3E-04	5.0E-03	1.59	8.3E-04	1.4E-02	1.73
10458663	Dpysl3	22240		2.3E-06	2.1E-04	1.54	5.9E-09	2.5E-06	1.68	1.8E-01	4.1E-01	
10427772	Tars	110960		4.7E-07	7.4E-05	1.54	6.8E-06	2.9E-04	1.51	3.3E-01	5.7E-01	
10461423	Fads3	60527		1.2E-05	7.0E-04	1.54	1.4E-04	2.5E-03	1.26	4.6E-03	4.0E-02	0.80
10462702	Hectd2	226098		2.2E-04	5.4E-03	1.54	3.9E-06	1.9E-04	1.72	1.1E-03	1.6E-02	0.67
10492682	Fam198b	68659		8.2E-05	2.8E-03	1.53	3.4E-07	3.6E-05	1.73	4.4E-04	9.3E-03	0.77
10550906	Plaur	18793		1.4E-03	1.9E-02	1.53	6.1E-05	1.4E-03	1.81	1.1E-03	1.6E-02	1.58
10345482	Cnnm4	94220		2.4E-05	1.2E-03	1.53	2.2E-06	1.3E-04	1.93	1.7E-01	4.0E-01	
10514133	Ttc39b	69863		1.4E-04	4.0E-03	1.53	1.1E-05	4.1E-04	1.47	8.1E-01	9.1E-01	
10439710	Phldb2	208177		9.0E-06	5.8E-04	1.53	1.9E-05	6.1E-04	1.38	6.2E-07	3.7E-04	0.66
10540795	Irak2	108960		1.7E-04	4.7E-03	1.52	1.7E-05	5.5E-04	1.57	9.5E-01	9.8E-01	
10459930	Ctdp1	67655		9.5E-07	1.3E-04	1.52	1.3E-07	1.9E-05	1.74	5.7E-02	2.0E-01	
10494817	Ngf	18049		7.1E-04	1.2E-02	1.52	2.4E-06	1.4E-04	2.67	5.2E-03	4.3E-02	0.73
10475623	Fbn1	14118	*	7.1E-06	4.9E-04	1.52	4.6E-05	1.1E-03	1.65	6.1E-01	7.9E-01	
10355530	Tns1	21961		1.2E-05	7.0E-04	1.52	1.2E-07	1.8E-05	2.24	8.4E-01	9.2E-01	
10426889	Sec61b	66212		6.9E-05	2.4E-03	1.52	4.7E-03	3.4E-02	1.26	6.1E-03	4.8E-02	1.33
10494753	ENSMUST00000121385			2.1E-04	5.2E-03	1.51	1.1E-03	1.2E-02	1.43	8.9E-03	6.1E-02	1.25
10554839	Picalm	233489		8.5E-07	1.2E-04	1.51	2.8E-07	3.1E-05	1.49	3.3E-02	1.4E-01	
10465185	Ehbp1l1	114601		8.6E-07	1.2E-04	1.51	3.2E-07	3.4E-05	1.60	6.1E-02	2.1E-01	
10443463	Cdkn1a	12575		5.0E-05	1.9E-03	1.51	6.2E-06	2.7E-04	1.70	1.7E-02	9.4E-02	1.25
10564272	Chrna7	11441		5.8E-03	5.3E-02	1.51	1.4E-06	9.5E-05	1.89	6.6E-01	8.3E-01	
10551009	Tmsb10	19240		9.3E-06	5.9E-04	1.51	8.6E-06	3.4E-04	1.42	1.2E-01	3.3E-01	
10466410	Psat1	107272		1.3E-05	7.4E-04	1.51	8.5E-03	5.3E-02	1.30	1.8E-01	4.1E-01	
10511888	ENSMUST00000120523			1.2E-04	3.7E-03	1.51	4.8E-06	2.2E-04	1.72	1.1E-02	7.1E-02	0.77

Table 6.3: Up-regulated probesets in invading and non-invading TGFβ1-treated fibroblasts.

Gene expression lists for microarrays conducted at 96 hours of MLg fibroblast invasion in the presence or absence of TGFβ1 (5 ng/ml). Data are shown for up-regulated probesets with > 1.5-fold regulation. Data are sorted by 96 h inv. (TGFβ1/n.t.). Statistical analysis: limma t-test and Benjamini-Hochberg multiple testing correction.(n.t. = non-treated, BH = Benjamini-Hochberg, FDR = False discovery rate, inv. = invading, non-inv. = non-invading, T = TGFβ1, C = Control).

Down-regulated probesets in TGFβ1/untreated

				96 h inv. (TGFβ1/n.t.) Statistical analysis, limma t-test, BH			96 h non-inv. (TGFβ1/n.t.) Statistical analysis, limma t-test, BH			96 h TGFβ1 (inv./non-inv.) Statistical analysis, limma t-test, BH		
Probe_set	Gene symbol or ID	Entrez	Unclear annotation	rawp	BH	Ratio (T/C), significant FDR<10%, ratio>1.5x (679)	rawp	BH	Ratio (T/C), significant FDR<10%, ratio>1.5x (1013)	rawp	BH	Ratio (G/M), significant FDR<10%, ratio>1.5x (620)
10403291	Akr1c14	105387		3.2E-08	1.1E-05	0.09	7.4E-09	2.9E-06	0.05	9.3E-02	2.8E-01	
10428619	Enpp2	18606		1.8E-07	4.0E-05	0.14	3.4E-05	9.2E-04	0.40	5.8E-03	4.6E-02	1.81
10580663	Ces1f	234564		1.4E-06	1.6E-04	0.15	2.7E-06	1.5E-04	0.29	2.1E-01	4.5E-01	
10422598	Sepp1	20363		6.2E-09	4.8E-06	0.17	4.5E-10	4.4E-07	0.18	3.7E-01	6.1E-01	
10580635	Ces1d	104158		1.3E-10	1.2E-06	0.17	9.1E-07	7.0E-05	0.27	1.2E-01	3.1E-01	
10502552	Clca1	12722		1.6E-08	7.3E-06	0.17	1.1E-10	1.6E-07	0.11	1.6E-01	3.8E-01	
10472538	Dhrs9	241452		2.2E-09	3.4E-06	0.17	6.3E-11	1.3E-07	0.11	5.7E-01	7.7E-01	
10398075	Serpina3n	20716		4.3E-06	3.3E-04	0.19	6.6E-08	1.2E-05	0.24	2.6E-03	2.7E-02	2.97
10523120	Cxcl5	20311		3.3E-05	1.4E-03	0.20	1.9E-06	1.2E-04	0.07	1.3E-02	7.8E-02	3.57
10405063	Ogn	18295		5.2E-06	3.8E-04	0.23	3.1E-09	1.5E-06	0.15	2.6E-04	6.8E-03	0.41
10493307	ENSMUST00000157979			2.2E-08	8.3E-06	0.24	6.2E-05	1.4E-03	0.40	1.2E-05	1.3E-03	2.14
10376765	Aldh3a1	11670		1.6E-06	1.7E-04	0.24	6.3E-04	7.8E-03	0.42	1.1E-04	4.3E-03	1.67
10556076	Olfml1	244198		1.4E-07	3.3E-05	0.25	1.8E-05	5.9E-04	0.40	8.9E-03	6.1E-02	1.30
10364072	Ggt5	23887		1.2E-07	2.9E-05	0.25	2.0E-08	5.8E-06	0.35	1.1E-01	3.0E-01	
10502565	Clca1	12722	*	2.1E-06	2.0E-04	0.26	1.5E-08	4.7E-06	0.15	9.7E-01	9.9E-01	
10562812	Spib	272382		1.2E-06	1.5E-04	0.26	2.5E-07	2.8E-05	0.42	2.2E-01	4.6E-01	
10531994	Gbp10	626578	*	1.4E-09	3.3E-06	0.27	8.3E-08	1.3E-05	0.29	2.0E-02	1.0E-01	
10547740	C1s	50908	*	1.5E-06	1.6E-04	0.28	1.1E-07	1.6E-05	0.17	1.7E-02	9.3E-02	1.90
10547752	Gm5077	317677		1.2E-06	1.4E-04	0.28	1.9E-06	1.2E-04	0.22	3.6E-02	1.5E-01	
10466127	AW112010	107350		3.0E-06	2.6E-04	0.29	1.4E-07	1.9E-05	0.32	5.5E-01	7.5E-01	
10563597	Saa3	20210		2.8E-04	6.5E-03	0.29	4.1E-05	1.0E-03	0.13	1.2E-02	7.6E-02	3.85
10450242	C4a	625018	*	5.6E-08	1.7E-05	0.30	2.1E-07	2.5E-05	0.47	8.5E-01	9.3E-01	
10403579	Prl2c5	107849	*	1.6E-07	3.6E-05	0.30	1.1E-03	1.2E-02	0.42	2.7E-06	6.6E-04	3.06
10441902	Smoc2	64074		3.7E-07	6.2E-05	0.30	7.2E-07	5.9E-05	0.27	6.5E-01	8.2E-01	
10519497	Steap4	117167		7.4E-05	2.6E-03	0.30	9.5E-06	3.6E-04	0.16	7.6E-03	5.5E-02	2.94
10560624	Apoe	11816		4.2E-08	1.4E-05	0.30	5.7E-04	7.3E-03	0.45	3.5E-03	3.4E-02	1.35
10508721	Snora44	100217418		1.6E-09	3.3E-06	0.31	4.4E-05	1.1E-03	0.62	8.5E-02	2.6E-01	
10344952	Rdh10	98711		2.9E-09	3.9E-06	0.32	2.2E-08	6.1E-06	0.27	5.0E-01	7.2E-01	
10587323	Gsta2	14858	*	7.0E-05	2.4E-03	0.32	1.8E-04	3.1E-03	0.58	2.7E-02	1.2E-01	
10531980	Gbp9	236573		2.3E-08	8.6E-06	0.32	1.8E-08	5.4E-06	0.31	7.1E-01	8.5E-01	
10606369	Itm2a	16431		3.0E-06	2.6E-04	0.32	7.6E-04	9.0E-03	0.67	8.2E-01	9.1E-01	
10523151	Cxcl1	14825		2.4E-07	4.9E-05	0.32	4.0E-06	2.0E-04	0.28	1.6E-03	2.0E-02	1.65
10603099	Figf	14205		2.9E-07	5.4E-05	0.33	3.8E-08	8.5E-06	0.25	8.6E-01	9.3E-01	
10580678	Ces1g	12623		2.1E-05	1.1E-03	0.33	3.0E-05	8.2E-04	0.48	1.4E-01	3.6E-01	
10543939	Fam180a	208164		3.2E-09	4.0E-06	0.34	3.2E-08	7.6E-06	0.47	3.8E-05	2.4E-03	1.41
10587331	Gsta2	14858	*	9.2E-05	3.0E-03	0.34	5.4E-04	7.0E-03	0.66	5.9E-02	2.1E-01	
10480734	Ptgds	19215		1.9E-06	1.9E-04	0.34	2.1E-07	2.5E-05	0.40	7.1E-02	2.3E-01	
10607499	Phex	18675		5.6E-08	1.7E-05	0.35	3.7E-08	8.5E-06	0.27	6.1E-01	7.9E-01	
10462618	Ifit3	15959		6.3E-06	4.5E-04	0.36	3.4E-04	5.0E-03	0.37	8.6E-01	9.3E-01	
10431935	Amigo2	105827	*	1.6E-08	7.3E-06	0.36	3.1E-11	9.9E-08	0.21	######	1.0E+00	
10423654	Osr2	107587		1.7E-06	1.8E-04	0.36	1.4E-07	1.9E-05	0.28	2.5E-02	1.2E-01	
10496580	Gbp3	55932		1.5E-07	3.4E-05	0.36	3.0E-06	1.6E-04	0.42	8.5E-01	9.3E-01	
10407797	Prl2c4	26421	*	1.6E-07	3.6E-05	0.37	1.0E-04	2.0E-03	0.39	2.8E-06	6.7E-04	3.25
10497051	Negr1	320840		3.6E-09	4.0E-06	0.37	4.1E-08	8.7E-06	0.22	9.9E-01	1.0E+00	
10428388	Rspo2	239405		1.1E-06	1.4E-04	0.38	1.2E-08	4.1E-06	0.21	4.7E-03	4.1E-02	1.74
10408689	Nrn1	68404		6.5E-07	9.5E-05	0.38	3.6E-07	3.7E-05	0.33	3.5E-02	1.5E-01	
10484463	Serping1	12258		1.4E-06	1.6E-04	0.38	1.8E-09	9.8E-07	0.21	3.9E-03	3.6E-02	1.62
10501586	S1pr1	13609		4.1E-05	1.7E-03	0.38	2.0E-05	6.2E-04	0.34	9.7E-01	9.9E-01	
10513208	Svep1	64817		3.7E-06	3.0E-04	0.39	4.3E-07	4.2E-05	0.27	1.2E-02	7.3E-02	0.64
10495285	Sort1	20661		1.6E-08	7.3E-06	0.39	4.0E-08	8.6E-06	0.31	5.7E-01	7.7E-01	
10419261	Bmp4	12159		4.6E-06	3.6E-04	0.39	5.8E-12	4.1E-08	0.12	8.6E-01	9.3E-01	
10424119	Nov	18133		3.0E-06	2.6E-04	0.40	6.5E-01	8.2E-01		6.0E-01	7.9E-01	
10384396	ENSMUST00000157365			6.5E-08	1.9E-05	0.40	1.2E-03	1.3E-02	0.68	2.1E-04	6.1E-03	1.35
10346164	Sdpr	20324		2.9E-05	1.3E-03	0.40	6.6E-10	5.7E-07	0.23	4.9E-02	1.9E-01	
10461979	Aldh1a1	11668		9.7E-07	1.3E-04	0.41	1.5E-09	9.3E-07	0.26	4.2E-02	1.7E-01	
10441813	Snora20	100303746		1.8E-06	1.8E-04	0.41	4.1E-02	1.6E-01		4.4E-01	6.8E-01	
10360398	Ifi202b	26388		2.9E-06	2.5E-04	0.41	3.0E-05	8.2E-04	0.52	6.5E-01	8.2E-01	
10536635	A430107O13Rik	214642		5.3E-09	4.6E-06	0.41	4.5E-07	4.3E-05	0.45	5.6E-03	4.5E-02	0.75
10452316	C3	12266		2.9E-05	1.3E-03	0.42	2.5E-06	1.4E-04	0.22	9.2E-03	6.2E-02	2.08
10531737	Hpse	15442		6.9E-06	4.8E-04	0.42	3.3E-02	1.4E-01		2.6E-01	5.1E-01	
10492165	ENSMUST00000082652			3.2E-06	2.7E-04	0.43	5.1E-04	6.7E-03	0.37	1.0E-04	4.2E-03	0.23
10370037	Mmp11	17385		7.9E-10	2.8E-06	0.43	8.2E-07	6.6E-05	0.49	1.2E-04	4.5E-03	1.36
10545865	Cml3	93674		1.7E-07	3.7E-05	0.43	5.0E-06	2.3E-04	0.55	2.4E-01	4.8E-01	
10496438	Adh1	11522		3.8E-09	4.0E-06	0.43	2.0E-08	5.9E-06	0.36	1.5E-06	5.4E-04	1.88
10440522	Adamts1	11504		1.6E-09	3.3E-06	0.43	1.1E-09	7.5E-07	0.27	4.3E-02	1.7E-01	
10571567	Sorbs2	234214		9.5E-05	3.1E-03	0.43	7.5E-10	5.9E-07	0.21	3.2E-02	1.4E-01	
10403842	Elmo1	140580		2.4E-06	2.2E-04	0.43	5.7E-07	5.1E-05	0.28	1.8E-01	4.2E-01	
10545869	Cml3	93674		4.0E-07	6.6E-05	0.44	3.8E-06	1.9E-04	0.56	3.6E-01	6.1E-01	

10360406	**Ifi205**	226695		1.2E-05	7.2E-04	0.44	1.2E-03	1.3E-02	0.45	2.9E-01	5.4E-01	
10587315	**Gsta4**	14860		1.8E-06	1.8E-04	0.44	2.2E-07	2.6E-05	0.31	4.6E-04	9.4E-03	1.99
10360306	**Slamf8**	74748		4.1E-06	3.2E-04	0.44	4.5E-07	4.3E-05	0.57	6.2E-02	2.1E-01	
10392560	**Abca9**	217262		7.2E-07	1.0E-04	0.44	8.3E-08	1.3E-05	0.35	7.3E-01	8.6E-01	
10529979	**Ppargc1a**	19017		1.8E-04	4.7E-03	0.44	5.7E-03	4.0E-02	0.42	1.9E-01	4.2E-01	
10502240	**Npnt**	114249		1.2E-06	1.5E-04	0.45	1.3E-09	9.1E-07	0.35	7.2E-01	8.6E-01	
10541678	**C1ra**	50909		1.1E-04	3.4E-03	0.45	6.7E-07	5.7E-05	0.29	1.5E-02	8.8E-02	1.70
10366052	**Kitl**	17311		2.6E-05	1.2E-03	0.45	4.1E-07	4.0E-05	0.35	1.0E-01	2.9E-01	
10374197	**Ramp3**	56089		3.9E-05	1.6E-03	0.45	1.5E-02	8.0E-02	0.67	3.4E-02	1.5E-01	
10359689	**Atp1b1**	11931		5.1E-07	7.9E-05	0.45	3.7E-04	5.4E-03	0.61	4.4E-02	1.7E-01	
10357870	**Prelp**	116847		2.0E-05	1.0E-03	0.45	4.0E-07	3.9E-05	0.34	3.5E-01	5.9E-01	
10601044	**Gdpd2**	71584		9.8E-06	6.1E-04	0.45	2.2E-08	6.1E-06	0.32	7.0E-03	5.2E-02	1.35
10595148	**Gsta1**	14857	*	1.8E-04	4.7E-03	0.46	1.6E-03	1.5E-02	0.75	1.3E-02	8.0E-02	1.30
10389207	**Ccl5**	20304		6.4E-08	1.9E-05	0.46	6.6E-03	4.4E-02	0.77	6.6E-01	8.2E-01	
10531972	**Gbp8**	76074		1.6E-08	7.3E-06	0.46	2.1E-07	2.5E-05	0.47	5.3E-01	7.4E-01	
10541683	**C1ra**	50909	*	2.1E-05	1.1E-03	0.46	6.6E-06	2.8E-04	0.28	2.1E-02	1.1E-01	
10409833	**Gas1**	14451		1.2E-07	3.0E-05	0.46	1.0E-08	3.7E-06	0.34	1.8E-01	4.1E-01	
10450367	**Hspa1b**	15511	*	1.1E-04	3.3E-03	0.46	1.8E-03	1.7E-02	0.65	3.3E-01	5.8E-01	
10545862	**Cml3**	93674		3.2E-06	2.7E-04	0.46	5.7E-05	1.3E-03	0.64	8.9E-01	9.5E-01	
10569456	**ENSMUST00000083184**			6.4E-07	9.4E-05	0.47	8.3E-07	6.6E-05	0.64	2.5E-01	4.9E-01	
10503334	**Gem**	14579		2.6E-05	1.2E-03	0.47	3.1E-04	4.7E-03	0.59	1.4E-02	8.1E-02	1.50
10416503	**Snora31**	100303751		3.2E-06	2.7E-04	0.47	9.3E-02	2.7E-01		2.5E-04	6.7E-03	1.95
10400143	**Stxbp6**	217517		1.1E-07	2.7E-05	0.47	4.7E-06	2.2E-04	0.63	2.9E-01	5.4E-01	
10508723	**Snora61**	100217440		6.3E-07	9.4E-05	0.47	1.3E-03	1.4E-02	0.68	1.3E-02	8.1E-02	1.37
10587339	**Gsta2**	14858	*	2.4E-04	5.7E-03	0.47	1.8E-03	1.7E-02	0.76	5.9E-03	4.7E-02	1.35
10529977	**Ppargc1a**	19017		2.2E-03	2.7E-02	0.47	2.3E-02	1.1E-01		6.8E-01	8.4E-01	
10422760	**Fyb**	23880		8.5E-09	5.4E-06	0.48	3.6E-02	1.4E-01		6.4E-01	8.1E-01	
10394593	**Fam49a**	76820		7.0E-05	2.4E-03	0.48	4.5E-02	1.7E-01		8.7E-02	2.6E-01	
10478633	**Mmp9**	17395		1.3E-06	1.5E-04	0.48	1.7E-04	3.0E-03	0.62	4.9E-05	2.7E-03	1.65
10434778	**Rtp4**	67775		1.6E-05	8.7E-04	0.48	5.9E-05	1.3E-03	0.46	4.3E-01	6.6E-01	
10501229	**Gstm1**	14862		9.3E-09	5.5E-06	0.49	4.8E-10	4.6E-07	0.36	4.5E-06	8.2E-04	1.63
10348354	**Ugt1a6a**	94284	*	7.9E-08	2.2E-05	0.49	3.8E-07	3.8E-05	0.43	1.8E-03	2.2E-02	1.48
10538082	**Atp6v0e2**	76252		3.9E-07	6.5E-05	0.49	3.4E-09	1.6E-06	0.40	6.6E-03	5.0E-02	1.30
10496251	**Bdh2**	69772		3.5E-07	6.1E-05	0.49	8.2E-08	1.3E-05	0.40	2.0E-04	5.9E-03	1.54
10356329	**Snora75**	100303740		5.0E-04	9.6E-03	0.50	4.4E-02	1.6E-01		6.8E-04	1.2E-02	0.70
10484371	**Calcrl**	54598		1.3E-04	3.8E-03	0.50	2.7E-05	7.6E-04	0.53	3.4E-02	1.5E-01	
10473604	**ENSMUST00000155234**			1.4E-05	7.9E-04	0.50	1.7E-04	2.9E-03	0.63	6.5E-01	8.2E-01	
10607484	**Ptchd1**	211612		2.9E-03	3.2E-02	0.50	4.1E-03	3.1E-02	0.49	4.3E-01	6.6E-01	
10543785	**AB041803**	232685		3.7E-07	6.2E-05	0.50	8.5E-06	3.4E-04	0.49	1.4E-01	3.6E-01	
10394674	**Socs2**	216233	*	1.1E-05	6.7E-04	0.50	4.4E-09	2.0E-06	0.27	3.8E-02	1.6E-01	
10530145	**Tlr1**	21897		1.7E-06	1.7E-04	0.50	4.4E-11	1.1E-07	0.42	7.7E-01	8.9E-01	
10351491	**Olfml2b**	320078		3.9E-05	1.6E-03	0.50	5.4E-08	1.0E-05	0.30	4.7E-03	4.1E-02	1.44
10527961	**ENSMUST00000157506**			4.2E-08	1.4E-05	0.50	6.6E-03	4.4E-02	0.72	9.1E-02	2.7E-01	
10532085	**Tgfbr3**	21814		1.3E-08	6.5E-06	0.50	5.6E-09	2.4E-06	0.38	9.9E-05	4.1E-03	1.51
10412921	**Nid2**	18074	*	8.8E-07	1.2E-04	0.51	2.0E-07	2.4E-05	0.31	9.9E-01	1.0E+00	
10439009	**Apod**	11815		6.0E-05	2.2E-03	0.51	1.4E-05	4.7E-04	0.42	4.6E-01	6.9E-01	
10485711	**Fibin**	67606		5.0E-06	3.7E-04	0.51	4.0E-08	8.6E-06	0.41	4.0E-03	3.7E-02	0.74
10607712	**Grpr**	14829		1.0E-03	1.6E-02	0.51	2.6E-02	1.2E-01		4.2E-03	3.8E-02	0.46
10506201	**Ror1**	26563		1.0E-06	1.3E-04	0.51	9.2E-05	1.9E-03	0.56	3.8E-01	6.3E-01	
10462621	**I830012O16Rik**	667370		4.8E-06	3.6E-04	0.52	7.7E-03	4.9E-02	0.63	3.8E-01	6.2E-01	
10361091	**Atf3**	11910		1.0E-02	7.7E-02	0.52	1.5E-01	3.6E-01		9.2E-01	9.7E-01	
10489569	**Pltp**	18830	*	2.3E-07	4.7E-05	0.52	2.8E-05	7.9E-04	0.54	5.5E-05	2.9E-03	1.65
10601878	**Tceal1**	237052		2.9E-04	6.5E-03	0.52	1.1E-04	2.1E-03	0.66	3.6E-01	6.0E-01	
10478847	**1500012F01Rik**	68949	*	3.4E-07	6.0E-05	0.52	1.9E-06	1.2E-04	0.66	1.5E-01	3.7E-01	
10498024	**Slc7a11**	26570		1.5E-03	2.1E-02	0.53	9.7E-01	9.9E-01		3.0E-02	1.3E-01	
10385747	**Phf15**	76901		2.2E-07	4.6E-05	0.53	3.0E-08	7.4E-06	0.54	4.3E-04	9.1E-03	1.32
10523161	**Mthfd2l**	665563		3.5E-05	1.5E-03	0.53	5.8E-05	1.3E-03	0.71	4.7E-03	4.0E-02	1.35
10490950	**Bhlhe22**	59058		2.2E-06	2.1E-04	0.53	2.9E-03	2.4E-02	0.78	4.3E-01	6.6E-01	
10496592	**Gbp2**	14469		2.0E-06	2.0E-04	0.53	7.8E-07	6.3E-05	0.51	3.2E-01	5.7E-01	
10525185	**ENSMUST00000082907**			1.5E-08	7.3E-06	0.53	9.4E-02	2.7E-01		1.4E-01	3.6E-01	
10566366	**Trim30d**	209387		1.8E-04	4.7E-03	0.53	3.4E-05	9.0E-04	0.43	7.2E-02	2.4E-01	
10565567	**4632427E13Rik**	666737		2.0E-05	1.0E-03	0.53	2.1E-05	6.5E-04	0.54	1.7E-05	1.6E-03	0.44
10569335	**H19**	14955		3.6E-03	3.8E-02	0.53	1.1E-05	4.1E-04	0.15	9.8E-01	9.9E-01	
10466712	**Mamdc2**	71738		3.4E-03	3.7E-02	0.53	2.4E-01	4.8E-01		1.8E-05	1.6E-03	1.80
10376950	**Pmp22**	18858		5.7E-05	2.1E-03	0.54	1.3E-06	9.3E-05	0.42	1.7E-01	4.0E-01	
10602692	**Rragb**	245670		8.2E-06	5.4E-04	0.54	3.0E-06	1.6E-04	0.54	1.4E-01	3.5E-01	
10503659	**Epha7**	13841		4.6E-04	9.1E-03	0.54	2.0E-04	3.4E-03	0.50	3.9E-01	6.3E-01	
10543959	**Ptn**	19242		5.8E-04	1.1E-02	0.54	1.4E-02	7.4E-02	0.57	5.8E-01	7.7E-01	
10444814	**H2-gs10**	436493	*	1.7E-06	1.8E-04	0.54	9.1E-05	1.9E-03	0.59	5.9E-04	1.1E-02	1.63
10362314	**Ptprk**	19272		5.1E-08	1.6E-05	0.54	4.5E-08	9.2E-06	0.43	8.0E-02	2.5E-01	
10360391	**Ifi203**	15950		2.7E-07	5.2E-05	0.54	1.5E-08	4.7E-06	0.43	2.0E-02	1.0E-01	
10556297	**Adm**	11535		1.4E-05	7.9E-04	0.54	4.7E-06	2.2E-04	0.22	4.0E-01	6.4E-01	
10594044	**Islr**	26968		7.0E-06	4.8E-04	0.54	9.6E-07	7.3E-05	0.38	1.9E-01	4.3E-01	
10522503	**Pdgfra**	18595		2.0E-08	8.3E-06	0.54	3.2E-07	3.3E-05	0.52	6.4E-01	8.1E-01	
10597945	**Tmem158**	72309		5.6E-07	8.5E-05	0.54	9.2E-04	1.0E-02	0.69	1.7E-03	2.1E-02	1.30
10422822	**Lifr**	16880		6.3E-05	2.3E-03	0.54	1.2E-06	8.7E-05	0.35	1.4E-01	3.5E-01	

10577315	**Angpt2**	11601		7.2E-06	4.9E-04	0.55	1.0E-04	2.0E-03	0.71	3.9E-03	3.6E-02	1.28
10409014	**ENSMUST00000082624**			9.5E-08	2.5E-05	0.55	1.4E-01	3.4E-01		3.0E-01	5.4E-01	
10507870	**ENSMUST00000082721**			7.2E-08	2.0E-05	0.55	2.2E-01	4.6E-01		1.3E-01	3.3E-01	
10455015	**Vaultrc5**	378472		2.1E-04	5.2E-03	0.55	1.8E-05	5.9E-04	0.41	1.5E-07	1.7E-04	4.72
10540275	**Gxylt2**	232313		1.1E-03	1.6E-02	0.55	4.5E-04	6.2E-03	0.40	2.4E-01	4.9E-01	
10580593	**Ces1a**	244595		7.7E-05	2.6E-03	0.55	1.5E-05	5.0E-04	0.51	3.5E-03	3.3E-02	1.53
10372324	**Syt1**	20979		1.5E-06	1.6E-04	0.56	1.8E-02	9.1E-02	0.83	2.0E-01	4.4E-01	
10506488	**Ppap2b**	67916		7.6E-06	5.1E-04	0.56	7.1E-06	3.0E-04	0.44	2.1E-03	2.4E-02	1.48
10507872	**ENSMUST00000083844**			1.3E-07	3.0E-05	0.56	2.3E-01	4.8E-01		4.5E-01	6.9E-01	
10443027	**A930001N09Rik**	77128		2.7E-06	2.4E-04	0.56	9.0E-07	7.0E-05	0.59	3.5E-01	5.9E-01	
10447190	**Plekhh2**	213556		2.1E-08	8.3E-06	0.56	1.0E-09	7.3E-07	0.37	4.7E-01	6.9E-01	
10353192	**Eya1**	14048		4.8E-06	3.6E-04	0.56	4.0E-08	8.6E-06	0.49	6.6E-01	8.2E-01	
10419566	**Ang2**	11731		1.2E-03	1.8E-02	0.56	5.0E-01	7.2E-01		7.2E-01	8.6E-01	
10452257	**Slc25a23**	66972		3.2E-06	2.7E-04	0.56	7.8E-08	1.3E-05	0.45	1.1E-02	7.0E-02	1.26
10462435	**Mlana**	77836		2.7E-07	5.2E-05	0.56	1.4E-04	2.6E-03	0.72	2.1E-02	1.1E-01	
10466659	**Gda**	14544		5.7E-03	5.2E-02	0.56	1.5E-03	1.5E-02	0.52	9.0E-02	2.7E-01	
10351293	**Dpt**	56429		9.9E-04	1.5E-02	0.56	9.6E-02	2.7E-01		1.3E-01	3.4E-01	
10562211	**Fxyd1**	56188		4.9E-06	3.6E-04	0.56	1.0E-07	1.5E-05	0.48	8.9E-04	1.4E-02	1.30
10522467	**Rasl11b**	68939		3.5E-05	1.5E-03	0.56	7.2E-05	1.6E-03	0.64	5.4E-01	7.5E-01	
10455961	**Iigp1**	60440		5.3E-06	3.9E-04	0.57	1.2E-04	2.2E-03	0.63	6.5E-01	8.2E-01	
10449284	**Dusp1**	19252		2.5E-04	5.9E-03	0.57	4.9E-04	6.5E-03	0.48	5.8E-02	2.0E-01	
10567010	**Dkk3**	50781		1.4E-05	7.9E-04	0.57	8.8E-02	2.6E-01		3.5E-02	1.5E-01	
10366266	**Pawr**	114774		1.7E-05	8.8E-04	0.57	1.8E-03	1.7E-02	0.84	9.6E-02	2.8E-01	
10505187	**Ugcg**	22234		6.6E-06	4.7E-04	0.57	4.7E-04	6.3E-03	0.67	1.6E-04	5.3E-03	0.59
10539617	**Alms1**	236266		1.8E-07	4.0E-05	0.57	1.2E-08	4.2E-06	0.45	1.4E-01	3.6E-01	
10354649	**Pgap1**	241062		2.2E-06	2.0E-04	0.57	1.3E-06	9.1E-05	0.54	4.4E-03	3.9E-02	0.75
10497381	**Cyp7b1**	13123		1.6E-04	4.4E-03	0.57	1.9E-03	1.8E-02	0.65	3.3E-02	1.4E-01	
10346374	**Aox1**	11761		1.3E-05	7.5E-04	0.57	5.2E-05	1.2E-03	0.56	6.2E-03	4.9E-02	1.25
10607486	**Ptchd1**	211612		7.6E-03	6.4E-02	0.57	1.5E-04	2.8E-03	0.42	6.3E-01	8.1E-01	
10462623	**Ifit1**	15957		2.3E-04	5.6E-03	0.58	6.1E-03	4.1E-02	0.55	4.8E-01	7.1E-01	
10431697	**Abcd2**	26874		9.1E-06	5.8E-04	0.58	6.3E-05	1.4E-03	0.62	8.7E-01	9.4E-01	
10542880	**4833442J19Rik**	320204		1.5E-05	8.1E-04	0.58	5.6E-05	1.3E-03	0.68	4.9E-02	1.8E-01	
10399823	**ENSMUST00000083266**			2.1E-07	4.4E-05	0.58	2.4E-05	7.1E-04	0.74	3.2E-01	5.7E-01	
10566993	**Galntl4**	233733		2.9E-03	3.3E-02	0.58	4.3E-04	6.0E-03	0.34	2.3E-02	1.1E-01	
10581538	**Nqo1**	18104		6.7E-06	4.7E-04	0.58	2.4E-02	1.1E-01		9.8E-05	4.1E-03	1.64
10366275	**ENSMUST00000083719**			1.8E-06	1.8E-04	0.58	8.5E-02	2.5E-01		2.8E-06	6.6E-04	1.77
10475932	**Fbln7**	70370		9.9E-04	1.5E-02	0.58	1.5E-04	2.7E-03	0.51	1.6E-02	8.9E-02	1.23
10572130	**Lpl**	16956		1.1E-04	3.4E-03	0.58	1.0E-03	1.1E-02	0.57	2.9E-04	7.3E-03	1.46
10580733	**Bbs2**	67378		9.6E-06	6.1E-04	0.58	1.4E-06	9.5E-05	0.56	2.4E-03	2.6E-02	1.23
10350742	**Rnasel**	24014		3.6E-08	1.2E-05	0.59	8.2E-05	1.7E-03	0.54	1.9E-01	4.2E-01	
10501608	**Vcam1**	22329		3.5E-05	1.5E-03	0.59	1.1E-05	4.1E-04	0.60	2.6E-01	5.1E-01	
10357345	**Nckap5**	210356		3.1E-04	6.8E-03	0.59	1.4E-04	2.6E-03	0.51	6.9E-01	8.4E-01	
10438769	**Cldn1**	12737		2.0E-04	5.1E-03	0.59	2.3E-07	2.6E-05	0.17	2.5E-01	5.0E-01	
10548871	**BC049715**	320135	*	3.7E-06	3.0E-04	0.59	7.3E-03	4.7E-02	0.81	8.8E-01	9.4E-01	
10476740	**Slc24a3**	94249		3.5E-06	2.9E-04	0.59	6.8E-07	5.7E-05	0.34	2.7E-01	5.2E-01	
10395414	**Tmem195**	319660		1.5E-04	4.2E-03	0.59	6.1E-05	1.4E-03	0.56	5.1E-02	1.9E-01	
10368277	**Rps12**	20042		1.6E-04	4.3E-03	0.59	8.4E-02	2.5E-01		5.6E-03	4.5E-02	1.36
10421924	**Pcdh9**	211712		5.7E-08	1.7E-05	0.59	1.1E-06	8.1E-05	0.43	1.0E-04	4.2E-03	0.62
10421932	**Pcdh9**	211712		1.1E-06	1.4E-04	0.59	2.8E-06	1.5E-04	0.42	1.0E-04	4.1E-03	0.59
10501879	**Usp53**	99526		5.4E-07	8.3E-05	0.59	1.9E-05	6.0E-04	0.65	1.9E-03	2.3E-02	0.79
10365983	**Lum**	17022		1.4E-03	1.9E-02	0.59	1.5E-04	2.7E-03	0.49	1.1E-01	3.1E-01	
10481101	**Snhg7**	72091	*	1.4E-05	8.1E-04	0.59	1.3E-01	3.3E-01		1.8E-01	4.1E-01	
10348739	**Sned1**	208777		1.1E-04	3.4E-03	0.59	4.3E-06	2.1E-04	0.57	2.7E-01	5.1E-01	
10419563	**Rnase1**	19752		4.2E-06	3.3E-04	0.59	1.8E-01	4.0E-01		5.4E-02	2.0E-01	
10594798	**ENSMUST00000083236**			7.6E-05	2.6E-03	0.59	7.8E-02	2.4E-01		1.6E-01	3.8E-01	
10591535	**Mir199a-1**	387194		1.4E-06	1.5E-04	0.60	3.1E-06	1.7E-04	0.57	9.1E-04	1.4E-02	0.74
10352448	**Dusp10**	63953		4.8E-05	1.9E-03	0.60	6.8E-05	1.5E-03	0.69	3.3E-02	1.4E-01	
10452815	**Xdh**	22436		5.0E-06	3.7E-04	0.60	1.0E-05	3.8E-04	0.49	4.5E-05	2.6E-03	2.01
10538715	**Fam190a**	232035		6.1E-05	2.2E-03	0.60	2.5E-05	7.4E-04	0.48	4.4E-01	6.7E-01	
10546710	**Shq1**	72171		1.5E-05	8.1E-04	0.60	3.1E-05	8.4E-04	0.54	2.3E-04	6.5E-03	1.55
10556206	**Snora3**	100302499		5.3E-05	2.0E-03	0.60	2.5E-04	4.0E-03	0.69	2.0E-02	1.0E-01	
10435787	**ENSMUST00000093651**			8.5E-04	1.4E-02	0.60	2.1E-02	1.0E-01		2.5E-02	1.2E-01	
10349174	**Serpinb8**	20725		1.4E-04	4.0E-03	0.60	1.1E-03	1.1E-02	0.58	5.6E-02	2.0E-01	
10581448	**ENSMUST00000150001**			5.7E-07	8.6E-05	0.60	9.0E-02	2.6E-01		5.3E-02	1.9E-01	
10582862	**Sp140**	434484	*	1.0E-04	3.2E-03	0.60	1.9E-05	6.1E-04	0.70	4.2E-02	1.7E-01	
10496519	**Unc5c**	22253		7.9E-03	6.6E-02	0.60	3.6E-02	1.4E-01		8.4E-01	9.3E-01	
10598064	**NC_005089**			4.4E-03	4.4E-02	0.61	1.1E-02	6.4E-02	0.77	4.1E-03	3.7E-02	0.61
10583310	**Taf1d**	75316		3.5E-06	2.9E-04	0.61	1.8E-02	8.9E-02	0.80	2.4E-01	4.8E-01	
10539640	**Alms1**	236266		3.1E-05	1.4E-03	0.61	3.9E-08	8.6E-06	0.50	4.3E-02	1.7E-01	
10461408	**Rab3il1**	74760		1.1E-04	3.4E-03	0.61	2.7E-05	7.6E-04	0.47	1.1E-02	7.2E-02	1.41
10475625	**Eid1**	58521		1.0E-04	3.3E-03	0.61	2.0E-05	6.3E-04	0.62	1.2E-01	3.2E-01	
10497646	**Phc3**	241915		4.9E-04	9.5E-03	0.61	2.3E-03	2.1E-02	0.78	1.4E-03	1.9E-02	0.66
10530536	**Tec**	21682		9.8E-06	6.1E-04	0.61	6.5E-01	8.2E-01		4.2E-04	8.9E-03	1.43
10539632	**Alms1**	236266		4.0E-05	1.6E-03	0.61	1.6E-07	2.1E-05	0.50	4.6E-02	1.8E-01	
10368356	**Akap7**	432442		1.4E-05	8.1E-04	0.61	1.9E-05	6.0E-04	0.70	4.3E-02	1.7E-01	
10473109	**Gm14461**	329436		3.7E-06	3.0E-04	0.61	8.7E-02	2.6E-01		9.6E-01	9.9E-01	

10400405	**Nfkbia**	18035		4.7E-06	3.6E-04	0.61	1.4E-05	4.9E-04	0.63	6.0E-03	4.8E-02	1.31
10362511	**Gstm3**	14864		3.6E-06	3.0E-04	0.61	2.8E-09	1.4E-06	0.50	4.0E-05	2.5E-03	1.43
10540233	**Fam19a1**	320265		1.7E-05	9.2E-04	0.61	1.8E-02	9.0E-02	0.81	9.6E-01	9.8E-01	
10566326	**Trim12a**	76681		2.0E-04	5.1E-03	0.61	9.9E-05	2.0E-03	0.66	2.7E-02	1.3E-01	
10490989	**Cp**	12870		1.4E-04	4.0E-03	0.61	5.3E-05	1.3E-03	0.37	1.2E-04	4.4E-03	2.78
10523145	**Cxcl15**	20309		8.2E-04	1.3E-02	0.61	1.1E-04	2.1E-03	0.49	5.9E-01	7.8E-01	
10414706	**Gm8635**	667441		4.4E-04	8.8E-03	0.61	2.5E-04	3.9E-03	0.66	1.6E-01	3.9E-01	
10570432	**Snora3**	100302499		6.4E-05	2.3E-03	0.61	2.0E-04	3.4E-03	0.69	2.2E-02	1.1E-01	
10511580	**Pdp1**	381511		9.8E-07	1.3E-04	0.61	3.0E-07	3.2E-05	0.64	2.2E-01	4.6E-01	
10399605	**Adam17**	11491		7.4E-06	5.0E-04	0.61	6.7E-07	5.7E-05	0.59	1.8E-01	4.1E-01	
10450369	**Hspa1a**	193740		1.2E-03	1.7E-02	0.61	1.1E-02	6.3E-02	0.74	3.0E-01	5.5E-01	
10531987	**Gbp4**	17472		1.5E-04	4.2E-03	0.61	9.1E-05	1.9E-03	0.68	5.8E-01	7.8E-01	
10407803	**Gpr137b**	83924		2.9E-06	2.5E-04	0.61	7.9E-02	2.4E-01		5.3E-03	4.4E-02	1.24
10362294	**Arhgap18**	73910		3.9E-05	1.6E-03	0.61	2.6E-08	6.8E-06	0.52	2.9E-02	1.3E-01	
10483178	**Cobll1**	319876		9.7E-08	2.5E-05	0.61	3.9E-07	3.9E-05	0.52	2.0E-03	2.3E-02	1.22
10376425	**Gm12258**	237769		2.9E-04	6.6E-03	0.61	1.4E-04	2.5E-03	0.62	1.2E-04	4.6E-03	0.56
10402512	**Scarna13**	100306943		1.2E-04	3.6E-03	0.62	2.3E-02	1.0E-01		9.1E-01	9.6E-01	
10399874	**Bcap29**	12033		1.2E-04	3.6E-03	0.62	6.8E-02	2.2E-01		6.5E-03	5.0E-02	0.73
10581992	**Maf**	17132		3.0E-07	5.5E-05	0.62	4.9E-05	1.2E-03	0.61	9.0E-03	6.2E-02	1.24
10371296	**Glt8d2**	74782	*	3.2E-05	1.4E-03	0.62	4.4E-06	2.1E-04	0.51	5.0E-02	1.9E-01	
10506050	**Nfia**	18027		2.3E-06	2.1E-04	0.62	6.4E-07	5.5E-05	0.41	9.4E-02	2.8E-01	
10472820	**Itga6**	16403		3.7E-03	3.9E-02	0.62	3.8E-04	5.5E-03	0.61	1.2E-02	7.3E-02	1.53
10590791	**Birc2**	11797		5.6E-05	2.1E-03	0.62	5.4E-04	7.0E-03	0.73	7.3E-02	2.4E-01	
10420668	**Mir15a**	387174		7.9E-04	1.3E-02	0.62	2.5E-05	7.3E-04	0.52	5.5E-03	4.5E-02	0.72
10523595	**Ptpn13**	19249		4.7E-04	9.1E-03	0.62	3.6E-05	9.4E-04	0.46	2.5E-02	1.2E-01	
10356274	**Csprs**	114564	*	1.3E-06	1.5E-04	0.62	9.0E-07	7.0E-05	0.59	5.7E-03	4.6E-02	0.82
10450038	**Angptl4**	57875		1.5E-05	8.1E-04	0.62	2.7E-06	1.5E-04	0.51	8.7E-02	2.7E-01	
10399908	**Prkar2b**	19088		2.1E-05	1.0E-03	0.62	1.3E-04	2.4E-03	0.61	1.3E-03	1.8E-02	1.45
10453759	**Gm10554**	100038541		2.8E-05	1.3E-03	0.62	4.0E-05	1.0E-03	0.58	6.2E-01	8.0E-01	
10379535	**Ccl8**	20307		3.7E-03	3.9E-02	0.63	7.7E-01	8.9E-01		1.6E-02	8.9E-02	2.23
10347915	**Gm7609**	665378	*	1.4E-06	1.6E-04	0.63	2.0E-06	1.2E-04	0.60	1.4E-02	8.4E-02	0.84
10529068	**Slc30a3**	22784		1.3E-05	7.5E-04	0.63	4.0E-07	3.9E-05	0.54	8.2E-01	9.1E-01	
10404792	**Phactr1**	218194		2.8E-05	1.3E-03	0.63	8.1E-04	9.5E-03	0.61	2.7E-01	5.2E-01	
10569341	**Mir675**	735280	*	4.0E-03	4.2E-02	0.63	1.6E-04	2.8E-03	0.31	4.9E-01	7.1E-01	
10468691	**Ablim1**	226251		1.8E-04	4.7E-03	0.63	1.2E-06	8.9E-05	0.49	8.6E-01	9.3E-01	
10601659	**Srpx2**	68792		7.8E-03	6.5E-02	0.63	2.1E-01	4.5E-01		9.1E-02	2.7E-01	
10457071	**Cyb5**	109672		1.9E-05	9.8E-04	0.63	1.7E-06	1.1E-04	0.65	2.5E-02	1.2E-01	
10566358	**Trim30a**	20128		2.8E-05	1.3E-03	0.63	3.6E-06	1.8E-04	0.53	8.4E-01	9.2E-01	
10407350	**Fgf10**	14165		6.3E-04	1.1E-02	0.63	4.4E-07	4.2E-05	0.53	2.3E-03	2.6E-02	1.62
10454807	**Snora74a**	436583		1.5E-04	4.1E-03	0.63	1.9E-02	9.4E-02	0.79	2.0E-03	2.3E-02	1.45
10453636	**Svil**	225115		6.0E-06	4.3E-04	0.63	2.6E-07	2.9E-05	0.49	1.6E-01	3.8E-01	
10465831	**5730408K05Rik**	67531		3.1E-05	1.4E-03	0.63	7.5E-02	2.3E-01		2.5E-01	5.0E-01	
10497490	**Naaladl2**	635702		3.0E-05	1.4E-03	0.63	6.8E-07	5.7E-05	0.45	3.3E-04	7.9E-03	0.70
10532019	**Gbp11**	634650	*	1.9E-05	9.8E-04	0.63	6.2E-03	4.2E-02	0.74	3.9E-01	6.3E-01	
10429564	**Ly6a**	110454		9.6E-04	1.5E-02	0.63	8.3E-06	3.3E-04	0.51	2.7E-01	5.2E-01	
10357280	**Insig2**	72999		1.1E-04	3.3E-03	0.63	3.8E-07	3.8E-05	0.61	2.0E-01	4.3E-01	
10582879	**Csprs**	114564	*	8.8E-07	1.2E-04	0.63	2.3E-06	1.3E-04	0.60	4.4E-03	3.9E-02	0.81
10462035	**Ldhb**	16832		7.9E-06	5.2E-04	0.63	1.0E-07	1.6E-05	0.60	2.8E-02	1.3E-01	
10498998	**D930015E06Rik**	229473		1.7E-06	1.8E-04	0.63	4.1E-04	5.8E-03	0.68	5.3E-02	1.9E-01	
10347925	**Gm7609**	665378	*	1.7E-06	1.8E-04	0.63	1.3E-06	9.0E-05	0.60	1.9E-02	1.0E-01	
10582888	**ENSMUST00000099042**			5.5E-04	1.0E-02	0.63	5.9E-04	7.5E-03	0.59	5.1E-04	9.9E-03	0.51
10520612	**Khk**	16548		1.3E-07	3.2E-05	0.63	6.1E-06	2.7E-04	0.63	7.8E-01	8.9E-01	
10500183	**Adamtsl4**	229595		4.1E-06	3.2E-04	0.64	8.3E-06	3.3E-04	0.59	1.8E-01	4.1E-01	
10523506	**Bmp3**	110075		1.3E-05	7.6E-04	0.64	8.2E-08	1.3E-05	0.38	5.8E-01	7.8E-01	
10423941	**Ttc35**	66736		1.5E-04	4.3E-03	0.64	1.4E-06	9.7E-05	0.61	6.6E-02	2.2E-01	
10516908	**Snora73a**	100306944		1.8E-04	4.7E-03	0.64	6.6E-01	8.3E-01		1.5E-03	1.9E-02	1.46
10453231	**Slc8a1**	20541		8.0E-03	6.6E-02	0.64	5.2E-01	7.4E-01		1.4E-03	1.8E-02	0.59
10383025	**C1qtnf1**	56745		2.2E-03	2.7E-02	0.64	7.8E-03	4.9E-02	0.79	7.5E-03	5.5E-02	1.46
10471424	**Fam102a**	98952		1.8E-06	1.8E-04	0.64	1.3E-04	2.4E-03	0.66	2.8E-07	2.3E-04	2.11
10556302	**Ampd3**	11717		7.9E-05	2.7E-03	0.64	8.9E-05	1.8E-03	0.61	4.2E-03	3.8E-02	1.35
10568436	**Fgfr2**	14183		4.9E-07	7.7E-05	0.64	4.0E-05	1.0E-03	0.74	3.1E-02	1.4E-01	
10503835	**Rragd**	52187		1.2E-03	1.8E-02	0.64	3.9E-02	1.5E-01		2.2E-03	2.5E-02	1.49
10501629	**Cdc14a**	229776		1.2E-06	1.5E-04	0.64	1.4E-05	4.8E-04	0.63	1.4E-01	3.5E-01	
10572897	**Hmox1**	15368		2.5E-05	1.2E-03	0.64	2.0E-06	1.2E-04	0.57	2.0E-07	2.0E-04	1.58
10480751	**C8g**	69379		1.9E-04	5.0E-03	0.64	3.1E-02	1.3E-01		4.0E-01	6.4E-01	
10428398	**Eif3e**	16341		1.0E-04	3.3E-03	0.64	1.8E-06	1.1E-04	0.61	2.7E-02	1.3E-01	
10357472	**Cxcr4**	12767		3.5E-06	2.9E-04	0.64	3.5E-02	1.4E-01		1.3E-01	3.4E-01	
10362811	**Sesn1**	140742		1.6E-05	8.8E-04	0.64	1.9E-07	2.3E-05	0.54	8.9E-01	9.5E-01	
10462535	**Pten**	19211		4.6E-03	4.5E-02	0.64	5.9E-04	7.4E-03	0.59	2.1E-06	6.0E-04	0.32
10537227	**Tmem140**	68487	*	1.1E-04	3.4E-03	0.64	3.1E-05	8.5E-04	0.58	3.1E-03	3.1E-02	1.44
10517287	**Man1c1**	230815		1.6E-06	1.7E-04	0.64	1.1E-04	2.2E-03	0.59	5.0E-01	7.2E-01	
10594404	**Smad3**	17127		7.5E-07	1.1E-04	0.65	1.1E-07	1.6E-05	0.56	5.5E-02	2.0E-01	
10583203	**Phxr4**	18689		1.1E-03	1.7E-02	0.65	2.5E-04	3.9E-03	0.41	4.2E-04	8.9E-03	0.40
10489235	**9430008C03Rik**	68108		2.3E-04	5.5E-03	0.65	2.5E-02	1.1E-01		3.2E-01	5.7E-01	
10469867	**Pnpla7**	241274		2.8E-07	5.4E-05	0.65	2.1E-05	6.4E-04	0.72	8.2E-01	9.1E-01	
10483150	**Fign**	60344		5.7E-05	2.1E-03	0.65	1.0E-05	3.8E-04	0.51	4.4E-01	6.8E-01	

10598771	Maoa	17161		1.0E-05	6.4E-04	0.65	4.1E-03	3.1E-02	0.86	8.7E-01	9.4E-01	
10531724	Plac8	231507		7.1E-06	4.9E-04	0.65	3.0E-06	1.6E-04	0.57	2.5E-03	2.7E-02	1.33
10492355	Mme	17380		1.3E-04	3.9E-03	0.65	2.6E-04	4.1E-03	0.59	6.3E-01	8.1E-01	
10546853	Srgap3	259302		2.4E-07	5.0E-05	0.65	4.5E-04	6.1E-03	0.68	1.8E-01	4.1E-01	
10351026	Gas5	14455		6.6E-05	2.4E-03	0.65	2.3E-02	1.1E-01		4.6E-06	8.3E-04	0.41
10506335	Pde4b	18578		2.4E-04	5.8E-03	0.65	5.3E-06	2.4E-04	0.60	7.2E-02	2.3E-01	
10561212	Ltbp4	108075		3.5E-04	7.4E-03	0.65	6.5E-06	2.8E-04	0.48	5.2E-01	7.3E-01	
10538753	Atoh1			1.3E-03	1.9E-02	0.65	3.0E-03	2.5E-02	0.74	4.1E-01	6.5E-01	
10462091	Klf9	16601	*	1.3E-05	7.5E-04	0.65	2.3E-04	3.7E-03	0.72	3.4E-01	5.8E-01	
10538163	Abp1	76507		3.4E-04	7.3E-03	0.65	6.1E-01	8.0E-01		2.2E-03	2.5E-02	1.25
10556242	ENSMUST00000082666			2.5E-03	2.9E-02	0.65	3.3E-03	2.7E-02	0.81	1.5E-04	5.1E-03	0.67
10381006	Thra	21833	*	1.0E-07	2.6E-05	0.65	3.0E-08	7.4E-06	0.53	9.2E-02	2.7E-01	
10438017	Fgd4	224014		1.1E-04	3.4E-03	0.65	2.9E-05	8.0E-04	0.65	8.4E-01	9.2E-01	
10523579	Arhgap24	231532		1.3E-06	1.5E-04	0.65	2.9E-07	3.1E-05	0.55	9.9E-01	1.0E+00	
10383479	Hmga1-rs1	111241	*	8.1E-04	1.3E-02	0.65	7.5E-03	4.8E-02	0.72	2.2E-04	6.2E-03	1.87
10466304	Dtx4	207521		5.6E-06	4.1E-04	0.65	1.0E-05	3.8E-04	0.58	1.3E-01	3.3E-01	
10603166	Trappc2	66226		1.7E-04	4.5E-03	0.65	9.2E-04	1.0E-02	0.79	1.5E-03	1.9E-02	0.69
10426891	Mettl7a1	70152		2.0E-04	5.1E-03	0.65	1.3E-04	2.4E-03	0.68	5.9E-02	2.1E-01	
10405693	Dapk1	69635		1.8E-04	4.7E-03	0.65	1.5E-03	1.5E-02	0.83	8.4E-01	9.2E-01	
10422227	Spry2	24064		3.2E-05	1.4E-03	0.65	1.6E-06	1.1E-04	0.34	1.0E-01	2.9E-01	
10425066	Csf2rb	12983		2.3E-04	5.5E-03	0.66	4.2E-01	6.6E-01		2.6E-01	5.1E-01	
10570639	2610005L07Rik	381598		1.7E-03	2.2E-02	0.66	5.4E-04	7.0E-03	0.73	4.9E-06	8.6E-04	0.42
10574149	Nlrc5	434341		1.8E-04	4.7E-03	0.66	6.9E-03	4.5E-02	0.75	4.3E-01	6.7E-01	
10592023	Aplp2	11804		2.2E-06	2.1E-04	0.66	7.2E-08	1.2E-05	0.51	9.4E-02	2.8E-01	
10377429	Snord118	100216530		3.4E-05	1.5E-03	0.66	7.1E-01	8.6E-01		8.5E-02	2.6E-01	
10399428	Snord118	100216530		3.4E-05	1.5E-03	0.66	7.1E-01	8.6E-01		8.5E-02	2.6E-01	
10358894	Sord	20322		3.8E-05	1.6E-03	0.66	8.9E-05	1.8E-03	0.61	8.0E-04	1.3E-02	1.53
10362674	Rnu3a	19850		2.3E-05	1.1E-03	0.66	2.6E-01	5.1E-01		7.5E-02	2.4E-01	
10499655	Il6ra	16194		1.5E-06	1.6E-04	0.66	1.2E-07	1.7E-05	0.54	8.6E-02	2.6E-01	
10457250	Arhgap12	75415		1.8E-04	4.7E-03	0.66	5.7E-06	2.5E-04	0.67	3.6E-02	1.5E-01	
10367475	ENSMUST00000102458			1.3E-05	7.5E-04	0.66	4.2E-04	5.8E-03	0.56	3.7E-06	7.5E-04	0.50
10444824	LOC68395	68395	*	1.4E-06	1.6E-04	0.66	2.5E-04	3.9E-03	0.72	1.4E-01	3.5E-01	
10453857	Gata6	14465		4.0E-05	1.7E-03	0.66	4.7E-03	3.4E-02	0.84	3.7E-01	6.1E-01	
10483819	Ttc30b	72421		6.4E-03	5.7E-02	0.66	6.2E-05	1.4E-03	0.70	6.9E-02	2.3E-01	
10518167	Trappc2	66226		4.4E-04	8.8E-03	0.66	7.7E-03	4.9E-02	0.80	3.1E-03	3.1E-02	0.69
10495967	Tifa	211550		3.6E-03	3.8E-02	0.66	1.2E-01	3.2E-01		8.1E-02	2.5E-01	
10432573	Slc11a2	18174		1.9E-05	9.9E-04	0.66	4.9E-04	6.5E-03	0.73	2.4E-03	2.6E-02	1.30
10526943	Gpr146	80290		2.1E-06	2.0E-04	0.66	3.6E-06	1.8E-04	0.69	7.4E-03	5.5E-02	1.14
10447084	Galm	319625		4.1E-06	3.2E-04	0.66	3.0E-04	4.6E-03	0.71	5.9E-04	1.1E-02	1.38
10512949	Abca1	11303		5.2E-03	5.0E-02	0.66	1.4E-02	7.6E-02	0.84	2.3E-02	1.2E-01	
10516906	Snora73b	100306945		1.1E-04	3.4E-03	0.66	2.9E-01	5.4E-01		1.8E-04	5.7E-03	1.56
10402268	Lgmn	19141		1.2E-05	7.2E-04	0.66	1.4E-05	4.7E-04	0.65	5.0E-03	4.2E-02	1.26
10353475	Eif3m	98221		3.3E-04	7.2E-03	0.66	5.3E-03	3.7E-02	0.79	5.0E-01	7.2E-01	
10602221	Mir680-2	751551		1.9E-04	5.0E-03	0.66	4.0E-04	5.6E-03	0.60	5.5E-04	1.0E-02	0.63
10570957	Sfrp1	20377		1.4E-02	9.6E-02	0.66	6.0E-04	7.6E-03	0.49	5.7E-02	2.0E-01	
10383214	Rnf213	672511		3.6E-07	6.2E-05	0.66	2.2E-07	2.6E-05	0.62	4.3E-01	6.7E-01	
10450145	Psmb9	16912		3.6E-06	3.0E-04	0.66	1.2E-04	2.3E-03	0.67	2.2E-02	1.1E-01	
10541670	C1rl	232371		3.3E-04	7.2E-03	0.66	9.2E-05	1.9E-03	0.66	3.8E-02	1.6E-01	
10418702	Sh3bp5	24056		2.2E-06	2.1E-04	0.66	4.8E-07	4.5E-05	0.53	5.3E-01	7.4E-01	
10537051	Cpa1	109697		1.4E-04	4.0E-03	0.66	3.6E-06	1.9E-04	0.29	7.0E-01	8.5E-01	
10436600	Mir99a	387229		3.9E-03	4.1E-02	0.66	1.4E-06	9.5E-05	0.40	3.4E-05	2.3E-03	0.57

Table 6.4: Down-regulated probesets in invading and non-invading TGFβ1-treated fibroblasts.

Gene expression lists for microarrays conducted at 96 hours of MLg fibroblast invasion in the presence or absence of TGFβ1 (5 ng/ml). Data are shown for down-regulated probesets with > 1.5-fold regulation. Data are sorted by 96 h inv. (TGFβ1/n.t.). Statistical analysis: limma t-test and Benjamini-Hochberg multiple testing correction.(n.t. = non-treated, BH = Benjamini-Hochberg, FDR = False discovery rate, inv. = invading, non-inv. = non-invading, T = TGFβ1, C = Control).

ACKNOWLEDGEMENTS

Foremost, I would like to express my special thanks to my supervisor Prof. Dr. Oliver Eickelberg, for giving me the opportunity to work on this interesting research project, for great scientific guidance, for providing an outstanding research environment, and the chance to gain valuable new experiences at diverse conferences.

I am very grateful to PD Dr. Silke Meiners for her kind and excellent supervision, encouraging support, and extensive scientific discussions during the past four years.

I would also particularly like to thank Dr. Gerald Burgstaller for his great contribution to this work, his enthusiasm, for his mentoring and for always finding the time for a coffee.

Prof. Dr. Alexander Dietrich, Prof. Dr. Stephan Kröger, and Prof. Dr. Michael Kiebler are acknowledged for evaluating my work and participating in my PhD examination.

I am thankful to Prof. Dr. Rachel Chambers for serving as my committee member. Furthermore, I want to acknowledge our collaboration partners Dr. Martin Irmler, PD Dr. Johannes Beckers, and Dr. Eric White for excellent scientific support and continuous interest in my research project.

I am grateful to all current and former members of the Eickelberg group, Dr. Katharina Heinzelmann, Dr. Nikica Miše-Racek, Dr. Claudia Staab-Weijnitz, Dr. Isis Fernandez, Dr. Viktoriya Tomiatti, Dr. Natalia Smirnova, Dr. Olga Bermudez, Andrea Schamberger, Jessica Grün, Larissa Knüppel, Nina Noskovicova, Elisabeth Hennen, Kyra Peters, Katharina Lippl, Ann-Christin Beitel, Daniela Dietel, Dibora Tibebu, Konstanze Heise, and Tiffany Hwang for contribution of ideas, their kind support, for outstanding technical assistance, and for the fun time in and outside the lab. This also accounts for many more great colleagues at the CPC, especially Dr. Kathrin Mutze, Dr. Verena Aumiller, Dr. Sabine van Rijt, and Dr. Tina Pritzke.

During my time at the CPC I have benefitted from participating in the research school “Lung Biology and Disease” – many thanks to Dr. Dr. Melanie Königshoff, Camille Beunèche, and Dr. Doreen Franke.

I furthermore highly appreciated the companion and friendship of my fellow PhD students. In particular Sabine Bartel, Franziska Uhl, Nora Semren, Nunja Habel-Ungewitter, Lilia Zvintzou, Murali Sarguru, Emmanuelle Genoyer, and Birgitta Heckl have supported me in many ways and highly contributed in making my time at the CPC especially memorable.

Special thanks to Andrea Schamberger – for your great optimism and help, and the fun we had traveling together. To Juliane Bartmann – for your talent in cheering me up and being the best

neighbor ever! To Barbara Berschneider – not only for carefully proofreading my thesis and late-night sushi delivery to the institute, but especially for always being there for me.

Warmest thanks also to my long-standing friend Jessica Kast for your help, in times you were busy with your own thesis, and for always encouraging me.

I dearly thank my family for their unconditional help and support, for always encouraging me, and their understanding. My deepest thanks to Florian – thank you for being the best support one could wish for.